

**FLUORESCENT LABELING REAGENTS OPTIMIZED FOR CAPILLARY
ELECTROPHORETIC SEPARATIONS**

A Dissertation

by

ROY TONACAO ESTRADA, III

Submitted to the Office of Graduate Studies of
Texas A&M University
in partial fulfillment of the requirements for the degree of

DOCTOR OF PHILOSOPHY

May 2010

Major Subject: Chemistry

**FLUORESCENT LABELING REAGENTS OPTIMIZED FOR CAPILLARY
ELECTROPHORETIC SEPARATIONS**

A Dissertation

by

ROY TONACAO ESTRADA, III

Submitted to the Office of Graduate Studies of
Texas A&M University
in partial fulfillment of the requirements for the degree of

DOCTOR OF PHILOSOPHY

Approved by:

Chair of Committee,	Gyula Vigh
Committee Members,	Kevin Burgess
	Paul A. Lindahl
	Emile A. Schweikert
	Victor M. Ugaz
Head of Department,	David H. Russell

May 2010

Major Subject: Chemistry

ABSTRACT

Fluorescent Labeling Reagents Optimized for Capillary Electrophoretic Separations.

(May 2010)

Roy Tonacao Estrada, III, B.S., University of San Carlos

Chair of Advisory Committee: Dr. Gyula Vigh

Fluorescent labeling can improve the detection sensitivity in capillary electrophoretic (CE) separations down to attomolar concentrations. However, most fluorescent labels are not compatible with CE because their fluorescence properties and charge states are pH-dependent, they are often hydrophobic and they have a tendency to significantly change the properties of the analytes after labeling.

A group of fluorescent labeling reagents have been prepared whose fluorophores have properties that are optimized for CE separations. These fluorophores have fluorescence properties and charge states that are independent of pH in the $2 < \text{pH} < 11$ range. Their excitation maxima are also compatible with the 488 nm line of the Argon ion laser. A mono-cationic acridine-based fluorescent label was prepared and was found to not shift the pI of a labeled model protein in capillary isoelectric focusing separation (cIEF). Lower loading, due to increased sensitivity, led to better resolution of closely spaced isoform peaks having a $\Delta\text{pI} = 0.05$. A tri-anionic pyrene-based fluorescent labeling reagent was also synthesized and was used in the sodium dodecyl sulfate – capillary gel electrophoresis (SDS-CGE) separation of proteins. The fluorophore led to an LOQ in

the nM range, and did not alter the migration behavior of proteins in the sieving matrix. A third fluorescent labeling reagent was developed as a solid phase reagent (SPR) where the fluorophore was immobilized on a solid surface through a cleavable anchor. The fluorophore is di-anionic and is based on pyrene. The SPR was designed to allow the simultaneous capture and labeling of an analyte and the efficient release of the label-analyte conjugate under mild acidic conditions. The use of the SPR allowed the labeling of a diamine whose concentration was in the low nanomolar range. The SPR opens up the possibility for mono-labeling and proportional multiple labeling of proteins.

To my wife, Faye, who is my home and the reason that I am.

To my children, Francesca and Benedict, who give the simplest, most beautiful pleasures.

To Mommy Suzette and Daddy Dong, who took care of us no matter what and taught us patience, forgiveness and love.

To Mama Vering, who is always there for us and taught us so many of life's values.

To Mama Winda, who made so many things possible through her prayers and support.

ACKNOWLEDGEMENTS

I thank Dr. Gyula Vigh for instilling in me a passion for life. He has taught me with tremendous enthusiasm and patience. I thank him for taking care of me as a father would.

I express my gratitude to the members of our group, both past and present. Thanks to Brent, Silvia, Kingsley, Omar, Shulan, Ann, Evan, Nellie, Sanjiv, Peniel, Brian, Rob, Edward, Ming-Chien and Mavreen for being such good friends.

Thanks to Dr. Kevin Burgess who has provided a lot of useful insights on the organic chemistry part of my research.

I also give my thanks to Bill, Stephanie, Brad, Vanessa, Shane and Yohannes for their enormous help in acquiring (and re-acquiring) numerous mass spectra.

I acknowledge Beckman Coulter and the Gradipore Chair of Separation Science for making this work possible through their financial support.

And most of all, all praise, honor, glory and thanksgiving to God who can never be outdone in His generosity, mercy and love.

TABLE OF CONTENTS

	Page
ABSTRACT	iii
DEDICATION	v
ACKNOWLEDGEMENTS	vi
TABLE OF CONTENTS	vii
LIST OF FIGURES	xiii
LIST OF TABLES	xxiv
1 INTRODUCTION	1
1.1 Capillary Electrophoretic Separation of Proteins	1
1.2 Fluorescence Detection of Proteins	1
1.3 Fluorescent Labeling of Proteins	2
1.4 Limitations of Existing Fluorescent Labeling Reagents	3
1.4.1 Hydrophobicity	3
1.4.2 pH-dependent Fluorescence	5
1.4.3 pH-dependent Charge States	6
1.4.4 Changes in the Properties of Proteins after Labeling	7
2 DEVELOPMENT OF A pH-INDEPENDENT ACRIDINE-BASED FLUORESCENT LABELING REAGENT	9
2.1 Design and Synthesis	9
2.1.1 Background and Objectives	9
2.1.1.1 Charge State	9
2.1.1.2 pH-independent Fluorescence Properties	14
2.1.1.3 Tether and Reactive Arm	17
2.1.2 Materials and Methods	18
2.1.2.1 Synthesis of Sulfopropylated Acridine Orange 6	19
2.1.2.2 Recrystallization of Sulfopropylated Acridine Orange 6	20
2.1.2.3 Synthesis of Sulfonyl Chloride 7	20
2.1.2.4 Synthesis of Sulfonamide 8	21

	Page
2.1.2.5 Synthesis of Acridine Orange Carboxylic Acid 9	21
2.1.2.6 Synthesis of Acridine Orange N- Hydroxysuccinimidyl Ester 10	21
2.1.3 Results and Discussion	22
2.1.3.1 Quaternarization of Acridine Orange	22
2.1.3.2 Extension of the Tether	27
2.1.3.3 Activation of the Carboxylate to the Amine-reactive Group	31
2.1.3.4 Water Solubility and Hydrophilicity	32
2.2 Spectral Properties	33
2.2.1 Background and Objectives	33
2.2.2 Materials and Methods	34
2.2.3 Results and Discussion	34
2.3 Labeling Reactions Using the Acridine Orange-based Fluorescent Label	39
2.3.1 Background and Objectives	39
2.3.2 Materials and Methods	40
2.3.2.1 Labeling of Small Amines and Their Analysis by CE-LIF	40
2.3.2.2 Protein Labeling and Their Analysis by SDS-CGE-LIF	41
2.3.2.3 Synthesis of the Fluorescent pI Markers	42
2.3.2.4 Labeling of Chicken Ovalbumin and Its Analysis by SDS-CGE-LIF	43
2.3.3 Results and Discussion	44
2.3.3.1 Labeling of Small Amines	44
2.3.3.2 Synthesis of Fluorescent pI Markers for cIEF-LIF	47
2.3.3.3 cIEF Analysis of Labeled Chicken Ovalbumin	55
2.4 Concluding Remarks	60
3 DEVELOPMENT OF A pH-INDEPENDENT PYRENE-BASED FLUORESCENT LABELING REAGENT	61
3.1 Introduction	61
3.2 Optimization of the Sulfonamidation Step	64
3.2.1 Background and Objectives	64
3.2.2 Materials and Methods	65
3.2.2.1 Synthesis of 2,2-Dimethylpropyl Ethenesulfonate 18	65

	Page
3.2.2.2 Synthesis of 2,2-Dimethylpropyl 2-(methylamino)ethanesulfonate 19	66
3.2.2.3 Synthesis of 8-Aminopyrene-1,3,6-trisulfonyl Chloride 20	67
3.2.2.4 Synthesis of 8-Aminopyrene-1,3,6-trisulfonamide 21	67
3.2.3 Results and Discussion.....	69
3.2.3.1 Sulfonamidation with N-Methyltaurine	69
3.2.3.2 Sulfonamidation with Neopentyl Ester 19	72
3.3 Optimization of Alkylation of the Anilinic Amino Group.....	74
3.3.1 Background and Objectives	74
3.3.2 Materials and Methods.....	75
3.3.2.1 Synthesis of Styrene Glycol 23	75
3.3.2.2 Synthesis of Dioxolane 24	76
3.3.2.3 Synthesis of Tetraethyleneglycol-decorated Dioxolane 25	77
3.3.2.4 Synthesis of Dioxolane/Carboxylic Acid-terminated Tetraethyleneglycol 26	78
3.3.2.5 Synthesis of Ketone/Carboxylic Acid-terminated Tetraethyleneglycol 27	79
3.3.2.6 Synthesis of PEG-based Fluorophore Tether Intermediate 28	80
3.3.2.7 Synthesis of Alkylated APTS Trisulfonamide 29	81
3.3.3 Results and Discussion.....	84
3.4 Optimization of the Removal of the Neopentyl Protecting Group and Purification of the Sulfonic Acid by Preparative Hydrophilic Interaction Liquid Chromatography (Prep HILIC)	91
3.4.1 Background and Objectives	91
3.4.2 Materials and Methods	92
3.4.2.1 Synthesis of Sulfonic Acid 32 (Removal of the Neopentyl Protecting Group)	93
3.4.2.2 Hydrolysis of Methyl Ester 32 to Form Carboxylic Acid 33	94
3.4.2.3 Semi-preparative HILIC of Tetra-anion 33	94
3.4.3 Results and Discussion.....	96
3.4.3.1 Removal of the Neopentyl Protecting Group	96
3.4.3.2 Purification of Sulfonic Acid 33 by Semi-prep HILIC.....	105
3.5 Spectral Properties.....	110
3.5.1 Background and Objectives	110
3.5.2 Materials and Methods	111

	Page
3.5.3 Results and Discussion.....	112
3.6 Fluorescence Labeling Tests with the Pyrene-based Label	116
3.6.1 Background and Objectives	116
3.6.2 Materials and Methods	116
3.6.2.1 Activation of Fluorophore 33 as a Pentafluorophenyl Ester	117
3.6.2.2 Labeling of Small Diamines.....	117
3.6.2.3 CE-LIF of Small Diamines.....	117
3.6.2.4 Labeling of Proteins for SDS-CGE-LIF.....	119
3.6.3 Results and Discussion.....	119
3.7 Concluding Remarks	126
4 DEVELOPMENT OF SCALER (SIMULTANEOUS CAPTURE AND LABELING, EFFICIENT RELEASE) FLUORESCENT LABELING REAGENT	128
4.1 Introduction	128
4.1.1 General Scheme.....	128
4.1.2 Anticipated Advantages that are Specific to the Proposed SCALER Solid Phase Reagent.....	131
4.1.3 General Objectives	133
4.2 Design and Synthesis of the Cleavable Anchor	134
4.2.1 Background and Objectives	134
4.2.2 Materials and Methods	136
4.2.2.1 Synthesis of Monotosylated Tetra(ethylene glycol) 35	137
4.2.2.2 Synthesis of Tetra(ethylene glycol)-decorated 4-Hydroxybenzaldehyde 36	137
4.2.2.3 Synthesis of Tosylated Aldehyde 37	139
4.2.2.4 Synthesis of Azido Aldehyde 38	139
4.2.2.5 Synthesis of Dioxolane 39	140
4.2.2.6 Synthesis of Tosylated Dioxolane 40	141
4.2.2.7 Synthesis of Tetra(ethylene glycol)-decorated Dioxolane 41	142
4.2.2.8 Synthesis of Diol-terminated Tetra(ethylene glycol) 42	143
4.2.2.9 Synthesis of Cleavable Anchor Intermediate 43	144
4.2.3 Results and Discussion.....	145
4.2.3.1 Hydrolysis Rates of Different Dioxolanes	145
4.2.3.2 Synthesis of the Cleavable Anchor	147
4.3 Attachment of the Cleavable Arm to the Fluorophore.....	151

	Page
4.3.1 Background and Objectives	151
4.3.2 Materials and Methods	152
4.3.2.1 Synthesis of Fluorophore 44	152
4.3.2.2 Synthesis of Fluorophore 45	154
4.3.3 Results and Discussion.....	155
4.3.3.1 Rationale for the Direct Attachment of the Cleavable Anchor to the Fluorophore	155
4.3.3.2 Attachment of the Cleavable Anchor Intermediate.....	161
4.3.3.3 Test Cleavage of Fluorophore 45	162
4.3.3.4 Fluorescence Properties of Fluorophore 46	166
4.4 Synthesis of the Solid Phase and Immobilization of the Fluorophore Through the Cleavable Anchor	167
4.4.1 Background and Objectives	167
4.4.2 Materials and Methods	169
4.4.2.1 Bifunctionalization of the Capillary Melting Point (MP) Tubes	170
4.4.2.2 HEMA-based Monolith Synthesis in Melting Point Capillaries	170
4.4.2.3 Activation of the Monolith Surface.....	172
4.4.2.4 Immobilization of Fluorophore 45 on the Activated Monolith Surface	172
4.4.2.5 Determination of Cleavage Rate of the Immobilized Fluorophore.....	173
4.4.2.6 Preparation of the Monolith Pipette Tip Cartridge.....	174
4.4.3 Results and Discussion.....	175
4.4.3.1 Preparation of the Monolithic Support for SCALER SPR.....	175
4.4.3.2 Immobilization of the Fluorophore onto the Monolith Support	177
4.4.3.3 Format of the Monolithic SPR	179
4.4.3.4 Rate of Cleavage of the Cleavable Group After Immobilization.....	181
4.5 Labeling Tests using the SCALER SPR	184
4.5.1 Background and Objectives	184
4.5.2 Materials and Methods	185
4.5.2.1 Activation of the Fluorophore	185
4.5.2.2 Labeling of Small Amines.....	185
4.5.2.3 Labeling of Diamines at Low Concentrations...	186
4.5.2.4 Labeling of Amino Acids	186
4.5.2.5 Labeling of N-Acetyl-L-Lysine-Amide	187

	Page
4.5.3 Results and Discussion.....	187
4.5.3.1 Activation of the SCALER SPR Amine- reactive Group	187
4.5.3.2 Labeling of Diamines and Their Analysis by CE-LIF at Different pH Values	189
4.5.3.3 Labeling of Diamines at Low Concentrations...	190
4.5.3.4 Labeling of Amino Acids	193
4.6 Concluding Remarks	196
5 CONCLUSION	199
5.1 Fluorescent Labeling Reagents Optimized for Capillary Electrophoretic Separations	199
5.2 Acridine-based Fluorescent Label.....	200
5.3 Pyrene-based Fluorescent Label.....	200
5.4 SCALER Solid Phase Fluorescent Labeling Reagent.....	202
REFERENCES.....	205
APPENDIX A	210
APPENDIX B	221
APPENDIX C	238
VITA	266

LIST OF FIGURES

FIGURE	Page
1.1 Calculated log P values of conjugates of common fluorophores and ethanolamine. Log P values calculated using Advanced Chemistry Development (ACD/Labs) ChemSketch V12.01 (Copyright 1994-2009 ACD/Labs).....	4
1.2 Net charge of ethanolamine labeled with fluorescein, rhodamine and aminoquinoline calculated with Eqn.1 using the pK _a values as follows: 2.51, 6.57 (fluorescein derivative); 2.39, 10.26 (rhodamine derivative); 4.52 (aminoquinoline derivative)	7
2.1 Calculated shifts of the pI values of three different proteins labeled with either a dianionic, a neutral or a monocationic fluorescent label	12
2.2 Structures of cyanine dyes used by Unlu and others for the minimal labeling of proteins for 2D-PAGE	14
2.3 Fluorescent dyes synthesized by Wolfbeis and Urbano from heterocyclic aromatic amines	16
2.4 Quaternarization of acridine orange to form zwitterion 6	22
2.5 PreMCE-LIF analysis of a reaction mixture obtained by Method C showing leftover acridine orange (AO), the desired product (compound 6) and an unknown anionic byproduct	24
2.6 Compound 6 before and after workup consisting of digestions in acetone and recrystallizations from formamide	26
2.7 ¹ H-NMR of compound 6 in d ₆ -DMSO with 10% triflic acid	27
2.8 Extension of the tether of the fluorescent label	28
2.9 Quantitative conversion of sulfonyl chloride 7 to stable sulfonamide 11 prior to CE analysis	28

FIGURE	Page
2.10 CE analysis of a 40-minute sample of the chlorination reaction of sulfonate 6 . The desired sulfonyl chloride product 7 was quantitatively coupled to morpholine to form sulfonamide 11 prior to CE analysis	29
2.11 CE-LIF analysis of (A) morpholine sulfonamide 11 , which is indicative of the starting material sulfonylchloride 7 , (B) coupling of 7 with methyl-6-aminocaproate and (C) hydrolysis of methyl ester 8 to carboxylic acid 9 . μ_{eff} values are expressed in $10^{-5} \text{ cm}^2/\text{Vs}$ units	30
2.12 Activation of carboxylate 9 to NHS ester 10	31
2.13 CE-LIF analysis of the activation of carboxylic acid 9 (A) to NHS ester 10 (B). μ_{eff} values are expressed in $10^{-5} \text{ cm}^2/\text{Vs}$ units	32
2.14 UV absorbance spectra of acridine orange and its quaternarized derivative, 6	35
2.15 Fluorescence emission spectra of compound 6 in different aqueous buffers from pH 2 to 11.....	36
2.16 Fluorescence intensities of fluorophore 6 in carrier ampholyte fractions of different pH ranges. The signals were taken using a Beckman PA800 with a LIF detection system (488 nm excitation, 520 nm detection).....	37
2.17 Absorbance and fluorescence emission spectra at different concentrations of Rhodamine 6G and carboxylic acid 9	38
2.18 Plot of integrated fluorescence emission versus absorbance for Rhodamine 6G (\blacktriangle) and carboxylic 9 (\blacksquare)	39
2.19 CE-LIF analysis of fluorescent labeling reagent 10 (A), labeled AEM (B) and labeled DEAPA (C)	46
2.20 CE-LIF analysis of fluorescent labeling reagent 10 (A), labeled aspartic acid (B), labeled iminodiacetic acid (C) and labeled glutamic acid (D).....	46
2.21 SDS-CGE analysis of labeled proteins using LIF detection.	47
2.22 General scheme for the synthesis of acidic pI markers using the acridine orange-based core fluorophore as the titrating group	49

FIGURE	Page
2.23 General scheme for the synthesis of basic pI markers based on HPTS as the core fluorophore and titrating group	50
2.24 Simulated net charges of pI markers 12 to 17 as a function of pH. The simulated pI is the pH at which the net charge of the molecule is equal to zero. The pKa values in Tables 2 and 3 were used in Equation 1.1 to calculate the net charge	52
2.25 Determination of the operational pI value of pI marker 13 . (A) A portion of the mobilization trace of the cIEF-UV analysis of 13 with UV-absorbing pI markers of known pI values. (B) Plot of pI values of the UV-absorbing pI markers versus their migration times (♦) and determination of the operational pI value of 13 (■) based on its migration time	53
2.26 cIEF analysis of pI markers 12 , 13 and 16 with UV (a) and LIF (b) detection. The peaks with the pI values boxed in red are those of the new fluorescent pI markers. The rest of the peaks are those of the UV-absorbing markers	55
2.27 Mobilization traces obtained in the cIEF analysis of (a) unlabeled chicken ovalbumin and (b) labeled chicken ovalbumin.....	57
2.28 Mobilization traces obtained in the cIEF run of the labeled chicken ovalbumin using (a) UV detection and (b) LIF detection	58
2.29 Reproducibility in (a) cIEF-LIF analysis of the same labeling reaction mixture and (b) cIEF-LIF analysis of different labeling reactions of the same chicken ovalbumin sample. The mobilization traces are normalized to the highest peak.....	59
3.1 Structure of 8-aminopyrene-1,3,6-trisulfonic acid (APTS), trisodium salt	61
3.2 General structure of the pyrene-based fluorescent label. R1 is H or alkyl, R2, and R3 are alkyl or heteroalkyl groups. LG is a leaving group	63
3.3 Structure of the tris sulfonamide using N-methyl taurine as the aminoalkanesulfonic acid	69

FIGURE	Page
3.4 HILIC analyses of APTS (A) and the sulfonamidation reaction mixture obtained with N-methyltaurine (B). Binary gradient elution: 1 mL/min, 95 to 65% B in 20 min. (A: 100mM ammonium formate in water; B: ACN)	71
3.5 Overlay of the UV absorbance spectra of APTS and sulfonamidation product 22 . The traces are normalized on the 237 / 238 nm peaks	71
3.6 Preparation of neopentyl ester 19	72
3.7 CE analysis with indirect UV detection of the reaction mixture before (A) and after (B) removal of methylamine	73
3.8 Sulfonamidation using sulfonate ester 19 to form tris sulfonamide 21 ...	73
3.9 RP-HPLC of the reaction mixture (A), product from the first recrystallization step (B) and product from the second recrystallization step (C) of trisulfonamide 21 . Detection wavelength set at 300 nm. The chromatograms are normalized on the major peak and purities calculated from the peak areas are shown	74
3.10 Michael addition reaction between methyl vinyl ketone and tris sulfonamide 22	84
3.11 Overlay of the UV absorbance spectra of amine 22 and its MVK-alkylated derivative 30 . The spectra are normalized on the 239 nm peak	85
3.12 Reductive amination using amine 21 and ethyl-4-acetylbutyrate	86
3.13 RP-HPLC monitoring (detection at 300 nm) of the reductive amination of ethyl-4-acetylbutyrate with amine 21 . The reaction proceeded only with excess amounts of each reagent. (A) is the chromatogram for starting material 21 . (B) through (D) are those of the reaction mixture with increasing amounts of the reagents ketone / NaBH ₃ CN / MSA: 21 / 14 / 20 equiv. (B), 36 / 24 / 60 equiv. (C), 51 / 34 / 100 equiv. (D), and 81 / 44 / 140 equiv. (E). The tallest peaks are normalized	87

FIGURE	Page
3.14 RP-HPLC analysis of starting material 21 (A) and the reductive amination reaction mixture at 20 minutes (B) and 50 min (C). The reaction was done in the presence of H ₃ PO ₄ /P ₂ O ₅ with 20 equiv. ethyl-4-acetylbutyrate, 10 equiv. sodium cyanoborohydride and DMF as solvent	88
3.15 Synthesis scheme for the preparation of tetraethyleneglycol-based fluorophore tether / reactive arm 28	89
3.16 Preparation of alkylated tris sulfonamide 29 from 21 by reductive amination under dehydrating conditions	90
3.17 RP-HPLC of starting material 21 (A) and the reductive amination reaction mixture containing 20 equiv. ketone 28 and 10 equiv. NaBH ₃ CN in the presence of H ₃ PO ₄ /P ₂ O ₅ in DMF after 30-minute (B)..	91
3.18 Sample loop configuration that allows in-line “Taylor” dilution of a sample loaded in a strong solvent for prep HPLC	96
3.19 Deprotection of test compound tris neopentyl ester 21 showing the partially deprotected intermediates (mono and bis) and the fully deprotected 22	96
3.20 Cleavage of the neopentyl sulfonate esters of 21 using TMACl in DMF at 120°C after 3 hours (A), 6 hours (B) and 21 hours (C) reaction time	98
3.21 Possible structures of the byproducts from cleavage of the neopentyl sulfonate esters	98
3.22 Cleavage of the neopentyl sulfonate esters of 21 using 1M HCl in water/n-propanol at 80 to 90 °C after 3 hours (A), and at 100 °C after 17 hours thereafter (B)	99
3.23 Summary of the degree of byproduct formation for different conditions used for the cleavage of the neopentyl sulfonate esters of 21	101

FIGURE	Page
3.24 Deprotection of tris neopentyl sulfonate ester 29 to produce fully deprotected sulfonate 22	103
3.25 HILIC analysis of the deprotection of tris neopentyl sulfonate ester 29 using TEACl in DMSO at 120 °C at 0 min (A), 15 min (B), 60 min (C), 2.4 h (D) and 4 h (D) reaction times	103
3.26 Plot of the percent of the intact neopentyl esters as a function of reaction time (♦). The equation of the fitted exponential decay curve (...) was used to predict the completion time of the reaction	104
3.27 HILIC analysis of methyl ester 32 (A) and a 10-minute sample of its hydrolysis to carboxylic acid 33 using 0.1M NaOH at room temperature (B)	105
3.28 Semi-prep tests with a Luna HILIC 150 mm x 4.6 mm column. The amount and volume of the sample loaded were: 0.1 mg 22 in 0.2 mL mobile phase (A), 1 mg 22 in 2 mL mobile phase (B), 5 mg 22 in 10 mL mobile phase (C) and 2.5 mg 22 in 50 µL water (D). The mobile phase composition (E) is in % B (A: 10 mM NH ₄ HCO ₂ in water; B: 10 mM NH ₄ HCO ₂ in ACN). Flow rate was 1 mL/min. The flat peak tops are due to detector signal overrange	106
3.29 Semi-prep HILIC separation of 5 mg 22 dissolved in 10-mL mobile phase injected using conventional sample injection (A) and 5 mg 22 dissolved in 50-µL water injected using the Taylor dilution-mediated injection technique (B). In the inset, the target peaks are manually aligned and expanded	108
3.30 Semi-prep HILIC separation of 45 mg 22 dissolved in 200 µL water using Taylor dilution-mediated injection. Inset: expanded view of the front end of the target peak showing a partially resolved impurity peak	109
3.31 Semi-prep HILIC separation of 33 (A). Inset shows the analytical HILIC separation of the crude (B) and the fractionated material (C). The target peaks are normalized	110
3.32 Overlay of the UV absorbance spectra of APTS, trisulfonamide 22 and alkylated trisulfonamide fluorophore 33	113

FIGURE	Page
3.33 Fluorescence spectra of fluorophore 33 at different pH values	113
3.34 UV absorbance at 510 nm as a function of the concentration of fluorophore 33	114
3.35 Relative fluorescence quantum yield determination for fluorophore 33 using Rhodamine 6G as standard. (a) UV absorbance and their respective fluorescence emission spectra at different concentrations. (b) Plot of integrated fluorescence emission of fluorophore 33 (▲) and Rhodamine 6G (■) as a function of UV absorbance	115
3.36 CE-LIF of labeled 4-(2-aminoethyl)morpholine and N-methylpiperazine (both marked with *) at different pH values	121
3.37 CE-LIF of a blank labeling reaction (A) and the labeled diamine mixture (B) at pH 7.1	122
3.38 SDS-CGE analysis of labeled proteins: α -lactalbumin (A), carbonic anhydrase (B), chicken ovalbumin (C) and bovine serum albumin (D) ..	123
3.39 SDS-CGE of a mixture of proteins individually labeled at a tag-to-protein ratio of 1:1	124
3.40 Plot of the logarithm of protein molecular weight as a function of the migration time of the proteins labeled at a 1:1 tag-to-protein ratio	124
3.41 SDS-CGE of a mixture of proteins individually labeled at a tag-to-protein ratio of 10:1	125
3.42 Plot of the logarithm of protein molecular weight as a function of protein migration time for proteins labeled at a 10:1 tag-to-protein ratio	126
4.1 A cartoon of the proposed general structure of SCALER (Simultaneous Capture and Labeling, Efficient Release) solid phase reagent	130
4.2 General schematic of the derivatization process using SCALER SPR for the fluorescent labeling of proteins	131

FIGURE	Page
4.3 Synthesis scheme for the preparation of the benzaldehyde side of the cleavable anchor. Refer to Sections 4.2.2.1 to 4.2.2.4 for synthesis details	136
4.4 Synthesis scheme for the preparation of the <i>vic</i> -diol side of the cleavable anchor. Refer to Sections 4.2.2.5 to 4.2.2.8 for synthesis details	140
4.5 Formation of cleavable anchor intermediate 43 from aldehyde 38 and diol 42 . Refer to Section 4.2.2.9 for synthesis detail	144
4.6 Structures of the dioxolanes used in the cleavage experiments	146
4.7 Synthesis scheme for the preparation of the benzaldehyde side of the cleavable anchor	148
4.8 Synthesis scheme for the preparation of the 1,2-diol side of the cleavable anchor	150
4.9 Formation of cleavable anchor intermediate 43 from aldehyde 38 and diol 42	150
4.10 Structure of trisulfonamide 22 which was used in the stability tests	155
4.11 HILIC analysis of the reaction mixture after treatment of trisulfonamide 22 with sodium hydroxide in a mixture of water and methanol at 65 °C for t = 0 h (A), 0.5 h (B) and 2.2 h (C)	157
4.12 Overlay of the UV absorbance spectra of trisulfonamide 22 and the unknown byproduct	158
4.13 Possible structure of the byproduct from the treatment of trisulfonamide 22 with a mixture of water, methanol and NaOH	158
4.14 Treatment of trisulfonamide 22 with different alcohols under basic conditions. The alcohols used were methanol (A), ethanol (B), tetra(ethylene glycol) (C) and glycerol (D)	159
4.15 Fluorescence emission spectra of trisulfonamide 22 (red solid line) and the byproduct obtained in basic ethanol (blue dashed line). Both samples have the same molar absorbance at 480 nm	160

FIGURE	Page
4.16 Fluorescence emission spectra of trisulfonamide 22 (red solid line) and the byproduct obtained in basic glycerol (blue dashed line). Both samples have the same molar absorbance at 480 nm	160
4.17 Scheme for the attachment of hydroxyl-terminated cleavable anchor intermediate 43 to fluorophore 33 and the subsequent reduction of the azido group to the amino group	161
4.18 HPLC monitoring of the attachment of cleavable anchor intermediate 43 to fluorophore 33 showing the chromatograms for the starting material (A), the reaction mixture after 13 hours (B), the reaction mixture after 30 hours (C) and the target after semi-prep HILIC purification (D)	162
4.19 Cleavage of the cleavable group of fluorophore 45 to release diol-terminated fluorophore 46	163
4.20 Plot of the normalized peak areas versus sampling time for the hydrolysis of the cleavable group at pH 3.1 (◆), pH 3.5 (■) and pH 4.2 (▲). The dark lines are the fitted exponential curves. The respective k' and R^2 values are indicated	164
4.21 Plot of the k' values as a function of $[H_3O^+]$ in the hydrolysis buffers ..	166
4.22 Fluorescence spectra of fluorophore 46 recorded at different pH values	167
4.23 Cutting of the melting point tube containing the monolith solid phase reagent using a ceramic cutting tool and a cutting guide/holder consisting of a part of a 1-mL syringe barrel and a polyethylene tube ...	174
4.24 Syringe tool for removing the monolith segment from the glass MP tubing mold	175
4.25 Schematic representation of the synthesis of the HEMA-based monolith 47	176
4.26 Activation of a hydroxyl group on the surface of the HEMA-based monolith using DSC and subsequent immobilization of the fluorophore	177

FIGURE	Page
4.27 Plot of the normalized peak area of the internal standard fluorophore 46 (◆) and fluorophore 45 (■) versus the effluent volume. Peak areas of 46 were normalized to the largest peak area and their respective volumes. Peak areas of 45 were normalized to the peak areas of the internal standard	179
4.28 Photograph of the pipette tip monolithic SPR with the immobilized fluorophore (A) and after cleaving off the fluorophore (B). The 10-μL volume of the cleaving solution used was collected in a 0.2 mL tube (C)	180
4.29 Photograph of the pipette tip monolithic SPR shown in Figure 4.28 under a UV lamp. The designations are the same as in Figure 4.28	181
4.30 PDA signal at 507 nm obtained for the cleaving effluent leaving the 1.5 mm long SPR segment. A pH 3.1 buffer was used as cleaving solution and eluent	183
4.31 Plot of $A_{immob}(t)$ with respect to time. $A_{immob}(t)$ is the area that represents the concentration of the fluorophore as a function of time	184
4.32 Activation of the carboxylic acid of the immobilized fluorophore using PFP-TFA to form the activated SCALER SPR 50	187
4.33 CE-LIF analysis of the cleaving solutions of an unactivated SCALER SPR (A), SPR quenched with morpholine immediately after activation (B) and SPR quenched with morpholine 100 minutes after activation (C). The fluorescent neutral marker is a trisulfonamide derivative of APTS obtained with diethanolamine	189
4.34 CE-LIF analysis, at different pH values, of the cleaving solutions obtained from the diamine labeling experiments	190

FIGURE	Page
4.35 CE-LIF analysis of the cleaving solutions from the labeling of the diamine samples having concentrations from 1mM down to 1μM. The electropherograms are normalized to the area of the labeled AEM peak	192
4.36 Plot of the normalized peak areas of MP against their concentrations. Inset is an expansion for the concentration range of 0 to 0.1 mM. The trend line was fitted from 1×10^{-5} to 0.1 mM (10 nM to 100 μM). The two highest concentration data points deviate from this linearity and are not included in the fit	193
4.37 CE-LIF of cleaving solution from the labeling of a 20μL sample of 0.2mM aspartic and glutamic acid. BGE: 12.5mM acetic acid titrated to pH 4.5 with LiOH	194
4.38 CE-LIF of the cleaving solution from the labeling of a 20μL sample of 0.2mM histidine and arginine. BGE: 13mM CHES titrated to pH 4.5 with LiOH	195
4.39 CE-LIF of cleaving solution from the labeling of a 20μL solution of 0.2mM N-acetyl-L-lysine amide. Different labeling reactions whose samples were passed through the SPR twice (A), 5 times (B), 10 times (C) and 20 times (D) were conducted	196

LIST OF TABLES

TABLE	Page
2.1 Summary of the results of different reactions used to quaternarize acridine orange	25
2.2 Calculated pK_a values of the buffering and titrating groups of pI markers 12 and 13	49
2.3 Calculated pK_a values of the buffering and titrating groups of pI markers 14 to 17	51
2.4 Summary of the determined operational pI values of the synthesized fluorescent pI markers	54
3.1 Buffers used in the fluorescence versus pH experiments for compound 33	111
3.2 Background electrolytes used for the CE analysis of small diamines	118
4.1 Summary of the results of the dioxolane hydrolysis experiments	147
4.2 Summary of the $t_{0.5}$ and $t_{0.01}$ values for the hydrolysis of the cleavable group of fluorophore 45 at different pH	165

1. INTRODUCTION

1.1 Capillary Electrophoretic Separation of Proteins

The analytical separation of proteins is integral in proteomic studies, production of therapeutic proteins and profiling of disease marker proteins in clinical diagnostics. Among the various separation techniques used, capillary electrophoresis (CE) has proven to be very beneficial because of its higher separation efficiency, small sample volume requirement, short analysis time and less need for manual intervention. CE separation of proteins can be done in any of a number of modes. Two of the more powerful CE separation techniques that are being used at present are capillary Isoelectric Focusing (cIEF) and Sodium Dodecylsulfate – Capillary Gel Electrophoresis (SDS-CGE). The former exploits the differences in the isoelectric points (pI) of proteins, the latter uses differences in protein sizes to attain separation selectivity.

1.2 Fluorescence Detection of Proteins

In these analytical separations, the detection of low protein concentrations is of tremendous importance. In proteomic studies, the number of cellular receptors or transcription factors, for example, can be as low as 100-1000 molecules per cell [1]. In the manufacturing of therapeutic recombinant monoclonal antibodies, degradation

This dissertation follows the style and format of *Electrophoresis*.

products and potentially adverse protein impurities can be present in very low levels relative to the active component [2]. Since the limit of detection in CE with the more widely used UV detector is relatively high at $\sim 10\mu\text{g/mL}$ [3], a more sensitive detection technique, such as laser induced fluorescence (LIF), has to be used. With LIF, attomolar concentrations or as low as a few molecules in a $1\mu\text{L}$ sample solution have been detected [4].

1.3 Fluorescent Labeling of Proteins

Proteins have intrinsic fluorescence due to the presence of the aromatic amino acid residues tyrosine and tryptophan. Therefore, proteins can be detected using LIF in their native form. This can provide detection sensitivity down to the nanomolar level [5-7]. However, since excitation occurs in the UV range where a lot of other molecules fluoresce, background noise from the separation matrix and other extraneous compounds is usually a problem. Moreover, UV lasers tend to be more expensive than those used in the visible region [8].

To go around the background noise problem, excitation can be done in the visible or higher wavelengths. However, only a very small number of proteins have native fluorescence above the UV region. To effectively use LIF as a detection method, proteins have to be labeled with fluorophores that can be excited with visible light. These fluorescent labels can either be covalently or noncovalently attached to the proteins. Covalent fluorescent reagents are more robust, more universal and can allow

further handling of the derivatized proteins without losing the attached fluorophore. Depending on the reactive group on the fluorescent label, the fluorophore can be attached to any of a number of functional groups on a protein including the ϵ -amino group of lysine residues, terminal amino group, thiol group of cysteine residues, phenolic group of tyrosine residues, imidazole of histidine and aliphatic alcohol group of serine and threonine residues. Most of the fluorescent labels available have reactive groups that are specific for the ϵ -amino group of lysine residues which are abundant in most proteins.

1.4 Limitations of Existing Fluorescent Labeling Reagents

Although fluorescent labels used in CE usually have desirable fluorescence properties, they usually do not possess the chemical properties that make them optimized for electrophoretic separations. These labels were developed primarily as fluorophores for bioanalytical assays, analytical HPLC and other applications, not for CE. The available fluorescent derivatization reagents that are not optimized for CE separations may even hinder the effective separation and detection of the labeled analytes.

1.4.1 Hydrophobicity

Most fluorophores have fused multi-ring systems as their core structures resulting in large hydrophobic areas. The hydrophobicity of the fluorescent label is important because separations in CE are usually done in aqueous or hydro-organic media. Hydrophilic dyes are preferred in order to prevent adsorption on the capillary wall as

well as aggregation of the dye-protein conjugates. A good measure of hydrophobicity is the logarithm of its partition coefficient between n-octanol and water ($\log P$). The higher the $\log P$ value, the more hydrophobic is the compound. Figure 1.1 lists the calculated $\log P$ values of the ethanolamine conjugates of some common fluorescent labels. Of the six fluorophores, only Alexa 488 has been designed to be a water-soluble fluorescent label having a $\log P$ value that is significantly lower than that of the others.

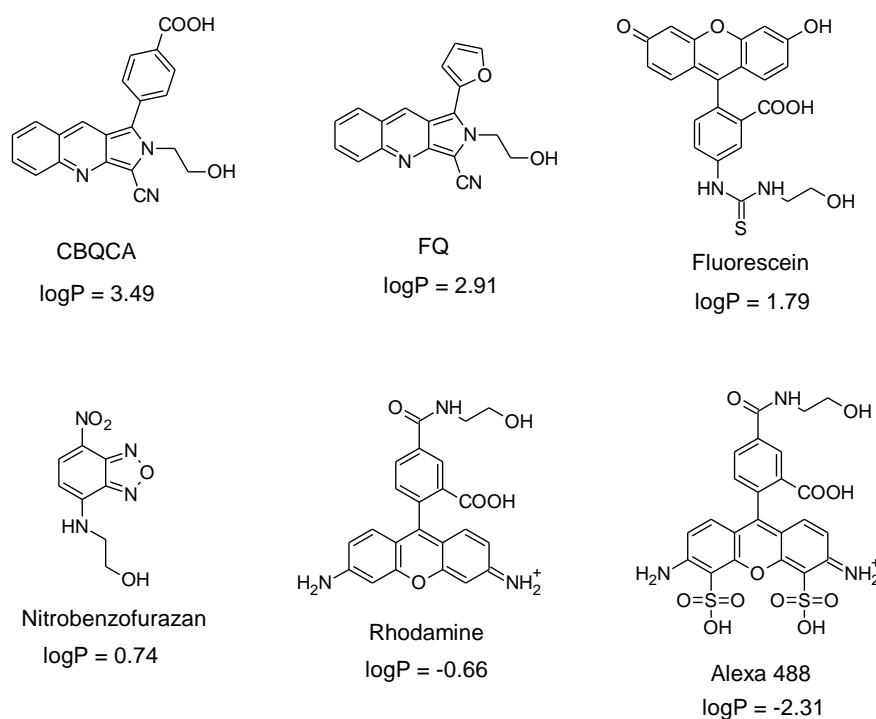


Figure 1.1. Calculated $\log P$ values of conjugates of common fluorophores and ethanolamine. $\log P$ values calculated using Advanced Chemistry Development (ACD/Labs) ChemSketch V12.01 (Copyright 1994-2009 ACD/Labs).

1.4.2 pH-dependent Fluorescence

The majority of the available fluorescent labels have functional groups conjugated to the aromatic ring structures for improved fluorescence quantum efficiency, photostability and excitation and emission wavelength shifting [9, 10]. These substituents are usually weakly acidic groups (e.g., carboxylic acids, thiols, phenols, sulfonamides) or weakly basic groups (e.g., amino groups) that have pK_a values within the operating pH range of CE separations. Since the electronic density and dipole moment of the fluorophore change with the protonation state of the conjugated weak acids or bases, the fluorescence properties of these fluorophores change with pH. Fluorescein, for example, has carboxylic acid and phenolic functional groups on its core aromatic structure resulting in a fluorescence intensity that is pH-dependent [11].

pH is one of the important parameters in CE that has to be set and controlled for optimum separation. CE analysis at different pH values can also be used to determine certain thermodynamic and physical properties of the analytes. It is desirable to have fluorescence properties that are pH-independent so that the fluorophore can be utilized anywhere in the operating pH range of CE. This allows the analysis of the same labeled analyte at different pH values in capillary zone electrophoresis (CZE) without having to derivatize with another fluorescent label. In cIEF where the analytes are separated along a pH gradient in the capillary, the fluorophore has to maintain its fluorescence in any part of the pH gradient to allow detection of all the labeled analytes in a single cIEF run.

1.4.3 pH-dependent Charge States

The net charge, Z , of a labeled analyte is a function of pH as shown in Equation 1.1:

$$Z = \sum_i \left[\frac{1}{1 + 10^{(pH - pK_{a,i})}} \right] - \sum_j \left[\frac{1}{1 + 10^{(pK_{a,j} - pH)}} \right] \quad (1.1)$$

where i and j are basic and acidic functionalities, respectively. These ionizable groups improve the water solubility of a fluorophore when its net charge is not zero. However, for fluorophores with weakly basic and weakly acidic groups, the overall charge can approach zero at certain pH ranges (Figure 1.2) forming either a zwitterionic or a neutral species. In these charge states, water solubility is at a minimum making the fluorophore-analyte conjugate more susceptible to aggregation and adsorption to the wall of the capillary during CE separation.

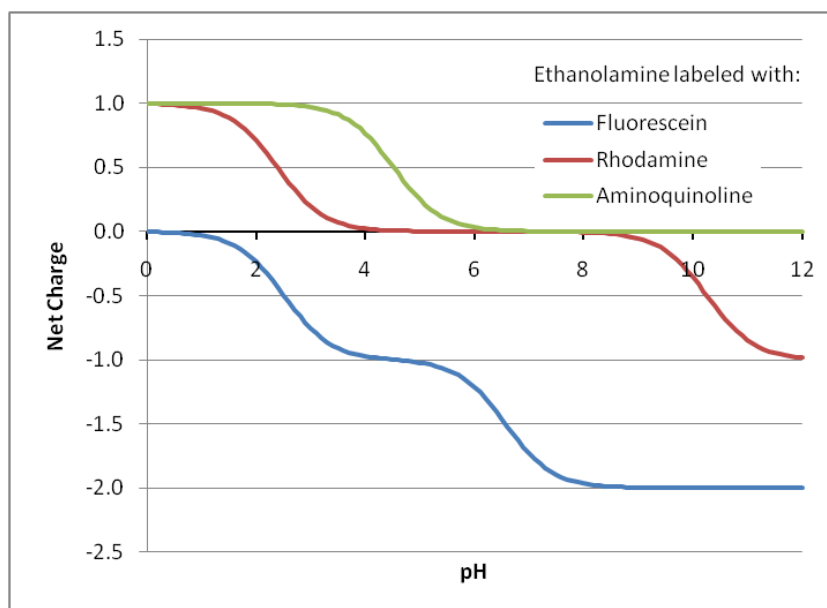


Figure 1.2. Net charge of ethanolamine labeled with fluorescein, rhodamine and aminoquinoline calculated with Eqn.1 using the pK_a values as follows: 2.51, 6.57 (fluorescein derivative); 2.39, 10.26 (rhodamine derivative); 4.52 (aminoquinoline derivative).

1.4.4 Changes in the Properties of Proteins after Labeling

The majority of proteins have multiple sites to which fluorescent labels can be attached during derivatization. Since the fluorescent label is not directed to any single site on the protein, the attachment site of the fluorophore is randomly selected. Moreover, the degree of labeling is dictated by the ratio of the amounts of the reactive label and protein, the number of available derivatization sites on the protein and their reactivity differences. The number of fluorophores attached to a single protein usually follows a statistical distribution. Both the randomness in the selection of the labeling site and the distribution in the degree of labeling produce multiple species which are significantly

different in their size and charge states. This can manifest as broadened peaks or even multiple peaks during CE separations [2, 12, 13]. In cases where all of the labeling sites are derivatized, a single species can be obtained [14]. However, this will result in a significant change in the properties for the protein (e.g., size, pI) rendering the analytical information unreliable for use in protein identification and characterization.

2. DEVELOPMENT OF A pH-INDEPENDENT ACRIDINE-BASED FLUORESCENT LABELING REAGENT

2.1 Design and Synthesis

2.1.1 Background and Objectives

An amine-reactive fluorescent label specifically suited for use in the cIEF separation of proteins needs to be developed. Most of the currently available fluorophores are not compatible with this separation technique. In order for it to be cIEF-compatible, the new fluorescent label must *(i)* minimize the labeling-induced pI shift of proteins and *(ii)* have fluorescence properties that are pH-independent. The fluorophore must also *(iii)* have an excitation wavelength around 488 nm, making it compatible with the commonly used 488 nm Argon ion laser. Three major parts of the fluorescent label development that are necessary to achieve the above objectives are discussed below.

2.1.1.1 Charge State

cIEF separates proteins by the difference in their pI values. The pI of a protein is dictated by the number and the pK_a values of its acidic and basic functional groups. Any derivatization that will add and/or take away any of these ionizable groups will therefore change the pI of the protein. For instance, an amine-reactive reagent that forms an amide with any of the primary amino groups of a protein takes away the ability of that amino group to become protonated, thus shifts the pI of the protein. The magnitude and

direction of the shift in pI of a protein is dependent on the charge state of the label and the number of labels attached to each protein molecule.

Several groups have studied the effects of fluorescence labeling on the pI values of proteins using readily available fluorophores. Pawliszyn and others [13] have labeled albumin, insulin and casein with fluorescein isothiocyanate (FITC) and separated them by cIEF. Although the detection sensitivity has improved by about four orders of magnitude compared to UV absorbance detection, derivatization resulted in broadening and splitting of the peaks and in a considerable shift of the pI values of the labeled proteins. Dovichi's group labeled green fluorescent protein (GFP) with 3-(2-furoyl)quinoline-2-carboxaldehyde (FQ) and looked into the effects of labeling on the pI value of GFP [12]. The use of a naturally fluorescent protein enabled them to monitor the shift of pI value from that of the native to that of its derivatives. Labeling not only significantly shifted the pI value in the acidic direction but also produced at least six different peaks. Using the same reagent to label myoglobin, Krylov and others encountered the same problem, multiple peak generation, with the pI values spanning about 1.5 pH units [15]. Krull et al. prevented this heterogeneity of the labeled proteins by using a large excess of the fluorescent label, 6-aminoquinolyl-N-hydroxysuccinimidylcarbamate (AQC), with respect to the protein thereby exhaustively labeling all the amino groups and producing only a single, fully labeled species. The peak width values of the labeled proteins were found to be smaller than those of the native proteins. However, the shift in the pI value was as large as 3 pH units. They also

encountered problems with precipitation, especially for the more basic proteins, probably due to having more of the hydrophobic dye on the basic proteins – a consequence of the basic protein having more ϵ -amino groups than the acidic ones [14].

Pawliszyn explored the use of noncovalent fluorescent reagents to improve the detection limits for proteins without changing their pI values [16]. This was expected because, unlike in covalent labeling, none of the ionizable groups on the protein was to be derivatized and the charge state was to remain unchanged. Bovine serum albumin (BSA) and hemoglobin were analyzed by cIEF using NanoOrange, Sypro Red, Sypro Orange and Sypro Tangerine. Although the noncovalently labeled BSA peak was well defined and had no significant shift in its pI value, hemoglobin did not produce a peak at all [16]. Stoyanov and others followed this technique but did not get any fluorescent peaks for any of their test proteins [17].

Ideally, the amino group-reactive fluorescent label has to have as close a pK_a as possible to that of the amino group it is reacting with for the pI shift to be minimal. It is impossible though for the label to have exactly the same pK_a value as that of the amino group because the latter will always vary depending on the amino acid residues adjacent to it and on its local environment in the three dimensional structure of the protein [18].

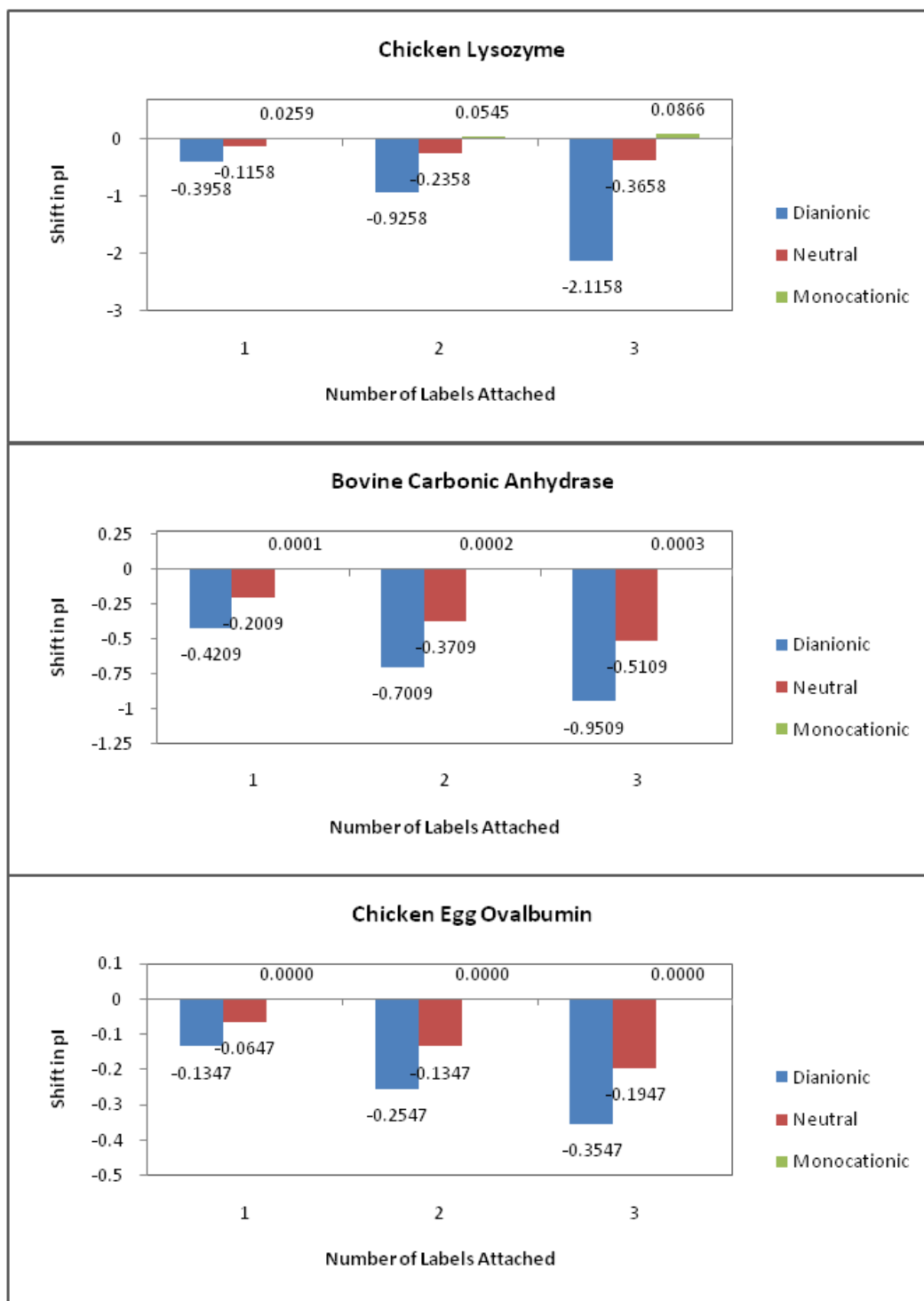


Figure 2.1. Calculated shifts of the pI values of three different proteins labeled with either a dianionic, a neutral or a monocationic fluorescent label.

Figure 2.1 shows the calculated shift in pI of three proteins after derivatization with three hypothetical fluorescent labels with different charge states. The labels are a dianionic fluorophore with pK_a values of 2.5 and 6.5 (to simulate fluorescein), a neutral fluorophore and a monocationic fluorescent label with a pK_a value of 14. For any of the fluorescent labels, the shift in pI value increases with increasing number of the attached labels. The deviation is most pronounced for the dianionic fluorophore where it can be as high as 0.5 for a singly labeled protein and still higher for every additional conjugation.

The shift in pI value is the lowest for the monocationic label. The pI shift is negligible for the slightly acidic protein, chicken egg albumin, and the neutral protein, bovine carbonic anhydrase. However, the pI shift is noticeable for the more basic chicken lysozyme, where it can be as high as 0.1 for three attached labels. The main reason for this larger shift is that for lysozyme - and for most of the basic proteins in general - the ϵ -amino groups of the lysine residues are the ionizable groups that are responsible for setting the pI value of the protein. Any derivatization of any one of these amino groups will therefore have a larger effect on the pI value for the basic proteins than for the more acidic ones. Thus, of the three possibilities, the monocationic labels are the most suitable reagents for the cIEF analysis of most proteins, especially if the number of labels attached to each protein molecule is kept to a minimum. This was demonstrated by Unlu and others who used monocationic fluorescent cyanine dyes (Figure 2.2) for the minimal labeling of proteins in two-dimensional polyacrylamide gel electrophoresis

(2D-PAGE) [19]. Minimal labeling was achieved by keeping the amount of the fluorescent label low with respect to the protein: only a minority of the protein molecules became labeled and only with a single fluorophore. Using 2D-PAGE, they did not observe a change in the pI value of the protein.

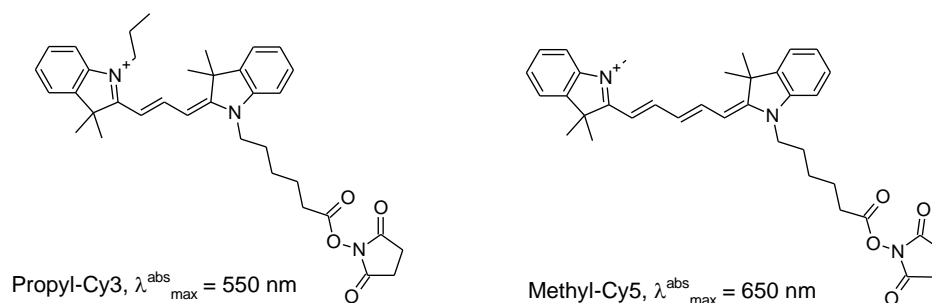


Figure 2.2. Structures of cyanine dyes used by Unlu and others for the minimal labeling of proteins for 2D-PAGE [19].

2.1.1.2 pH-independent Fluorescence Properties

Having pH-independent fluorescence properties for a fluorescent label is more important in cIEF than in any other mode of CE. For a fluorophore to be insensitive of pH within a certain range, its fluorescent core structure either must not have weakly acidic or basic functional groups or must have ionizable groups that have pK_a values well outside of the desired pH range. For cIEF, this range is normally $3 < \text{pH} < 10$, sometimes $2 < \text{pH} < 11$. A number of the available fluorophores are pH-insensitive through most of the operating pH range of cIEF, but may not otherwise be compatible with cIEF. For example, rhodamine dyes are pH-insensitive between 4 and 9 and have very desirable

fluorescence properties [20, 21]. However, these dyes are relatively hydrophobic and tend to cause aggregation problems [22]. Another group of fluorophores, the Alexa Fluor dyes have pH-independent fluorescence properties between 4 and 10 [23]. They are based on the coumarin and rhodamine core structures and are sulfonated to improve water solubility and fluorescence properties. The sulfonate groups however give them negative net charges and render them incompatible with cIEF. Borondipyrromethene (BODIPY) fluorophores are pH-insensitive dyes and are so even outside the operating pH range of cIEF. This is due to the absence of weakly acidic and weakly basic functional groups on their aromatic core structure. These fluorophores have excellent photostability and quantum yields [24]. Currently, however, the BODIPY dyes are only available in the neutral or sulfonated forms. The cyanine dyes used by Unlu et al. (Figure 2.2) in the development of differential gel electrophoresis (DIGE) are both pH-insensitive and monocationic and proved to be suitable for isoelectric focusing in 2D-PAGE [19]. Unfortunately, these fluorophores are fairly hydrophobic. The calculated log D value of Cy3 in its N-hydroxysuccinimide (NHS) form is 6.23 at pH 7 (calculated using SPARC Online Calculator v4.5 [25]).

Heterocyclic aromatic amines (e.g., quinoline, acridine) can be used as core fluorophore structures for a cIEF-compatible fluorescent label. The nitrogen atom in these heterocyclic structures can be conveniently alkylated and quaternarized making the fluorophore pH-insensitive and, at the same time, providing the single positive charge necessary for cIEF applications. Wolfbeis and Urbano synthesized a group of highly

fluorescent dyes by quaternarizing heterocyclic aromatic amines (Figure 2.3) [26]. These dyes were designed to be pH-insensitive fluorescent standards in near neutral pH regions. Fluorescent dye **4**, which is derived from acridine orange, is a good candidate for the core fluorophore. It has a $\lambda_{\max}^{\text{ex}}$ of 494 nm, which is very close to the 488 nm emission line of the Argon-ion laser. Acridine orange is based on the acridine structure and has N,N-dimethylamino substituents in the 3 and 6 positions. These substituents are necessary to shift the excitation wavelength maximum from 415 nm in acridine to 494 nm in acridine orange. The pK_a values of these weak anilinic amino groups are calculated to be less than 2 (calculated using SPARC Online Calculator v4.5 [25]). Consequently, these amino groups are not going to become ionized and change the fluorescence properties of the core within the operating pH range of cIEF.

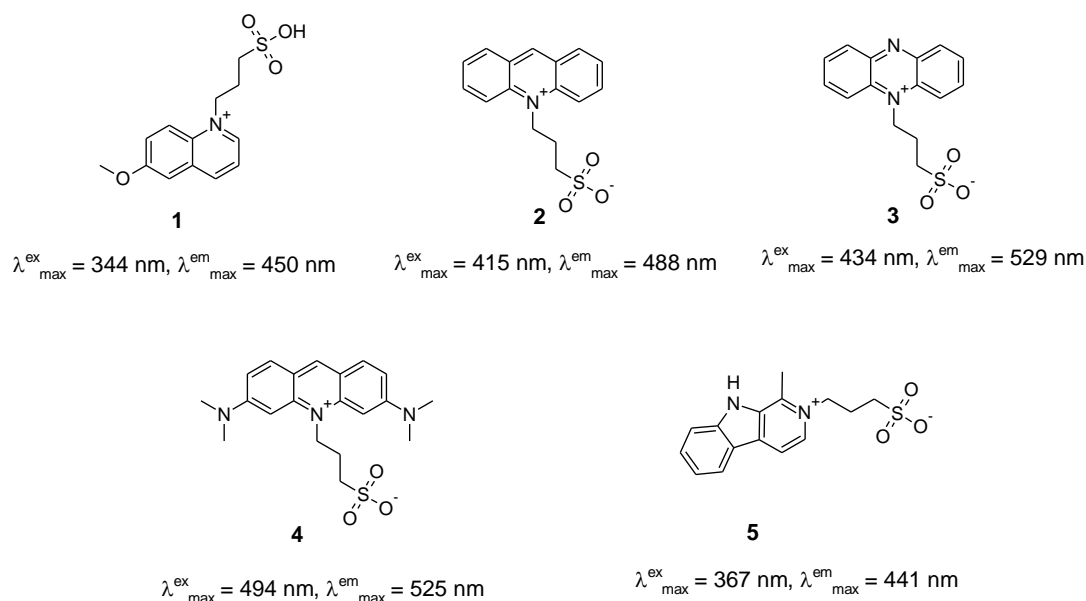


Figure 2.3. Fluorescent dyes synthesized by Wolfbeis and Urbano from heterocyclic aromatic amines [26].

2.1.1.3 Tether and Reactive Arm

A tether that separates the fluorophore and the labeled protein is necessary to minimize the effect of the analyte on the fluorescence of the label. A tether, or at least a part of it, can be attached to the nitrogen atom in the aromatic heterocycle of the acridine orange core fluorophore using haloalkanes [27], alkyl triflates ([28, 29] or 1,3-propane sultone [26, 30]. 1,3-Propane sultone is an attractive option because it is inexpensive and readily available. Wolfbeis and Urbano reported the use of 1,3-propane sultone to quaternarize the heterocyclic nitrogen atom of acridine orange in a solventless reaction system. The reaction was done with 2 equivalents of the sultone, between 110 and 120 °C, for 1 hour, resulting in a yield of 60% [26]. Adamczyk and others reported the use of propane sultone to make sulfopropylated chemiluminescent acridine-based labels using a 10-fold excess of the sultone at 125 °C for 5 hours [29]. Adamczyk and Rege later employed less harsh conditions by conducting the reaction in a microwave reactor. They obtained a yield of 68% for acridine orange as substrate for a reaction time of only 15 seconds [30].

The sulfonate produced after the reaction of acridine orange with 1,3-propane sultone can then be activated and coupled with an amino acid to extend the tether. The ensuing carboxylic acid can in turn be activated as a NHS ester to form the amine-reactive group of the fluorescent label thus forming the complete fluorescent labeling reagent.

2.1.2 Materials and Methods

Acridine orange (AO) as a hemi(zinc chloride) salt, 1,3-propane sultone, oxalyl chloride, morpholine, 6-aminocaproic acid, N-hydroxysuccinimide (NHS) and N,N'-dicyclohexylcarbodiimide (DCC) were purchased from Sigma-Aldrich Corporation. Free base acridine orange was used in the synthesis and was obtained by treating the hemi(zinc chloride) salt with aqueous sodium hydroxide and EDTA and extracting it into dichloromethane. 6-Aminocaproic acid, which was used as part of the fluorophore tether, was first refluxed in methanol with a catalytic amount of hydrochloric acid to obtain the methyl ester.

The reactions were monitored by capillary electrophoresis (CE) either with photodiode array (PDA) or LIF detection using a Beckman PA800 system. Fifty micron I.D., 360 μm O.D. bare fused silica capillaries having total and inlet-to-detector lengths of 30.2 and 20.0 cm, respectively, were used. The quaternarization reactions were monitored using pressure mediated capillary electrophoresis (PreMCE) [31] having the following run details: $t_{\text{inj}} = 3$ s, $t_{\text{trans}} = 120$ s, $t_{\text{migr}} = 1$ min, $U_{\text{appl}} = 15$ kV, negative to positive polarity. The background electrolyte (BGE) was a mixture of 8 parts 20 mM chloroacetic acid adjusted to pH 2.7 with lithium hydroxide in water and 2 parts dimethylsulfoxide (DMSO). The reaction mixtures obtained during extension of the fluorophore tether and NHS-activation of the carboxylic acid were analyzed by conventional CE at 30 kV, positive to negative polarity. The BGE was a mixture of 2

parts 20 mM acetic acid adjusted to pH 4.7 with lithium hydroxide in water and 1 part formamide.

2.1.2.1. Synthesis of Sulfopropylated Acridine Orange **6**

Method C:

80 g (655 mmol) of 1,3-propane sultone was heated to 100 °C and mixed with 19.5 g (73.5 mmol) of free base acridine orange while stirred with a mechanical stirrer. After 45 minutes, 300 mL of N,N-dimethylformamide (DMF) was added with vigorous stirring. Heating was turned off after 15 minutes and the mixture was stirred at room temperature overnight. The resulting slurry was then mixed with 300 mL acetone and filtered. The solid was digested in 100 mL DMF at 110 °C for 2 hours and was carefully added to 1.5 L of a 70:30 mixture of hot acetone : TEA while stirring. This was allowed to cool with stirring in a water bath and was filtered. The DMF digestion and acetone/TEA precipitation was repeated (18 g, 63% yield). The reaction and the workup were monitored by conventional CE.

Method D:

0.418 g (1.6 mmol) free base acridine orange was added to 2.5 mL methyl isobutyl ketone (MIBK) and heated to 80 °C in a 100 mL round bottom flask with an attached water cooled condenser. 0.234 g (1.9 mmol) 1,3-propane sultone was then added to the reaction mixture after which the temperature was raised to 125 °C. Once in every 15 minutes, solids sticking to the wall of the flask were scraped off and placed back into the

bulk reaction mixture. Heating was stopped after 1 hour and the reaction mixture was analyzed by conventional CE.

2.1.2.2. Recrystallization of Sulfopropylated Acridine Orange **6**

85 grams of **6** from multiple reaction batches and 1.2 L formamide were combined in a 2-L round bottom flask with an attached mechanical stirrer. The flask was placed in an oil bath and the temperature of the slurry was raised to 140 °C to dissolve all the solids and allowed to stay at this temperature for 15 more minutes. Stirring was stopped and the mixture was allowed to cool slowly by controlling the rate of decrease of the temperature at about 0.5 °/ min. The mixture was allowed to stand at room temperature overnight. The solids were filtered out and slurried in 150 mL formamide and filtered again. The formamide recrystallization was repeated two more times.

2.1.2.3. Synthesis of Sulfonyl Chloride **7**

3.0 g (7.7 mmol) of sulfopropylated acridine orange **6**, 90 mL of dichloromethane and 24 µL of DMF were mixed and sonicated for about 10 minutes. While stirring in an ice bath, a 3.5 mL (approximately 13 mmol) portion of oxalyl chloride was added slowly to it. After addition, the reaction mixture was refluxed until CE analysis showed that chlorination did not proceed further. Chlorination was completed in 2 hours. The reaction mixture was mixed with 300 mL hexanes and 300 mL benzene, stirred and allowed to settle. The supernatant was decanted and the hexanes/benzene digestion was repeated. The solids (**7**) were used immediately in the next step.

2.1.2.4. Synthesis of Sulfonamide **8**

A mixture of 2.7 g (14.9 mmol) methyl-6-aminohexanoate, 85 mL DMF and 8.5 mL (61 mmol) triethylamine was quickly added to sulfonyl chloride **7**. Sulfonamide formation was monitored by CE which showed that conversion ceased to progress after 50 minutes at room temperature. The reaction mixture was then mixed with 250 mL ethyl acetate to precipitate the desired sulfonamide.

2.1.2.5. Synthesis of Acridine Orange Carboxylic Acid **9**

Sulfonamide **8** from the previous step was added into 100 mL of 1M HCl. The mixture was heated to 100 °C for 4 hours, cooled in an ice bath and filtered. The brick red solids were recrystallized by heating them in 100 mL 1M HCl at 100 °C and cooling again using an ice bath. The solids were then filtered and dried in a vacuum oven (2.4 g, 58% yield for 3 steps).

2.1.2.6. Synthesis of Acridine Orange N-Hydroxysuccinimidyl Ester **10**

2.4 g of carboxylic acid **9** was added to 120 mL DMF, 0.78 g (6.8 mmol) NHS and 1.48 g (7.2 mmol) DCC. The mixture was heated at 65 °C for 12 hours. 240 mL of petroleum ether and 120 mL acetone were then added to precipitate the desired compound. The slurry was centrifuged and the supernatant decanted. The remaining solid was digested twice in 120 mL of a 1:1 mixture of acetone : methyl ethyl ketone and filtered (2.8 g, 98%).

2.1.3 Results and Discussion

The synthesis of the amine-reactive acridine orange-based fluorescent label started with the quaternarization of the heterocyclic nitrogen atom using 1,3-propane sultone. The next step was the conversion of the sulfonate group to the sulfonyl chloride group. The product of this step was then coupled with methyl-6-aminocaproate and the methyl ester subsequently hydrolyzed to extend the tether. The final step was the activation of the carboxylate group as an NHS ester to make the amine-reactive component of the fluorescent label.

2.1.3.1 Quaternarization of Acridine Orange

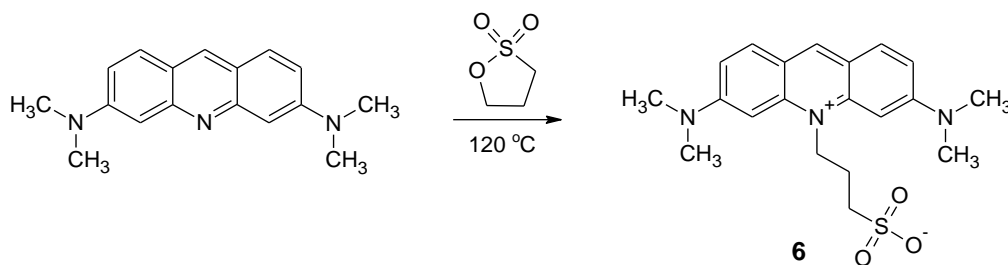


Figure 2.4. Quaternarization of acridine orange to form zwitterion **6**.

Quaternarization of acridine orange using 1,3-propane sultone to make acridine orange propylsulfonate **6** (Figure 2.4) was first attempted using the microwave method (method A) described by Adamczyk and Rege [30]. The reaction under microwave irradiation produced a lower conversion than what was published and an increase in the reaction time produced a considerable amount of unknown byproducts. The method reported by Wolfbeis and Urbano[26] was also tried where equal weights of both reagents (2.5

equivalents of the sultone) were reacted at 120 °C (method B). The reaction mixture was heterogeneous and was very difficult to stir even with a mechanical stirrer. Although conversion was good (64%), the reaction was difficult to implement at scales higher than 3 grams because of the high viscosity of the melt. The byproduct was only about 2% which is considerably less than in the microwave method. To achieve homogeneity, the next reactions were done with 10 equivalents of the sultone (method C) [29]. This resulted in a similar conversion as the previous method but had lower amounts of reaction byproducts. The reactions were monitored by PreMCE in the negative-inlet, positive-outlet polarity mode. An electropherogram of a sample taken at the end of the reaction using method C is shown in Figure 2.5. The purity of the product based on the relative peak areas is about 60% and the peak area of the anionic byproduct is less than 1%. About 85 grams of zwitterion **6** was synthesized in multiple 20-gram batches.

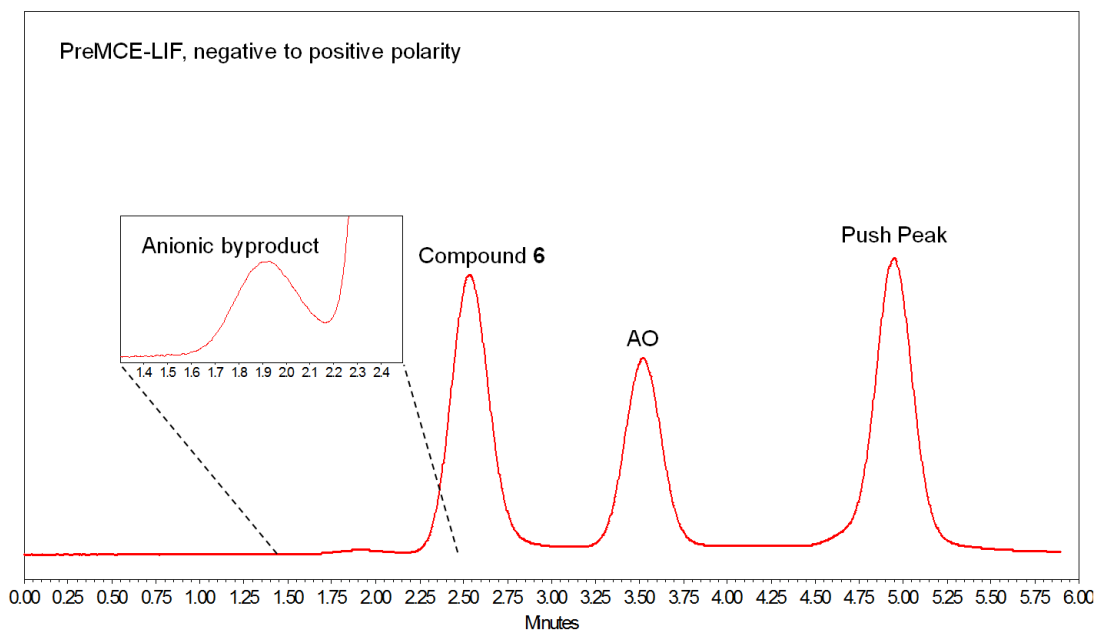


Figure 2.5. PreMCE-LIF analysis of a reaction mixture obtained by Method C showing leftover acridine orange (AO), the desired product (compound **6**) and an unknown anionic byproduct.

To address the problem caused by the large excess of sultone used in the quaternarization step, a new quaternarization method was also developed (method D). Methyl isobutyl ketone (MIBK), whose boiling point is at the temperature of the reaction, was used as a reaction solvent to dissolve acridine orange and 1.2 equivalent of propane sultone. In this system, the ionic product precipitated from MIBK, avoiding occlusion of any unreacted acridine orange, which is very probable in the solventless systems. The reaction had an 80 % conversion rate despite the smaller excess of propane sultone. A summary of the results for all of the above reaction methods is shown in Table 2.1.

Table 2.1. Summary of the results of different reactions used to quaternarize acridine orange.

Method	Conditions	Conversion	Remarks
A	20 eq. sultone 15 sec microwave irradiation 30 sec microwave irradiation	20% 38%	multiple byproducts (~ 40%)
B	2.5 eq. sultone, 120 °C, 1 h	64%	byproduct > 2% heterogeneous, very viscous
C	10 eq. sultone, 120 °C, 30 min	60 to 70%	byproduct < 1%
D	1.2 eq. sultone, S: MIBK, reflux, 1h	80%	byproduct < 1%

Workup first focused on the removal of most of the excess propane sultone and unreacted acridine orange by digestion in acetone and subsequently in a warm mixture of acetone and triethylamine. The use of triethylamine ensured full deprotonation of acridine orange making it more soluble in the organic solvents. This step increased the purity of zwitterion **6** from 60% to 90% after a series of digestions as determined by PreMCE. The solid was then recrystallized three times from formamide to remove the remaining impurities. Compound **6** crystallized out as brick red needles in the third crystallization step and had a purity of 99.5% by LIF-CE. Yields of up to 65% were attained. Figure 2.6 shows the PreMCE analysis of the material before and after a series of digestions and crystallizations: the total peak area of the impurities decreases to less than 1% as determined by CE using LIF detection.

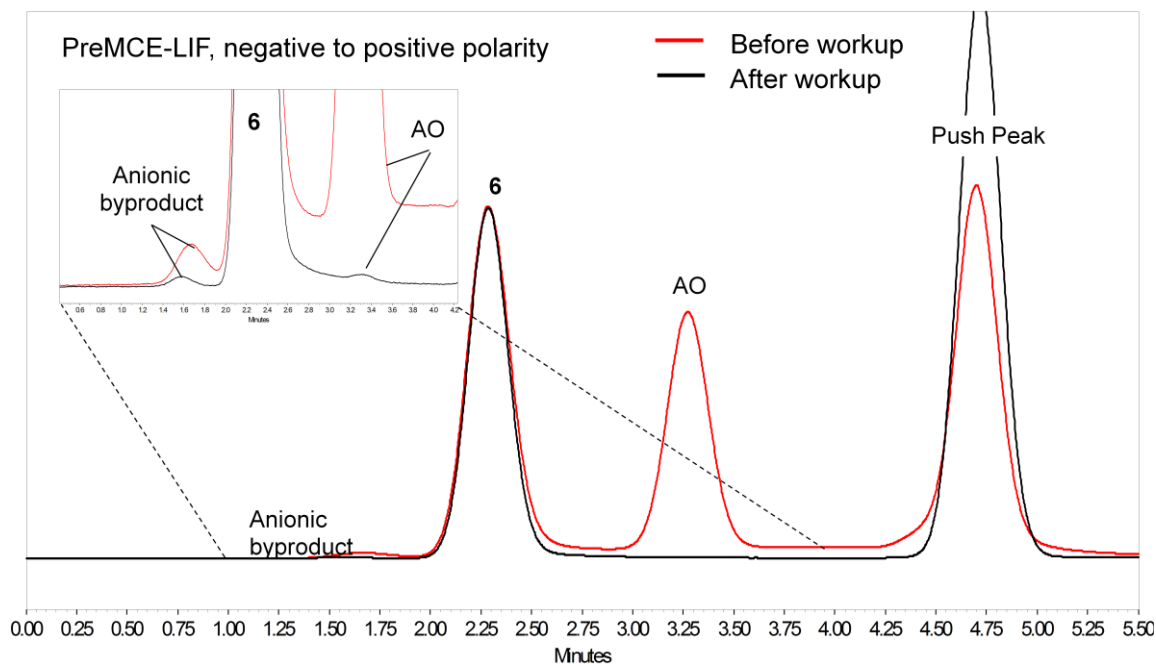


Figure 2.6. Compound **6** before and after workup consisting of digestions in acetone and recrystallizations from formamide.

The material is not appreciably soluble even in the more polar solvents used for NMR. In order to increase its solubility and obtain a better signal intensity in NMR, a hydrophobic strong acid, triflic acid, was added to the DMSO NMR sample to protonate the sulfonate group and have the triflate ion pair with the quaternary nitrogen atom. VT-NMR at a temperature of 110 °C was also used to improve dissolution. The ^1H -NMR spectrum shown in Figure 2.7 confirmed the structure of the compound. The single 9H peak shown in the inset indicates that the product is homogenous, that is, quaternarization occurred at a single location on the fluorophore. PreMCE runs, which show that the compound is neutral even at low pH, confirm that quaternarization occurred on the heterocyclic nitrogen atom.

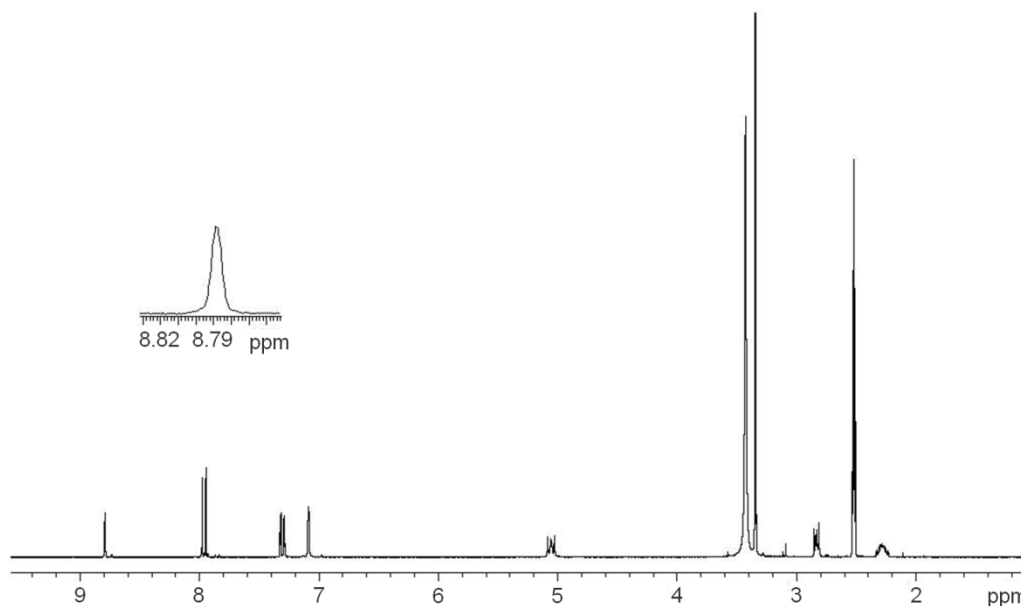


Figure 2.7. ^1H -NMR of compound **6** in d_6 -DMSO with 10% triflic acid.

2.1.3.2 Extension of the Tether

Compound **6** was refluxed with an excess of oxalyl chloride in dichloromethane with catalytic amounts of DMF to produce sulfonyl chloride derivative **7** (Figure 2.8). The reaction mixture was heterogeneous because compound **6** was not soluble in any of the solvents compatible with oxalyl chloride. In spite of this, the reaction proceeded very well and went above 90% completion as determined by CE. Sulfonyl chloride **7** was not directly analyzed because it was not stable in the aqueous background electrolyte solution. To go around this problem each sample containing sulfonyl chloride **7** was quantitatively reacted with an excess amount of morpholine to form stable sulfonamide derivative **11** prior to each CE analysis (Figure 2.9). The chlorination reaction did not

proceed any further after 40 minutes of reaction time. Analysis of a sample taken at the end of the chlorination reaction as shown in Figure 2.10 gives a conversion of 93%.

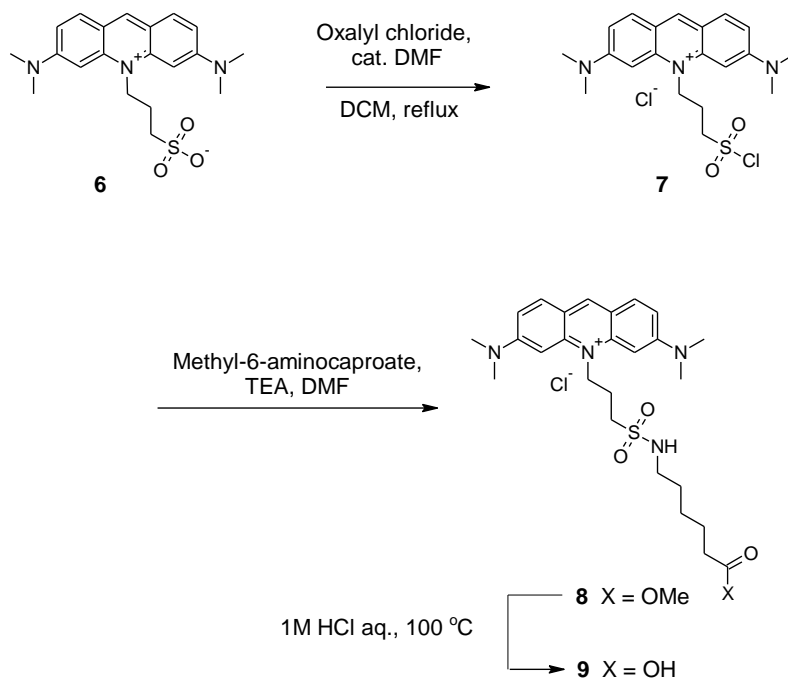


Figure 2.8. Extension of the tether of the fluorescent label.

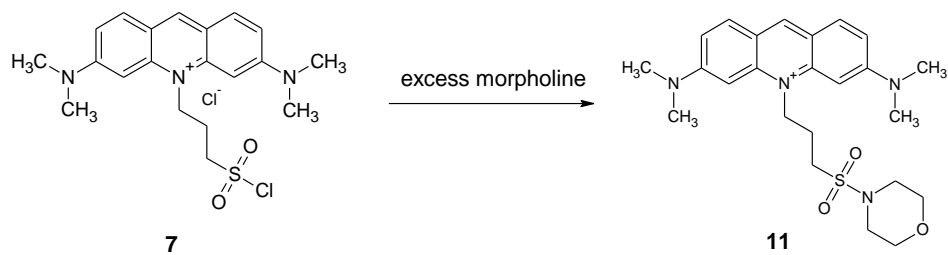


Figure 2.9. Quantitative conversion of sulfonyl chloride **7** to stable sulfonamide **11** prior to CE analysis.

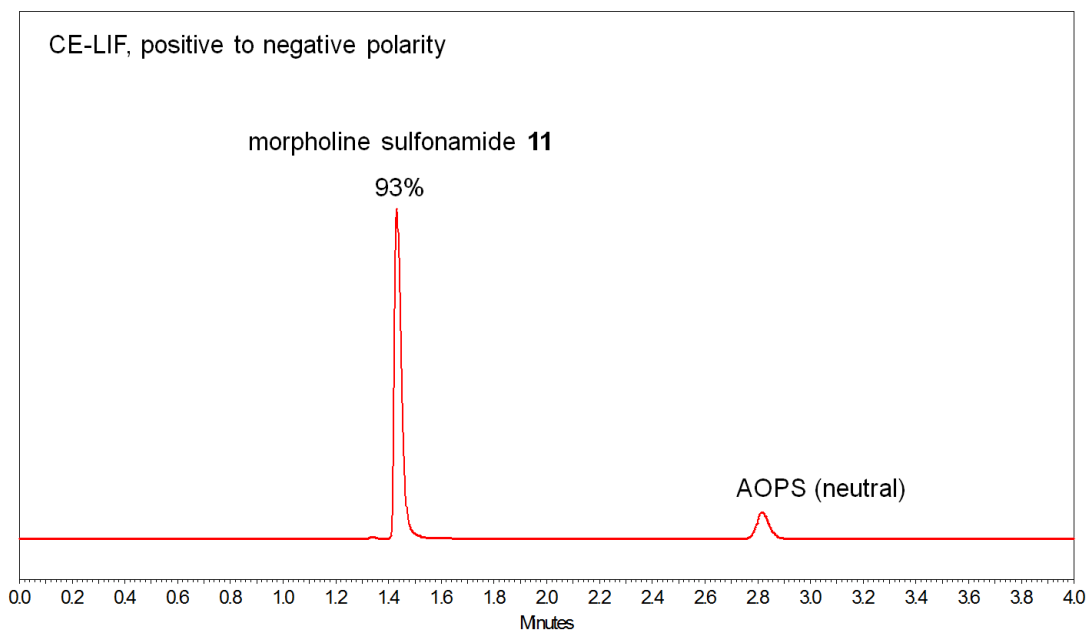


Figure 2.10. CE analysis of a 40-minute sample of the chlorination reaction of sulfonate **6**. The desired sulfonyl chloride product **7** was quantitatively coupled to morpholine to form sulfonamide **11** prior to CE analysis.

Conjugation of sulfonylchloride **7** with methyl-6-aminocaproate to form the full length of the tether was done in DMF in the presence of TEA. The reaction is rapid and goes to 83% conversion in less than an hour. The methyl ester was then hydrolyzed to the carboxylic acid under acidic conditions (1M HCl in water). Basic hydrolysis in this step was avoided to prevent the irreversible formation of a byproduct due to an attack of hydroxide ion on the 9 position of quaternarized acridine orange **6** [26]. Hydrolysis went smoothly achieving completion in 4 hours. The product was recrystallized from 1M aqueous HCl giving a yield of 58% for the tether extension steps. Figure 2.11 shows the CE-LIF analysis of the product for each step of the tether extension process. The

effective mobilities, μ_{eff} are consistent with what is expected of each of the species based on their molecular weights and their charge states in the background electrolyte.

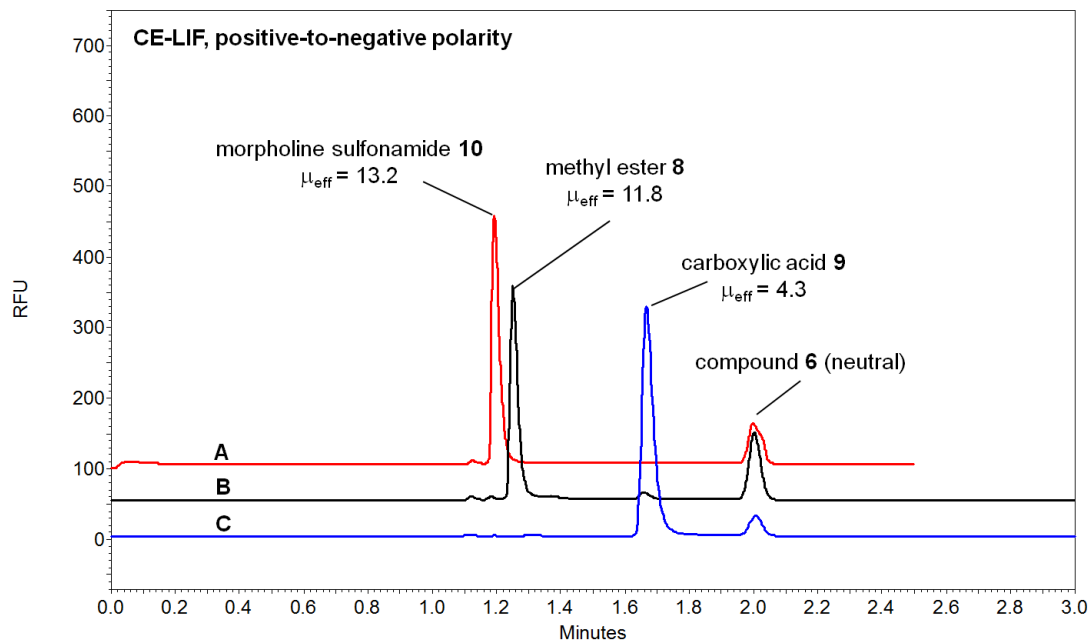


Figure 2.11. CE-LIF analysis of (A) morpholine sulfonamide **11**, which is indicative of the starting material sulfonylchloride **7**, (B) coupling of **7** with methyl-6-aminocaproate and (C) hydrolysis of methyl ester **8** to carboxylic acid **9**. μ_{eff} values are expressed in $10^{-5} \text{ cm}^2/\text{Vs}$ units.

2.1.3.3 Activation of the Carboxylate to the Amine-reactive Group

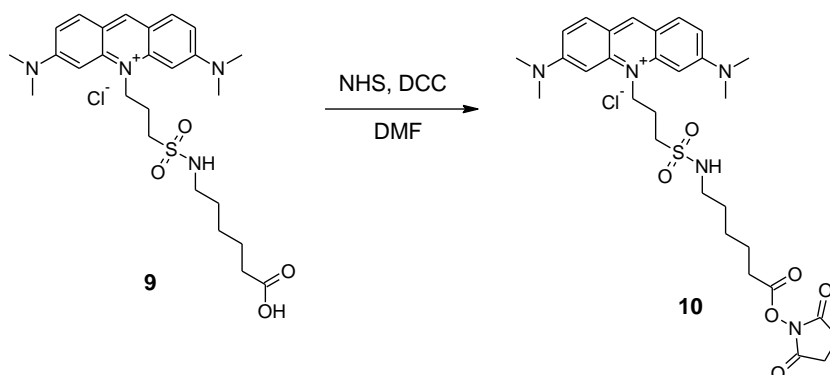


Figure 2.12. Activation of carboxylate **9** to NHS ester **10**.

The carboxylic acid was then heated to 55 °C with NHS and N,N'-dicyclohexylcarbodiimide (DCC) in DMF for 3 hours to form the amine-reactive NHS ester (Figure 2.12). The material partially crystallized out from the reaction solvent and was completely precipitated using methyl tert-butyl ether (MTBE). The solids were redissolved and repeatedly precipitated using methyl ethyl ketone giving a yield of 98%. The material was used as-is as an amine-reactive fluorescent labeling reagent. Figure 2.13 shows the electropherograms of the fluorophore before and after activation with NHS. NHS ester **10** has a CE-LIF purity of 94% with **6** and **9** as contaminants. The increase of μ_{eff} corroborates the loss of the negative charge of the carboxylate group while the addition of mass from the NHS group gives it an μ_{eff} that is lower than that of ester **8**.

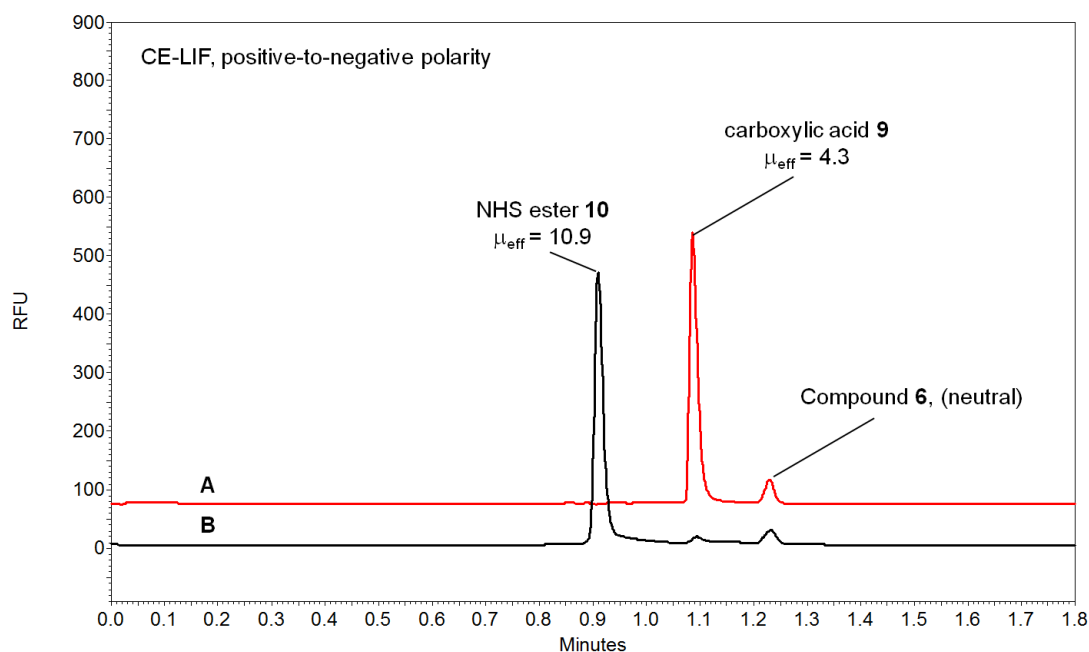


Figure 2.13. CE-LIF analysis of the activation of carboxylic acid **9** (A) to NHS ester **10** (B). μ_{eff} values are expressed in $10^{-5} \text{ cm}^2/\text{Vs}$ units.

2.1.3.4 Water Solubility and Hydrophilicity

An ethanamine conjugate of acridine orange-based fluorescent label **10** has a calculated $\log D_{\text{pH } 7}$ value of 1.1 indicating that **10** is 4 orders of magnitude less hydrophobic than the comparable fluorescent label, Cy3. However, the fluorescent label still has a limited solubility in water, comparable to that of rhodamine at approximately 5 g per 100 mL. In capillary zone electrophoresis, when using purely aqueous buffers, conjugates of label **10** with small molecules have tailing peak shapes which indicate hydrophobic interactions with the wall of the bare fused silica capillary. This problem was mitigated by using hydroorganic buffer solutions. The PreMCE and CE separations

of acridine orange and its derivatives shown above and in the next sections were run in background electrolyte solutions that contained up to 35% of either DMSO or formamide. Labeling of proteins using **10** at high tag to protein ratios also resulted in protein aggregation. It is clear that the hydrophilicity of the core fluorophore still needs to be further improved in order to attain better separation efficiencies in pure aqueous background electrolytes and also minimize the possibility of labeling-induced protein aggregation.

2.2 Spectral Properties

2.2.1 Background and Objectives

Fluorescent label **10** was based on the acridine orange core fluorophore to take advantage of the latter's $\lambda_{\text{max}}^{\text{ex}}$ which is around 490 nm thus making it compatible with the 488 nm line of the argon ion laser. It is important to ascertain that quaternarization of the fluorophore does not significantly shift $\lambda_{\text{max}}^{\text{ex}}$ nor does it adversely affect its fluorescence properties. It is also necessary for the derivatized fluorophore to have pH-independent fluorescence properties for it to be effective in CE and cIEF. When applied in cIEF separations, the fluorescent label is subject to relatively high concentrations of carrier ampholytes and electroosmotic flow (EOF) suppressing polymers (*e.g.*, methylcellulose). Matrix effects from these components of the cIEF system that may be detrimental to the fluorescence of the label must be determined.

2.2.2 Materials and Methods

The Pharmalyte and Servalyte carrier ampholyte fractions were purchased from Amersham Biosciences and Sigma Aldrich, respectively.

Fluorescence spectra at different pH values were taken using an Aminco Bowman Series 2 Luminescence Spectrometer. UV absorbance and fluorescence spectra for quantum yield determinations were acquired using a Varian 100 Bio UV-Vis spectrophotometer and a Varian Cary Eclipse fluorescence spectrophotometer, respectively.

2.2.3 Results and Discussion

Quaternarization of acridine orange to compound **6** did not significantly shift λ_{\max}^{ex} .

Acridine orange has its λ_{\max}^{ex} approximately at 493 nm, fluorophore **6** has it at 498 nm as shown in the UV absorbance spectra in Figure 2.14 which were taken using the photodiode array (PDA) detector of the PA 800. Excitation at 488 nm still can utilize approximately 90% of the maximum absorbance of **6**.

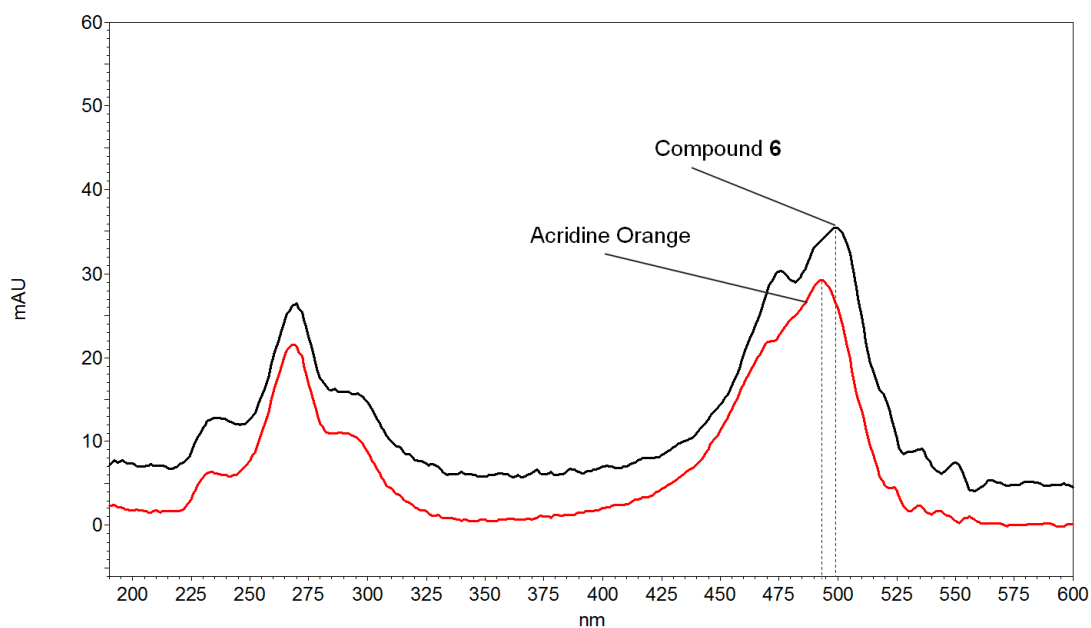


Figure 2.14. UV absorbance spectra of acridine orange and its quaternarized derivative, **6**.

The fluorescence emission spectra of fluorophore **6** were taken in aqueous solutions of different pH values. As shown in Figure 2.15, fluorescence did not change with pH indicating that the weakly basic dimethylamino functionalities of acridine orange do not change their ionization states in this pH range. This means that the fluorescent label can be used in background electrolytes of different pH values and suggests that the fluorophore is indeed suitable for use in cIEF separations.

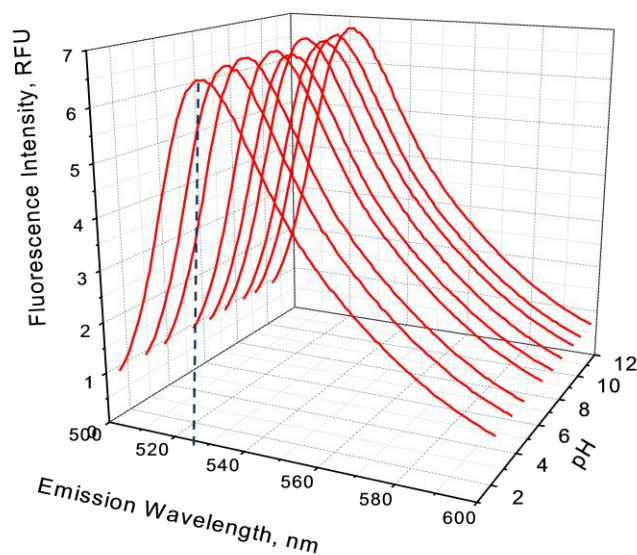


Figure 2.15. Fluorescence emission spectra of compound **6** in different aqueous buffers from pH 2 to 11.

In cIEF separations, different carrier ampholyte species in different regions of the pH gradient may have disparate matrix effects on the fluorescence of the core fluorophore. In order to investigate this possibility, the fluorescence emission intensity of fluorophore **6** was measured in different carrier ampholyte fractions having different narrow pH ranges. The fractions had pH ranges that spanned the entire operating pH range of cIEF. The fluorophore was dissolved at the same concentration in each of the carrier ampholyte fractions and their fluorescence signals as shown in Figure 2.16 were recorded using a CE-LIF system. The fluorescence intensity was practically the same for all of the samples except for the pH 9 to 11 fraction. This fraction contained Servalyte carrier ampholytes while the others had Pharmalyte carrier ampholytes

suggesting that carrier ampholytes from different manufacturers may either have different matrix effects on the fluorophore, have significantly different refractive indices or may have different levels of background fluorescence. Nevertheless, the fluorescence intensity of compound **6** in the different CA fractions produced by the same manufacturer is similar and does not prevent good quantitation.

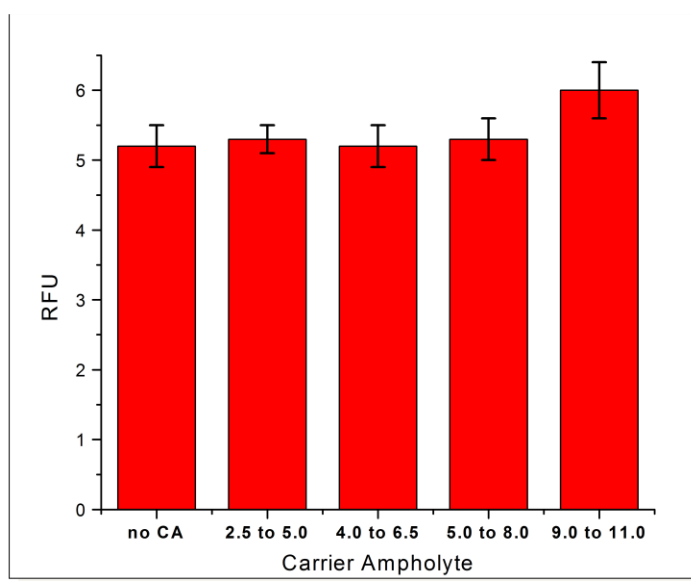


Figure 2.16. Fluorescence intensities of fluorophore **6** in carrier ampholyte fractions of different pH ranges. The signals were taken using a Beckman PA800 with a LIF detection system (488 nm excitation, 520 nm detection).

The absorbance and fluorescence emission spectra at different concentrations of Rhodamine 6G and carboxylic acid **9** were recorded as shown in Figure 2.17. The fluorescence emissions of both fluorophores were integrated and plotted against their respective absorbances (Figure 2.18). After ensuring that there was good linearity for

both plots, the slopes, S , were determined and used to calculate the relative fluorescence quantum yield, Φ_x , of carboxylic acid **9** with Rhodamine 6G as the standard. Φ_x was calculated using the following equation:

$$\Phi_x = \Phi_{st} \frac{S_x}{S_{st}} \left(\frac{\eta_x}{\eta_{st}} \right)^2 \quad (2.1)$$

where η is the refractive index of the solution. Subscripts x and st refer to the test and the standard fluorophore, respectively [32]. Φ_x of carboxylic acid **9** is 0.16 in a pH 9.0 0.1M aqueous sodium bicarbonate solution.

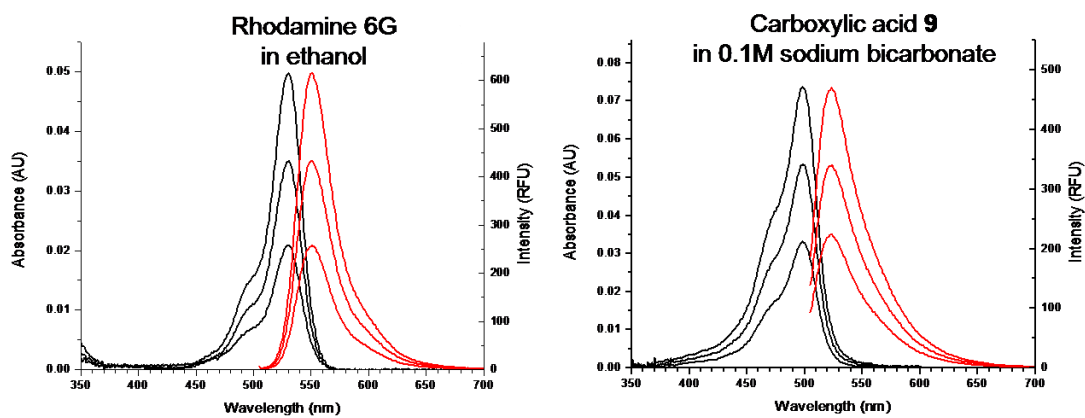


Figure 2.17. Absorbance and fluorescence emission spectra at different concentrations of Rhodamine 6G and carboxylic acid **9**.

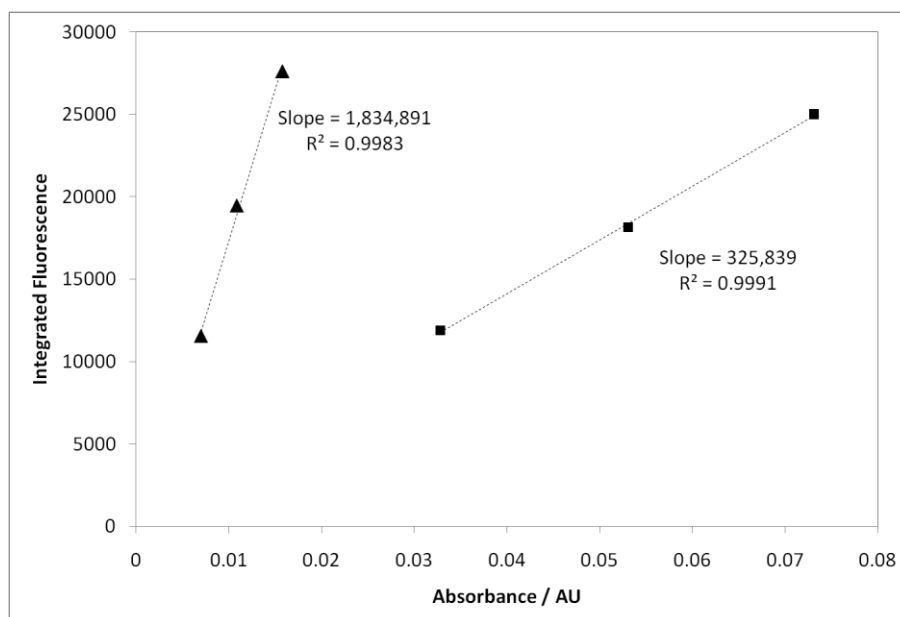


Figure 2.18. Plot of integrated fluorescence emission versus absorbance for Rhodamine 6G (▲) and carboxylic 9 (■).

2.3 Labeling Reactions Using the Acridine Orange-based Fluorescent Label

2.3.1 Background and Objectives

Most amino compounds are not fluorescent and are usually derivatized with a fluorescent label to allow their sensitive detection [33]. To test the applicability of the acridine orange-based fluorescent label for the analysis of small amines, 4-(2-aminoethyl)morpholine (AEM), 3-(diethylamino)propylamine (DEAPA) and the acidic amino acids aspartic acid (Asp), glutamic acid (Glu) and iminodiacetic acid (IDA) were labeled and analyzed by CE -LIF.

Model proteins were also derivatized and analyzed by SDS-CGE and cIEF. For cIEF, the effect of the decreased analyte loading – an anticipated beneficial consequence of LIF detection of the fluorescently labeled proteins – on the resolution of closely spaced isomers of the model protein was also determined.

cIEF pI markers are necessary to calibrate the pH gradient along the length of the separation capillary. There are numerous UV absorbing pI markers but only a few are available for fluorescence detection with 488 nm excitation. Fluorescent pI markers have been prepared by Shimura et al. by labeling commercially available peptides having defined pI values with 5-carboxytetramethylrhodamine [34, 35] but these markers are not commercially available. To allow the use of LIF detection in the cIEF analyses of acridine orange-labeled proteins, a facile strategy of synthesizing multiple pI markers had to be developed.

2.3.2 Materials and Methods

2.3.2.1 Labeling of Small Amines and Their Analysis by CE-LIF

Small amines were labeled in a pH 9, 0.1 M aqueous sodium bicarbonate buffer. A solution of the diamines and acidic amino acids were prepared in the labeling buffer at 10 mM and 5 mM concentrations, respectively. A solution of fluorescent label **10** in DMSO was also prepared at a concentration of 10 mg/mL (approximately 20 mM). A 10 μ L aliquot of the labeling reagent was added to 100 μ L of the test amine solution and

allowed to react for 1 hour. CE-LIF analyses were done at 3 minutes and 1 hour reaction times.

CE-LIF analyses of the labeled small amines were done using a Beckman PA800 CE unit with a 488 nm Argon ion laser detection system. A bare fused silica capillary having the following dimensions was used: 50 μm I.D., 360 μm O.D. and 30.2 cm / 20.0 cm total / inlet-to-detector lengths. The background electrolyte consisted of a mixture of 2 parts 20 mM acetic acid adjusted to pH 4.7 with lithium hydroxide in water and 1 part formamide. The separations were run with positive-to-negative polarity at 30 kV.

2.3.2.2 Protein Labeling and Their Analysis by SDS-CGE-LIF

A 100 μL aliquot of a 10 mg/mL solution of the test protein in pH 8.3 0.1 M aqueous sodium bicarbonate was mixed with 1 μL of a 1 mg/mL labeling reagent **10** solution in DMSO. The mixture was allowed to react for 1 hour at room temperature. An aliquot of the labeling reaction mixture was diluted 20 fold with the pH 8.3 0.1 M aqueous sodium bicarbonate buffer. An aliquot of this first diluted solution was further diluted 100 fold with the Beckman SDS-MW sample buffer. 5 μL of 2-mercaptoethanol was added to 100 μL of the twice-diluted labeled protein solution and the mixture was placed in a 100 $^{\circ}\text{C}$ water bath for 3 minutes. The reduced protein sample was then cooled to room temperature and analyzed by SDS-CGE.

SDS-CGE was carried out in a Beckman PA800 using a LIF detection system. The separation capillary was a bare fused silica capillary having the following dimensions: 50 μm I.D., 360 μm O.D. and 30.2 cm / 20.0 cm total / inlet-to-detector lengths. The capillary was preconditioned as recommended by Beckman for their SDS-MW analysis. Briefly, the capillary was rinsed with a 0.1 M aqueous sodium hydroxide solution at 50 psi for 5 min. This was followed by a 50 psi rinse with a 0.1 M aqueous hydrochloric acid solution for 2 min, then a 50 psi rinse with deionized water for 2 min. The capillary was then filled with the SDS-MW gel buffer solution at a pressure of 40 psi for 10 min. A 15.0 kV potential was applied (negative-to-positive polarity), with a ramp up time of 5 min and a 20 psi nitrogen blanket on both the inlet and outlet vials.

The SDS-CGE separation was performed by first introducing the protein sample by electrokinetic injection at 5.0 kV for 20 sec. Then the sample was separated by applying 15.0 kV with a 1 min ramp up time and 20 psi of pressure applied on both the inlet and outlet vials.

2.3.2.3 Synthesis of the Fluorescent pI Markers

The acridine orange-based pI markers were synthesized by reacting 4 equivalents of the amino acid with respect to fluorescent label **10** in DMF, in the presence of 20 equivalents of triethylamine. The reaction mixture was heated at 70 °C for 2 hours. The desired product was purified by HPLC.

pI markers based on 8-hydroxypyrene 1,3,6- trisulfonic acid (HPTS) were also made by first carefully mixing 1 g HPTS with 5 mL chlorosulfonic acid. The mixture was stirred at 75 °C for 2 hours. A 20 μ L aliquot of the reaction mixture was then added into 400 μ L of cold dichloromethane. The organic solution was then slowly added to 200 mg of ice in a 1 mL Eppendorf tube. After complete addition, the dichloromethane phase was dried with sodium sulfate and reacted with 20 equivalents of the diamine. The desired product was purified by HPLC.

2.3.2.4 Labeling of Chicken Ovalbumin and Its Analysis by SDS-CGE-LIF

Chicken ovalbumin was labeled in a pH 8.3 0.1 M aqueous sodium bicarbonate solution that also contained 3 M urea (labeling buffer). A 250 μ L aliquot of a 10 mg/mL solution of the protein in the labeling buffer was reacted with a 25 μ L portion of a 10 mg/mL solution of fluorescent label **10** in DMSO. The fluorophore-to-protein ratio was approximately 1 to 1. The labeling reaction was done at room temperature for 30 minutes. An aliquot of the labeled protein mixture was then diluted with the cIEF separation solution to get to the desired signal level. The cIEF separation solution consisted of 4 μ L of cIEF carrier ampholyte 3-10, 200 μ L of the cIEF gel, arginine (cathodic blocker) and iminodiacetic acid (IDA, anodic blocker), and the pI markers. The cIEF carrier ampholytes and the cIEF gel solution were provided by Beckman Coulter.

The separation capillary used had a neutral internal coating (Beckman Coulter). The dimensions of the capillary were 50 μm I.D., 360 μm O.D, 20 cm inlet-to-detector length and 30.2 cm total length. The capillary was prepared by rinsing it with a 10 mM phosphoric acid solution at 30 psi for 1 min, followed by a water rinse at 30 psi for 1 min. The capillary was then filled with the carrier ampholyte mixture at 30 psi for 1.5 min. The sample was loaded through the outlet end for 1 min at 2.0 psi. After loading the sample, the inlet and outlet ends of the capillary were immersed into the anolyte and catholyte solutions, respectively. The anolyte solution was a 200 mM phosphoric acid solution in cIEF gel, the catholyte was a 300 mM sodium hydroxide solution in deionized water. A potential of 25 kV was then applied for 6 min to carry out the focusing. After focusing, the contents of the capillary were mobilized through the detector by applying a pressure of 0.5 psi to the inlet vial while maintaining a potential of 21 kV.

2.3.3 Results and Discussion

2.3.3.1 Labeling of Small Amines

The small amines were labeled in a pH 9 0.1M aqueous sodium bicarbonate buffer at room temperature. Though labeling was almost complete after 3 minutes, the reaction mixture was allowed to stand for 1 hour. As expected, the products of the labeled diamines, AEM and DEAPA, migrate as cations that are faster than fluorescent label **10** as shown in Figure 2.19. The diamines were analyzed at a sample concentration of around 50 μM . The $\text{LOD}_{S/N=3}$ was calculated to be about 150 nM. For the acidic

amino acids, Asp, Glu and IDA (Figure 2.20), the labeled products migrated towards the anode. At the pH of the CE analysis the labeled species had a net negative charge, thus anionic mobilities. The loaded samples had a concentration of about 20 μM . The $\text{LOD}_{S/N=3}$ for labeled aspartic acid was around 50 nM.

Aside from the desired fluorescently labeled products, the labeling reactions also produced the hydrolyzed fluorescent label (*i.e.*, carboxylic acid **9**) and an unknown byproduct. There are also two contaminant peaks that are already present with the labeling reagent. The byproducts and contaminants, however, are the same for all labeling reactions and can, at least in principle, be anticipated and thus separated from the labeled analytes by careful design of the separation conditions.

β -Lactoglobulin, bovine serum albumin and immunoglobulin were labeled and analyzed by SDS-CGE with LIF detection after sample reduction with 2-mercaptoethanol. The electropherograms for each labeled protein are shown in Figure 2.21. Proteins were labeled at a low fluorophore-to-protein ratio to avoid (i) protein precipitation during the labeling reaction and (ii) peak broadening in the SDS-CGE analysis. The concentrations of the loaded protein samples in these SDS-CGE-LIF runs were one-to-two orders of magnitude lower than the recommended lower limits for the CE system used with UV detection. Despite the low sample loads the signal-to-noise ratio was very high. The $\text{LOD}_{S/N=3}$ was calculated to be in the low nanomolar (low $\mu\text{g/mL}$) range.

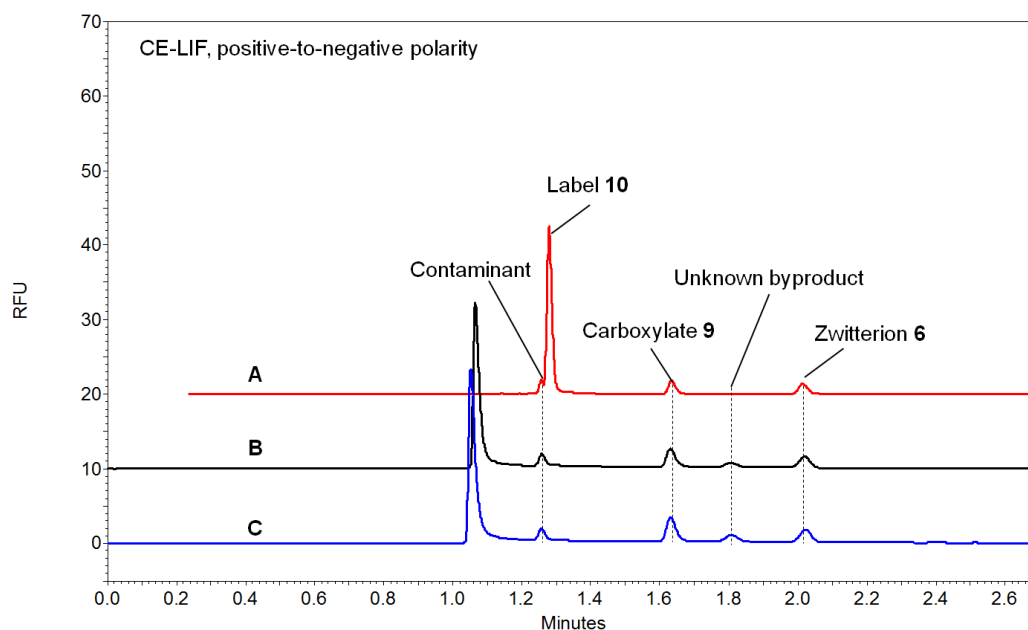


Figure 2.19. CE-LIF analysis of fluorescent labeling reagent **10** (A), labeled AEM (B) and labeled DEAPA (C).

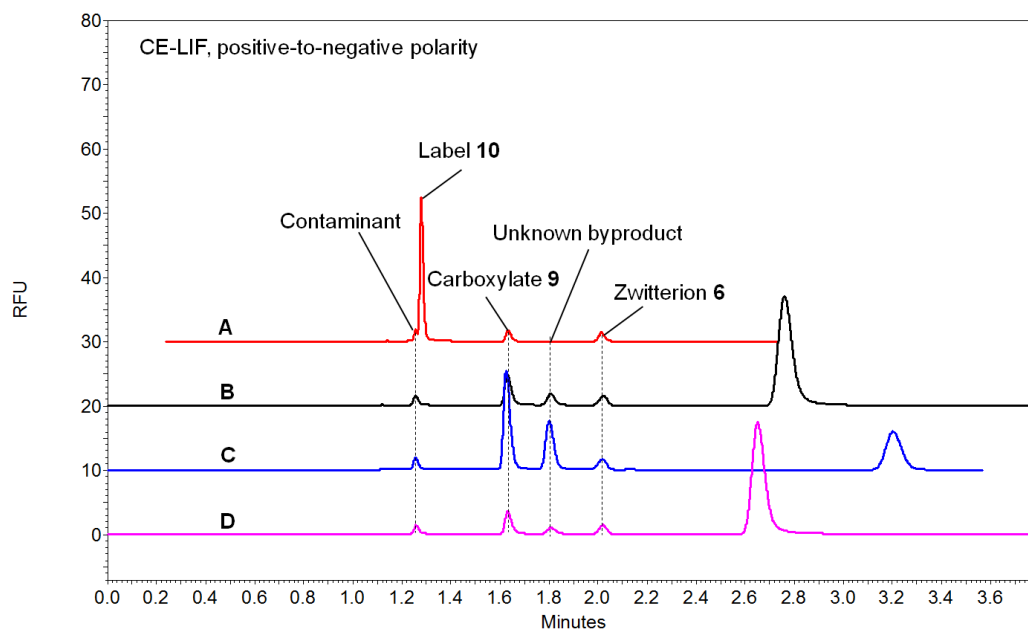


Figure 2.20. CE-LIF analysis of fluorescent labeling reagent **10** (A), labeled aspartic acid (B), labeled iminodiacetic acid (C) and labeled glutamic acid (D).

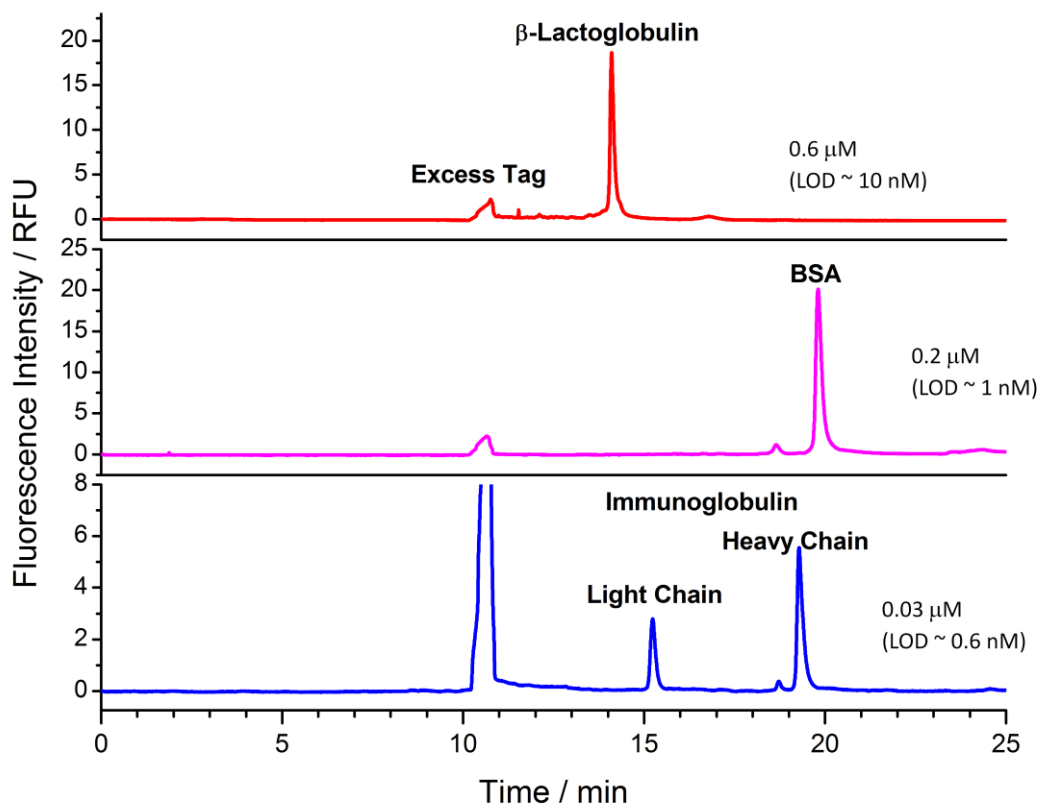


Figure 2.21. SDS-CGE analysis of labeled proteins using LIF detection.

2.3.3.2 Synthesis of Fluorescent pI Markers for cIEF-LIF

Two general synthetic schemes were developed for the synthesis of a ladder of pI markers. The markers have two main parts: (1) the titrating group, which also contains the fluorophore, and (2) the buffering group. Acridine orange-based fluorescent label **10** and 8-hydroxypyrene-1,3,6-trisulfonic acid (HPTS) were chosen as core fluorophores because of the presence of a positively charged quaternary nitrogen and a negatively charged phenolate group, respectively, which were used as the titrating groups in the

respective pI markers. These fluorophores were easily coupled to the corresponding buffering groups to make the complete pI marker. The synthetic schemes were designed to allow the use of different buffering species to produce pI markers with diverse pI values.

pI markers in the acidic pH region have been made using the acridine orange-based fluorescent label according to the scheme shown in Figure 2.22. Using this method, two pI markers have been synthesized: one from iminodiacetic acid (pI marker **12**), the other from aspartic acid (pI marker **13**). The buffering groups were chosen because by simulation their pI values were reasonably closely spaced in the acidic pH region (Figure 2.24). The pI values were simulated by plotting the calculated net charge of the molecule versus the pH using Equation 1.1 and determining the pH at which the net charge was equal to zero. The pK_a values used for the pI simulation of markers **12** and **13** are tabulated in Table 2.2.

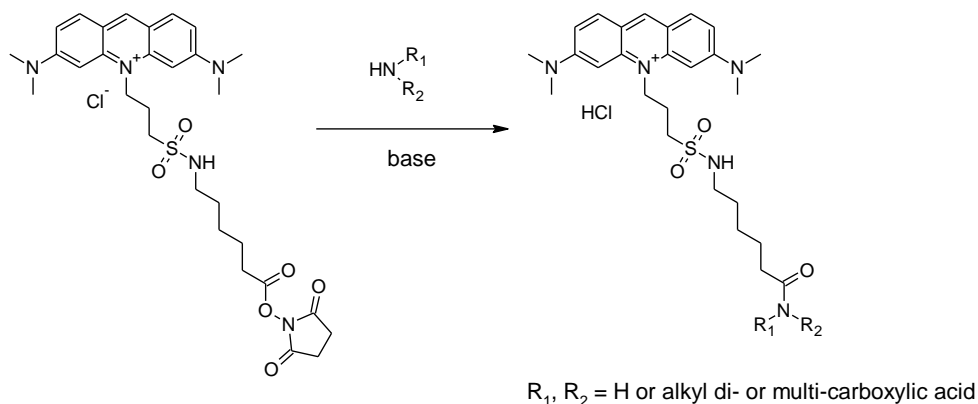


Figure 2.22. General scheme for the synthesis of acidic pI markers using the acridine orange-based core fluorophore as the titrating group.

Table 2.2. Calculated pK_a values of the buffering and titrating groups of pI markers **12** and **13**.

pI marker		pK _a values ^a
12		3.41, 4.29, 20 (quaternary nitrogen)
13		3.36, 4.97, 20 (quaternary nitrogen)

^a pK_a values were calculated using SPARC (SPARC Performs Automatic Reasoning in Chemistry) Online Calculator v4.5 [25].

For the neutral and basic pH region, HPTS was coupled to different diamines using the scheme shown in Figure 2.23. Simulation of the pI values of the pI markers derived from 4-(2-aminoethyl)morpholine (pI marker **14**), piperazine (pI marker **15**), N,N,N'-trimethylethylenediamine (pI marker **16**) and 3-(diethylamino)propylamine (pI marker

17) indicates that these diamines will produce pI markers with a well spaced ladder of pI values in the neutral and basic pH regions (Figure 2.24). Equation 1.1 was used to calculate the net charge of the pI markers as a function of pH using the pK_a values in Table 2.3. It is important to note that the calculated pK_a of the phenolate group of HPTS after attachment of the buffering groups is around 5. This means that the HPTS fluorophore will significantly lose fluorescence if subjected to a pH below 5 due to protonation of the phenolate group. pI markers derived from HPTS must therefore be designed to have pI values above this pH.

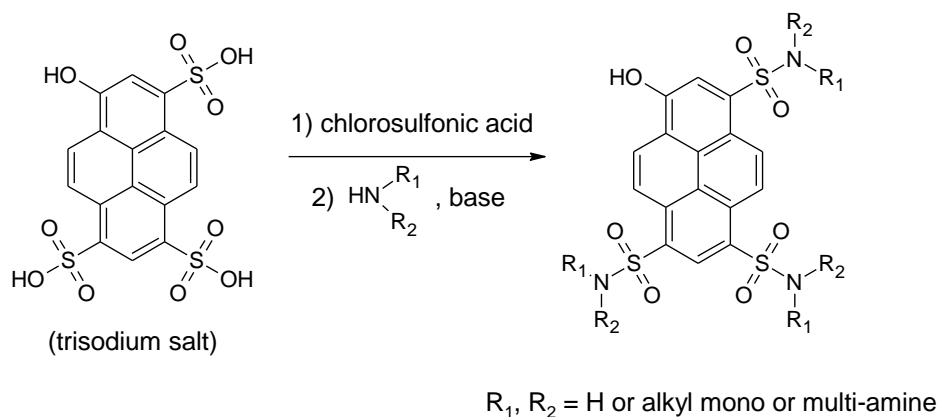
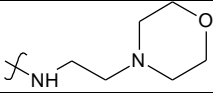
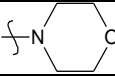
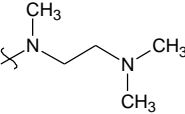
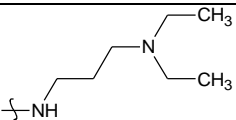


Figure 2.23. General scheme for the synthesis of basic pI markers based on HPTS as the core fluorophore and titrating group.

Table 2.3. Calculated pK_a values of the buffering and titrating groups of pI markers **14** to **17**.

pI marker		pK_a values ^a
14		4.91 (phenol), 6.36, 6.84, 7.32
15		4.59 (phenol), 7.85, 8.34, 8.83
16		4.93 (phenol), 8.93, 9.42, 9.90
17		5.03 (phenol), 9.13, 9.61, 10.09

^a pK_a values were calculated using SPARC (SPARC Performs Automatic Reasoning in Chemistry) Online Calculator v4.5 [25].

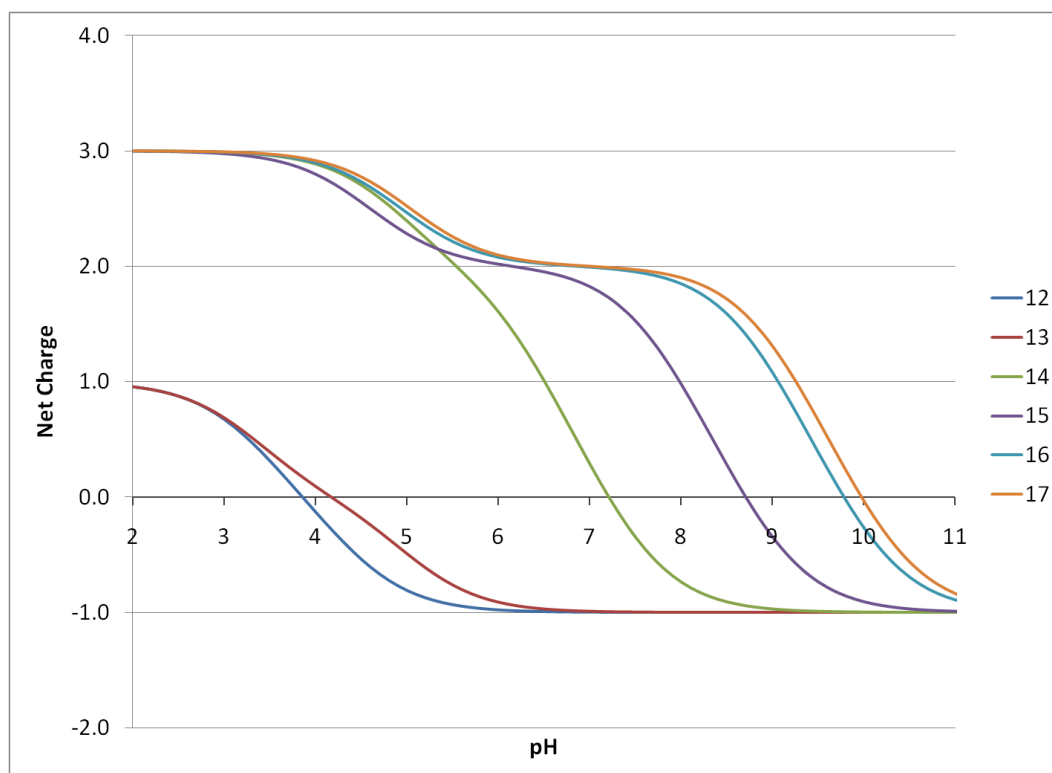


Figure 2.24. Simulated net charges of pI markers **12** to **17** as a function of pH. The simulated pI is the pH at which the net charge of the molecule is equal to zero. The pKa values in Tables 2 and 3 were used in Equation 1.1 to calculate the net charge.

The operational pI values of the markers were then determined by analyzing these in cIEF with UV detection using UV absorbing pI markers as calibrants. Figure 2.25a is the mobilization trace of a cIEF run of pI marker **13** with the calibrant pI markers. The pI values of the UV-absorbing pI markers were plotted against their migration times (Figure 2.25b) to determine the linearity of the pH gradient. The pH gradient in this case is linear because the Pearson R^2 value is very close to 1. The operational pI value of the new fluorescent pI marker can then be determined from its migration time. The

corresponding pI values of the other fluorescent pI markers were determined in a similar manner.

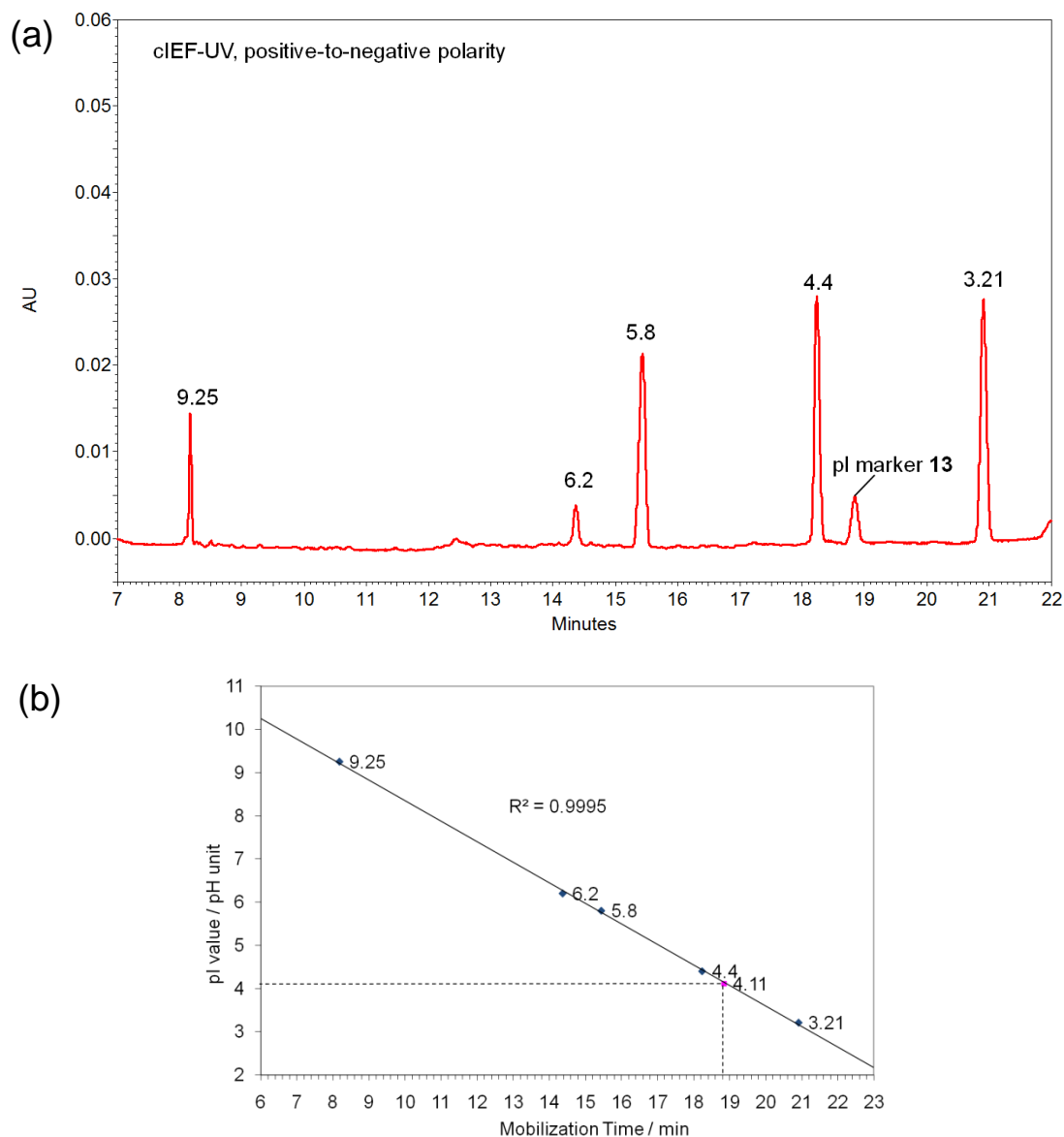


Figure 2.25. Determination of the operational pI value of pI marker **13**. (A) A portion of the mobilization trace of the cIEF-UV analysis of **13** with UV-absorbing pI markers of known pI values. (B) Plot of pI values of the UV-absorbing pI markers versus their migration times (◆) and determination of the operational pI value of **13** (■) based on its migration time.

A summary of the newly synthesized pI markers and their corresponding operational pI values are shown in Table 2.4

Three of the fluorescent pI markers were used in the cIEF analysis of the labeled model protein, chicken ovalbumin, in the next subsection. pI markers **12**, **13** and **16** were analyzed by cIEF with both UV and LIF detection and the mobilization traces of both detection methods were compared (Figure 2.26). The relative positions of the fluorescent pI markers are the same with both UV and LIF detection showing the utility of the markers for the calibration of the pH gradient in cIEF separations with LIF detection.

Table 2.4. Summary of the determined operational pI values of the synthesized fluorescent pI markers.

#	Core Fluorophore / Titrating Group	Buffering Group	Operational pI value
12	acridine orange	IDA	3.10 (n=3)
13	acridine orange	Asp	4.11 (n=3)
14	HPTS	AEM	6.38 (n=2)
15	HPTS	Piperazine	7.83 (n=2)
16	HPTS	TMEDA	8.72 (n=4)
17	HPTS	DEAPA	9.36 (n=2)

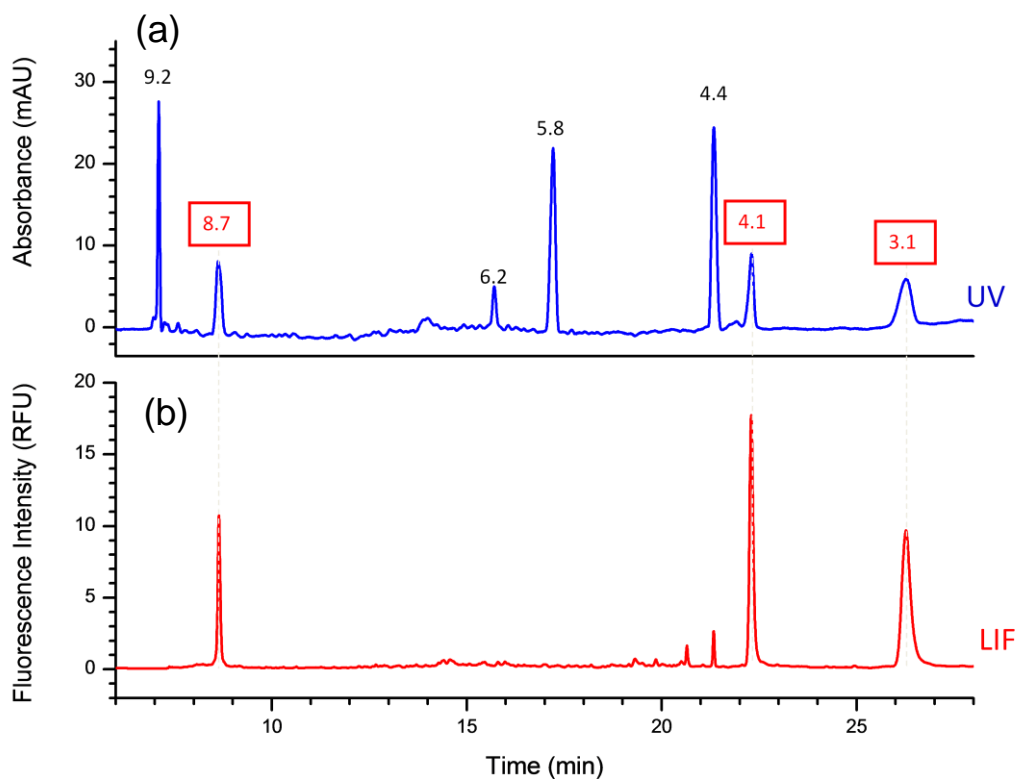


Figure 2.26. cIEF analysis of pI markers **12**, **13** and **16** with UV (a) and LIF (b) detection. The peaks with the pI values boxed in red are those of the new fluorescent pI markers. The rest of the peaks are those of the UV-absorbing markers.

2.3.3.3 cIEF Analysis of Labeled Chicken Ovalbumin

Chicken ovalbumin was labeled at a low fluorophore-to-protein ratio and analyzed by cIEF. The same set of fluorescent pI markers was used with both UV and LIF detection to allow consistent calibration of the pH gradient. Figure 2.27 is a comparison of the cIEF runs using UV detection of the unlabeled and labeled ovalbumin. This clearly shows that the isoform peak profiles are the same for both samples. This suggests that

derivatization using monocationic label **10** does not change noticeably the pI value of the isoforms of chicken ovalbumin.

The labeled chicken ovalbumin was then analyzed using both UV and LIF detection. The respective mobilization traces are shown in Figure 2.28. The peak groups in both traces appear in the same region of the pH gradient. However, detection by LIF produced more distinguishable peaks than detection by UV as shown in the inset. The more sensitive LIF detection allowed loading of a significantly lower sample amount and thus avoided the overloading of the isoforms in their respective focusing regions. This resulted in better resolution of each of the components of the ovalbumin sample. Moreover, the signal-to-noise ratio in the LIF detector trace is about five times better than in UV detector trace at the required sample loadings.

The reproducibility of the cIEF-LIF analysis and labeling of chicken ovalbumin was also investigated. Figure 2.29a is an overlay of three non-consecutive cIEF analysis runs of the same labeling reaction that shows that cIEF-LIF analysis of the labeled protein is indeed reproducible. The figure also shows that a pI difference of 0.05 pH unit can be easily resolved even with a wide range, pH 3 to 10 carrier ampholyte mixture. A narrower range of carrier ampholyte mixture may provide better resolution using LIF detection. Figure 2.29b is an overlay of the cIEF analyses of three separate labeling reactions done on three different days. The peak profiles in all three runs are almost the same demonstrating the reproducibility of the labeling reaction itself.

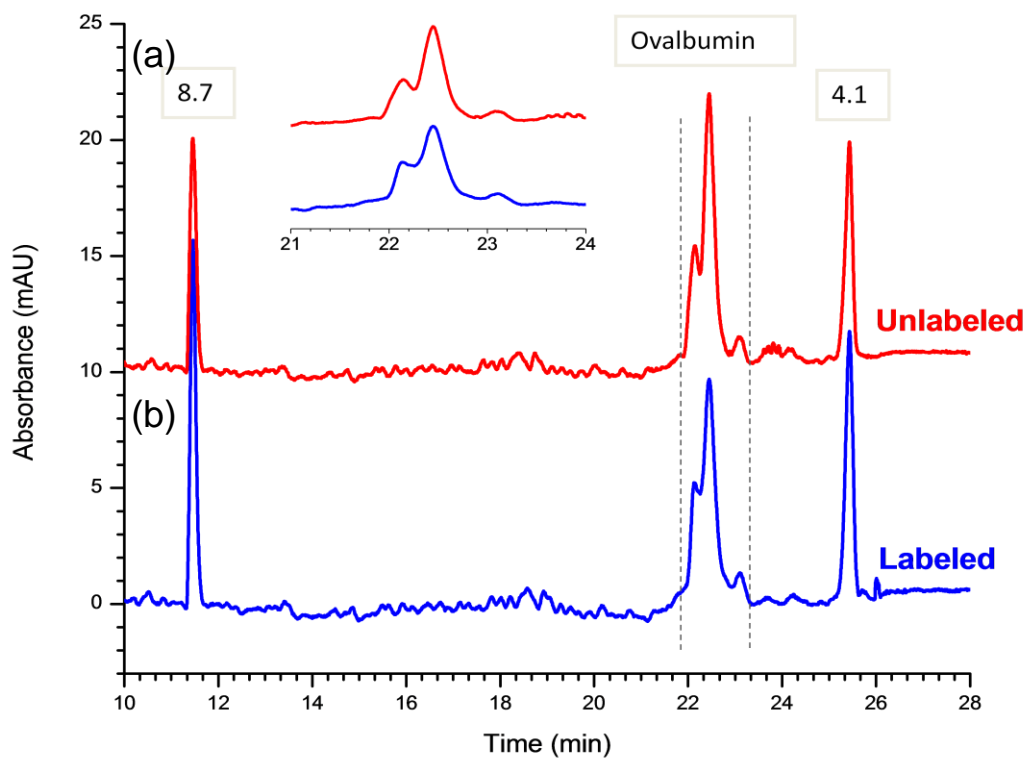


Figure 2.27. Mobilization traces obtained in the cIEF analysis of (a) unlabeled chicken ovalbumin and (b) labeled chicken ovalbumin.

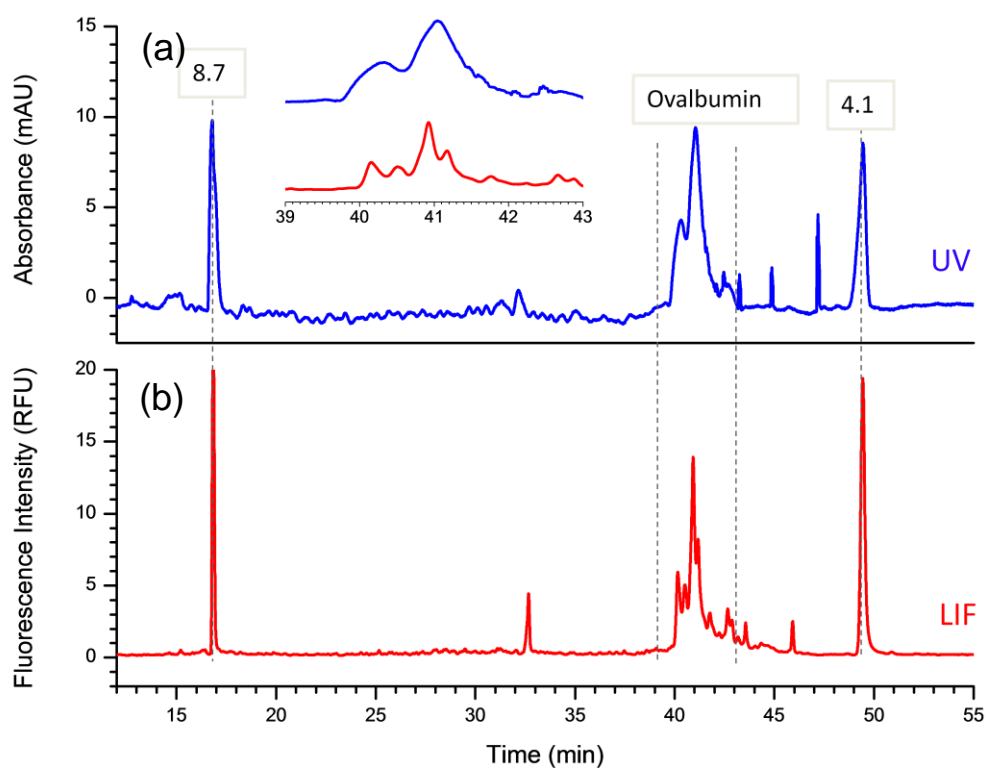


Figure 2.28. Mobilization traces obtained in the cIEF run of the labeled chicken ovalbumin using (a) UV detection and (b) LIF detection.

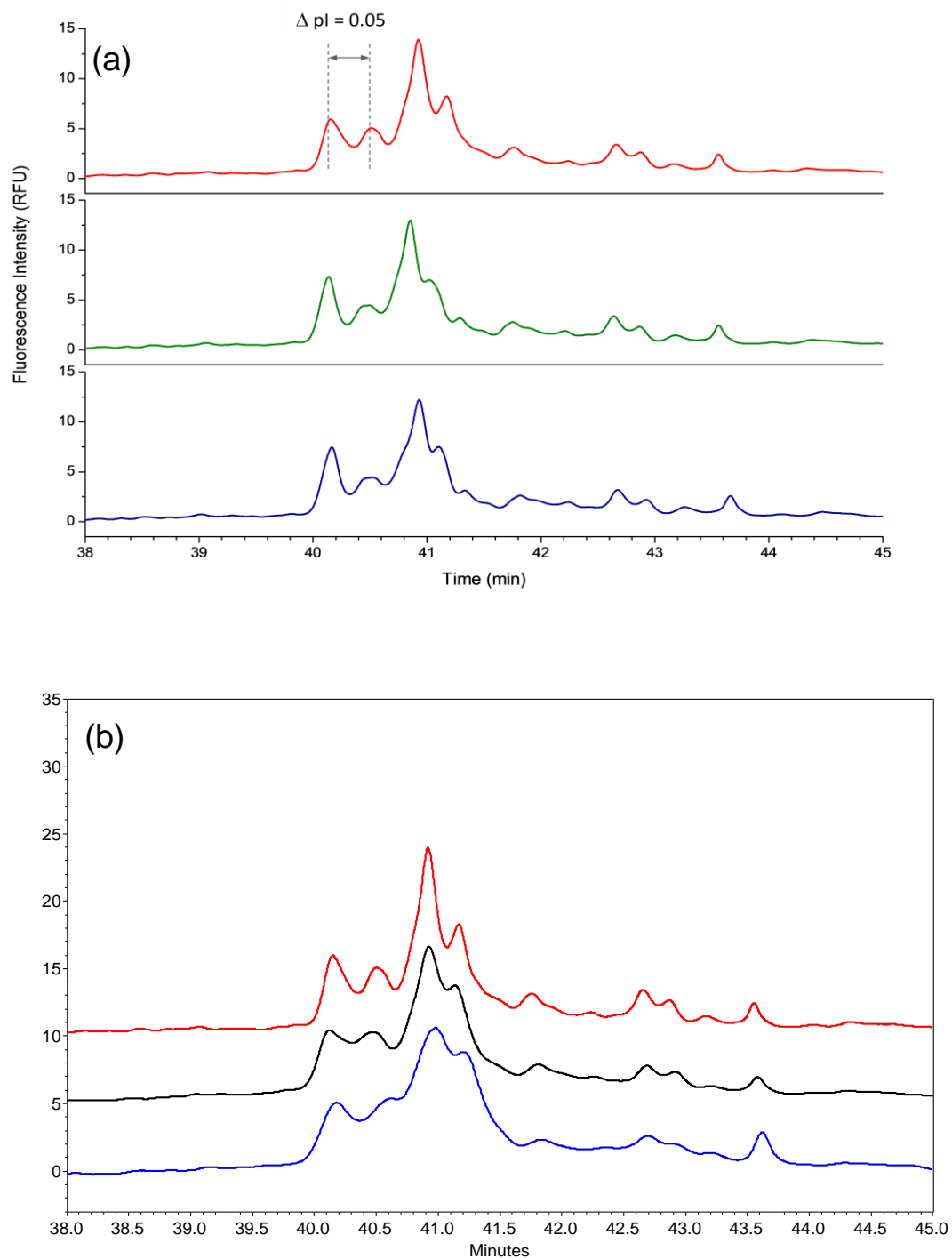


Figure 2.29. Reproducibility in (a) cIEF-LIF analysis of the same labeling reaction mixture and (b) cIEF-LIF analysis of different labeling reactions of the same chicken ovalbumin sample. The mobilization traces are normalized to the highest peak.

2.4 Concluding Remarks

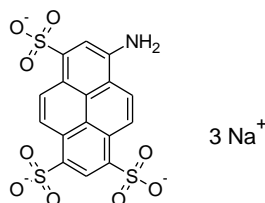
A new amine-reactive monocationic fluorescent labeling reagent based on acridine orange has been synthesized and characterized. Each step of the synthesis was effectively monitored and characterized by CE-LIF. The fluorescent label has a $\lambda_{\text{max}}^{\text{ex}}$ of 498 nm and has pH-independent fluorescent properties making it applicable in CE separations using background electrolytes with different pH values. The fluorophore is compatible with cIEF where the carrier ampholyte mixture does not have adverse matrix effects on its fluorescence. The fluorescent label was used to derivatize small amines and proteins which were then analyzed by CE. Labeled proteins were analyzed by SDS-CGE with an LOD in the low nanomolar (low $\mu\text{g/mL}$) range. The derivatization did not change the pI values of the model protein, chicken ovalbumin. cIEF analysis of the protein using LIF detection gave better resolution than UV detection: peaks with a ΔpI of about 0.05 could be resolved using a wide range, pH 3 to 10 carrier ampholyte mixture.

In order to get accurate results in the cIEF separations, a group of pI markers were synthesized using acridine orange-based label **10** and 8-hydroxypyrene-1,3,6-trisulfonic acid. Two synthetic strategies were developed which can be used to make a ladder of markers with different pI values by changing the buffering part of the molecules. Six pI markers were synthesized using these two synthetic schemes.

3. DEVELOPMENT OF A pH-INDEPENDENT PYRENE-BASED FLUORESCENT LABELING REAGENT

3.1 Introduction

An amine-reactive fluorophore that can be effectively utilized in the SDS-CGE separation of proteins and other macromolecules will have the following characteristics: (i) it will be negatively charged to minimize non-selective interactions with the SDS-protein complex, (ii) it will be highly soluble in aqueous background electrolytes to minimize protein aggregation even at high label-to-protein ratios, (iii) it will have fluorescence properties that do not vary with the pH of the background electrolyte between pH 3 and 10, and (iv) it will have a charge state that is pH-independent. As stated in the previous chapter, it would also be desirable for the fluorophore to have (v) an $\lambda_{\max}^{\text{ex}}$ that is compatible with the commonly used 488 nm argon ion laser assuring general utility in CE.



8-Aminopyrene-1,3,6-trisulfonic acid (trisodium salt)

$$\lambda_{\max}^{\text{ex}} = 420 \text{ nm}; \lambda_{\max}^{\text{em}} = 500 \text{ nm}$$

Figure 3.1. Structure of 8-aminopyrene-1,3,6-trisulfonic acid (APTS), trisodium salt.

Pyrene-based fluorophores have been known to have high molar absorbance and fluorescence quantum yield values [36-38]. In particular, 8-aminopyrene-1,3,6-trisulfonic acid (APTS), shown in Figure 3.1, has been extensively used to fluorescently label carbohydrates [39-41]. The multiple anionic charge of APTS insures good electrophoretic mobility and aqueous solubility of the labeled carbohydrates. The pK_a values of the sulfonate groups and the anilinic amino group are well below the operating pH range of CE making the effective mobilities (μ_{eff}) and fluorescence properties of the labeled carbohydrates pH-insensitive. These properties make APTS a good candidate core fluorophore for the proposed highly water-soluble pH-independent anionic fluorescent labeling reagent. The only drawback of APTS is that its $\lambda_{\text{max}}^{\text{ex}}$ is around 420 nm. Consequently, excitation at 488 nm makes use of only about 4% of its maximum absorbance [39].

The identity of the substituents on the aromatic core structure of a fluorophore has a profound effect on the core's fluorescence [9]. For APTS, altering the electron withdrawing / donating capability of the sulfonic acid and amino groups may provide incremental bathochromic shifts to $\lambda_{\text{max}}^{\text{ex}}$. It has been shown by Wolfbeis and coworkers that for the APTS analogue 8-hydroxypyrene-1,3,6-trisulfonic acid (HPTS), $\lambda_{\text{max}}^{\text{ex}}$ was redshifted by 20 nm and 65 nm for the acid and the conjugate base forms, respectively, when the sulfonic acid groups were converted to sulfonamides [42]. Evangelista also demonstrated that when APTS was used as a derivatizing agent for carbohydrates,

reductive alkylation of its anilinic amino group shifted $\lambda_{\text{max}}^{\text{ex}}$ by about 30 nm [39]. If sulfonamidation and amine alkylation do not negate the effect of the other, a total bathochromic shift of about 50 to 95 nm can be expected for the doubly-modified APTS.

The general objective for the development of the pyrene-based fluorophore is to build a complete fluorescent labeling reagent (fluorophore, tether and reactive group) out of the APTS core structure while preserving its desirable properties, as stated above, and simultaneously shifting its $\lambda_{\text{max}}^{\text{ex}}$ towards 488 nm. A general structure of the envisioned amine-reactive label is shown in Figure 3.2. The sulfonic acid groups can be sulfonamidated with an aminoalkanesulfonic acid to maintain multiple anionic charges on the molecule. A reactive arm terminated with a carboxylic acid, which is later on activated, can be used for attachment to the anilinic amino group.

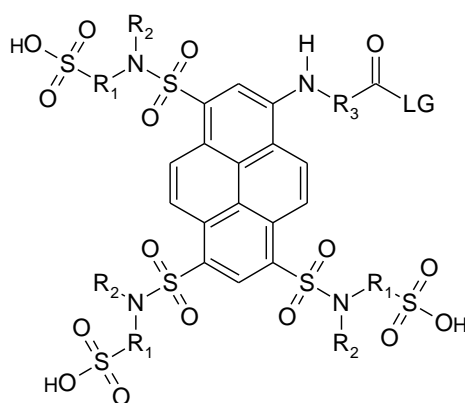


Figure 3.2. General structure of the pyrene-based fluorescent label. R1 is H or alkyl, R2, and R3 are alkyl or heteroalkyl groups. LG is a leaving group.

3.2 Optimization of the Sulfonamidation Step

3.2.1 Background and Objectives

There are some considerations to be made in choosing the aminoalkanesulfonic acid to be used for the sulfonamidation reaction. The amino group can either be a primary or a secondary amino group. The selection will determine the form of the sulfonamide nitrogen and may have an effect on the fluorescence properties of the molecule. The sulfonic acid group can come either unprotected or protected. Because these have very contrasting polarities (*i.e.*, one is ionic and the other is not) they may have important implications on the way the fluorophore will be prepared and purified.

There are a number of available aminoalkanesulfonic acids that are suitable for sulfonamidation of APTS, including taurine, N-methyltaurine, homotaurine, 2-cyclohexylamino-1-ethanesulfonic acid (CHES) and 3-cyclohexylamino-1-propanesulfonic acid (CAPS). Taurine and N-methyltaurine are more attractive because these have less hydrophobic alkyl parts than the others and have amino groups that are less sterically hindered in the sulfonamidation reaction.

Aminoalkanesulfonic acids with protected sulfonic acid groups are not readily available and will have to be synthesized if the bare sulfonic acid is found to be undesirable during work up of the reaction mixtures.

3.2.2 Materials and Methods

8-Aminopyrene-1,3,6-trisulfonic acid, trisodium salt was provided by Beckman Coulter.

2-Chloroethanesulfonyl chloride (95% purity) was purchased from TCI America.

Neopentyl alcohol, chlorosulfonic acid and triethylamine were purchased from Sigma

Aldrich. Methylamine was acquired from MC&B as a 40% solution in water. Bare

fused silica capillaries for CE analysis were purchased from Polymicro Technologies.

All HPLC columns used were purchased from Phenomenex.

CE analysis was carried out in a UV-detector equipped Beckman PA800 system. HPLC

analyses were run on a Beckman HPLC system that had a 508 autosampler, 126 pump

and 168 PDA detectors. UV absorbance spectra were taken with the PDA detectors.

Indirect UV detection response factors, degrees of electromigration dispersion and

system peak mobilities were simulated with the PeakMaster 5.2 software package [43] in

order to optimize the background electrolyte compositions for indirect UV detection CE.

pK_a values were calculated with the SPARC (SPARC Performs Automatic Reasoning in

Chemistry) Online Calculator v4.5 [25].

3.2.2.1 Synthesis of 2,2-Dimethylpropyl Ethenesulfonate **18**

10.0 g (61 mmol) of 2-chloroethanesulfonyl chloride was weighed in a 500-mL round

bottom flask. Dichloromethane (150 mL) was added followed by 5.2 g (59 mmol) of

neopentyl alcohol. While stirring in an ice bath, 41 mL of triethylamine was slowly

added in the span of 6 min. The reaction mixture was stirred at 0 °C for 40 min, then at room temperature for 30 min. Subsequently, the reaction mixture was extracted three times with 150 mL 20% aqueous sodium bisulfate, then once with 150 mL water. The organic phase was dried with anhydrous sodium sulfate and the solvent removed under reduced pressure to give an off-white oily residue (9.54 g, 91 % yield).

3.2.2.2 Synthesis of 2,2-Dimethylpropyl 2-(methylamino)ethanesulfonate **19**

Methylamine as a 40% solution in water (83 g, approximately 1 mol) was weighed in a stoppered 500-mL 3-neck round bottom flask with an attached ice water-cooled condenser. Vinylsulfonate **18** (9.5 g, 53 mmol) dissolved in 100 mL tetrahydrofuran (THF) was added to the stirred methylamine solution while in an ice bath. The reaction mixture was stirred for 2 hours at 0 °C and then overnight at room temperature. The solvents were then removed under reduced pressure until a clear oily residue was obtained (11.0 g, 99% yield).

The reaction mixture was analyzed by CE with indirect UV detection (254 nm) using a 10 mM acetic acid solution titrated to pH 4.4 with pyridine as BGE. The capillary used had 50 µm I.D., 360 µm O.D. with inlet-to-detector and total lengths of 20.3 cm and 30.4 cm, respectively.

3.2.2.3 Synthesis of 8-Aminopyrene-1,3,6-trisulfonyl Chloride **20**

8-Aminopyrene-1,3,6-trisulfonic acid, trisodium salt (4.0 g, 7.6 mmol) was carefully added to 75 mL chlorosulfonic acid while stirring in an ice bath. After addition, the reaction mixture was transferred to a 60 to 65 °C oil bath and was allowed to react for 1.5 hours. The extent of chlorination of APTS was determined by HPLC. An HPLC sample was prepared by adding a 20 μ L aliquot of the reaction mixture to 0.2 g of ice in a 1.5 mL Eppendorf tube. After addition, about 0.8 mL of water was added and the slurry was centrifuged. The supernatant was decanted and 50 μ L morpholine was added to the solid residue. The sample tube was vortexed for about 5 min and analyzed by HPLC using a Gemini C18 column (3 μ m, 100 Å, 150 mm x 4.6 mm) with isocratic elution using a binary eluent made of 55% B, at 1 mL/min (A: 2 mM N-methylmorpholine and 1mM acetic acid in water; B: 2 mM N-methylmorpholine and 1mM acetic acid in acetonitrile).

Once the reaction reached completion, the reaction mixture was cooled to room temperature and added dropwise, very carefully, to 800 g ice-water (the process is very exothermic!). The red precipitate formed was filtered and the pasty solid was used as-is in the next step.

3.2.2.4 Synthesis of 8-Aminopyrene-1,3,6-trisulfonamide **21**

Amine **19** (27 g, 129 mmol) was combined with 50 mL ACN in a beaker and added to 30 mL triethylamine. Sulfonyl chloride **20** was then added to the mixture and

transferred to a 250-mL round bottom flask. An additional 100 mL of ACN was used to wash all of the reaction mixture into the flask. The dark brown-red mixture was stirred at 55 °C for about 1 hour, then at room temperature overnight. Subsequently, the solvent was removed under reduced pressure to yield a viscous dark brown liquid. The residue was dissolved in 60 mL ACN and 160 mL formamide at 50 °C. Using a dropping funnel, 24 mL of water was added to the solution at a rate of about 1 drop per 3 to 5 seconds while stirring at 50 °C. The mixture was then allowed to cool to room temperature to precipitate the desired material. The solid was filtered out and the recrystallization step was repeated one more time. The solid was washed with water to remove excess formamide (3.8 g, 49% yield).

The reaction mixture and the products from the recrystallization steps were analyzed by RP-HPLC using the same column as in section 3.2.2.4. The sample was eluted with a binary gradient of 60% to 90% B in 20 min at 1 mL/min (A: 2 mM N-methylmorpholine and 1mM acetic acid in water; B: 2 mM N-methylmorpholine and 1mM acetic acid in ACN). The chromatograms were detected at 300 nm.

3.2.3 Results and Discussion

3.2.3.1 Sulfonamidation with N-Methyltaurine

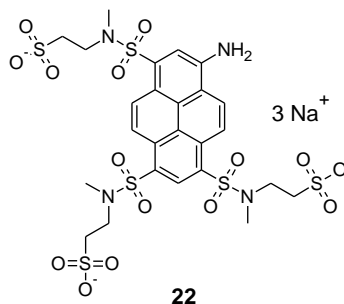


Figure 3.3. Structure of the tris sulfonamide using N-methyl taurine as the aminoalkanesulfonic acid.

Sulfonamidation using an aminoalkanesulfonic acid having a primary amine is an attractive option because this will produce a sulfonamide that has an available proton for hydrogen bonding thus making the fluorophore more water-soluble. However, the calculated pK_a value of this sulfonamido nitrogen is between 9 and 10, making it a weak acid. Deprotonation will affect the electron withdrawing ability of the sulfonamide group and the fluorescence of APTS around this pH region. Furthermore, nucleophilic substitution can also occur at this group. Because of these concerns, sulfonamidation was initially carried out with the commercially available N-methyltaurine. The sulfonic acid groups of APTS were first activated with chlorosulfonic acid and then reacted with N-methyltaurine to make tris sulfonamide **22** whose structure is shown in Figure 3.3. The starting material and reaction mixture were analyzed by hydrophilic interaction liquid chromatography (HILIC), as shown in Figure 3.4. HPLC analysis showed that there were several byproducts that eluted very closely to the target major peak. Their

efficient removal by preparative HPLC was only possible up to the second nearest peak. These byproducts were presumed to be under-sulfonamidated APTS molecules which would explain their higher retention and their spectra being an intermediate between those of APTS and compound **22**. The highly ionic nature of these byproducts and of the target overwhelms their hydrophobicity differences making selective recrystallization from polar solvents unsuccessful. These difficulties warranted the use of an aminoalkanesulfonic acid with a protected sulfonic acid group for the sulfonamidation reaction.

The UV absorbance spectra of APTS and tris sulfonamide **22** were compared to see if sulfonamidation indeed brought about the hoped-for, appreciable red shift in λ_{\max}^{ex} .

Figure 3.5 is an overlay of the UV absorbance spectra of APTS and product **22**: indeed, there is a 44 nm shift towards longer wavelength bringing λ_{\max}^{ex} of the fluorophore closer to 488 nm.

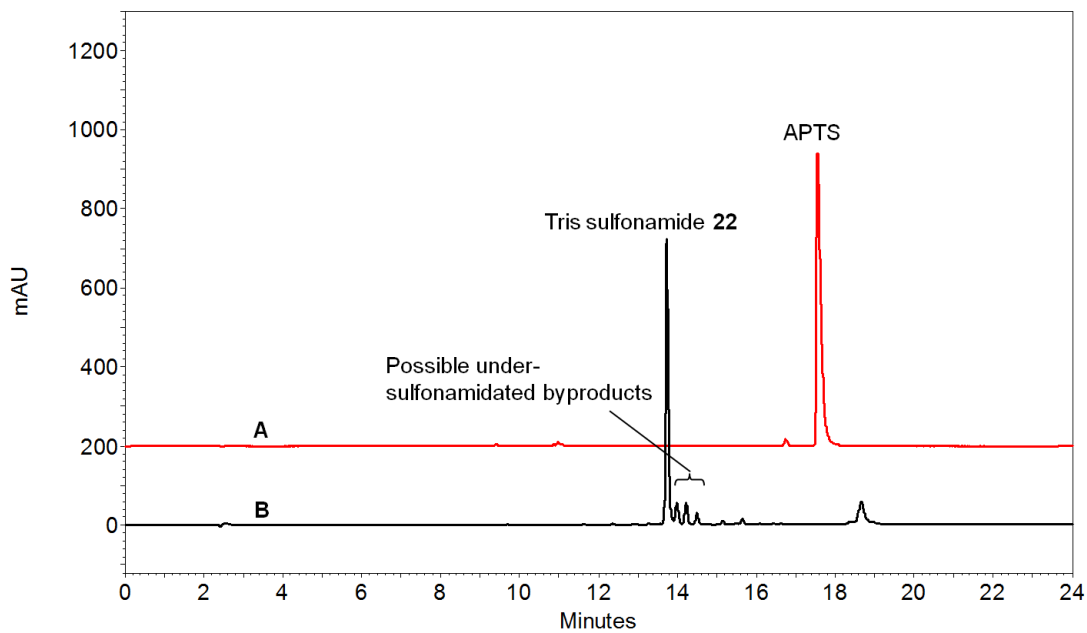


Figure 3.4. HILIC analyses of APTS (A) and the sulfonamidation reaction mixture obtained with N-methyltaurine (B). Binary gradient elution: 1 mL/min, 95 to 65% B in 20 min. (A: 100mM ammonium formate in water; B: ACN).

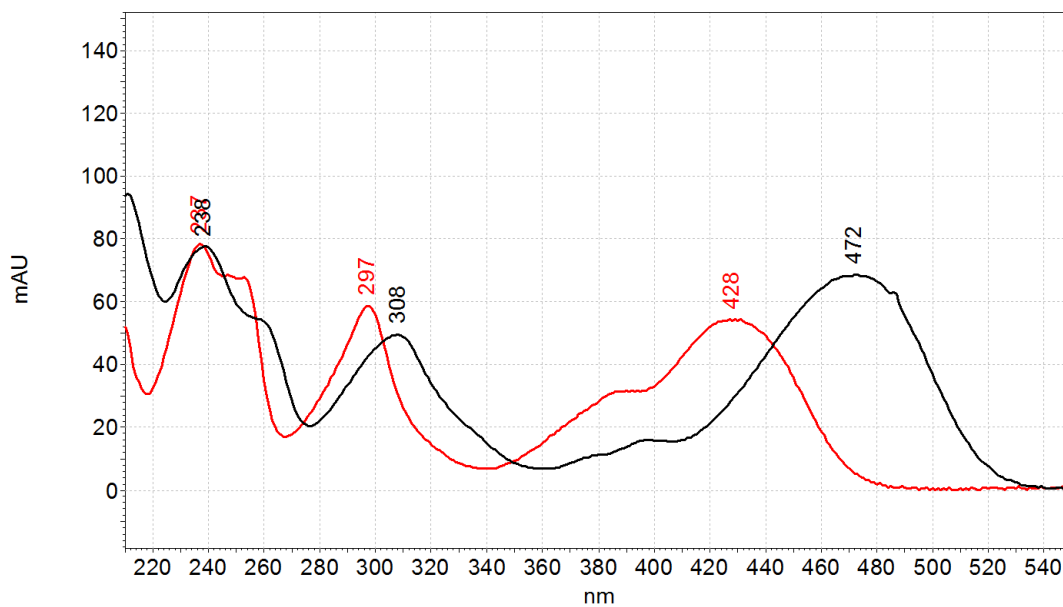
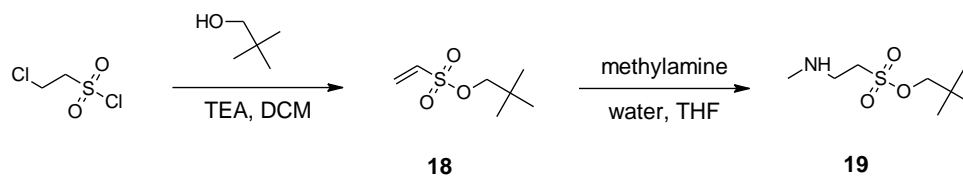


Figure 3.5. Overlay of the UV absorbance spectra of APTS and sulfonamidation product **22**. The traces are normalized on the 237 / 238 nm peaks.

3.2.3.2 Sulfonamidation with Neopentyl Ester **19**Figure 3.6. Preparation of neopentyl ester **19**.

A protected aminoalkanesulfonic acid was prepared from 2-chloroethanesulfonyl chloride (Figure 3.6). Reacting the sulfonyl chloride with neopentyl alcohol in the presence of a base formed neopentyl vinylsulfonate ester **18**. This was then reacted with excess methyl amine to produce **19**, a neopentyl ester of N-methyltaurine. The reaction and workup were monitored by CE with indirect UV detection. Figure 3.7 shows the presence of neopentyl ester **19** in the reaction mixture and the removal of methylamine from the final product.

Neopentyl ester **19** was then used for the sulfonamidation reaction after activation of the sulfonic acid groups of APTS with chlorosulfonic acid as shown in Figure 3.8. The reaction produced tris sulfonamide **21** with an assay purity of 74%. The reaction and work up were monitored by RP-HPLC as shown in Figure 3.9. Work up of the material was facile and consisted of two recrystallization steps in a solvent mixture of ACN, formamide and water. The final solid had a purity of 96% based on peak areas detected

at 300 nm. The UV absorbance spectrum of tris sulfonamide **21** is almost the same as that of **22** (λ_{max} at 239, 308, 476 nm).

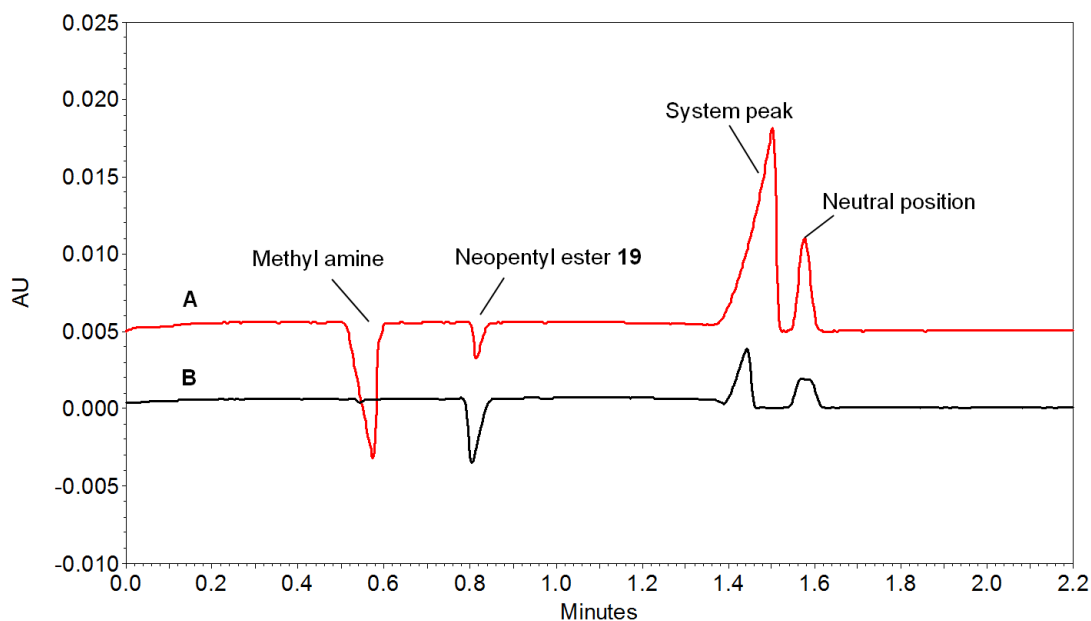


Figure 3.7. CE analysis with indirect UV detection of the reaction mixture before (A) and after (B) removal of methylamine.

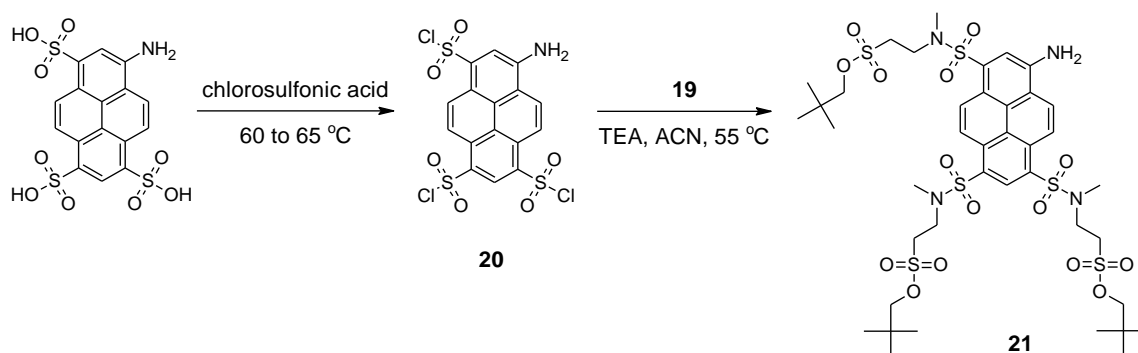


Figure 3.8. Sulfonamidation using sulfonate ester **19** to form tris sulfonamide **21**.

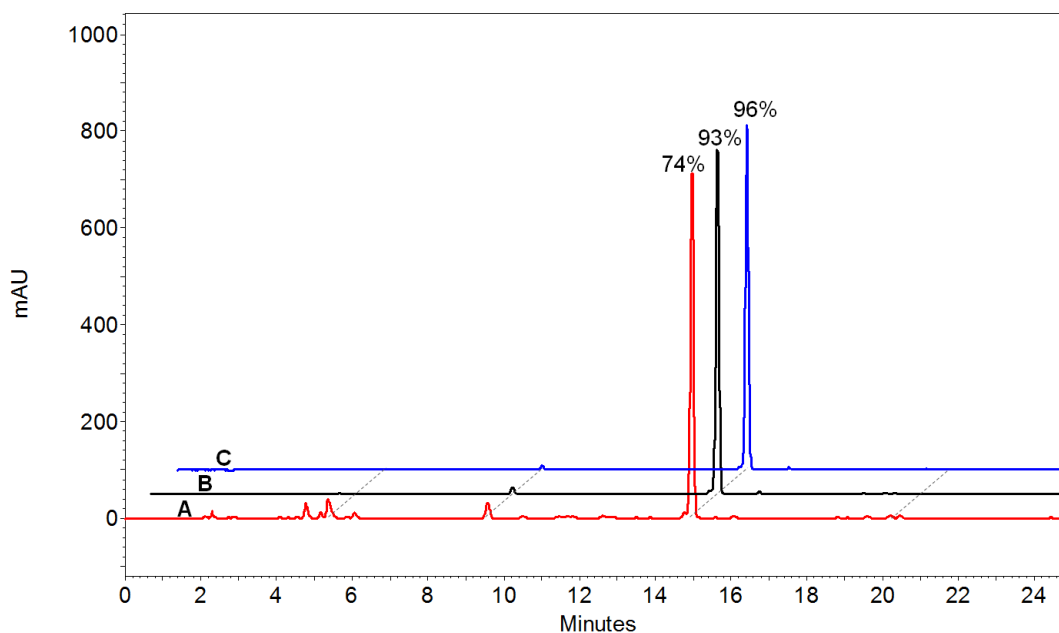


Figure 3.9. RP-HPLC of the reaction mixture (A), product from the first recrystallization step (B) and product from the second recrystallization step (C) of trisulfonamide **21**. Detection wavelength set at 300 nm. The chromatograms are normalized on the major peak and purities calculated from the peak areas are shown.

3.3 Optimization of Alkylation of the Anilinic Amino Group

3.3.1 Background and Objective

Alkylation of weak anilinic amines can be a challenge but can be accomplished by several methods. Two of the most accessible ones are alkylation by Michael addition and reductive amination. A large number of catalyzed or promoted Michael addition [44-47] and reductive amination [48-52] reactions have been reported but only a few used aniline substrates that are comparable in nucleophilicity to trisulfonamide **21**. For both types of reactions acid catalysis appears to be most effective [46, 49] and was thus tried for alkylation of amine **21**. Reductive amination in the presence of drying agents

such as molecular sieves and sodium sulfate has been explored by several groups [48, 50, 51]. This principle was also used in the development of a more efficient way to reductively alkylate amine **21**. It was also important to determine from the alkylation tests whether $\lambda_{\text{max}}^{\text{ex}}$ shifted towards 488 nm.

The tether being attached to the fluorophore in the above alkylation step had to be carefully considered. A hydrophilic heteroalkyl chain was preferred over a hydrophobic alkyl chain in order to reduce the likelihood of nonspecific interactions with the hydrophobic parts of proteins which may have significant and unpredictable effects on fluorescence. A poly(ethylene glycol)-based tether / reactive arm had to be designed that could be installed using the optimized alkylation method.

3.3.2 Materials and Methods

Acrylic acid, methyl ethyl ketone, ethyl-4-acetylbutyrate, sodium cyanoborohydride, phosphorus pentoxide, styrene oxide, 5-chloro-2-pentanone, sodium hydride (60% dispersion in oil), tetraethyleneglycol, and bromoacetic acid were purchased from Sigma Aldrich.

3.3.2.1 Synthesis of Styrene Glycol **23**

Styrene oxide (150 g) was added to 1.5 L of water and stirred for 3 hours at 60 °C, then for about half an hour at 90 °C. Subsequently, a 100 g portion of styrene oxide was added and heating was continued for 6 hours at 60 to 70 °C, then for 1.5 hours at 85 °C.

After cooling, water was evaporated under reduced pressure and the solid residue was recrystallized from toluene (twice) giving **23** in 97% purity by HPLC (detection at 270 nm).

3.3.2.2 Synthesis of Dioxolane **24**

A mixture of 23 g (167 mmol) styrene glycol **23**, 5.0 g (41.5 mmol) 5-chloro-2-pentanone, 78 mg (0.4 mmol) *p*-toluenesulfonic acid, monohydrate, and 200 mL toluene was refluxed in a 500 mL round bottom flask with an attached Dean-Stark apparatus.

Formation of the dioxolane ring was monitored by RP-HPLC. Reflux was stopped once HPLC showed complete conversion of the ketone to **24** (detection at 270 nm).

Subsequently, **24** was filtered from the cooled reaction mixture, digested with 100 mL toluene and filtered again. The toluene filtrates were combined, mixed with 5 g potassium carbonate, stirred and filtered. Toluene was then removed under reduced pressure. The residue was digested in 200 mL hexanes and filtered to remove most of the remaining styrene glycol. The hexanes filtrate was evaporated under reduced pressure and the remaining oil was digested in 48 mL *N,N*-dimethylformamide (DMF) and 120 mL water. The mixture was allowed to settle and the supernatant was decanted. The DMF/water digestion was repeated one more time on the bottom phase. The oil from the digestions was subsequently partitioned between 20 mL of toluene and 15 mL of water. The solvent from the organic phase was removed under reduced pressure giving a clear colorless oil (6.5 g, 65% yield).

The reaction and work up were monitored by RP-HPLC using a Gemini C18 column (3 μm , 100 \AA , 150 mm x 4.6 mm) with a binary gradient of 20% to 70% B in 25 min at 1 mL/min (A: 2 mM N-methylmorpholine and 1mM acetic acid in water; B: 2 mM N-methylmorpholine and 1mM acetic acid in ACN).

3.3.2.3 Synthesis of Tetraethyleneglycol-decorated Dioxolane **25**

Sodium hydride, as a 60% dispersion in oil (2.2 g, 55 mmol) was weighed in a 250 mL round bottom flask and was stirred in 50 mL hexanes under nitrogen blanket. The slurry was allowed to settle and the hexanes were cannulated out. Using a dropping funnel, a mixture of 53 g (273 mmol) tetraethyleneglycol and 50 mL THF was very carefully added dropwise to the stirred sodium hydride. Once gas evolution has ceased, the rate of alcohol addition was carefully increased. The solution was stirred at room temperature for about 10 min. After this, 0.9 g (5.4 mmol) of potassium iodide was dropped in. A mixture of 6.5 g (27 mmol) dioxolane **24** and 20 mL THF was added dropwise using a dropping funnel, then the temperature of the reaction mixture was increased to about 60 $^{\circ}\text{C}$ and THF was distilled off under a light vacuum. After complete removal of THF, the reaction temperature was increased to 80 $^{\circ}\text{C}$. The reaction was complete after 7 hours as determined by RP-HPLC. The reaction mixture was cooled to room temperature and partitioned between 100 mL dichloromethane and 200 mL 10% aqueous sodium chloride. The organic phase was extracted with 200 mL 10% aqueous sodium chloride two more times. The organic phase was dried with sodium sulfate and evaporated under reduced pressure yielding an oil (9.5 g 88% yield).

HPLC was carried out using a Gemini C18 column (3 μm , 100 \AA , 100 mm x 4.6 mm) with a binary gradient of 20% to 70% B in 20 min at 1 mL/min (A: 2 mM N-methylmorpholine and 1mM acetic acid in water; B: 2 mM N-methylmorpholine and 1mM acetic acid in ACN).

3.3.2.4 Synthesis of Dioxolane/Carboxylic Acid-terminated Tetraethyleneglycol **26**

Sodium hydride, as a 60% dispersion in oil (12.0 g, 300 mmol) was weighed in a 1-L round bottom flask and stirred in 100 mL hexanes under nitrogen blanket. The slurry was allowed to settle and the hexanes were cannulated out. 100 mL of THF was then added in. While stirring in a water bath, a mixture of 17.3 g (125 mmol) bromoacetic acid and 40 mL THF was carefully added dropwise using a dropping funnel. The addition rate was controlled to avoid excessive hydrogen formation. A mixture of 45 g (88 mmol) of dioxolane **25** (~77% purity) and 100 mL THF was then carefully added dropwise. Stirring was continued while in a water bath: the reaction was completed in 2 hours as shown by RP-HPLC. 50 mL of methanol was then slowly added followed by 250 mL of 10% aqueous sodium bicarbonate. The solvent was removed under reduced pressure. The wet solid residue was digested in 100 mL ACN at 80 $^{\circ}\text{C}$ for 5 min, cooled in an ice bath and filtered. The solids were washed with 150 mL ACN. More of the solids were forced out from the filtrate by adding 300 mL each of THF and methyl-t-butyl ether (MTBE) and slurry filtered. The filtrate was evaporated under reduced pressure. The oily residue was then redissolved in 100 mL THF to precipitate more of the inorganic solids and centrifuged. To the supernatant, 700 mL MTBE was added,

swirled and allowed to settle for 6 hours. Subsequently, the supernatant was decanted leaving a viscous liquid settled at the bottom. The THF-MTBE treatment was repeated one more time. Carried over solvent was evaporated from the bottom phase under reduced pressure to afford a light brown oil with a purity of about 85% as determined by HPLC (39 g, 82% yield).

HPLC analysis was done using a Gemini C18 column (3 μm , 100 \AA , 100 mm x 4.6 mm) with a binary gradient of 20% to 80% B in 20 min at 1 mL/min (A: 2 mM N-methylmorpholine and 1mM acetic acid in water; B: 2 mM N-methylmorpholine and 1mM acetic acid in ACN).

3.3.2.5 Synthesis of Ketone/Carboxylic Acid-terminated Tetraethyleneglycol **27**

Dioxolane **26** (39 g, 72 mmol) was combined with 500 mL 1:1 mixture of 1M aq. HCl : THF and stirred until dioxolane hydrolysis was complete as determined by RP-HPLC. The mixture was neutralized with sodium bicarbonate until gas evolution has stopped. The solvent was removed under reduced pressure. The residue was partitioned between 200 mL ethyl acetate and 100 mL water to remove styrene glycol. The aqueous phase was extracted two more times with 200 mL ethyl acetate. Carried over ethyl acetate was removed under reduced pressure and the remaining aqueous solution of the target was acidified with 11 mL concentrated HCl. This was then extracted with 200 mL MTBE six times. The acidic aqueous phase was then neutralized with sodium carbonate and water was removed under reduced pressure. The residue was digested in 200 mL ACN

and filtered. ACN was evaporated leaving a light caramel colored viscous residue (18.8 g, 73% yield). HPLC monitoring was done using a Gemini C18 column (3 μm , 100 \AA , 100 mm x 4.6 mm) with a binary gradient of 10% to 50% B in 16 min at 1 mL/min (for monitoring the dioxolane hydrolysis reaction: A: 2 mM N-methylmorpholine and 1mM acetic acid in water; B: 2 mM N-methylmorpholine and 1mM acetic acid in ACN; for monitoring the workup: A: 0.1% trifluoroacetic acid in water; B: 0.1 % trifluoroacetic acid in ACN).

3.3.2.6 Synthesis of PEG-based Fluorophore Tether Intermediate **28**

110 mL dichloroethane and 30 mL methanol were added to 18.8 g (53 mmol) carboxylate **27**. Sulfuric acid (2.8 g) was carefully added and the mixture was refluxed for about 4 hours or until methyl ester formation was complete as shown by RP-HPLC. The mixture was cooled, then quenched with about 1.5 g sodium bicarbonate in 20 mL water, making sure that the pH of the solution did not go above 7. The solvents were removed under reduced pressure. Subsequently, the residue was digested in 200 mL THF for about 30 min at 65 $^{\circ}\text{C}$, then cooled to room temperature and filtered. The solvent was evaporated under vacuum to afford a brown viscous oil (15.5 g, 84% yield).

HPLC monitoring was done using a Gemini C18 column (3 μm , 100 \AA , 100 mm x 4.6 mm) with a binary gradient of 10% to 50% B in 16 min at 1 mL/min (for monitoring the methyl ester formation reaction: A: 0.1% trifluoroacetic acid in water; B: 0.1% trifluoroacetic acid in ACN; for monitoring the workup: A: 2 mM N-methylmorpholine

and 1mM acetic acid in water; B: 2 mM N-methylmorpholine and 1mM acetic acid in ACN).

3.3.2.7 Synthesis of Alkylated APTS Trisulfonamide **29**

Method A:

Anhydrous DMF (15 mL) and 85% H₃PO₄ (2 mL) were combined in a 500-mL round bottom flask with an attached mechanical stirrer. While stirring in a water bath, ~12 g of P₂O₅ was slowly added to create a homogenous paste. Then, 3.4 g (9.7 mmol) of ketone **28** was added in. The mixture became more viscous and sticky after the addition of the ketone. This mixture was stirred further for 15 minutes before addition of 0.5 g (0.5 mmol) of amine **21**. The mixture was stirred for another 20 min, after which 2.5 mL of NaBH₃CN in anhydrous DMF was dropped in while stirring. The paste color turned from red-brown to red-orange seconds after the addition. The reaction was complete after 30 minutes as shown by RP-HPLC analysis.

A mixture of 27 g Na₂CO₃ and 200 mL water was added slowly to the reaction mixture while it was stirred in an ice bath. Ethyl acetate (200 mL) was then added and the mixture stirred for 30 min. The two phases were separated, the organic phase was dried with sodium sulfate and evaporated under reduced pressure. The sticky viscous residue was added to 25 mL water, swirled vigorously and allowed to settle for a few minutes. The supernatant was decanted and centrifuged to recover any carried over target material. Water digestion was repeated for the remaining residue. All the viscous

residue was dissolved in 50 mL dimethylsulfoxide (DMSO) and added drop by drop to a stirred, 50 mL portion of a 10% aqueous sodium chloride solution. The slurry was stirred and allowed to settle. The supernatant was decanted and centrifuged to recover the carried over solids. Precipitation was repeated one more time. The resulting sticky solid was dissolved in ethyl acetate, filtered and evaporated under reduced pressure to afford a dark red-orange residue (0.62 g, 91% yield).

HPLC analysis was done using a Gemini C18 column (3 μm , 100 \AA , 75 mm x 4.6 mm) with a binary gradient of 40% to 100% B in 18 min at 1 mL/min (A: 2 mM N-methylmorpholine and 1mM acetic acid in water; B: 2 mM N-methylmorpholine and 1mM acetic acid in ACN).

Method B:

1.2 g of P_2O_5 and 1.2 g orthophosphoric acid were weighed into a 25 mL round bottom flask. 10.2 mL anhydrous DMF was added and stirred. The flask was well sealed to keep moisture out. 4.06 g (11.6 mmol) of ketone **28** was added to the DMF mixture and was stirred for 3 minutes before addition of 0.40 g (0.6 mmol) tris sulfonamide **21**. The mixture was stirred for another 30 minutes at room temperature, after which 728 μL of 2M NaBH_3CN in anhydrous DMF was added. The color of the reaction mixture turned from red-brown to red-orange and conversion was complete after 16 hours as determined by RP-HPLC analysis.

The reaction mixture was partitioned between 75 mL ethyl acetate and 150 mL 10% aqueous sodium carbonate. The organic layer was extracted again with 150 mL aq. Na_2CO_3 . The aqueous layers were combined and back-extracted with 75 mL of ethyl acetate. The ethyl acetate phases were combined and washed with 150 mL 1M sodium phosphate, pH 5.6, to neutralize any carried-over sodium carbonate. The organic phase was dried with sodium sulfate and evaporated under reduced pressure. The remaining residue was a dark red brown liquid. To this was added 30 mL methanol, heated to reflux and, while stirring, slowly added 30 mL of water at a rate of 1 drop per second. Red-brown gum precipitated out from solution. The mixture was allowed to cool. The supernatant was decanted and centrifuged to recover carried over material. Precipitation was repeated three more times using 30 mL water and twice more using 15 mL water. Water and methanol residues were evaporated under reduced pressure (0.71 g, 86% yield).

HPLC analysis was done using a Gemini C18 column (3 μm , 100 \AA , 150 mm x 4.6 mm) with an isocratic elution of 80% B at 1 mL/min (A: 2 mM N-methylmorpholine and 1mM acetic acid in water; B: 2 mM N-methylmorpholine and 1mM acetic acid in ACN).

3.3.3 Results and Discussion

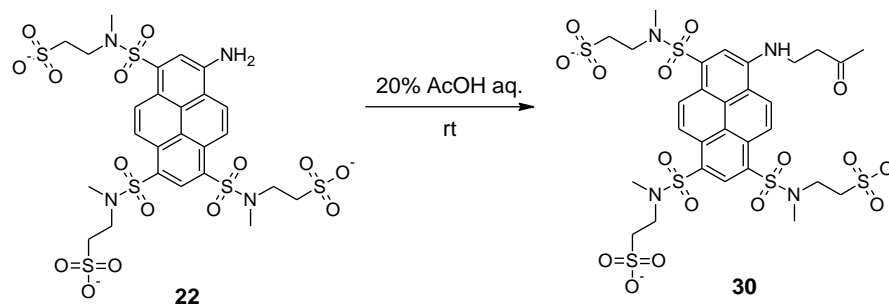


Figure 3.10. Michael addition reaction between methyl vinyl ketone and tris sulfonamide **22**.

Because of its reactivity, methyl vinyl ketone (MVK) was tried as an alkylating agent for APTS tris sulfonamide **22**. The reaction proceeded very well under mild conditions to form alkylated product **30** (Figure 3.10). The UV absorbance spectra of **22** and **30** are overlaid in Figure 3.11. Alkylation brought $\lambda_{\text{max}}^{\text{ex}}$ of the fluorophore to about 492 nm making the sulfonamidated-alkylated APTS compatible with the 488 nm argon ion laser. However, upon treatment with ammonium acetate at 60 °C, a new component having exactly the same UV absorbance spectrum as **22** was observed. This indicates that alkylated compound **30** was not stable and underwent dealkylation.

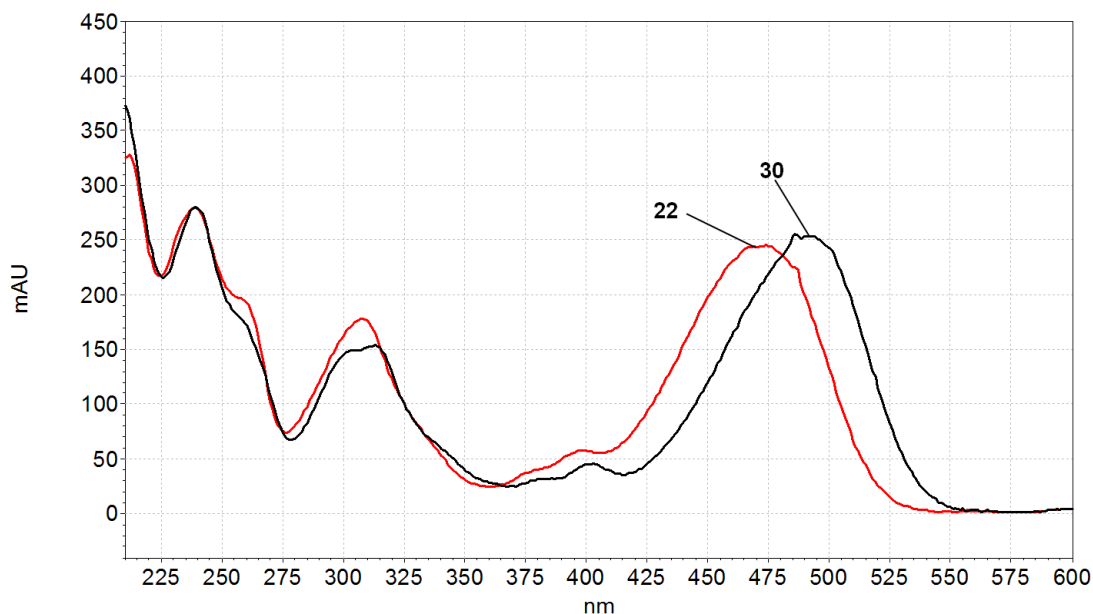


Figure 3.11. Overlay of the UV absorbance spectra of amine **22** and its MVK-alkylated derivative **30**. The spectra are normalized on the 239 nm peak.

Efforts to affect Michael addition with less active Michael acceptors without the use of a strong acid catalyst were not successful. Therefore, further attempts were tried only with strong acid catalysts. Methyl acrylate with methanesulfonic acid in a solventless Michael addition with tris sulfonamide **21** brought only about 15% conversion and the formation of numerous minor byproducts. When acrylic acid was used as acceptor and sulfuric acid as catalyst, formation of a putative alkylated product was significant but this in turn was rapidly converted into a byproduct with a much lower $\lambda_{\text{max}}^{\text{ex}}$.

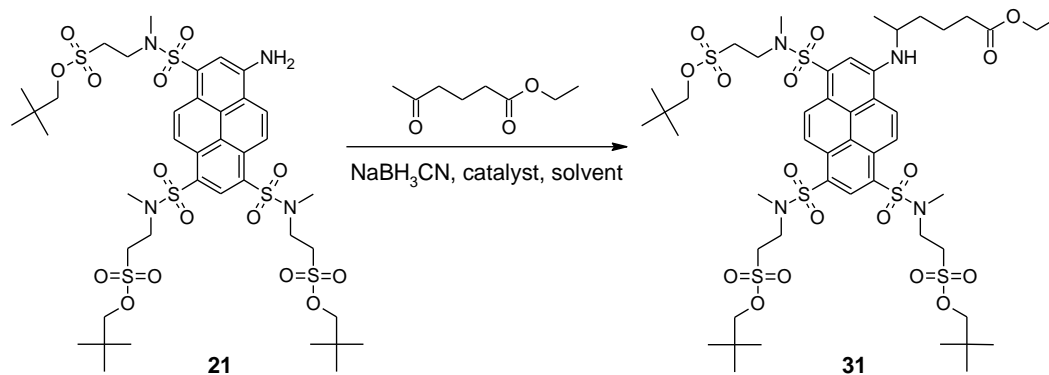


Figure 3.12. Reductive amination using amine **21** and ethyl-4-acetylbutyrate.

Reductive amination of tris sulfonamide **21** with ethyl-4-acetylbutyrate and sodium cyanoborohydride as shown in Figure 3.12 was carried out in an ACN/methanol solvent mixture with methanesulfonic acid as catalyst. The reaction yielded alkylated amine **31** (the methyl ester was observed due to transesterification) with a conversion of up to 95%. However, this was only after incremental addition of a very large excess of all the reagents as indicated in the chromatograms in Figure 3.13.

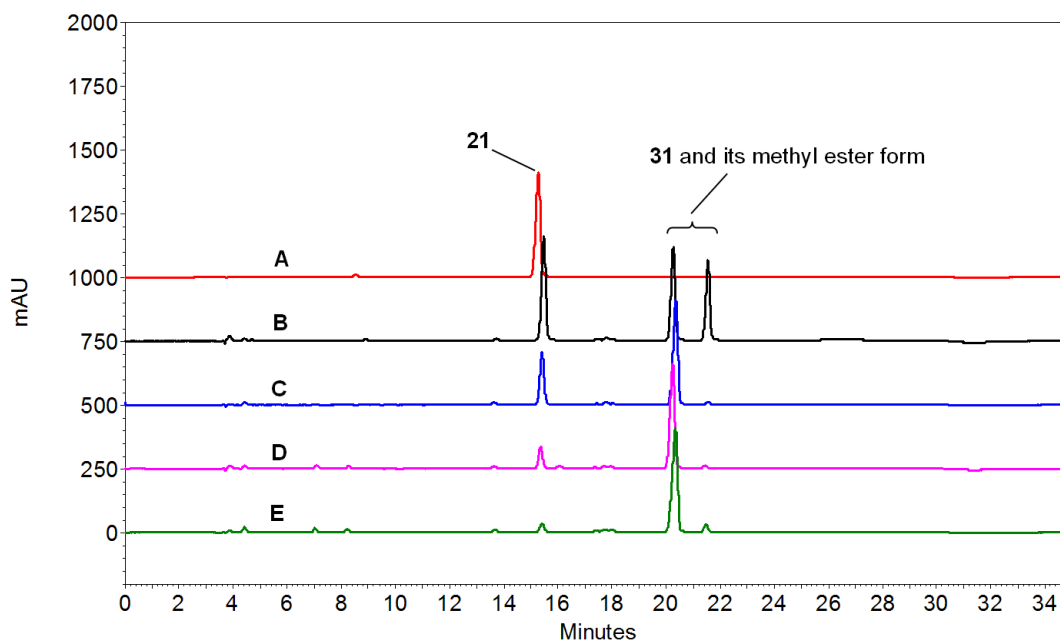


Figure 3.13. RP-HPLC monitoring (detection at 300 nm) of the reductive amination of ethyl-4-acetylbutyrate with amine **21**. The reaction proceeded only with excess amounts of each reagent. (A) is the chromatogram for starting material **21**. (B) through (D) are those of the reaction mixture with increasing amounts of the reagents ketone / NaBH₃CN / MSA: 21 / 14 / 20 equiv. (B), 36 / 24 / 60 equiv. (C), 51 / 34 / 100 equiv. (D), and 81 / 44 / 140 equiv. (E). The tallest peaks are normalized.

Knowing that the limiting step for the reductive amination of a ketone with weak amine **21** was the formation of an imine, a dehydrating strategy was considered to shift the equilibrium towards the latter. However, since compound **21** is an exceptionally weak nucleophile, dehydrating agents reported in the literature [53] may not effectively promote imine formation. This prompted the use of phosphorus pentoxide (P₂O₅) as a dehydrating agent. Reductive amination of 20 equivalents of ethyl-4-acetylbutyrate with amine **21** proceeded very quickly to completion in the presence of phosphoric acid (85% H₃PO₄) and P₂O₅ with 10 equivalents of sodium cyanoborohydride as reducing agent and DMF as solvent as shown in Figure 3.14. The reaction was carried out at room

temperature. The reaction mixture was very viscous and had to be mechanically stirred to effect good mixing.

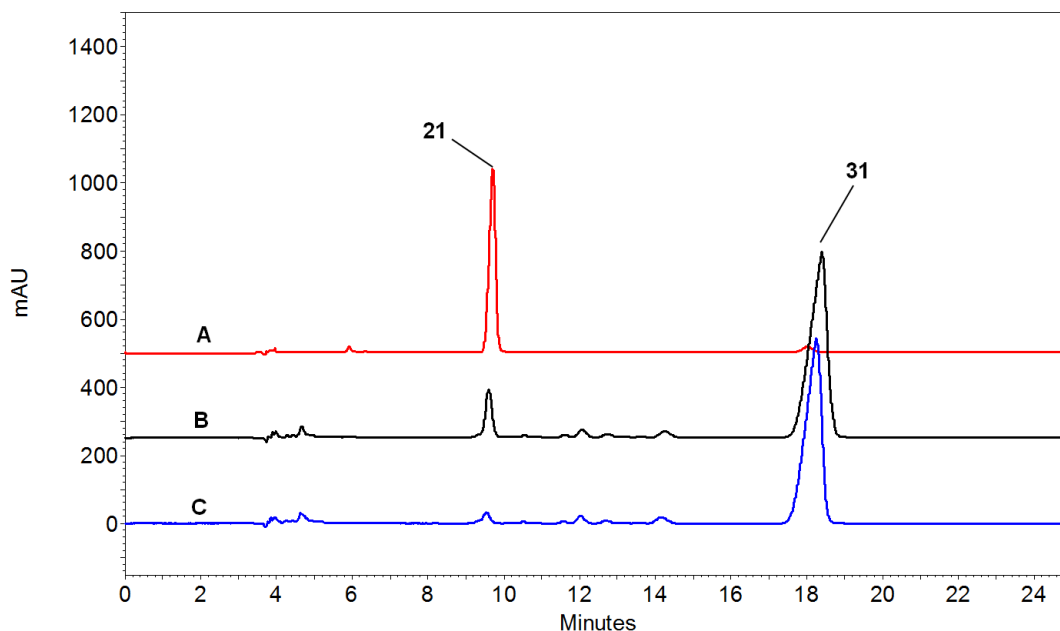


Figure 3.14. RP-HPLC analysis of starting material **21** (A) and the reductive amination reaction mixture at 20 minutes (B) and 50 min (C). The reaction was done in the presence of $\text{H}_3\text{PO}_4/\text{P}_2\text{O}_5$ with 20 equiv. ethyl-4-acetylbutyrate, 10 equiv. sodium cyanoborohydride and DMF as solvent.

Upon learning the necessary alkylation conditions, a tether based on tetraethyleneglycol was prepared according to the reaction scheme in Figure 3.15. The preparation started with 5-chloro-2-pentanone to provide the ketone needed for the fluorophore tether. The ketone was protected with **23** as a 1,3-dioxolane to give chloro derivative **24**. The latter was subsequently coupled to tetraethyleneglycol to form dioxolane-terminated PEG **25**. Bromoacetic acid was reacted with **25** in the presence of sodium hydride to produce dioxolane/carboxylic acid-terminated PEG **26**. The dioxolane group of **26** was then

hydrolyzed under acidic conditions to form carboxylic acid **27**. Since the free carboxylic acid would form an amide with amine **21** under the dehydrating conditions used for the reductive amination, **27** was converted into methyl ester **28** by refluxing in methanol and dichloroethane, with a catalytic amount of sulfuric acid.

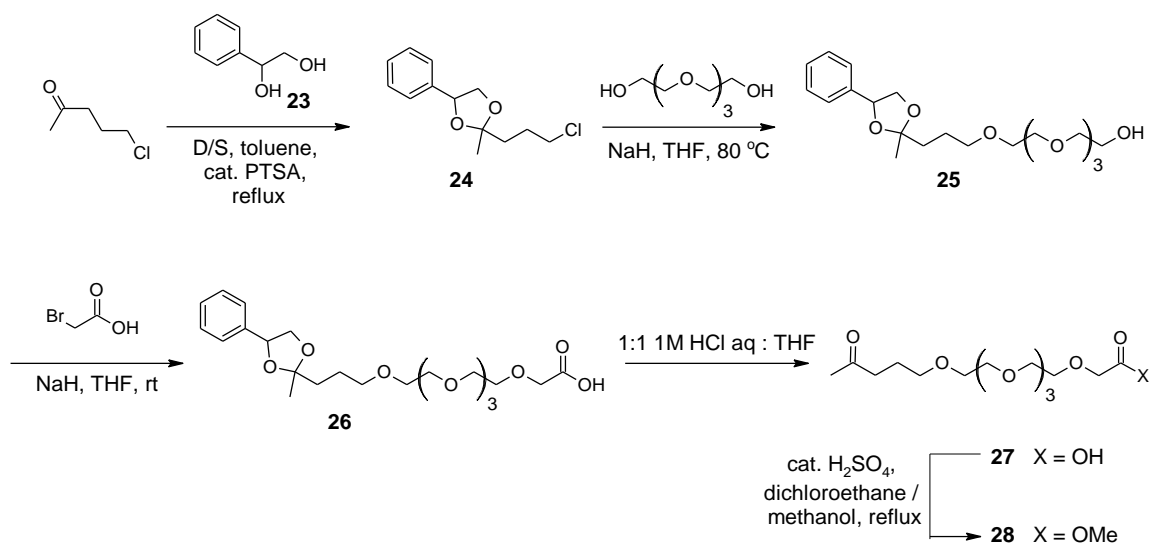


Figure 3.15. Synthesis scheme for the preparation of tetraethyleneglycol-based fluorophore tether / reactive arm **28**.

Fluorophore tether intermediate **28** was then used for the alkylation of tris sulfonamide **21** to obtain alkylated product **29** (Figure 3.16). With 20 equivalents of the ketone and 10 equivalents of sodium cyanoborohydride, the reaction went to completion in 30 minutes at room temperature as shown by the HPLC trace in Figure 3.17. A small amount of the carboxylate form of **29** was observed because about 5% of PEG-based tether intermediate **28** was present in the carboxylic acid form. However, this was not a

concern because the methyl ester was to be hydrolyzed to the carboxylic acid in a later step of the fluorophore preparation scheme. The reductive amination conditions were further optimized by lowering the amount of P_2O_5 and using orthophosphoric acid instead of 85% H_3PO_4 . Only about 2.5 equiv. of sodium cyanoborohydride were added. The ketone was still added in excess at 20 equiv., because a lower excess produced a small amount of an unknown byproduct. The reaction mixture obtained under the new conditions was considerably less viscous than the previous one, but the reaction took 16 hours to complete.

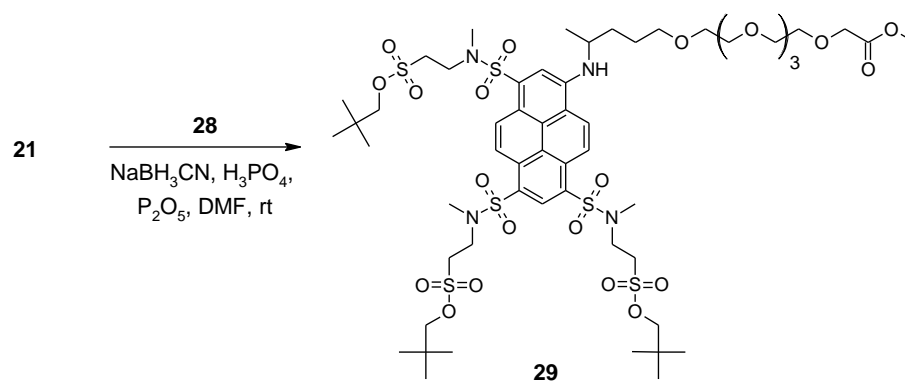


Figure 3.16. Preparation of alkylated tris sulfonamide **29** from **21** by reductive amination under dehydrating conditions.

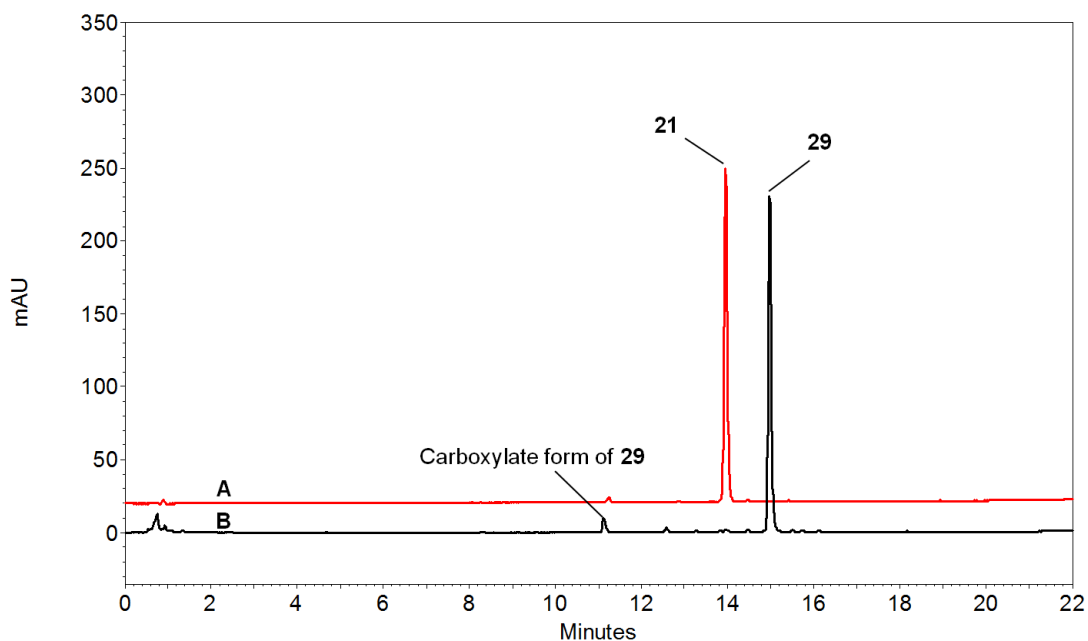


Figure 3.17. RP-HPLC of starting material **21** (A) and the reductive amination reaction mixture containing 20 equiv. ketone **28** and 10 equiv. NaBH_3CN in the presence of $\text{H}_3\text{PO}_4/\text{P}_2\text{O}_5$ in DMF after 30-minute (B).

3.4 Optimization of the Removal of the Neopentyl Protecting Group and Purification of the Sulfonic Acid by Preparative Hydrophilic Interaction Liquid Chromatography (Prep HILIC)

3.4.1 Background and Objective

Neopentyl sulfonate esters are extremely stable and require relatively harsh conditions to deprotect. Roberts *et al.* reported the cleavage of a neopentyl arylsulfonate ester by heating with tetramethylammonium chloride in DMF at 160 °C for 16 hours [54].

Adamczyk and others deprotected dyes having alkylsulfonate esters by refluxing them in

1N HCl for 4 to 8 hours [29]. These and other conditions had to be investigated to minimize the formation of byproducts.

Once deprotected, the fluorophore becomes tetra-anionic making purification by conventional methods difficult. The use of preparative liquid chromatography was a practical choice but different aspects of the separation had to be carefully considered. For instance, reverse phase liquid chromatography will not be suitable because the very polar compound will not have enough retention in the nonpolar stationary phase. The use of ion pairing agents may help but these will be difficult to remove from the target later on. Hydrophilic interaction liquid chromatography (HILIC) is another mode of liquid chromatography that is orthogonal to reverse phase in its selectivity and is usually used to separate polar compounds having little retention in the latter. However, there are only a few reports on the use of HILIC for semi-preparative or preparative fractionations [55-57] and none of these has a highly ionic compound as their target. A new approach for the semi-preparative HILIC purification of the tetra-anionic target compound had to be developed with the aim of maximizing throughput without sacrificing the integrity of the separation.

3.4.2 Materials and Methods

Tetramethylammonium chloride (TMACl), tetraethylammonium chloride (TEACl), benzyltrimethylammonium chloride (BnTMA), tetrabutylammonium hydroxide

(TBAOH) and sodium trifluoroacetate (NaTFA) were purchased from Sigma Aldrich. Analytical and semi-preparative HPLC columns were provided by Phenomenex.

3.4.2.1 Synthesis of Sulfonic Acid **32** (Removal of the Neopentyl Protecting Group)

0.6 g (0.44 mmol) neopentyl sulfonate ester **29** was dissolved in 10 mL DMSO. 1.0 g tetraethylammonium chloride was added and the mixture was heated to 115-120 °C. The reaction was monitored closely by HILIC and found to be complete after 4 hours. The target was precipitated by adding 100 mL of a 1:1 mixture of THF and MTBE. The heterogeneous mixture was then distributed into multiple centrifuge vials and centrifuged. The supernatant was decanted and the bottom viscous liquids were dissolved in a total of 10 mL ACN and combined. The target was again precipitated by adding an 80 mL portion of a 1:1 mixture of THF:MTBE. This dissolution-precipitation step in ACN and THF/MTBE was repeated one more time. The resulting red-brown viscous liquid was vortexed in 40 mL THF, centrifuged and decanted twice (the bottom phase was not flowing anymore). The material (**32** and carried over TEACl) was used as-is in the next step.

HILIC analysis was done using a Luna HILIC column (3 μm , 200 \AA , 150 mm x 4.6 mm) with a binary gradient of 95% to 75% B in 20 min at 1 mL/min (A: 10 mM 3-morpholinopropane-1-sulfonic acid (MOPS) and 5mM sodium hydroxide (NaOH) in water; B: 10 mM MOPS and 5mM NaOH in 5% water in ACN).

3.4.2.2 Hydrolysis of Methyl Ester **32** to Form Carboxylic Acid **33**

The solid from the previous step was dissolved in 5 mL 0.01M aqueous sodium hydroxide and stirred at room temperature. Complete ester hydrolysis was accomplished after 10 minutes as determined by HILIC. The base was then quenched by adding a mixture of 75 μ L trifluoroacetic acid, 140 μ L triethylamine and 0.5 mL water. The mixture was evaporated under vacuum to afford a dark red gummy solid residue. This was dissolved in 25 mL ACN and added dropwise to a solution of 5 g sodium trifluoroacetate (NaTFA) in 25 mL ACN while stirring. Excess NaTFA ensured that the counterion of **33** during semi-prep HILIC was sodium, not tetraethylammonium. The resulting slurry was centrifuged, decanted and the bottom solid phase set aside. The supernatant was evaporated. The residue went through a series of digestions, first with 100 mL of 1:1 THF:MTBE, then with 50 mL THF and lastly with 50 mL ACN. The red orange solid was combined with the previously set aside solid from the sodium ion exchange step and dissolved in about 3 mL of water. Some of the water was evaporated to reduce the volume to about 2 mL. At this volume, the concentration of **33** was high enough to have a high semi-prep HILIC throughput while the viscosity of the mixture was not too high allowing good injection in the sample loop. HILIC was done the same way as in section 3.4.2.1.

3.4.2.3 Semi-preparative HILIC of Tetra-anion **33**

A solution of **33** from the previous step was used as the feed for the semi-prep HILIC separation. About 200 to 250 μ L of the solution, corresponding to approximately 50 mg

of dissolved material, was injected. The sample loop configuration is shown in Figure 3.18. The sample loop used was a stainless steel 5-mL Rheodyne loop with an approximate I.D. of 1 mm. The semi-prep HILIC separations were carried out in a Beckman HPLC system equipped with a 508 autosampler, 126 pump and 168 photodiode array detector. The HILIC column was a Luna 5 μm HILIC column (250 mm x 10 mm) with a HILIC guard cartridge. The flowrate was 5 mL/min. After sample injection, there was a 4 min long isocratic elution segment at 92% B that was followed by a step change to 77% B. The eluent composition was maintained at this concentration until the desired component was eluted, followed by a 5-minute cleaning of the column at 40% B, before going back to the initial composition, 92% B (A: 20 mM sodium trifluoroacetate in water; B: 20 mM sodium trifluoroacetate in ACN). Solvents were filtered through a 0.65 μm PVDF membrane filter from Millipore.

The collected fractions had a total volume of 400 mL. A 40-mL aliquot was taken and evaporated under reduced pressure to afford a dark red-orange residue. The solid was then dissolved in 0.5 mL DMSO and reprecipitated with 7 mL ACN to remove sodium trifluoroacetate. The slurry was centrifuged and the resulting orange solid was redissolved and reprecipitated two more times using DMSO and ACN. Finally, the solid was washed with ACN and dried in vacuum over P_2O_5 (43 mg, 72% yield for the 40 mL aliquot taken through the deprotection and hydrolysis steps).

HILIC was done the same way as in section 3.4.2.1.

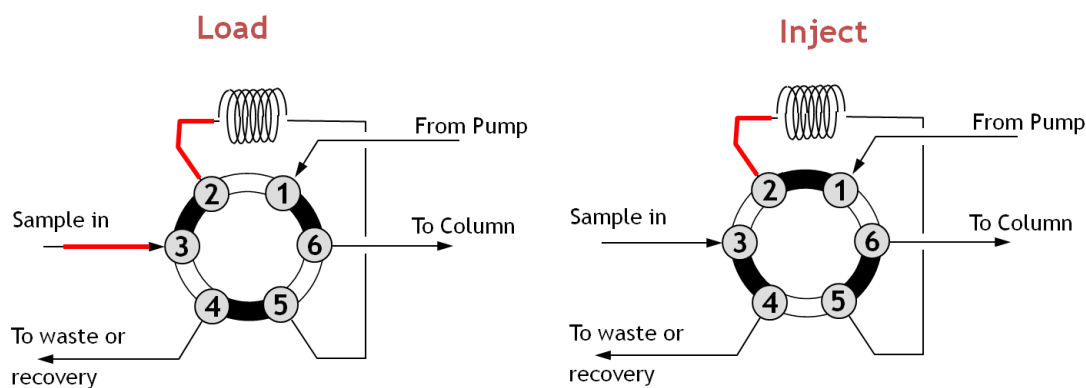


Figure 3.18. Sample loop configuration that allows in-line “Taylor” dilution of a sample loaded in a strong solvent for prep HPLC.

3.4.3 Results and Discussion

3.4.3.1 Removal of the Neopentyl Protecting Group

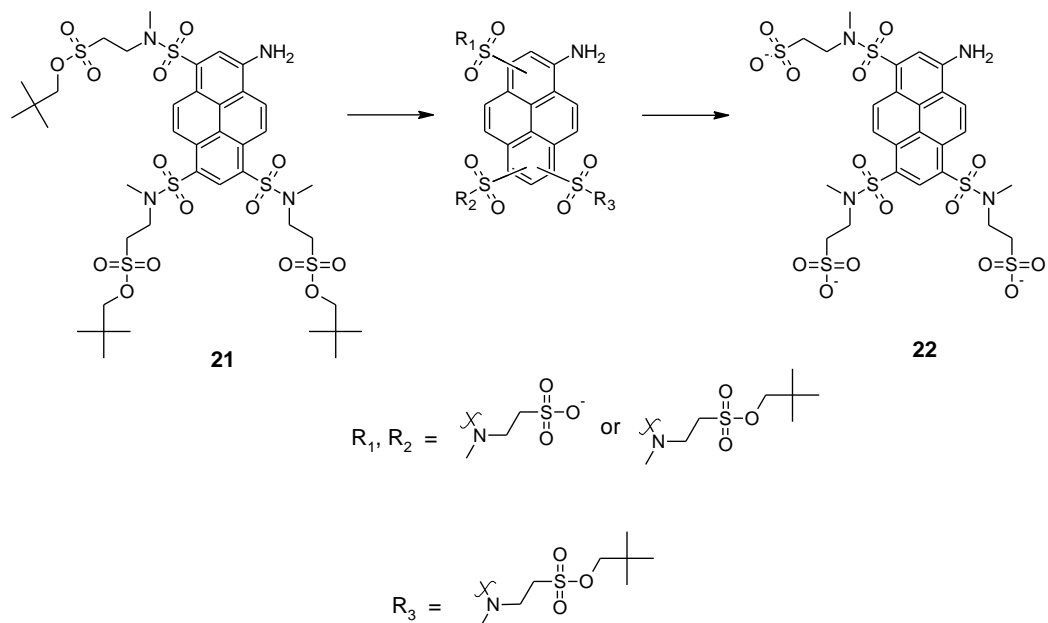


Figure 3.19. Deprotection of test compound tris neopentyl ester **21** showing the partially deprotected intermediates (mono and bis) and the fully deprotected **22**.

The neopentyl ester protected trisulfonamide **21** was used as test compound for the deprotection experiments to form **22**. A schematic of the reactions is shown in Figure 3.19. The method described by Roberts and coworkers employing trimethylammonium chloride in DMF was tried except that the reported temperature of 160 °C was lowered to 120 °C due to concerns about the stability of the fluorophore under such harsh conditions. Cleavage of the ester was complete after 21 hours. Figure 3.20 shows the HILIC analysis of the deprotection reaction mixtures after 3, 6 and 21 hours of heating at 120 °C. Decrease of the mono and bis neopentyl ester intermediates is evident as well as the increase of the single major product peak corresponding to target **22**. However, a closer look at the chromatogram of the 21-hour sample reveals several byproducts eluting very closely to the target which will make the purification of the target component by semi-prep HILIC very difficult. ESI-MS indicated the presence of sulfonamide dealkylation byproducts (Figure 3.21). These byproducts, which eluted between 6 to 6.3 min accounted for 10% of the total peak area in the HPLC analysis shown in Figure 3.20.

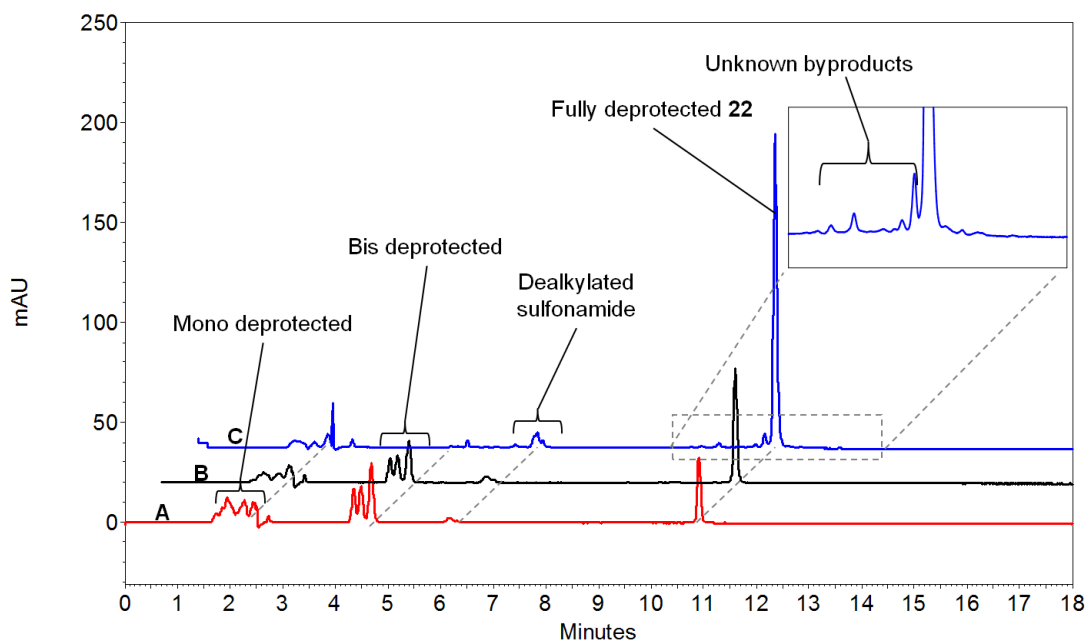


Figure 3.20. Cleavage of the neopentyl sulfonate esters of **21** using TMACl in DMF at 120°C after 3 hours (A), 6 hours (B) and 21 hours (C) reaction time.

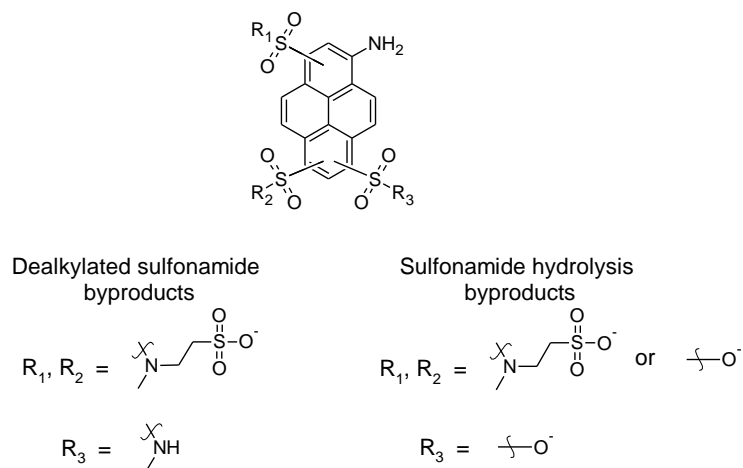


Figure 3.21. Possible structures of the byproducts from cleavage of the neopentyl sulfonate esters.

A modification of the deprotection method used by Adamczyk and others [29] was also tested. Figure 3.22 shows the HILIC analysis of the sample where deprotection was achieved by heating in 1N HCl in water and 1-propanol. When the temperature was maintained between 80 to 90 °C for 3 hours, no significant cleavage was observed. When the temperature was increased to 100 °C and kept for 17 hours, the amount of sulfonamide dealkylation products decreased and the closely eluting unknown byproducts that were significant in the previous test were not produced. However, there was a considerable amount of sulfonamide hydrolysis products (Figure 3.21) which represented about 20% of the total signal.

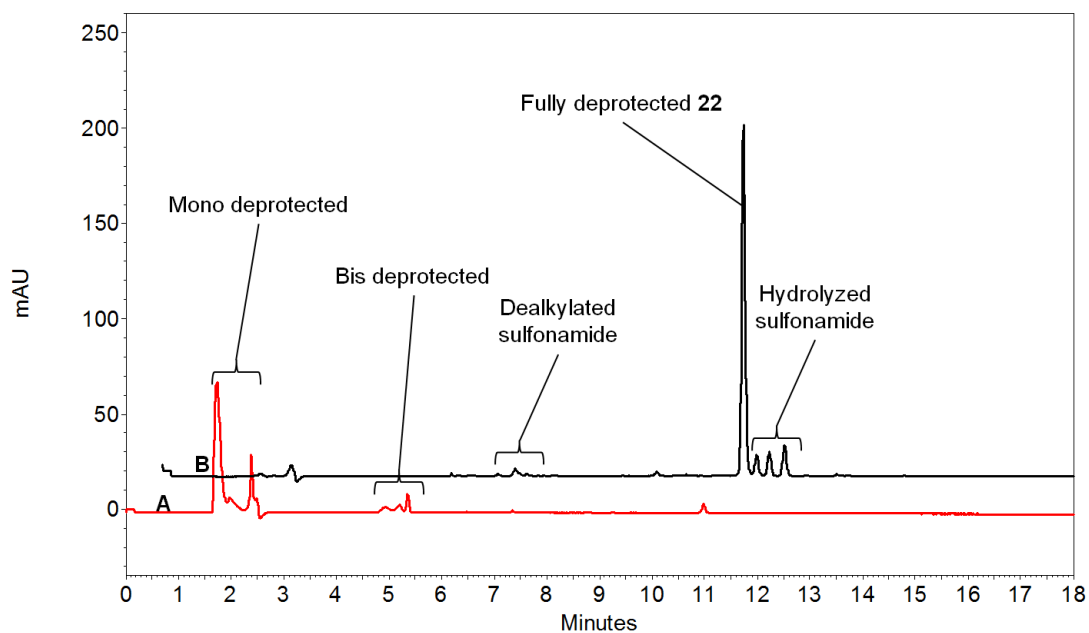


Figure 3.22. Cleavage of the neopentyl sulfonate esters of **21** using 1M HCl in water/n-propanol at 80 to 90 °C after 3 hours (A), and at 100 °C after 17 hours thereafter (B).

The formation of significant amounts of byproducts and the appearance of some of these close to the major target peak in HILIC prompted us to test other conditions for the deprotection reaction. The effect of the ammonium halide used was investigated by using TEACl, TMABr, and BnTMACl in DMF at 120 °C for cleavage of the neopentyl ester. TMABr led to the highest degree of byproduct formation. TEACl gave slightly better results than TMACl. TEACl was then used in another set of experiments to investigate the effects of the solvent on byproduct formation. DMF, N,N-dimethylacetamide (DMA), formamide and DMSO were used. The reactions were done at 100 °C except for DMSO which was done at 120 °C. DMA gave the most byproducts while DMSO, despite the higher temperature, led to the cleanest results. The DMSO reaction mixture was further subjected to a longer reaction time at 120 °C after deprotection was complete to see how the system behaved under thermal stress. These experiments resulted in the formation of an unknown byproduct which underlined the importance of close monitoring of the deprotection reaction. Cleavage under basic conditions (TBAOH) and use of an inorganic halide both gave good results but were not better than the TEACl-DMSO system. A summary of the deprotection experiments is shown in Figure 3.23.

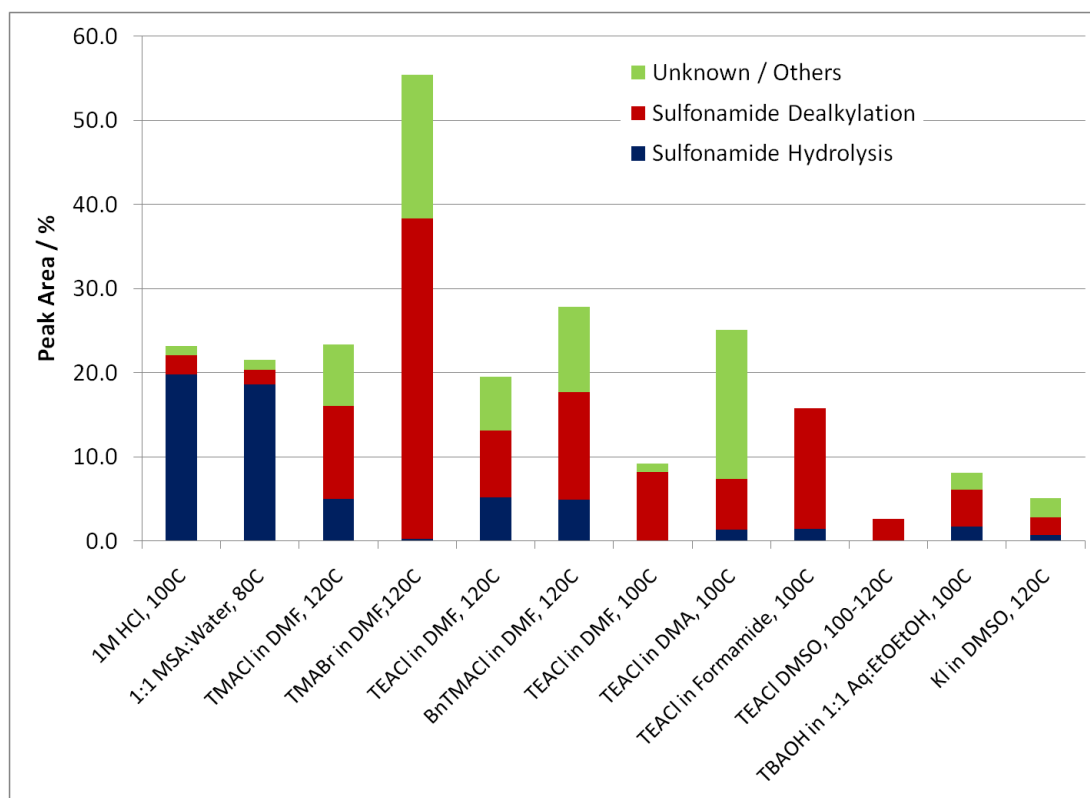


Figure 3.23. Summary of the degree of byproduct formation for different conditions used for the cleavage of the neopentyl sulfonate esters of **21**.

The best condition above was then used to remove the neopentyl protecting group from tris sulfonamide **29** as shown in Figure 3.24. The hope was that the results for test compound **21** can be translated to the actual fluorophore. HILIC monitoring of the cleavage of the neopentyl sulfonate ester of **29** does show minimal formation of byproducts (Figure 3.25). Since the deprotection reaction was very well behaved, the peak areas of the 15-minute, 60-minute and 2.4-hour samples were used to predict the time required to complete the reaction. The total area of the intact individual neopentyl

esters was determined by multiplying the peak area of the remaining starting compound **29** by a factor of 3, that of the mono-deprotected intermediate by 2, and that of the bis-deprotected intermediate by 1. These values were then added together and taken as the total area of the intact individual neopentyl ester, A_{neop} . The total area of the free individual sulfonic acids was calculated the same way but in reverse where the peak area of product **32** was multiplied by 3, that of the bis-deprotected by 2 and that of the mono-deprotected by 3. These were then added together to get the total area of the free individual sulfonic acid, A_{sulfo} . The percent area of intact individual neopentyl ester was calculated by taking the percentage of A_{neop} over the sum of A_{neop} and A_{sulfo} . The percentage of the intact neopentyl esters was then plotted against reaction time as shown in Figure 3.26. Assuming that the deprotection is a first-order reaction dependent only on the concentration of the neopentyl esters, the plot was fitted with an exponential decay curve and the resulting equation of the fitted line was used to predict the completion time of the reaction. The time at which the degree of deprotection was 99% was calculated to be at 252 min. therefore, the deprotection reaction was stopped after 4 hours (240 min) of total reaction time to minimize byproduct formation. This prediction was corroborated by the HPLC analysis of the 4-hour sample (Figure 3.25) which showed that the deprotection reaction was indeed complete.

After the deprotection step the methyl ester of compound **32** was hydrolyzed under basic conditions to form the carboxylic acid, tetra-anionic **33**. Figure 3.27 shows that hydrolysis was complete after 10 minutes in 0.1M NaOH at room temperature.

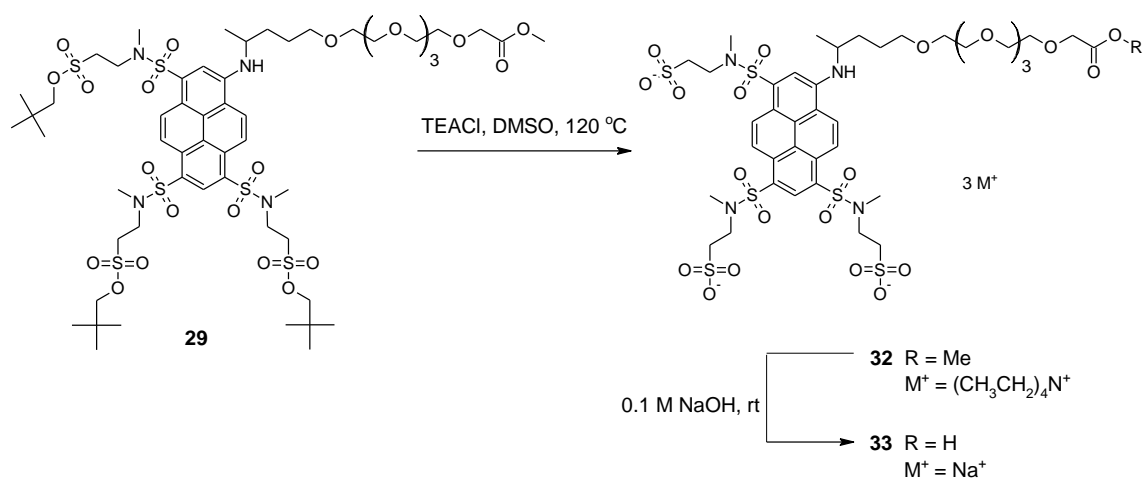


Figure 3.24. Deprotection of tris neopentyl sulfonate ester **29** to produce fully deprotected sulfonate **22**.

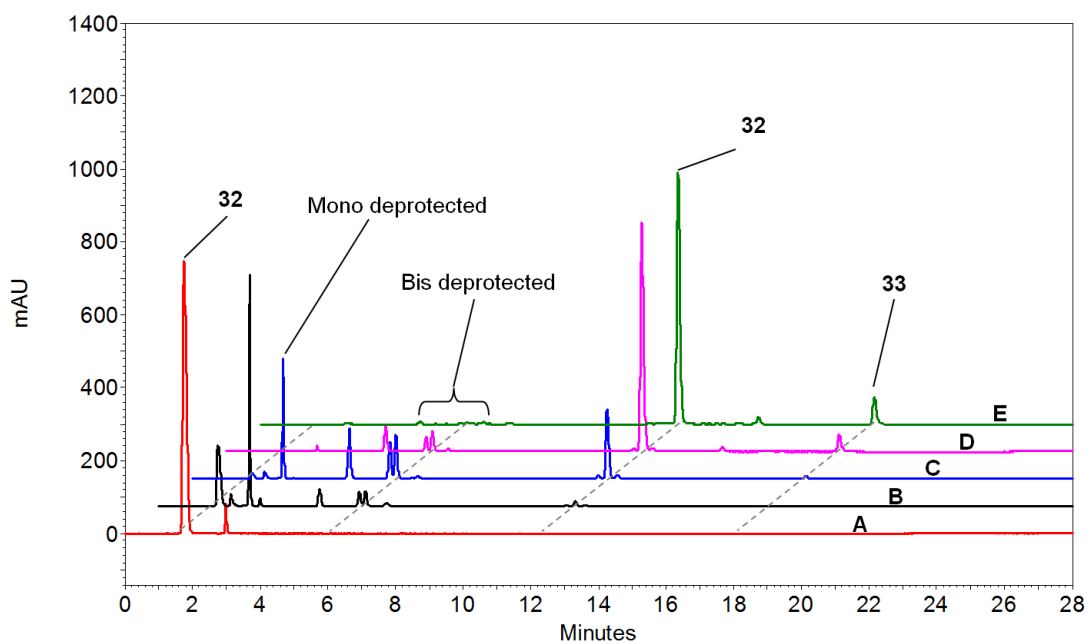


Figure 3.25. HILIC analysis of the deprotection of tris neopentyl sulfonate ester **29** using TEACl in DMSO at 120 °C at 0 min (A), 15 min (B), 60 min (C), 2.4 h (D) and 4 h (E) reaction times.

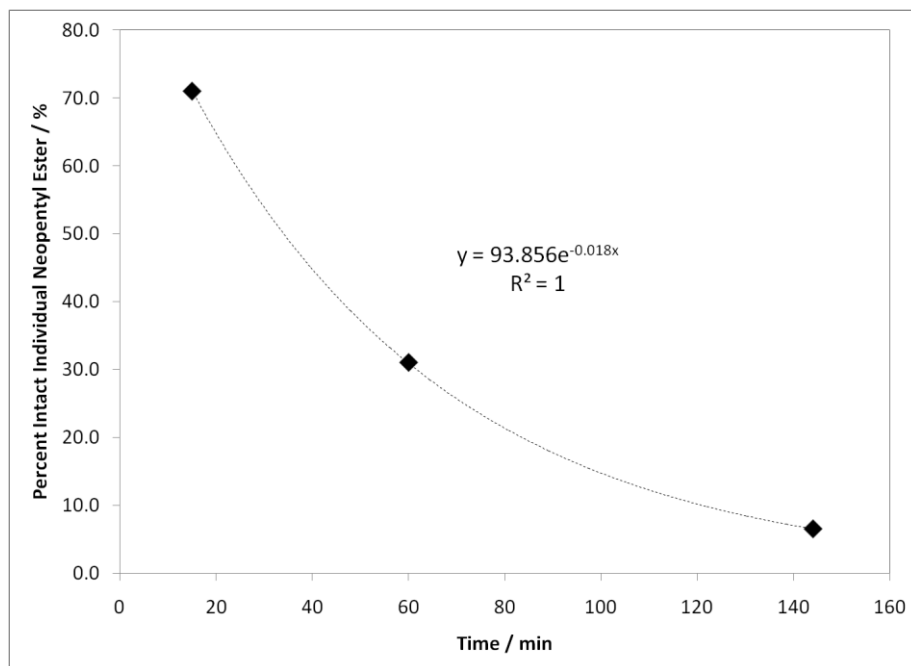


Figure 3.26. Plot of the percent of the intact neopentyl esters as a function of reaction time (♦). The equation of the fitted exponential decay curve (...) was used to predict the completion time of the reaction.

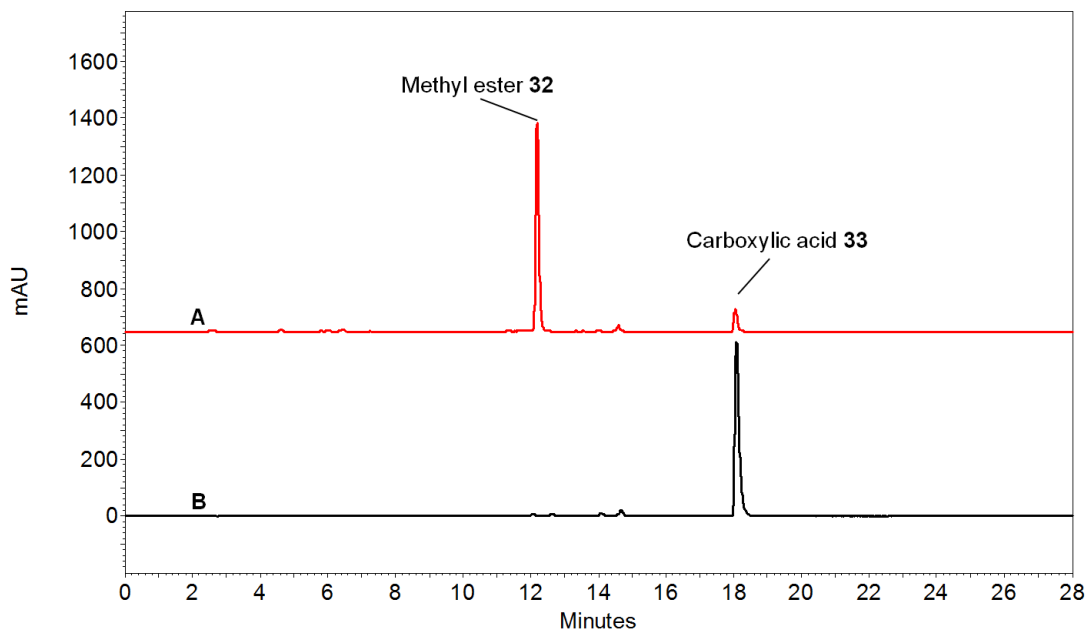


Figure 3.27. HILIC analysis of methyl ester **32** (A) and a 10-minute sample of its hydrolysis to carboxylic acid **33** using 0.1M NaOH at room temperature (B).

3.4.3.2 Purification of Sulfonic Acid **33** by Semi-prep HILIC

The first and obvious bottleneck in the semi-prep HILIC of tetra-anion **33** was its efficient loading into the column. In preparative chromatography, the sample must be loaded in a solvent that is weaker than the eluent to prevent unnecessary peak broadening. In the HILIC system used, the initial eluent contains 90 to 100% ACN. The amount of the tetra-anionic material that can be dissolved in this solvent is very small, consequently prohibitively large sample volumes would have to be injected to achieve the desired sample loads.

To investigate this problem, tri-anionic compound **22** was used as test compound.

Figure 3.28 is an overlay of the semi-prep HILIC runs obtained with a Luna HILIC 150 mm x 4.6 mm column for compound **22**. The 5-mg sample had to be loaded in a 10-mL

volume due to limited solubility of the highly ionic target in the run eluent (~95% ACN). The step gradient for the 5-mg sample had to be delayed until all of the sample volume was injected into the column adding an additional 10 minutes of elution time for the target peak in (C) lowering throughput. A 2.5-mg sample in a 50 μ L volume of pure aqueous solvent was also loaded to see if peak resolution could be maintained without the large sample volume. The peak shape was severely fronting (Figure 3.27, trace D) and eliminated altogether the resolution between the target and the early eluting impurities.

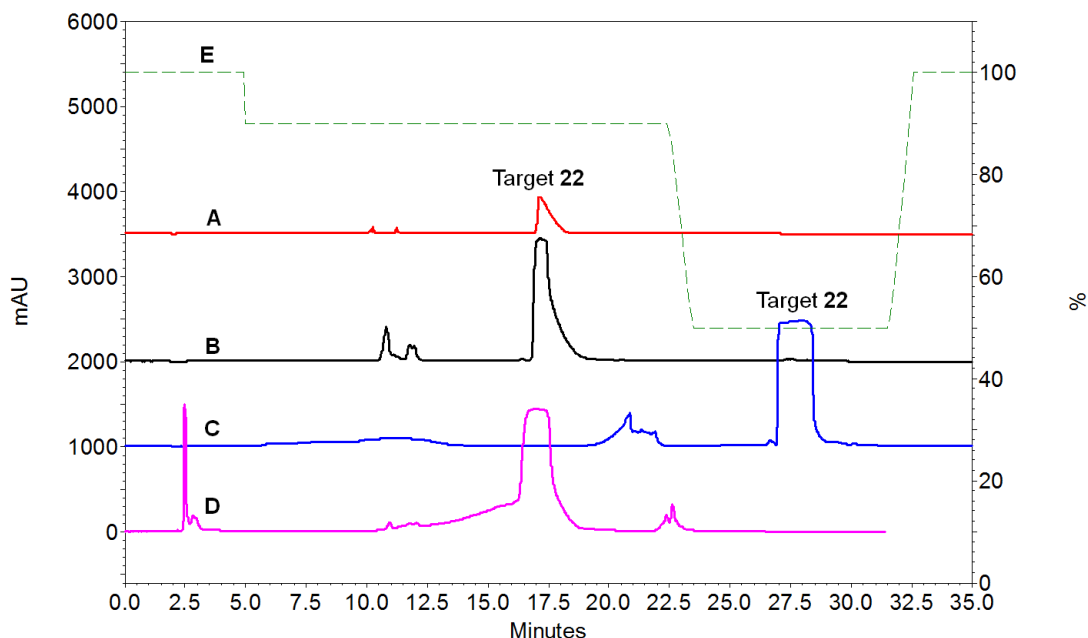


Figure 3.28. Semi-prep tests with a Luna HILIC 150 mm x 4.6 mm column. The amount and volume of the sample loaded were: 0.1 mg **22** in 0.2 mL mobile phase (A), 1 mg **22** in 2 mL mobile phase (B), 5 mg **22** in 10 mL mobile phase (C) and 2.5 mg **22** in 50 μ L water (D). The mobile phase composition (E) is in % B (A: 10 mM NH_4HCO_2 in water; B: 10 mM NH_4HCO_2 in ACN). Flow rate was 1 mL/min. The flat peak tops are due to detector signal overrange.

To go around this problem, Neue et al. developed a technique that allows the loading of samples which were dissolved in stronger solvent by diluting them at-column [58]. However, this required the use of an additional HPLC pump and reconfiguration of the HPLC plumbing. A simpler technique was developed to allow maximum loading of a sample prepared in a strong solvent without the need for additional equipment. The idea was to partially fill a sample loop with a plug of the sample in one end and then dilute the plug in-line with the eluent along the length of the loop during injection through Taylor dispersion. The extent of dilution increases with increasing I.D. and length of the sample loop. In the semi-prep HILIC experiments reported here, a 2.0-mL and a 5-mL sample loop, both with a nominal I.D. of 1 mm, were found to be sufficient to effect dilution for a 4.6 mm and 10.0 mm I.D. column, respectively. The sample loop was configured as shown in Figure 3.18 in the Materials and Methods section.

A comparison of a semi-prep HILIC separation of 5 mg **22** dissolved in 10 mL mobile phase and 5 mg **22** dissolved in 50 μ L water is shown in Figure 3.29. The latter was injected in Taylor dilution mode using a 2.0-mL sample loop. Both runs appear similar, except for the longer elution time for the 10-mL sample. However, a closer look at the impurities (Figure 3.29, inset) reveals that the 50 μ L injection with Taylor dilution had much better defined impurity peaks (i.e., these peaks were less broadened and thus better resolved from the target peak).

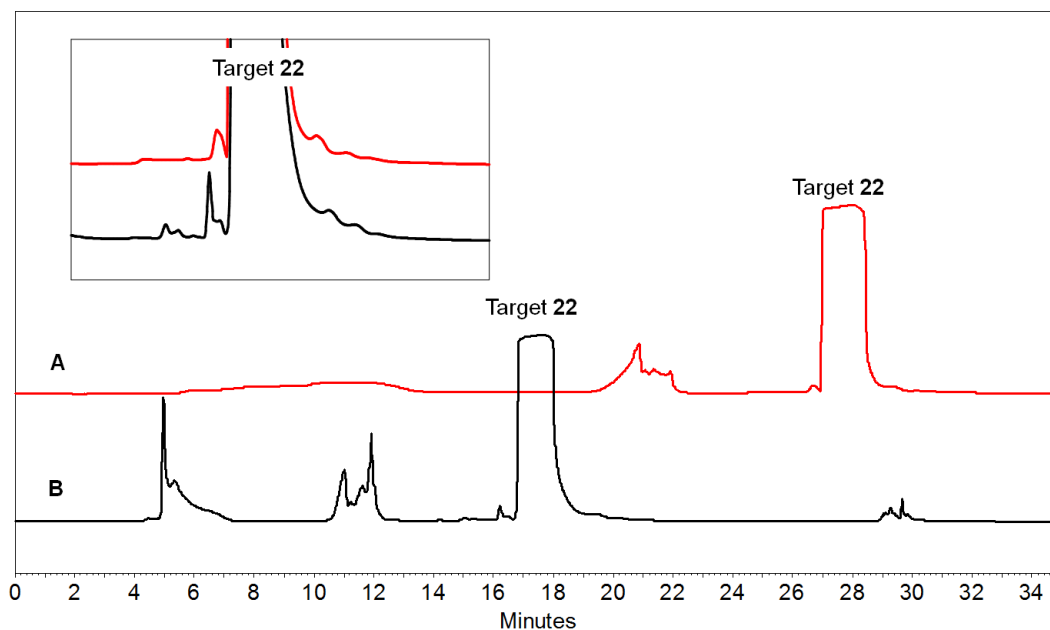


Figure 3.29. Semi-prep HILIC separation of 5 mg **22** dissolved in 10-mL mobile phase injected using conventional sample injection (A) and 5 mg **22** dissolved in 50- μ L water injected using the Taylor dilution-mediated injection technique (B). In the inset, the target peaks are manually aligned and expanded.

The Taylor dilution-mediated injection technique was then applied with a 10.0 mm I.D. HILIC column using a 5.0-mL sample loop. The sample injected was 45 mg **22** in 200 μ L water. Figure 3.30 shows a well defined target peak shape that is favorable for fractionation. An early eluting impurity peak is partially resolved (see inset). A conventional injection technique would have required the injection of a 90 mL sample, taking about 20 minutes.

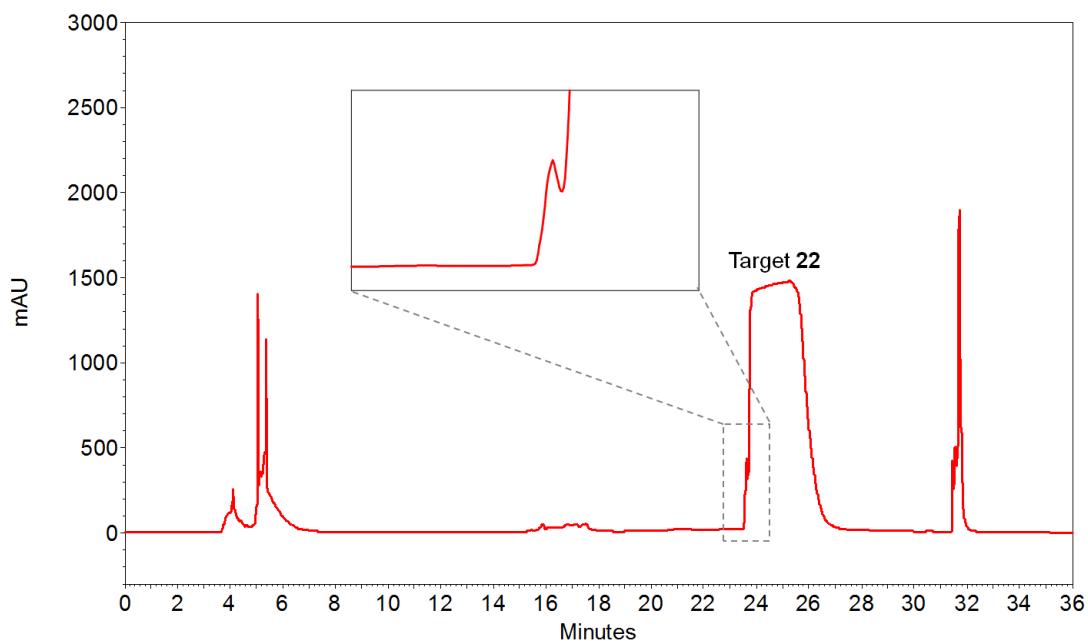


Figure 3.30. Semi-prep HILIC separation of 45 mg **22** dissolved in 200 μL water using Taylor dilution-mediated injection. Inset: expanded view of the front end of the target peak showing a partially resolved impurity peak.

Compound **33** was purified using semi-prep HILIC. To facilitate the removal of the buffer component from the target after fractionation, sodium trifluoroacetate (NaTFA) was used in place of ammonium formate in the HILIC eluent. Since NaTFA is soluble in ACN and the sodium salt of **33** is not, a simple precipitation from ACN can recover the target from the fractions. Figure 3.31 shows a semi-prep HILIC separation of 50 mg **33** dissolved in 200 μL water. Because the peaks were well defined, fractionation of the target peak was facile. The inset shows improvement in the purity of the target from 89% (crude) to 99.7% (fractionated material).

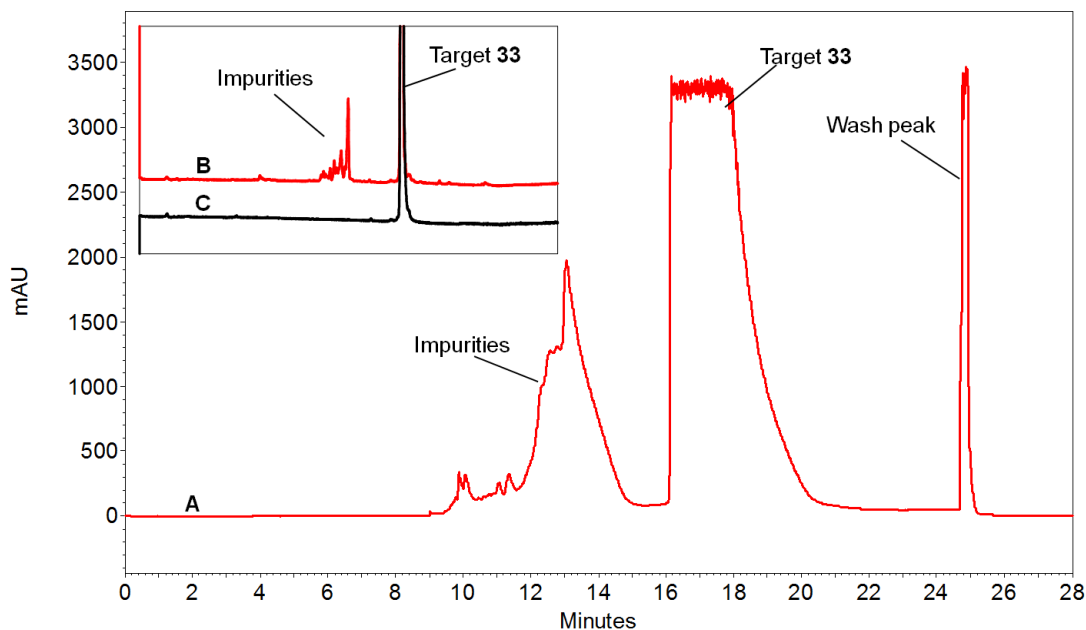


Figure 3.31. Semi-prep HILIC separation of **33** (A). Inset shows the analytical HILIC separation of the crude (B) and the fractionated material (C). The target peaks are normalized.

3.5 Spectral Properties

3.5.1 Background and Objectives

Fluorophore **33** was designed to have an $\lambda_{\text{max}}^{\text{em}}$ that is compatible with the 488 nm line of the Argon ion laser. It was also developed to have pH-independent fluorescence properties which are important for CE applications. The fluorescence spectra of **33** were recorded in aqueous buffers having different pH values in order to determine if pH had any influence on the fluorescence intensity and $\lambda_{\text{max}}^{\text{em}}$ of **33**. The molar absorbance and relative quantum yield values were also determined using Rhodamine 6G as a standard.

3.5.2 Materials and Methods

UV absorbance spectra were recorded using a Beckman 168 photodiode detector during the HILIC separations. The eluent compositions at the time of detection were 26 mM NH_4HCO_2 74% ACN/water for APTS, 24 mM NH_4HCO_2 76% ACN/water for trisulfonamide **22** and 10 mM MOPS with 5 mM NaOH in 76% ACN/water for **33**.

Fluorescence spectra at different pH values were recorded on a Shimadzu RF-5301PC spectrofluorometer. The buffers used are listed in Table 3.1 below:

Table 3.1. Buffers used in the fluorescence versus pH experiments for compound **33**.

pH	Composition	Ionic Strength
2.4	10.2 mM trifluoroacetic acid / 5mM NaOH	10
3.5	25 mM formic acid / 10 mM LiOH	10
4.1	50 mM acetic acid / 10 mM BisTris	10
5.5	50 mM MES / 10 mM LiOH	10
7.1	20 mM MOPS / 10mM LiOH	10
8.0	13 mM HEPES / 10 mM LiOH	10
9.0	50 mM boric acid / 20 mM NaOH	20
10.0	25 mM N,N-diethylethanolamine / 10 mM formic acid	10
11.2	30 mM piperidine / 7 mM acetic acid	10

UV absorbance and fluorescence spectra for the quantum yield determinations were acquired using a Varian 100 Bio UV-Vis spectrophotometer and a Varian Cary Eclipse fluorescence spectrometer, respectively. The samples were dissolved in a pH 9 0.1M aqueous sodium bicarbonate buffer.

3.5.3 Results and Discussion

The UV absorbance spectra of fluorophore **33**, APTS (starting material) and **22** (trisulfonamide intermediate) are overlaid in Figure 3.32. As anticipated, $\lambda_{\text{max}}^{\text{ex}}$ of the fluorophore increased with each modification of the functional groups on the pyrene ring. Sulfonamidation and alkylation increased $\lambda_{\text{max}}^{\text{ex}}$ to 502 nm. About 91% of the maximum molar absorbance can be harnessed at 488 nm

The fluorescence emission spectra of fluorophore **33** are virtually the same across the pH range as indicated in Figure 3.33. Moreover, $\lambda_{\text{max}}^{\text{em}}$ is constant at 559 nm across the entire pH range. Fluorescent intensity in the spectrum taken at pH 10 is slightly lower than in the ones at the neighboring pH values and may have been caused by a matrix effect that was specific for the buffer that was used.

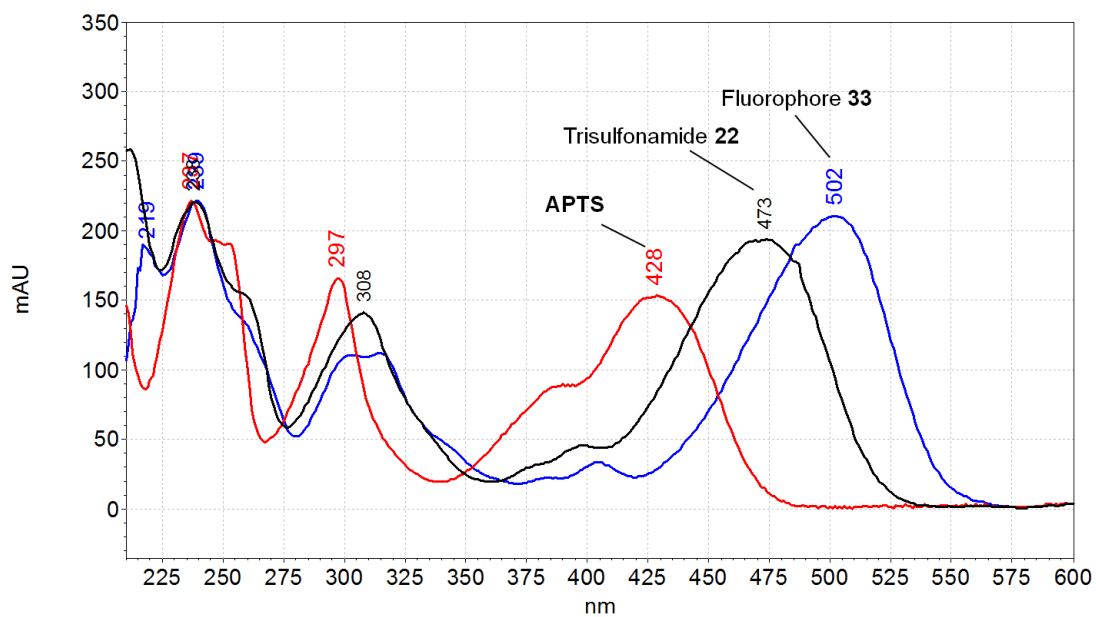


Figure 3.32. Overlay of the UV absorbance spectra of APTS, trisulfonamide **22** and alkylated trisulfonamide fluorophore **33**.

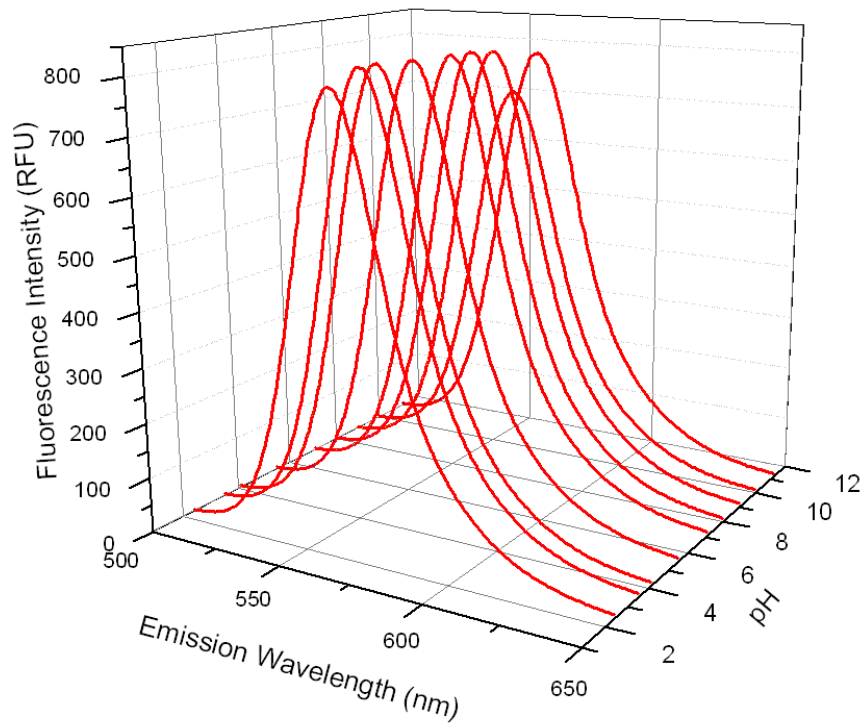


Figure 3.33. Fluorescence spectra of fluorophore **33** at different pH values.

The molar absorbance of fluorophore **33** at 510 nm, ϵ^{510nm} , was determined as shown in Figure 3.34 yielding a ϵ^{510nm} of about 32,000 $\text{cm}^{-1}\text{M}^{-1}$. The relative fluorescence quantum yield was also determined with Rhodamine 6G as standard (Figure 3.35) using equation 2.1 in Chapter 2. The relative quantum yield is 0.74 which is typical for pyrene-based fluorophores.

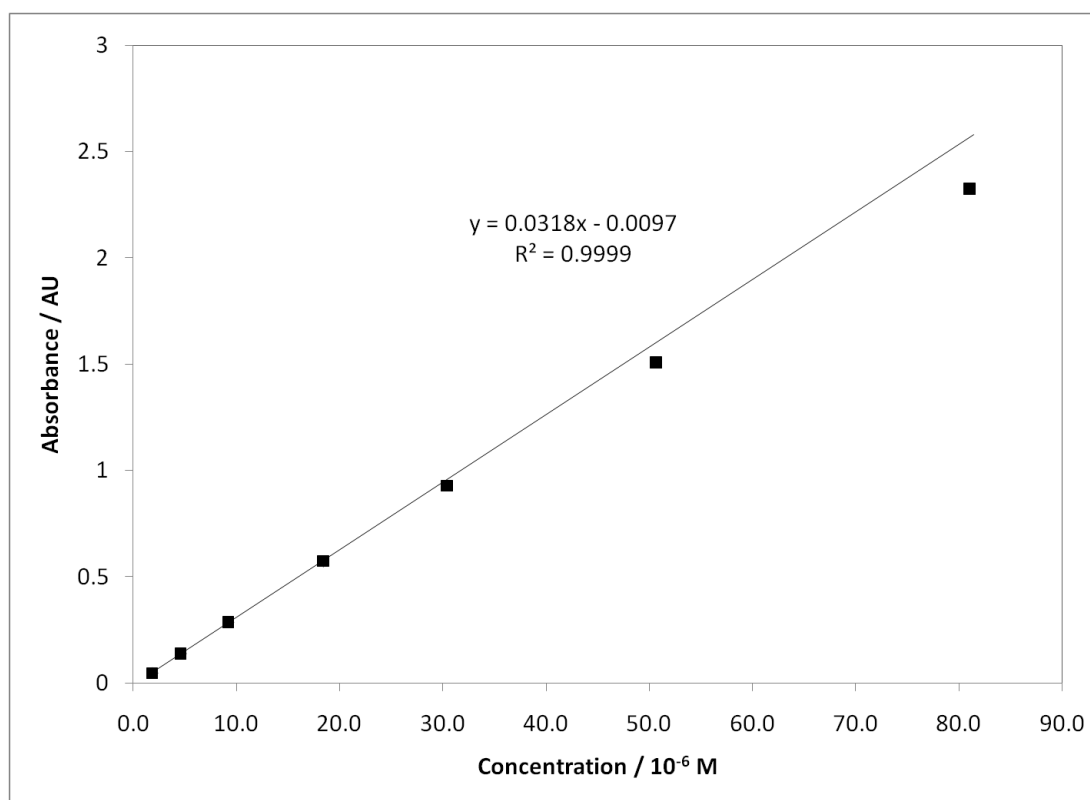


Figure 3.34. UV absorbance at 510 nm as a function of the concentration of fluorophore **33**.

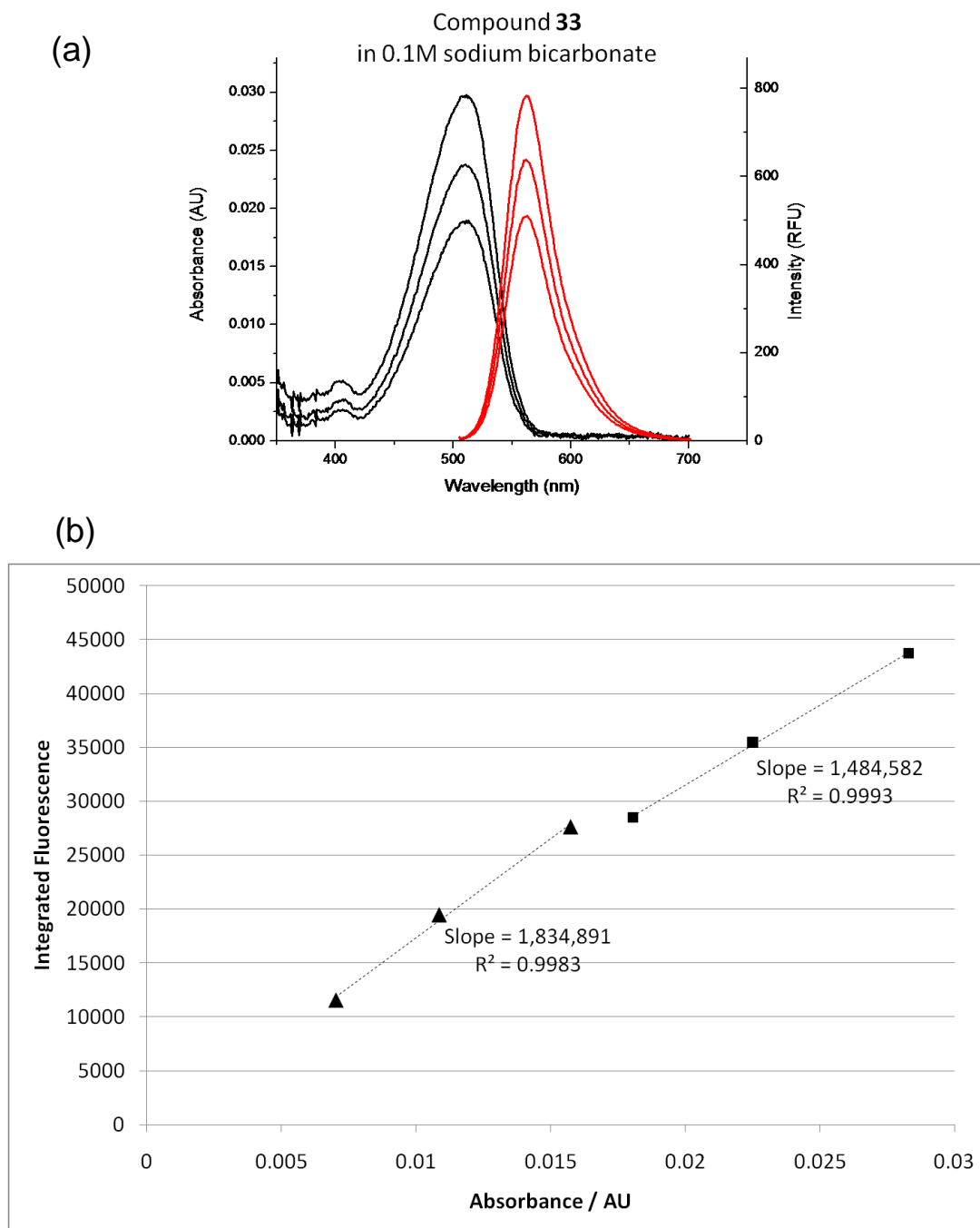


Figure 3.35. Relative fluorescence quantum yield determination for fluorophore **33** using Rhodamine 6G as standard. (a) UV absorbance and their respective fluorescence emission spectra at different concentrations. (b) Plot of integrated fluorescence emission of fluorophore **33** (▲) and Rhodamine 6G (■) as a function of UV absorbance.

3.6 Fluorescence Labeling Tests with the Pyrene-based Label

3.6.1 Background and Objectives

The utility of the fluorescent label in free zone capillary electrophoresis (CZE) had to be investigated. Small amines, 4-(2-aminoethyl)morpholine and N-methylpiperazine were labeled and analyzed by CZE in different pH BGEs to determine the effect of the latter on the fluorescence of the label.

Proteins of different sizes were also labeled and separated by SDS-CGE. The effect of labeling on the migration time of the proteins through the sieving matrix was investigated.

3.6.2 Materials and Methods

Pentafluorophenyl trifluoroacetate, 4-(2-aminoethyl)morpholine, N-methylpiperazine, polyvinylpyrrolidone (360 kDa), α -lactalbumin (Type III: calcium depleted from bovine milk, 85%), carbonic anhydrase (from bovine erythrocytes), chicken egg ovalbumin and bovine serum albumin were all purchased from Sigma Aldrich. SDSMW kits for the SDS-CGE separation of proteins were provided by Beckman Coulter. Ultrafree[®]-MC (10,000 NMWL, Biomax-10) centrifugal filter units were acquired from Millipore.

CE separations were completed in a PA800 system with a 488 nm argon ion LIF detector.

3.6.2.1 Activation of Fluorophore **33** as a Pentafluorophenyl Ester

7 μL of pentafluorophenyl trifluoroacetate, 385 μL anhydrous DMF and 11.5 μL triethylamine were mixed in a 1.5-mL Eppendorf tube. The mixture was immediately added to 10 mg of fluorophore **33**. After 2.5 hours at room temperature, MTBE was added, the slurry was centrifuged and the solids were washed with THF. The residue was dissolved in 100 μL DMSO and used as-is as an amine-reactive fluorescent labeling reagent.

3.6.2.2 Labeling of Small Diamines

A diamine sample containing 1 mM each of 4-(2-aminoethyl)morpholine and N-methylpiperazine in a buffer made from 50 mM boric acid and 20 mM sodium hydroxide was prepared. A 2 μL portion of the activated fluorophore solution in DMSO was added to 40 μL of the diamine mixture and allowed to react at room temperature for 30 minutes. The reaction mixture was then quenched with 3.2 μL of 0.25 M taurine in 0.1 M sodium hydroxide solution and allowed to stand for 5 minutes. The mixture was then analyzed by CE-LIF by diluting a 0.5 μL aliquot with 50 μL of 1:3 mixture of BGE:water.

3.6.2.3 CE-LIF of Small Diamines

CE-LIF was carried out in a fused silica capillary (50 μm I.D / 360 μm O.D; 20.35 cm / 30.39 cm inlet-to-detector length / total length) having a semi-permanent internal

coating. The new capillary was first preconditioned by flushing, sequentially, with water for 2 min, 0.1M NaOH for 3 min, 0.1M HCl for 3 min, water for 3 min, a 2% polyvinylpyrrolidone (360 kDa PVP) solution in water for 2 min and background electrolyte (BGE) for 1 min. All rinses were done at a pressure of 50 psi. The inlet and outlet of the capillary were then immersed in the BGE vials and a potential of 20 kV (negative-to-positive polarity) was applied for 10 min. Before each CE separation, the capillary was sequentially rinsed with water for 0.5 min, the 2% PVP solution for 1 min and the BGE for another 1 min, all at 50 psi. The sample was then injected by pressure at 0.5 psi for 3 sec and separated by applying 20 kV (negative-to-positive polarity).

The BGEs used for the CE separations are shown in Table 3.2.

Table 3.2. Background electrolytes used for the CE analysis of small diamines.

pH	Composition	Ionic Strength
2.4	10.2 mM trifluoroacetic acid / 5mM NaOH	10
4.1	50 mM acetic acid / 10 mM BisTris	10
6.1	20 mM histidine / 10mM propionic acid	10
7.1	20 mM MOPS / 10 mM LiOH	10
8.0	13 mM HEPES / 10 mM LiOH	10
10.0	13 mM CHES / 10 mM formic acid	10

3.6.2.4 Labeling of Proteins for SDS-CGE-LIF

A 50 μL portion of each 5 mg/mL protein solution in 0.1M sodium carbonate/bicarbonate buffer (pH 9) was added to the necessary amount of activated fluorophore. 1:1 and 10:1 tag-to-protein labeling ratios were tried. The labeling reactions were allowed to proceed for 20 min at room temperature. A 20 μL aliquot of each of the labeled protein mixture was then loaded into a 10,000 NMWL centrifugal filter unit followed by 200 μL of 0.1M sodium bicarbonate buffer. The units were centrifuged until approximately 10 to 20 μL of solution was left. This process of dilution and centrifugation was repeated twice for the 1:1 tag-to-protein labeling reactions and 5 times for the 10:1 tag-to-protein labeling reactions. The final protein solutions retained above the membrane were diluted with 100 μL of Beckman SDSMW sample buffer, mixed with 5 μL 2-mercaptoethanol and heated at 100 $^{\circ}\text{C}$ in a closed vial for 3 minutes. The solutions were cooled to room temperature and analyzed by SDS-CGE by diluting a 2 μL portion with a 100 μL aliquot of Beckman SDSMW run buffer.

SDS-CGE was carried out using the Beckman SDSMW protocol and the 488 nm LIF detector. The run details are the same as those in section 2.3.2.2.

3.6.3 Results and Discussion

Labeling of the small diamines produced the expected labeled species without the formation of byproducts. The labeled diamines were analyzed in different BGEs having pH values that were evenly spread across the operating pH range of CE. Separations

were obtained with negative-to-positive polarity in a capillary that had a semi-permanent coating to suppress electroosmotic flow. Of all the components, hydrolyzed fluorophore **33** is expected to have the highest anionic mobility at any pH due to its smallest size and highest anionic charge. This is evident in Figure 3.36 where the electropherograms of the same labeled diamine sample obtained at different pH values are overlaid. It is also clear from these electropherograms that the fluorescence signal stays basically the same across the pH range, irrespectively of the components of the BGE. The relative peak areas of the hydrolyzed fluorophore and the labeled diamines stay almost the same for all the runs (53 ± 1.5 and 47 ± 1.5). The pH scan was used to determine the approximate optimum pH for the separation of the diamines (marked with *). The diamines have good separation selectivity at pH 6.1 and 8.0 ($\alpha_{\text{pH}6.1} = 1.05$, $\alpha_{\text{pH}8.0} = 1.03$) but co-migrate outside this pH range. An intermediate pH of around 7 may therefore provide the optimum selectivity.

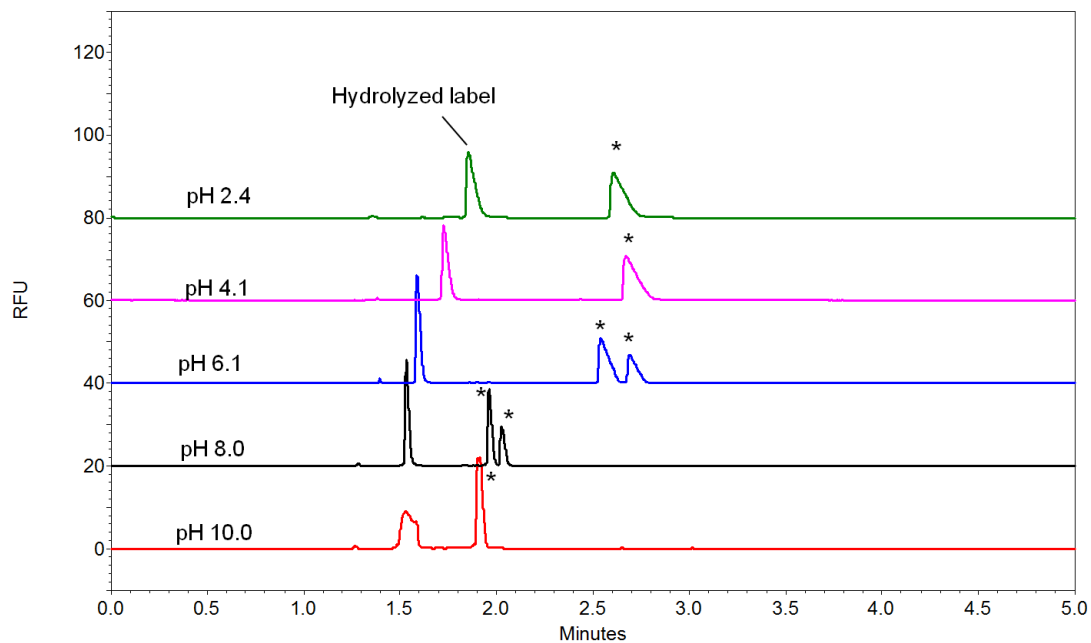


Figure 3.36. CE-LIF of labeled 4-(2-aminoethyl)morpholine and N-methylpiperazine (both marked with *) at different pH values.

At pH 7.1, separation selectivity for the labeled diamines is as high as $\alpha_{\text{pH}7.1} = 1.11$.

(Figure 3.37). The calculated $\text{LOD}_{S/N=3}$ for the labeled AEM is about 5 nM. For an injected volume of about 5 nL, the loaded amount of the analyte is in the low attomolar range.

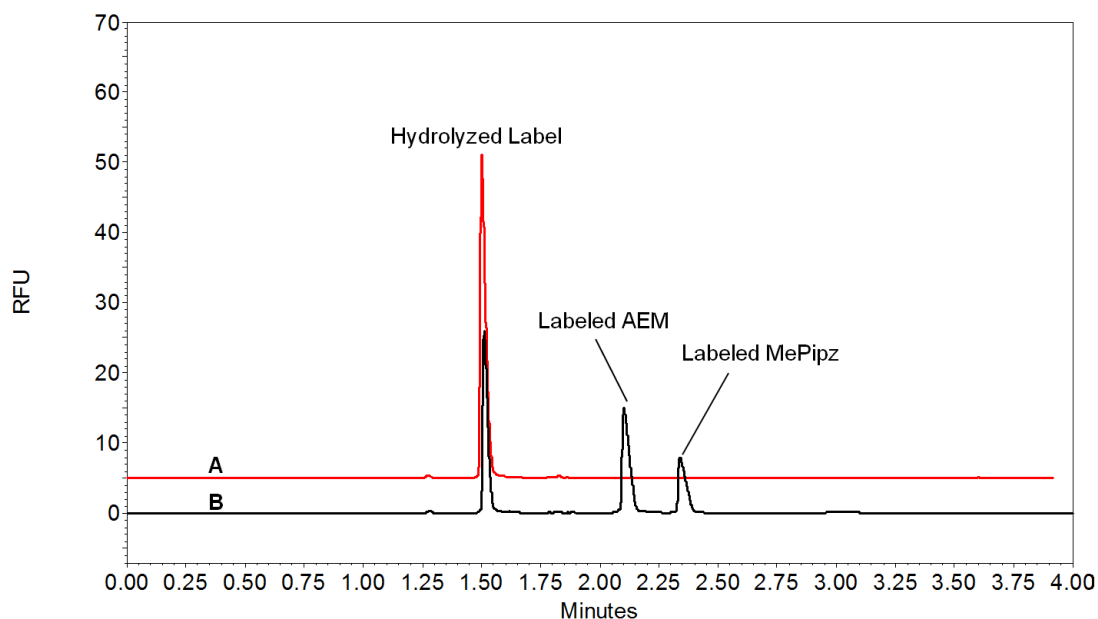


Figure 3.37. CE-LIF of a blank labeling reaction (A) and the labeled diamine mixture (B) at pH 7.1.

Proteins α -lactalbumin, carbonic anhydrase, chicken ovalbumin and bovine serum albumin were also labeled with the PFP activated fluorophore. Individual protein labeling reactions at both 1:1 and 10:1 tag-to-protein ratios (mol : mol) were carried out. The electropherograms of the labeled proteins obtained by SDS-CGE-LIF analysis are overlaid in Figure 3.38 showing the expected migration order for the proteins. The electropherogram of a sample containing each of the labeled proteins is shown in Figure 3.39. The logarithm of protein molecular weight ($\log MW$) was plotted against their corresponding migration times (T_m) in Figure 3.40 showing the expected linear correlation between $\log MW$ and T_m . This suggests that the migration behavior of the labeled proteins was not adversely affected when the tag-to-protein labeling ratio was 1:1.

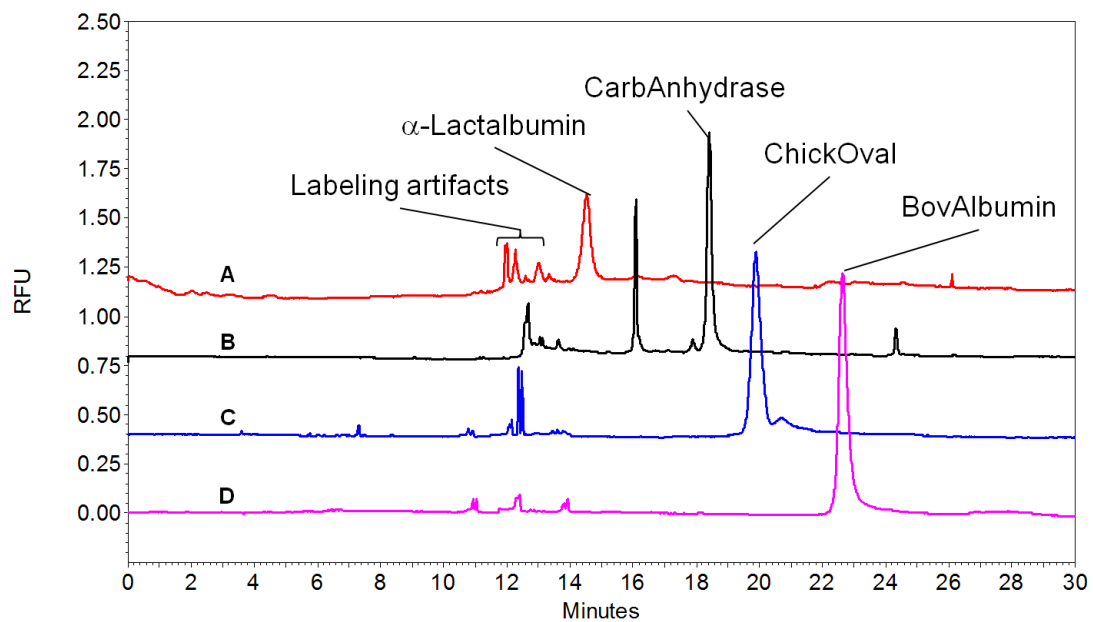


Figure 3.38. SDS-CGE analysis of labeled proteins: α -lactalbumin (A), carbonic anhydrase (B), chicken ovalbumin (C) and bovine serum albumin (D).

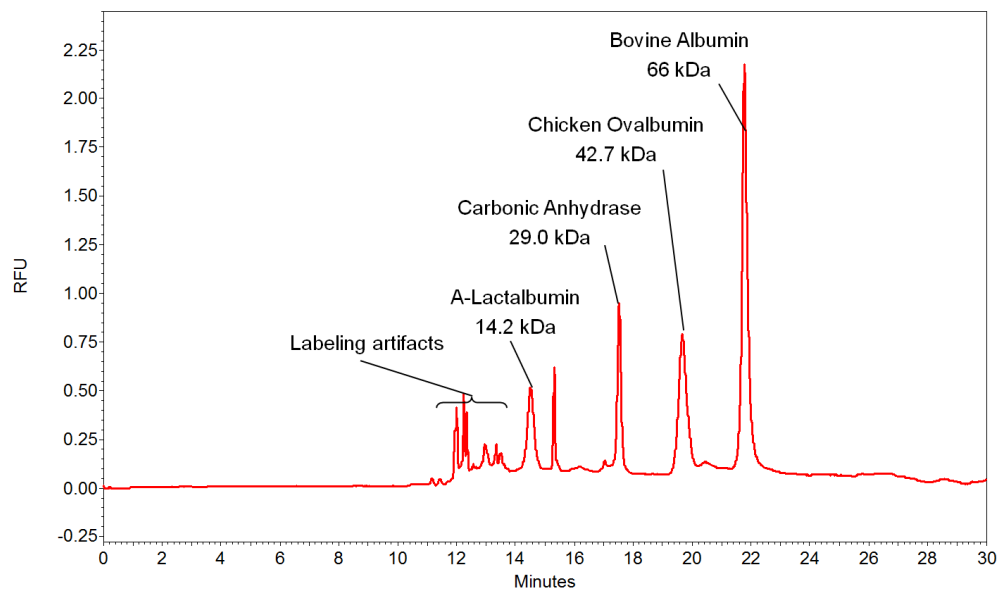


Figure 3.39. SDS-CGE of a mixture of proteins individually labeled at a tag-to-protein ratio of 1:1.

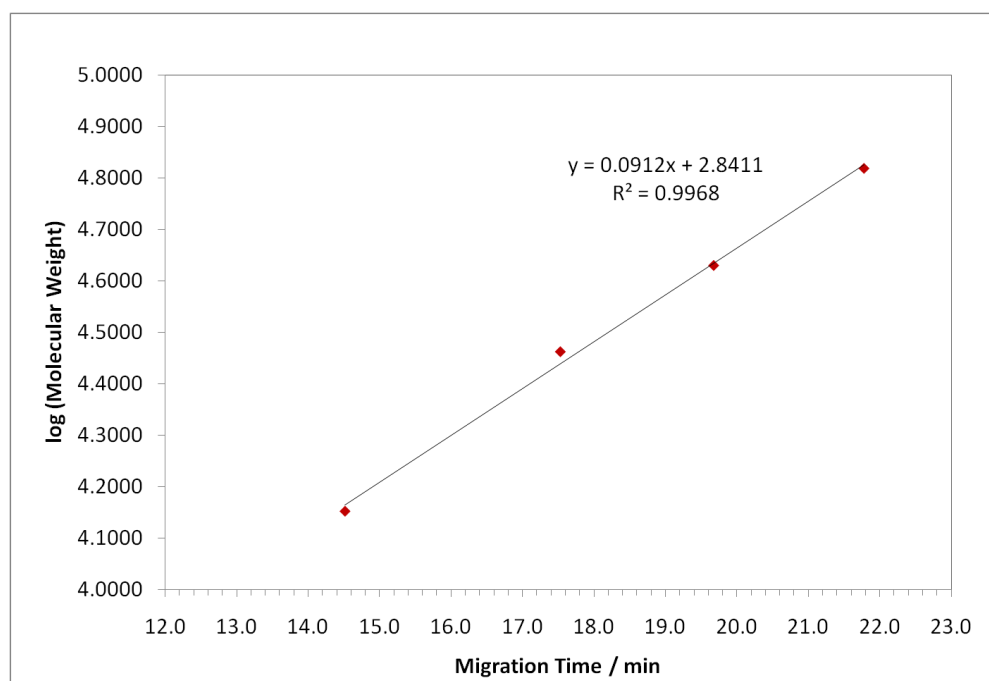


Figure 3.40. Plot of the logarithm of protein molecular weight as a function of the migration time of the proteins labeled at a 1:1 tag-to-protein ratio.

Increasing the tag-to-protein ratio in the labeling reaction can increase the response factor for the proteins. Therefore, labeling reactions at a 10:1 ratio were also attempted. A mixture of these labeled proteins was prepared and analyzed by SDS-CGE-LIF (Figure 3.41). The response factors increased for every protein, although at different rates. The $LOD_{S/N=3}$ values for the 1:1 labeling ratio were between 80 to 140 ng/mL except for α -lactalbumin which was about 1 μ g/mL. For the 10:1 labeling ratio, the $LOD_{S/N=3}$ values were between 20 to 40 ng/mL

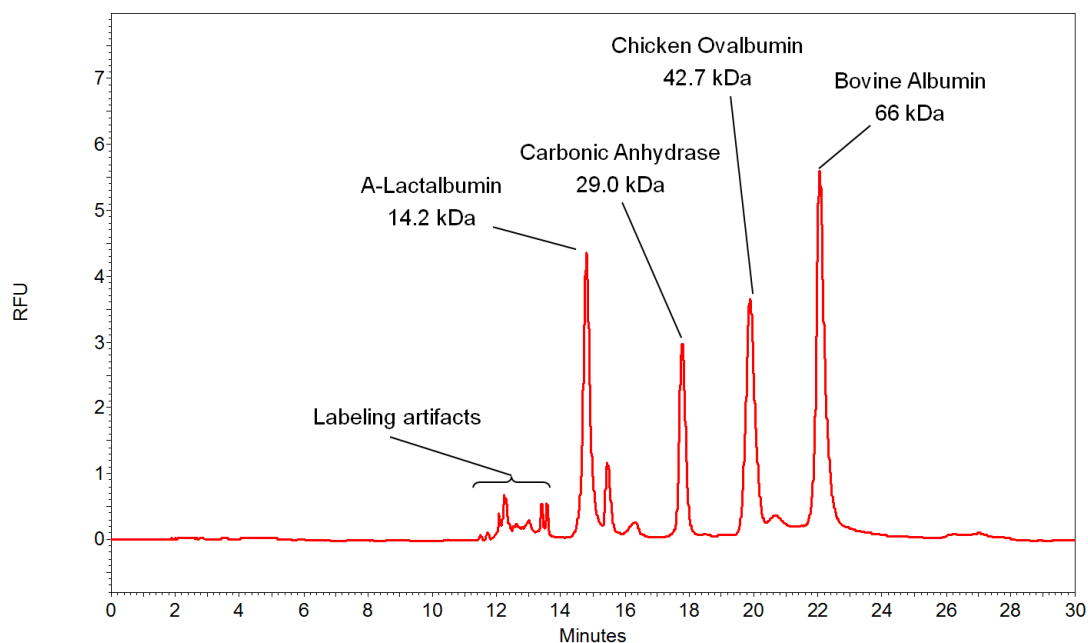


Figure 3.41. SDS-CGE of a mixture of proteins individually labeled at a tag-to-protein ratio of 10:1.

LogMW and T_m from the above SDS-CGE separations were then plotted to see if the higher label incorporation rates had any effect on protein migration. Figure 3.42 shows

that at this higher label-to-protein ratio the plot is still linear. The slope and y-intercept values for both the 1:1 and 10:1 labeling ratios are almost the same.

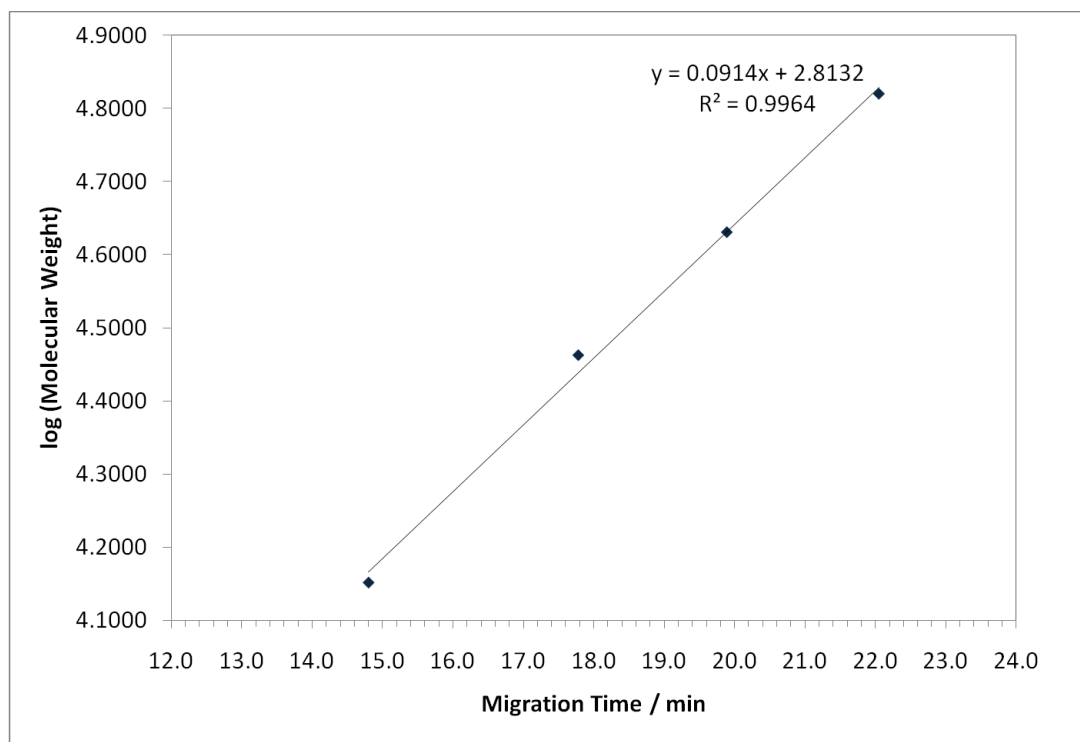


Figure 3.42. Plot of the logarithm of protein molecular weight as a function of protein migration time for proteins labeled at a 10:1 tag-to-protein ratio.

3.7 Concluding Remarks

A fluorescent labeling reagent based on the pyrene core structure has been synthesized. The fluorophore was derived from APTS and its development consisted of red-shifting its $\lambda_{\text{max}}^{\text{ex}}$ from 425 nm to 502 nm through sulfonamidation and alkylation. During synthesis, efficient methods were developed for the reductive amination of very weak

amines, cleavage of the neopentyl sulfonate ester protecting groups and semi-preparative HILIC purification of highly anionic compounds.

The new fluorescent label has pH-independent electrophoretic mobilities and fluorescence properties with a fluorescence quantum yield that is typical if not better ($\Phi_{fluor33} 0.76$) than those observed for other pyrene derivatives. The new reagent was successfully applied for the labeling of small diamines affording low nanomolar LODs (corresponding to low attomolar amounts) in their CE-LIF separations at different pH values. The new fluorophore has also been successfully used to label proteins for SDS-CGE-LIF analysis. Labeling did not affect the migration behavior of the labeled proteins as shown by their linear logMW vs T_m plots. The calculated LODs for the labeled proteins were in the low ng/mL or low nanomolar range.

It is important to note that the LIF detection system used for the above experiments had a detection band pass filter centered at 520 nm. At this wavelength only about 5% of the maximum emission of the fluorophore can be harnessed. This means that the limits of detection attained can still be improved by an order of magnitude by using a detection filter centered at around 560 nm.

4. DEVELOPMENT OF SCALER (SIMULTANEOUS CAPTURE AND LABELING, EFFICIENT RELEASE) FLUORESCENT LABELING REAGENT

4.1 Introduction

4.1.1 General Scheme

The immobilization of enzymes [59-63] and derivatizing reagents [64, 65] on solid phases has been studied by several groups. The main motivation for doing these reactions on a solid phase was the observation that reactivity could be increased when the reagents were immobilized compared to when the same reactions were carried out in solution. Krenkova and coworkers immobilized trypsin and endoproteinase LysC on an acrylate-based monolithic support and used these to digest protein samples for protein identification using mass spectrometry [59, 63]. They found that the immobilized enzymes accomplished results within a few minutes similar to what took 24 hours at elevated temperatures when the proteolysis was done in free solution. They observed similar results when peptide-N-glycosidase was immobilized and used for protein deglycosylation [60]. Zare and others confirmed these observations for trypsin when they attached the enzyme to a silica-based monolith and obtained 2,000 times faster proteolysis rates than in free solution. The increased reaction rates were attributed to the high local concentrations of the enzyme on the solid surface. Also, for proteases, immobilization prevented auto-proteolysis, thus maintaining their activity for longer periods of time.

Krull *et al.*, reported on several solid phase reagents (SPR) that had immobilized reactive UV-absorbing or fluorescent labels which were designed to improve the UV or fluorescence detection of small molecules and proteins [64-67]. The labels were attached to solid supports through an analyte-reactive tether that cleaved off simultaneously with the derivatization reaction thus transferring the label from the solid surface to the analyte in the bulk solution. These solid phase reagents were found to have good thermal and aqueous stability, good derivatization efficiency, they provided low detection limits and had fewer interferences from the unreacted labels. Krull *et al.* also claimed that the increased reaction rates were due to the high local concentrations of the labeling reagents on the solid support.

A cartoon of the proposed general structure of the SCALER fluorescent labeling SPR is shown in Figure 4.1. The distinguishing feature of this SPR is that the core fluorophore is covalently anchored to the solid support and, in addition, has an independent analyte-reactive moiety. The SCALER system immobilizes the analyte the moment it is derivatized or labeled (thus, the name, *Simultaneous Capture and Labeling*). The anchor of the label has to be designed in such a manner that it can be severed efficiently under relatively mild conditions to release the label-analyte conjugate (thus, *Efficient Release*). To facilitate efficient removal of the labeled analyte from the spent solid phase, the latter must be designed with minimized mass transfer limitations. As in the previous chapters, the fluorophore and the analyte-reactive group are separated by a tether to minimize the effects of the analyte on the fluorescence of the fluorophore.

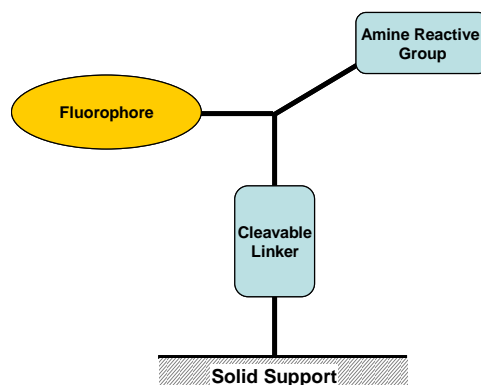


Figure 4.1. A cartoon of the proposed general structure of SCALER (Simultaneous Capture and Labeling, Efficient Release) solid phase reagent.

The general schematic of the labeling process with SCALER is presented in Figure 4.2. It starts by eluting the analyte (a protein is shown in the figure but the analyte can be any molecule with a derivatizable group) through the solid phase to allow contact with the reactive group that is attached to the label. The sample solution can be recirculated over the SPR in order to maximize conversion of the analyte to the labeled derivative. After this, the unreacted label is exhaustively reacted with a quenching compound. A cleaving agent is subsequently flushed through the solid phase to break the cleavable tether. The label-analyte conjugate is released into the bulk solution only at this point and can then be directly analyzed by CE or by any other applicable analytical method such as HPLC with UV, fluorescence or MS detection. The labeled analyte can also be used for biological studies after removal of the cleaving agent.

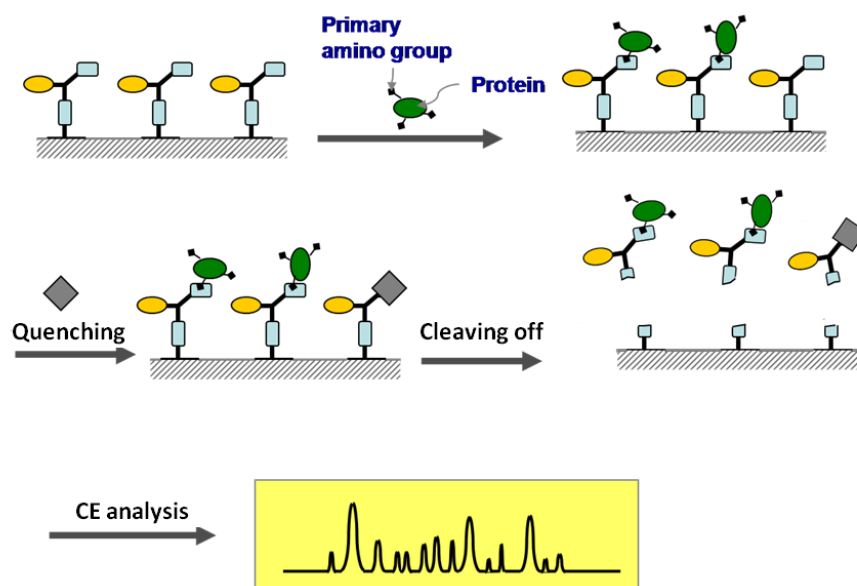


Figure 4.2. General schematic of the derivatization process using SCALER SPR for the fluorescent labeling of proteins.

4.1.2 Anticipated Advantages that are Specific to the Proposed SCALER Solid Phase Reagent

The first obvious benefit when using the above scheme is the *in situ* preconcentration of dilute samples during derivatization. Large sample volumes with low analyte concentrations can be eluted through the solid phase. During labeling, the analytes are pulled out of the bulk solution, into the much smaller volume of the solid support. After labeling, the tagged analytes can be cleaved off with a small volume of the concentrated cleaving agent, thus providing analyte enrichment.

Moreover, the simultaneous capture and labeling system will make the degree of analyte labeling more reproducible. When analytes having multiple reactive sites, such as proteins, are derivatized in solution phase, the number of labels incorporated into the analyte depends on the concentration of both reactants and the reaction time. Both the relative concentrations and the reaction time determine the probability of a collision between the analyte - whether unlabeled or already labeled - and a reactive label initiating the derivatization reaction. In the SCALER design, once the analyte is labeled and captured on the solid surface, it is prevented from reacting with a label from another part of the reaction space. The average number of labels attached to a certain analyte will now solely depend on the spacing of the reactive labels on the solid support surface and the number of active sites on the analyte.

If the distance between the anchored reactive labels is smaller than the gyration radius of the analyte, multiple labels will be attached to the analyte, but this will occur in a proportional manner. In this scenario, the incorporation rate depends on the number of active sites on the analyte *vis-à-vis* the surface density of the reactive label which will be the same for all SPR batches. Proportional multiple labeling in solution phase can only occur if labeling is done exhaustively, that is, when a large excess of the labeling reagent is used which does not have to be the case when using SCALER. For fluorescence detection, proportional multiple labeling using the SPR can give better quantitation than exhaustive derivatization because the former minimizes the possibility of fluorescence

self quenching. This is expected to result in reproducible response factors that are proportional to the number of reactive groups on the analyte.

However, if the distance between the anchored reactive labels (spacing) is larger than the gyration radius of the analytes, only mono-labeling can occur, no matter how many reactive sites the analytes carry. In solution phase, mono-labeling can only be achieved when the label-to-protein ratio is low [19]: this, unavoidably, leads to labeling only of a small portion of the analyte population. Because the number of reactive labels is limited, their attachment to – and distribution between - the analytes will depend on the respective reactivities of the latter. When done in the SPR format, mono-labeling is achieved even with an excess of reactive labels thereby producing an analyte population that is completely mono-labeled. Mono-labeling can be of high utility when pure standards of the analytes are not available to establish calibration curves, because mono-labeling leads to relative response factors that are more indicative of the molar ratios of the analytes. For proteins and other biological compounds, mono-labeling can be useful in biological assays because this can give optimal quantitation with a minimal change of the analyte structure.

4.1.3 General Objectives

The SCALER SPR will consist of at least three parts that will have to be designed and developed. The fluorophore that has been developed in Chapter 3 (fluorophore **33**) will be used in a proof-of-principle implementation of the SPR. This pyrene-based

fluorophore has excellent fluorescence properties and has very good water solubility, thereby eliminating any problems with aggregation and surface adsorption during its immobilization on the solid support and cleavage. The cleavable anchor has to be stable enough to survive the conditions used for the synthesis of the SPR and the derivatization reactions. At the same time, it has to be cleavable under mild conditions for facile release of the label-analyte conjugates. The solid phase needs to be optimized as well. It has to permit efficient transfer of the analytes to (during labeling) and from (after cleaving) the reactive sites.

The general objectives of this project are to *(i)* demonstrate that a SCALER SPR can be prepared, *(ii)* develop analytical methods for its characterization, *(iii)* demonstrate that the different parts of the reagent can function as designed once assembled and *(iv)* demonstrate the use of such a reagent.

4.2 Design and Synthesis of the Cleavable Anchor

4.2.1 Background and Objectives

The cleavable part of the anchor can be made from a number of existing cleavable linkers. Holmes [68, 69] reported that photolabile *o*-nitrobenzyl linkers could be rapidly cleaved by irradiating with 365 nm UV light. Gupta and others [70, 71] developed reusable solid phase supports for oligonucleotide synthesis that relied on a disulfide moiety for the cleavable group. The disulfide bond was broken using a reducing agent such as dithiothreitol.

Although not for a solid phase application, a 1,3-dioxolane-based cleavable linker was described by Jaeger and coworkers who designed surfactants for use as vesicular media for reaction catalysis [72, 73]. One of these dioxolanes could be cleaved under relatively mild acidic conditions. The linker had a half life of 56 minutes in a pH 3 aqueous buffer. ALS, standing for acid-labile surfactant, is another 1,3-dioxolane-containing surfactant that was developed by Waters Corporation as an alternative to SDS in gel electrophoresis. Several groups reported improved MS analysis of tryptic peptides when ALS was used instead of SDS due to improved peptide recovery after decomposition of the surfactant at low pH [74-77]. Yu and others reported a half life of 8 minutes for ALS at pH 2 [77].

A 1,3-dioxolane group was chosen as the cleavable group of the SCALER SPR due to its simplicity, ease of cleavage and its stability in both neutral and basic solutions. However, since the half life of 1,3-dioxolanes reported by Jaeger is rather long, the effect of the substituents around the dioxolane ring on the hydrolysis rate was looked into to find the structure with the desired rate of cleavage. The synthesis of the cleavable anchor was designed to allow its insertion between the solid surface and the fluorophore. Spacers consisting of well-defined oligo(ethylene glycol) chains were used to maximize hydrophilicity of the construct.

4.2.2 Materials and Methods

Tetra(ethylene glycol), 4-hydroxybenzaldehyde, benzylacetone, sodium azide, sodium hydride (60% dispersion in oil), p-toluenesulfonyl chloride (tosyl chloride) and p-toluenesulfonic acid monohydrate (PTSA) were purchased from Sigma Aldrich. Glycerol was from EM Science. Xterra[®] MS C18 HPLC column was acquired from Waters. Gemini C18 column was from Phenomenex.

HPLC analyses were done in a Beckman HPLC system equipped with a 508 autosampler, 126 pump and 168 photodiode array detector.

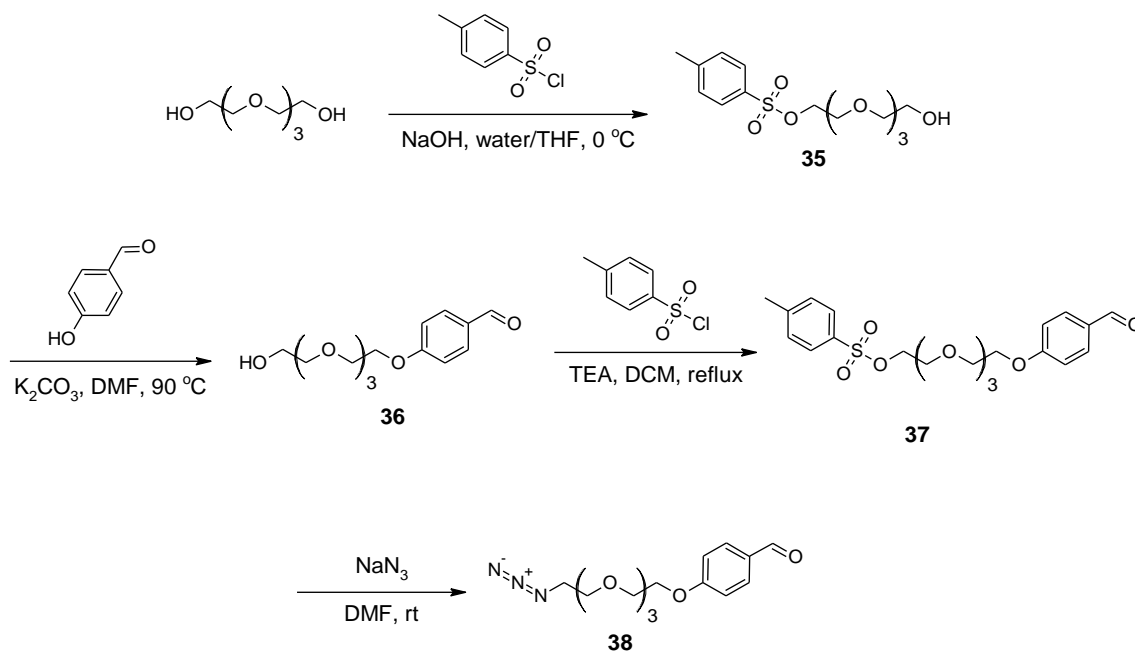


Figure 4.3. Synthesis scheme for the preparation of the benzaldehyde side of the cleavable anchor. Refer to Sections 4.2.2.1 to 4.2.2.4 for synthesis details.

4.2.2.1 Synthesis of Monotosylated Tetra(ethylene glycol) **35**

Compound **35** (Figure 4.3) was prepared by a procedure similar to what was outlined by Ashton and others [78]. 175.6 g (904 mmol) tetra(ethylene glycol) and 25 mL THF were charged into a 3-neck 500-mL flask. While mechanically stirred in an ice bath, a mixture of 5.47 g (137 mmol) of NaOH and 30 mL water was incrementally added to the solution. The temperature increased to 30 °C due to the addition. After the temperature went back down to 3°C, 16.7 g (87.6 mmol) of tosyl chloride in 90 mL THF was added, while stirring vigorously, in the span of 1.5 hours using a syringe pump. Stirring was continued for an additional 2 hours in the ice bath. The reaction was monitored by RP-HPLC. 500 mL of ice water was dumped into the reaction mixture. The hazy mixture was extracted three times with 100 mL dichloromethane. The organic phases were combined and washed twice with 50 mL water. The dichloromethane solution was dried with sodium sulfate and the solvent was removed under vacuum to afford a colorless oil (27.37 g, 90% yield).

HPLC was done using an Xterra[®] MS C18 column (3.5 µm, 150 mm x 2.1 mm) with a binary gradient of 30% to 70% B in 20 min at 0.3 mL/min (A: water; B: ACN).

4.2.2.2 Synthesis of Tetra(ethylene glycol)-decorated 4-Hydroxybenzaldehyde **36**

80 g (230 mmol) of the monotosyl derivative of tetra(ethylene glycol), **35**, 30 g (246 mmol) p-hydroxybenzaldehyde and 500 mL DMF were put together in a 2-L round bottom flask, followed by the addition of 93 g (673 mmol) potassium carbonate. The

reaction mixture was placed in a heating mantle and its temperature was increased to 90 °C in 30 minutes while stirring with a mechanical stirrer. The reaction was complete in 60 minutes as determined by RP-HPLC. The mixture was allowed to cool and most of DMF was removed under reduced pressure. The resulting residue was partitioned between 1 L dichloromethane and 1 L water. The organic phase was then extracted twice with 1 L 10% aqueous sodium chloride. The dichloromethane solution was then evaporated under vacuum leaving a brownish oil having an assay purity of 90% with p-hydroxybenzaldehyde as the main contaminant. This oil was extracted using a solvent system consisting of 500 mL ACN, 50 mL toluene and 1 L water. The aqueous bottom phase contained 70% of the target as determined by HPLC and was set aside. The top phase was mixed with 400 mL ACN and 1 L water, allowed to form two phases and separated. The aqueous phases from the two extraction steps were combined and the solvent was removed under reduced pressure to give a light brown oil (56.1 g , 96.5 % yield).

HPLC was carried out using a Gemini C18 column (3 μm , 100 \AA , 75 mm x 4.6 mm) with a binary gradient of 20% to 70% B in 15 min at 1 mL/min (A: 2 mM N-methylmorpholine and 1mM acetic acid in water; B: 2 mM N-methylmorpholine and 1mM acetic acid in ACN).

4.2.2.3 Synthesis of Tosylated Aldehyde **37**

56 g (188 mmol) of **36** was dissolved in 500 mL dichloromethane. 72.3 g (379 mmol) tosyl chloride was then added followed by 105 mL (755 mmol) triethylamine. The mixture was heated to reflux for 2 hours. After determining by HPLC that conversion of **36** was complete, 38 mL (113 mmol) N,N-diethylethanolamine was added to quench excess tosyl chloride and reflux was continued for 40 more minutes. The reaction mixture was cooled to room temperature and extracted twice with 500 mL aqueous monosodium phosphate, then twice with 500 mL water to extract N,N-diethylethanolamine and its tosyl ester into the aqueous phase. The dichloromethane phase was dried with sodium sulfate and the solvent was removed under reduced pressure affording an oil having an HPLC assay purity (detection at 265 nm) of 90% (85.7 g, 90% yield).

HPLC was carried out using a Gemini C18 column (3 μm , 100 \AA , 75 mm x 4.6 mm) with a binary gradient of 20% to 80% B in 18 min at 1 mL/min (A: 2 mM N-methylmorpholine and 1mM acetic acid in water; B: 2 mM N-methylmorpholine and 1mM acetic acid in ACN).

4.2.2.4 Synthesis of Azido Aldehyde **38**

85 g (~180 mmol) tosylate **37** was mixed with 55 g (85 mmol) sodium azide in 500 mL DMF. The mixture was stirred at 65 °C for 20 minutes and at room temperature overnight. DMF was then removed under reduced pressure. The resulting residue was

partitioned between 300 ml dichloromethane and 300 mL water. The dichloromethane phase was washed with 300 mL water and then with 450 mL 7% aqueous sodium chloride. The organic phase was dried with sodium sulfate and the solvent removed under reduced pressure to produce a light brown oily residue (60.7 g, ~100% yield).

HPLC was carried out the same way as in Section 4.2.2.3.

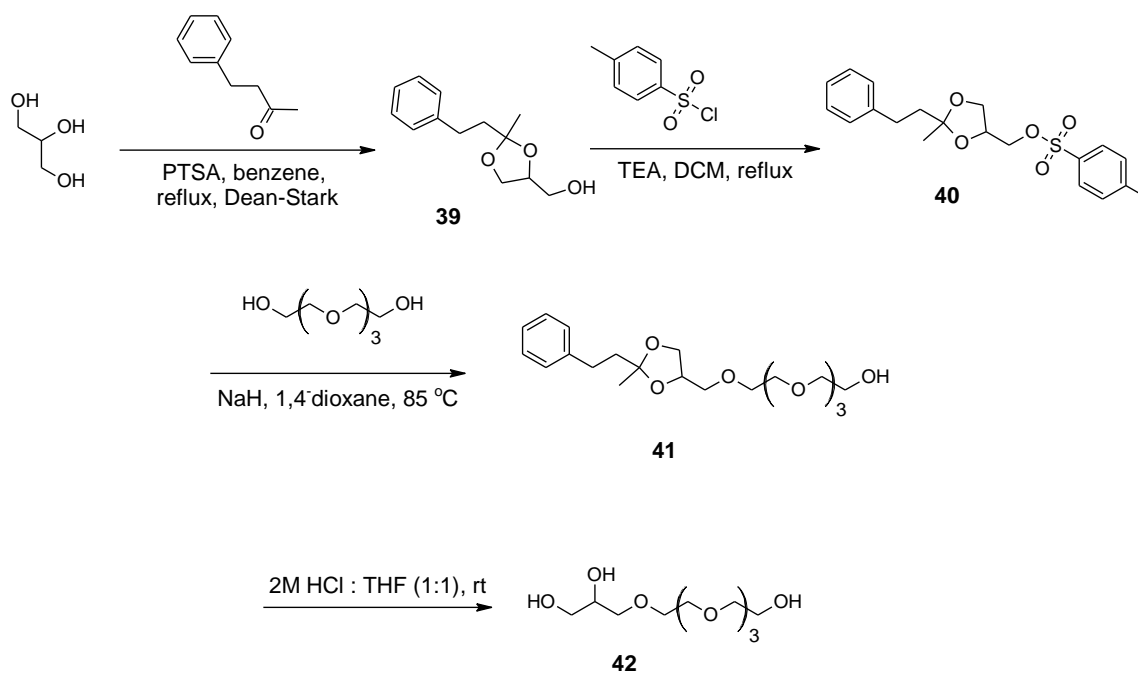


Figure 4.4. Synthesis scheme for the preparation of the *vic*-diol side of the cleavable anchor. Refer to Sections 4.2.2.5 to 4.2.2.8 for synthesis details.

4.2.2.5 Synthesis of Dioxolane **39**

15 g (101 mmol) benzylacetone, 45 g (489 mmol) glycerol and 0.194 g (1 mmol) p-toluenesulfonic acid were added to 200 mL benzene in a 500 mL round bottom flask

with an attached Dean-Stark apparatus. A two phase system was formed. The mixture was refluxed until conversion was complete (about 11 hours) as determined by HPLC with detection at 212 nm. The reaction mixture was then cooled to room temperature and extracted twice with 200 mL of 0.5% aqueous sodium carbonate and once with 200 mL water. The benzene phase was dried with sodium sulfate and the solvent was removed under vacuum (20.6 g, 92% yield).

HPLC was carried out using a Gemini C18 column (3 μm , 100 \AA , 100 mm x 4.6 mm) and isocratic elution with 40% B at 1 mL/min (A: 2 mM N-methylmorpholine and 1mM acetic acid in water; B: 2 mM N-methylmorpholine and 1mM acetic acid in ACN).

4.2.2.6 Synthesis of Tosylated Dioxolane **40**

20 g (90 mmol) of dioxolane **39** and 100 mL dichloromethane were weighed into a 500 mL round bottom flask. 38 mL (273 mmol) triethylamine was added followed by 19 g (100 mmol) tosyl chloride. 50 mL more dichloromethane was used to wash-in tosyl chloride. The mixture was refluxed and analyzed by HPLC after 10 and 30 minutes. An additional 3.45 g (18 mmol) tosyl chloride was added and refluxing was continued for 15 more minutes when HPLC indicated complete conversion of **39** to **40**. At this point, 5 g diethylethanolamine was added to quench excess tosyl chloride. The mixture was further refluxed for 30 minutes and then stirred at room temperature overnight. 150 mL toluene was added to the cooled reaction mixture and extracted twice with 600 mL 1M, pH 6 sodium dihydrogenphosphate buffer and once with 600 mL of 10% aqueous

sodium chloride. The organic phase was evaporated under reduced pressure yielding a colorless oil with a 97% purity as determined by HPLC with 262 nm detection (33.0 g, 97% yield).

HPLC was done using a Gemini C18 column (3 μm , 100 \AA , 100 mm x 4.6 mm) with a binary gradient of 40% to 75% B in 14 min at 1 mL/min (A: 2 mM N-methylmorpholine and 1mM acetic acid in water; B: 2 mM N-methylmorpholine and 1mM acetic acid in ACN).

4.2.2.7 Synthesis of Tetra(ethylene glycol)-decorated Dioxolane **41**

8.5 g (213 mmol) sodium hydride (60% dispersion in oil) was digested in 160 mL of hexanes, allowed to settle and the hexanes were canulated out. A nitrogen blanket was applied over the reaction mixture to prevent moisture contamination. The hexanes rinse was repeated one more time. 100 mL of 1,4-dioxane was then added and to this, a mixture of 165 g (845 mmol) tetra(ethylene glycol) and 160 mL 1,4-dioxane was carefully added, dropwise, using a dropping funnel. Care was taken not to produce too much pressure during this addition. After this, a solution of 32 g (85 mmol) of tosylate **40** and 50 mL 1,4-dioxane was poured in. The mixture was then stirred in a 85 °C oil bath until conversion was complete (about 7 hours) as determined by HPLC and then was stirred overnight at room temperature. The solvent was removed under vacuum and the residue was partitioned between 1 L dichloromethane and 2 L of 5% aqueous sodium chloride. The organic phase was extracted two more times with the same volume of the

aqueous sodium chloride. The workup was monitored with HPLC with and without labeling of the residual tetra(ethylene glycol). Tetra(ethylene glycol) labeling was done by first drying a 100 μL aliquot of the dichloromethane phase with sodium sulfate. Then, 20 μL of that solution was added to 5 μL of 5% 4-(dimethylamino)pyridine in DMF, 50 μL DMF, 20 μL triethylamine and 10 μL benzoyl chloride. The mixture was vortexed, allowed to react for about 5 to 10 minutes and analyzed by HPLC with the UV detector set at 262 nm. The amount of unreacted tetra(ethylene glycol) left in the reaction mixture decreased below detection limit by the second extraction. The dichloromethane phase was then dried with sodium sulfate and the solvent was evaporated under reduced pressure (31.2 g, 92% yield).

HPLC monitoring was the same as in Section 4.2.2.6.

4.2.2.8 Synthesis of Diol-terminated Tetra(ethylene glycol) **42**

Tetra(ethylene glycol)-decorated dioxolane **41** (30 g, 75 mmol) was added to a mixture of 300 mL of 2M aqueous HCl and 300 mL THF. Hydrolysis of the dioxolane ring was almost complete by 30 minutes at room temperature as shown by HPLC analysis. The reaction mixture was stirred for an additional 1.5 hours, after which sodium carbonate was carefully added until bubble formation ceased. Water and THF were removed under vacuum and the remaining residue was digested in 500 mL THF at room temperature overnight. The slurry was filtered and the filtrate was evaporated yielding an oil. This was then partitioned between 200 mL toluene and 200 mL water. The

aqueous phase was extracted with dichloromethane after addition of 10 g sodium chloride. The aqueous solution was evaporated and the residue was digested in a mixture of 120 mL THF and 80 mL MTBE. The slurry was filtered and the solvent was removed under vacuum to afford a light tan viscous oil (17.3 g, 86% yield).

Dioxolane hydrolysis was monitored by HPLC in the same manner as in Section 4.2.2.5, workup as in Section 4.2.2.6.

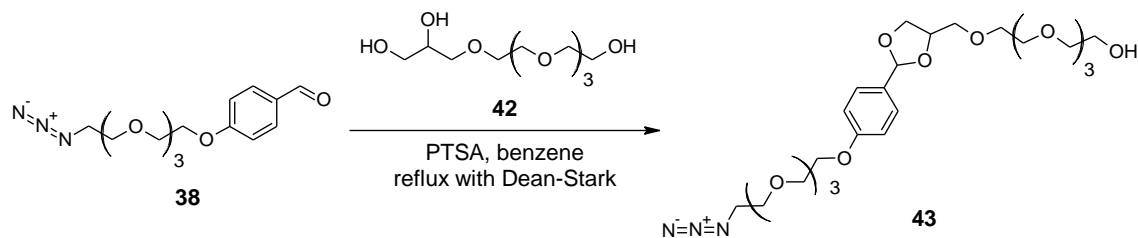


Figure 4.5. Formation of cleavable anchor intermediate **43** from aldehyde **38** and diol **42**. Refer to Section 4.2.2.9 for synthesis detail.

4.2.2.9 Synthesis of Cleavable Anchor Intermediate **43**

A mixture of 17.2 g (64 mmol) of diol-terminated tetra(ethylene glycol) **42**, 21 g (65 mmol) aldehyde **38**, 122 mg (0.64 mmol) PTSA and 200 mL benzene was refluxed in a 500 mL round bottom flask with an attached Dean-Stark apparatus. Dioxolane formation was monitored by HPLC at 224 nm which showed that the reaction stopped progressing after about 24 hours of reflux. The benzene mixture was cooled to room temperature and mixed with 200 mL dichloromethane and 300 mL of an aqueous solution containing 30 g sodium chloride and 0.5 g sodium carbonate. The organic

phase was dried with sodium sulfate and evaporated under vacuum to afford 30.4 g of oil with a purity of 64% (HPLC, detection at 224 nm). The oil was stored by adding about 0.1% v/v worth of triethylamine to scavenge any acid that may have contaminated the batch. A 5 g portion of this oil was purified by silica gel flash chromatography using 2 column volumes of ethyl acetate with 0.1% v/v triethylamine followed by 3 column volumes of a 1:1 mixture of acetone and ethyl acetate with 0.1% v/v triethylamine. The fractions containing target compound **43** were combined and evaporated to give a 95% pure colorless oil (6.78 g from 2 x 5 g portions, 56% yield after reaction and workup). Again, triethylamine was added to prevent hydrolysis of the dioxolane ring during storage.

Dioxolane formation was monitored by HPLC using a Gemini C18 column (3 μm , 100 \AA , 100 mm x 4.6 mm) with a binary gradient of 20% to 70% B in 15 min at 1 mL/min. The fractions from flash column chromatography were analyzed by HPLC using a Gemini C18 column (3 μm , 100 \AA , 150 mm x 4.6 mm) with a binary gradient of 20% to 80% B in 17 min at 1 mL/min (A: 2 mM N-methylmorpholine and 1mM acetic acid in water; B: 2 mM N-methylmorpholine and 1mM acetic acid in ACN).

4.2.3 Results and Discussion

4.2.3.1 Hydrolysis Rates of Different Dioxolanes

Hydrolysis rate of the dioxolane ring as a function of the ring substituents was studied first. Four dioxolanes were prepared (structures shown in Figure 4.6). Two of the

dioxolanes were formed from an aryl 1,2-diol with an alkyl ketone and an alkyl aldehyde as partner, respectively. The other two used dioxolanes derived from an alkyl 1,2-diol with an aryl ketone and an aryl aldehyde as partner, respectively. Hydrolyses rates of these dioxolanes at different pH values were monitored at room temperature and their half lives, $t_{1/2}$, were determined at the highest pH value where there was appreciable hydrolysis within an hour. A summary of the experiments is shown in Table 4.1. The dioxolanes derived from aryl diol / alkyl carbonyl have very slow hydrolysis rates, even at around pH 1. Based on Jaeger's report that $t_{1/2}$ of their alkyl diol / alkyl carbonyl-derived dioxolane was 56 min at pH 3, the aromatic substituent on the diol does not seem to increase hydrolysis rate. On the other hand, the alkyl diol / aryl carbonyl dioxolanes have relatively short half lives at pH 3.5 which suggests that an aromatic substituent, specifically, a p-alkoxyphenyl substituent on the carbonyl group increases the hydrolysis rate in general. These dioxolanes were also found to be stable at pH values 7 and above. Therefore, a dioxolane derived from a p-alkoxybenzaldehyde and an alkyl 1,2-diol was chosen as the cleavable element of the anchor group in SCALER due to its favorable cleavage rate.

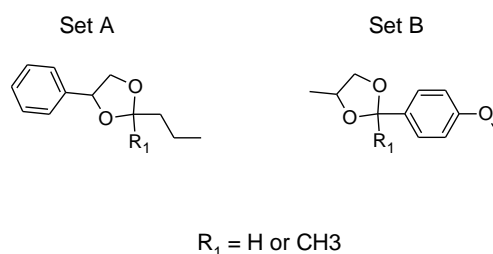


Figure 4.6. Structures of the dioxolanes used in the cleavage experiments.

Table 4.1. Summary of the results of the dioxolane hydrolysis experiments.

Diol	Carbonyl	Buffer solution	$t_{1/2}$
styrene glycol	butyraldehyde	1N HCl : THF (2:3)	--- ^a
styrene glycol	methyl ethyl ketone	1N HCl : THF (2:3)	85 min
1,2-propanediol	4-methoxybenzaldehyde	pH 3.5 formic acid with LiOH, 20% ACN	5 min
1,2-propanediol	4-methoxyacetophenone	pH 3.5 formic acid with LiOH, 20% ACN	24 min

^ano detectable hydrolysis within 50 minutes

4.2.3.2 Synthesis of the Cleavable Anchor

The cleavable group will be flanked by two spacers, one that connects it to the solid phase and another that connects it to the fluorophore. We elected to have spacers based on a well-defined oligo(ethylene glycol) (OEG) in order to maintain good water solubility of the fluorophore and local hydrophilicity of the cleavable anchor.

Tetra(ethylene glycol) was chosen as the oligo(ethylene glycol) since it is readily available in high purity. We also planned to build the cleavable anchor in a convergent manner where dioxolane formation comes last. Therefore, synthesis of the cleavable anchor was divided into two parts: the first the preparation of the benzaldehyde side, the second the preparation of the alkyl diol side. The benzaldehyde side of the cleavable anchor was prepared as shown in Figure 4.7.

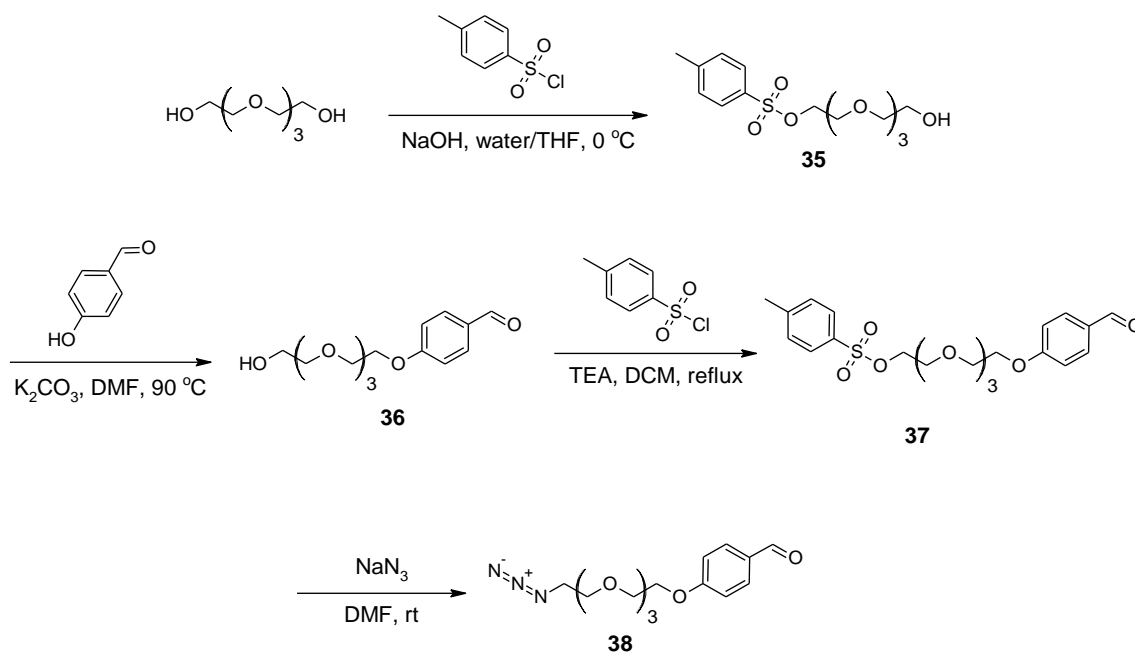


Figure 4.7. Synthesis scheme for the preparation of the benzaldehyde side of the cleavable anchor.

The synthesis started with monotosylation of tetra(ethylene glycol) where monotosylate **35** was obtained in 90% yield (based on tosyl chloride) with a purity of 96%. The procedure used a large excess of tetra(ethylene glycol) to minimize bis-tosylation. This step was improved later by another member of our group, Ming-Chen Li, who achieved a similar degree of monotosylation, at comparable purity, with only 1.2 equivalents of tetra(ethylene glycol). She used Ca(OH)₂ as base instead of silver oxide suggested in the literature [79]. Monotosylate **35** was then coupled with 4-hydroxybenzaldehyde to form compound **36** which was subsequently activated with tosyl chloride to allow azido substitution and produce compound **38**. The azido group was to be easily converted later on to an active group (*i.e.*, amino group) for attachment to the solid phase.

The alkyl diol part was synthesized according to the scheme depicted in Figure 4.8. Glycerol was used as the starting material where the 1,2-diol part was protected as a 1,3-dioxolane ring using benzyl acetone to make compound **39**. Benzyl acetone was specifically chosen for two reasons. First, the presence of an aromatic ring simplified HPLC analysis. Second, the carbonyl group separated from the aromatic ring by a short alkyl chain was expected to mimic the behavior of acetone which selectively forms the dioxolane ring with the 1,2-diol, not the 1,3-diol. The hydroxyl group of compound **39** was then activated with tosyl chloride, followed by coupling with tetra(ethylene glycol). Disappearance of the latter was analyzed by HPLC using UV detection by first derivatizing the glycol with benzoyl chloride. Tetra(ethylene glycol)-decorated dioxolane **41** was then subjected to acidic conditions to free the diol and form 1,2-diol-terminated tetra(ethylene glycol) **42**.

The aldehyde and the diol sides of the cleavable anchor were then put together as shown in Figure 4.9 using conventional methods to form cleavable anchor intermediate **43**. One end of **43** had an azido group which could be later converted to $-NH_2$ for connection to the solid phase. The other end had a hydroxyl group which was to be used to couple with the fluorophore. The reasons for the choice of hydroxyl as the terminating group for **43** are discussed in the next section.

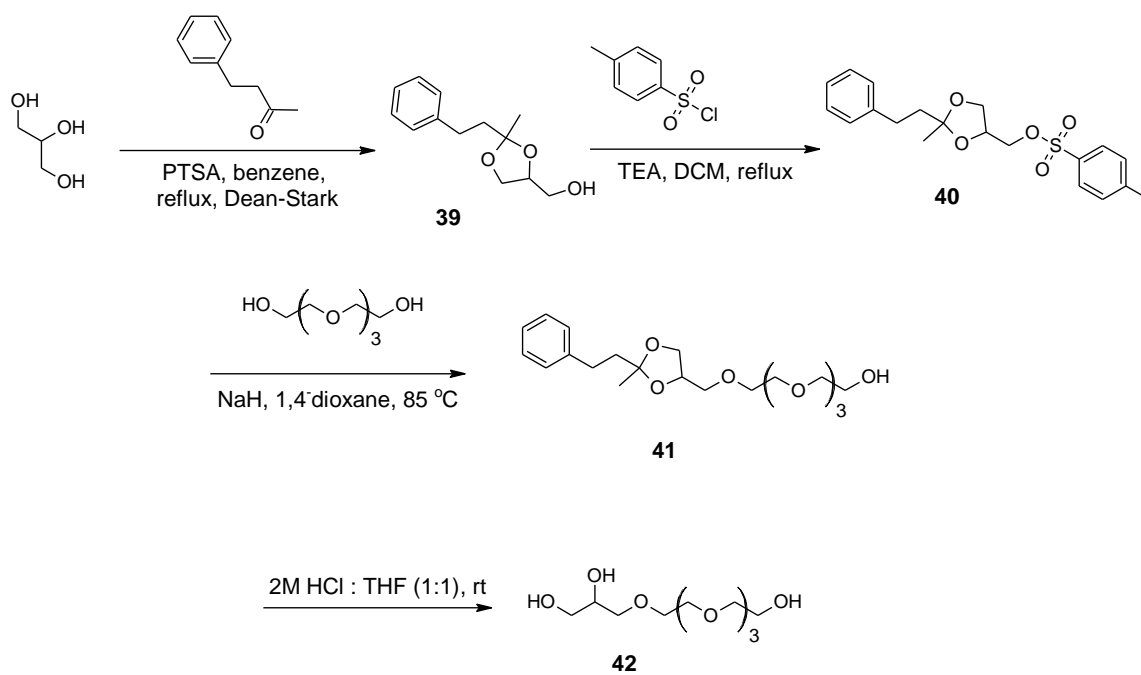


Figure 4.8. Synthesis scheme for the preparation of the 1,2-diol side of the cleavable anchor.

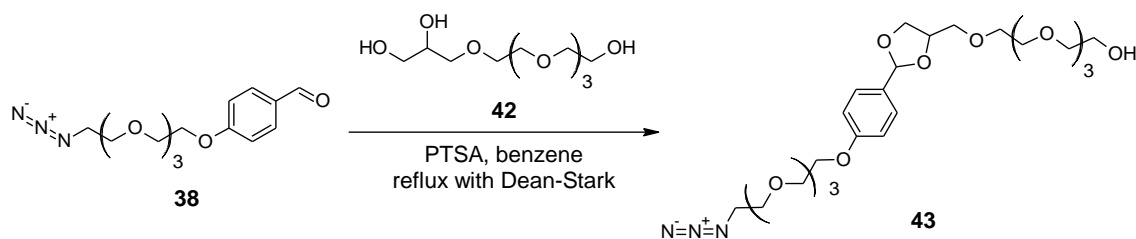


Figure 4.9. Formation of cleavable anchor intermediate **43** from aldehyde **38** and diol **42**.

4.3 Attachment of the Cleavable Arm to the Fluorophore

4.3.1 Background and Objectives

The cleavable anchor can be attached to the fluorophore either indirectly or directly.

An indirect attachment requires the use of a trifunctional scaffold that can connect the three main parts of SCALER together. An example of such a trifunctional scaffold would be based on lysine, where, through proper protection and deprotection strategies, one of the amino groups would be connected to the cleavable anchor, the other amino group would be coupled to the fluorophore, and the carboxylate group would be connected to a tethered reactive arm. Such a scaffold would allow the use of practically any amine-reactive fluorescent label in the SCALER SPR format.

Direct attachment involves connecting the anchor either to one of the existing substituents or to the core aromatic ring of the fluorophore. This coupling must not impair the fluorescence of the fluorophore or the ability of the reactive arm to derivatize the analyte. The type of coupling to be selected is specific to the type of the fluorophore used for SCALER. We opted to use compound **33** as the amine-reactive fluorophore for the SPR in the direct coupling mode to capitalize on a serendipitously observed conversion of the trisulfonamide APTS core that allowed easy attachment of the cleavable group and simultaneously improved its fluorescence properties.

4.3.2 Materials and Methods

1,3-propanedithiol, dimethylsulfoxide (DMSO), trifluoroacetic acid (TFAA) and sodium trifluoroacetate (NaTFA) were purchased from Sigma Aldrich. Sodium hydroxide, pyridine and triethylamine (TEA) were supplied by EMD. 40 μm silica gel for preparative LC was acquired from J.T. Baker Chemical Co.

HPLC analyses and semi-preparative HILIC separations were done in a Beckman HPLC system equipped with a 508 autosampler, 126 pump and 168 photodiode array detector.

4.3.2.1 Synthesis of Fluorophore **44**

50 mg (41 μmol) of fluorophore **33** was dissolved in 700 μL DMSO and added to a mixture of 700 mg (1.2 mmol) cleavable anchor intermediate **43** and 250 μL of a 50% aqueous solution of sodium hydroxide. After addition, the reaction mixture turned dark blue/violet. The reaction mixture was placed into 55-60 $^{\circ}\text{C}$ oil bath. The reaction was monitored by HILIC and was found to be complete in about 20 hours. After cooling to room temperature, a mixture of 757 μL TEA and 377 μL TFA was added to neutralize sodium hydroxide and buffer the system. The color of the reaction mixture turned dull orange. A 15 mL portion of MTBE containing a few drops of TEA was then used to precipitate out the target compound. The heterogeneous mixture was vortexed, centrifuged and the supernatant was decanted. The bottom phase was a viscous liquid containing the target, sodium trifluoroacetate, triethylammonium trifluoroacetate, water and DMSO. 15 mL of MTBE was used to digest the bottom phase twice in order to

remove most of DMSO and triethylammonium trifluoroacetate without solubilizing the target. After MTBE, the residue was digested twice with the more polar solvent mixture consisting of 5 mL THF and 10 mL MTBE. The resulting red/brown residue was mixed with 1 mL water, centrifuged and the target compound was recovered from the supernatant by semi-prep HPLC as described in section 3.4.2.3 using a Luna 5 μm HILIC column (250 mm x 10 mm I.D.) with a HILIC guard cartridge. The flow rate was 5 mL/min. After sample injection, there was a 4 min long isocratic elution segment at 98% B that was followed by a step change to 85% B. The eluent composition was maintained at this concentration until the desired component was eluted, followed by a 5-minute cleaning of the column at 50% B. The material that eluted during this wash step was collected and analyzed to confirm that it was free of the target compound. The presence of the target in this fraction would have indicated a severely tailing peak resulting from precipitation of the component during in-line Taylor dilution-mediated injection (refer to Chapter 3). The solvent composition was then changed back to 98% B (A: 20 mM sodium trifluoroacetate in water; B: 20 mM sodium trifluoroacetate in ACN). Solvents were filtered through a 0.65 μm PVDF membrane filter from Millipore.

The fractions containing the target were combined and the solvent was removed under vacuum. To remove NaTFA, the residue was eluted through a 1 cm I.D. x 14 cm column packed with 40 μm silica in HILIC mode using a buffer consisting of 10 mM TEA and 5 mM TFA. A step gradient elution was used starting at 100% ACN (sample loading), followed by an elution at 5% water/ACN composition, then at 10% and lastly

at 15% water/ACN. Each step used 5 column volumes. The target fractions were then evaporated and the residue was dissolved in the least amount of ACN and precipitated out with 2 mL MTBE that contained a few drops of TEA. The dissolution – precipitation process was repeated five times to remove triethylammonium trifluoroacetate from the target. The solid was dried under vacuum (42 mg, 57% yield).

Note: After drying, the solids were stored without addition of triethylamine. After 1 day, HILIC analysis showed hydrolysis of 10% of the cleavable anchor. Addition of a few drops of triethylamine prevented this hydrolysis even after days of storage at room temperature.

HILIC analysis was done using a Luna HILIC column (3 μm , 200 \AA , 150 mm x 4.6 mm) with a binary gradient of 95% to 75% B in 20 min at 1 mL/min (A: 10 mM 3-morpholinopropane-1-sulfonic acid (MOPS) and 5mM NaOH in water; B: 10 mM MOPS and 5mM NaOH in 5% water in ACN).

4.3.2.2 Synthesis of Fluorophore **45**

The reduction of azido fluorophore **44** to the amine was accomplished by mixing 42 mg of **44** with 600 μL water, 420 μL triethylamine, 2 mL pyridine and 302 μL 1,3-propanedithiol. The reaction was complete after about 2 hours as determined by HPLC. The reaction mixture was concentrated by adding 30 mL MTBE to take in most of the solvent and reagent without solubilizing the product. After centrifuging, the phases were

separated. The bottom phase was a red/brown viscous liquid while the top phase was colorless. 20 mL MTBE with a few drops of TEA was again added, the mixture vortexed, centrifuged and the phases separated. The digestion step was repeated with a more polar solvent mixture consisting of 10 mL THF and 20 mL MTBE, followed by digestion with a still more polar solvent, 20 mL THF. The solvent in each step contained a few drops of triethylamine. The residue was dissolved in 200 μ L DMF that contained some triethylamine and precipitated out with 20 mL THF. The solid was dissolved in 400 mL DMSO to give an approximate amine-terminated fluorophore **45** (as triethylammonium salt) concentration of 90 mg/mL. The material had the 10% “hydrolyzed” fluorophore contaminant as noted in Section 4.3.2.1 and was stored in the freezer.

4.3.3 Results and Discussion

4.3.3.1 Rationale for the Direct Attachment of the Cleavable Anchor to the Fluorophore

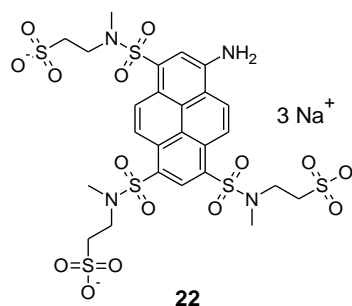


Figure 4.10. Structure of trisulfonamide **22** which was used in the stability tests.

During the development of fluorophore **33** in Chapter 3 we wanted to know the stability of the trisulfonamide derivative of APTS when subjected to various, relatively harsh conditions. One of the tests conducted was digestion of trisulfonamide **22** (structure shown in Figure 4.7) with sodium hydroxide in water and methanol at an elevated temperature. Byproduct formation was observed by HPLC in half an hour as shown in Figure 4.8. The UV absorbance spectrum of the byproduct was significantly different from that of trisulfonamide **22** (Figure 4.9). There was a bathochromic shift of about 15 nm and the broad peak profiles in the UV range gave way to narrower, more defined ones. Both of these observations pointed to a change in the aromatic core of the fluorophore. MS analysis of the byproduct showed that it had a $[M-H]^-$ value of 648.12 corresponding to the putative structure presented in Figure 4.10 where one of the sulfonamide groups was replaced by a methoxy group. To test if the transformation was exclusive to methanol, different alcohols were tested under the same basic conditions. Each alcohol gave its own byproduct peak in HILIC as shown in Figure 4.11. However, all byproducts had the same UV absorbance spectra. This suggested that their core fluorophore structures were also the same and only the alkoxy substituent was different which would account for the differences in their retention times in HILIC. It was subsequently determined that the exchange of the sulfonate group to the alkoxy group did not take place with APTS as the fluorophore substrate.

As of the writing of this dissertation, no efforts have been made to ascertain the location of the alkoxy substitution. The fluorophore is most likely a single isomer though, basing

on HILIC analysis and NMR. HILIC analysis was able to separate different groups of isomers in the neopentyl sulfonate ester cleavage experiments (Chapter 3, Section 3.4.3.1). Isomers of disulfonamide of APTS (from the hydrolysis of trisulfonamide APTS), mono-neopentyl sulfonate ester of trisulfonamide APTS (an intermediate of the neopentyl sulfonate ester cleavage) and those of the mono-dealkylated trisulfonamide APTS (a byproduct of the neopentyl sulfonate ester cleavage) were all resolved from each other. Basing on the singularity of the peak of the alkoxy substituted fluorophores, it is safe to assume that the substitution occurs at a single place on the pyrene ring. Moreover, the aromatic region of the NMR spectra of the completely assembled fluorophore showed homogeneity of the peaks for the protons on the pyrene ring.

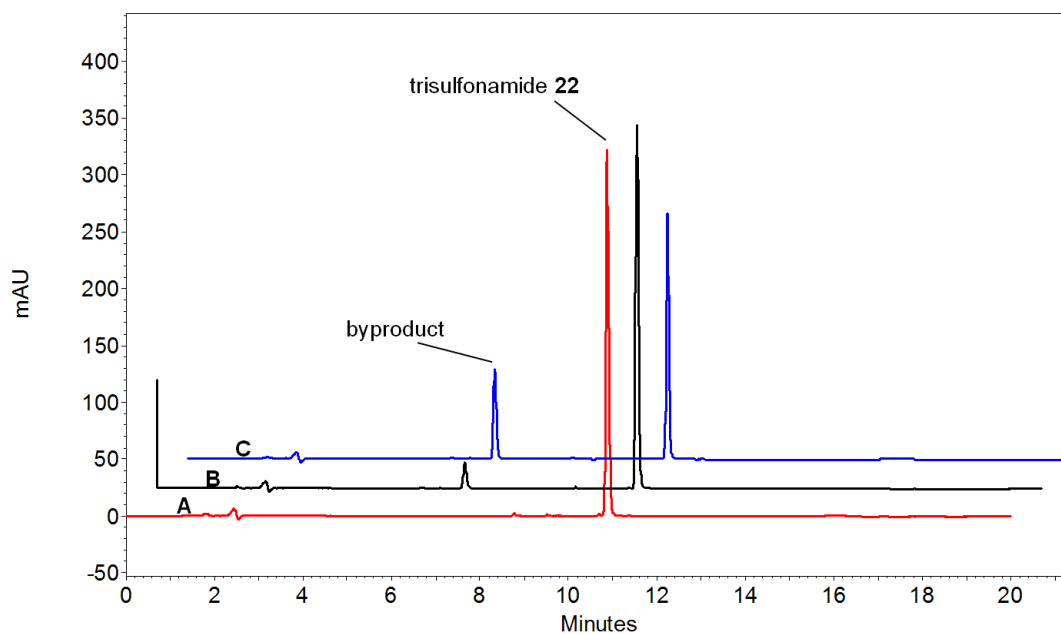


Figure 4.11. HILIC analysis of the reaction mixture after treatment of trisulfonamide **22** with sodium hydroxide in a mixture of water and methanol at 65 °C for $t = 0$ h (A), 0.5 h (B) and 2.2 h (C).

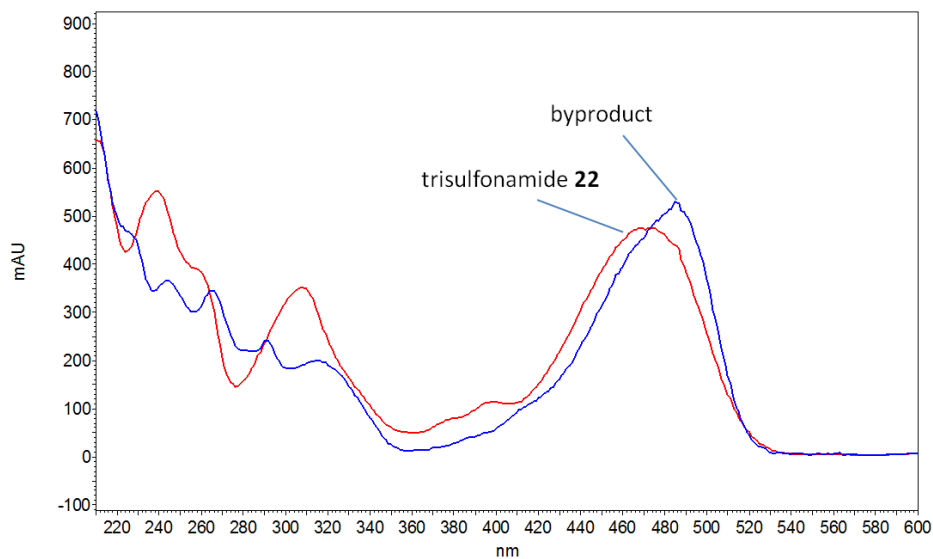


Figure 4.12. Overlay of the UV absorbance spectra of trisulfonamide **22** and the unknown byproduct.

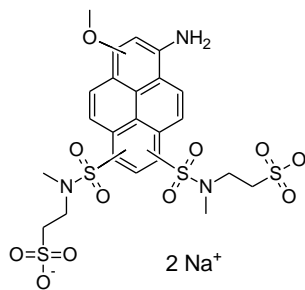


Figure 4.13. Possible structure of the byproduct from the treatment of trisulfonamide **22** with a mixture of water, methanol and NaOH.

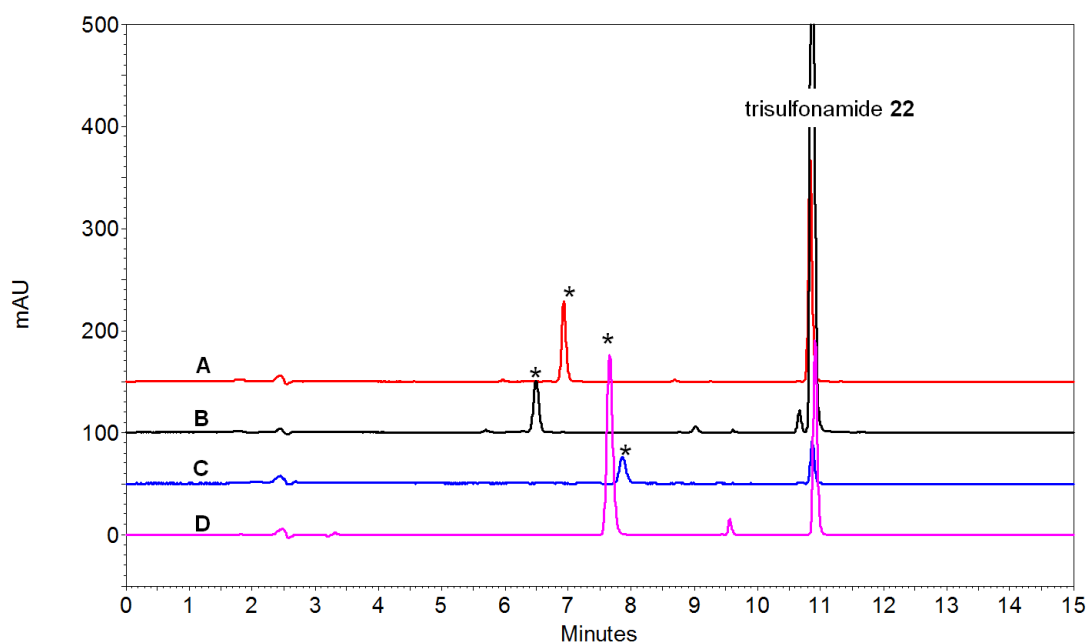


Figure 4.14. Treatment of trisulfonamide **22** with different alcohols under basic conditions. The alcohols used were methanol (A), ethanol (B), tetra(ethylene glycol) (C) and glycerol (D).

To have a qualitative idea of how fluorescence changed due to the alkoxy substitution, the fluorescence spectra of an ethoxy and a glycerol derivative were taken and compared with that of trisulfonamide **22** (Figure 4.12 and Figure 4.13, respectively). The samples in each pair of measurements had the same UV absorbance at 480 nm. The higher fluorescence intensities of the alkoxy derivatives suggested that there was an increase of the fluorescence quantum yield due to the alkoxy substitution. The figures also show a hypsochromic shift of the $\lambda_{\text{max}}^{\text{em}}$ of the alkoxy derivatives to 525 from the 540 nm value of trisulfonamide **22**. These observations prompted us to exploit the sulfonamide to alkoxy group exchange for the attachment of the cleavable anchor to the APTS core. Also, this

decision mandated the synthesis of a cleavable anchor with a terminal primary hydroxyl group for connection to the fluorophore.

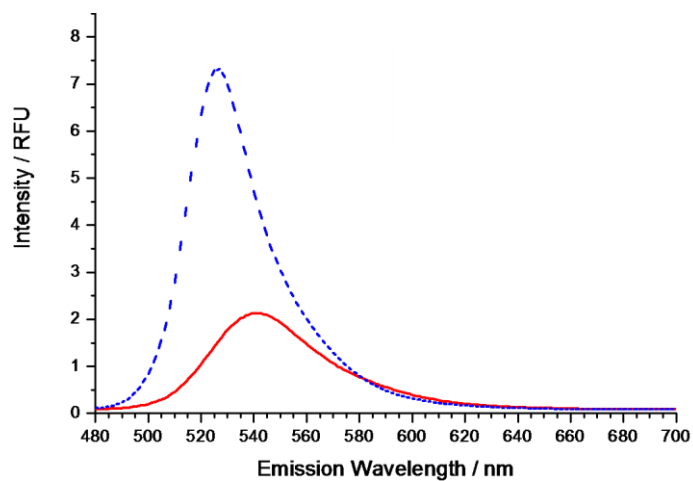


Figure 4.15. Fluorescence emission spectra of trisulfonamide **22** (red solid line) and the byproduct obtained in basic ethanol (blue dashed line). Both samples have the same molar absorbance at 480 nm.

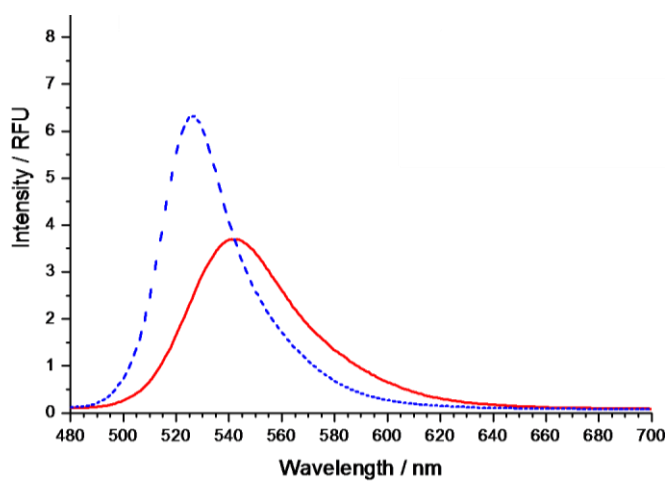


Figure 4.16. Fluorescence emission spectra of trisulfonamide **22** (red solid line) and the byproduct obtained in basic glycerol (blue dashed line). Both samples have the same molar absorbance at 480 nm.

4.3.3.2 Attachment of the Cleavable Anchor Intermediate

Hydroxyl-terminated cleavable anchor intermediate **43** was connected to fluorophore **33** by reacting the two in the presence of a high concentration of sodium hydroxide in water and DMSO at 50-60 °C (scheme shown in Figure 4.14). HPLC monitoring as shown in Figure 4.15 indicated that the reaction was complete after 30 hours. The reaction mixture was purified by semi-preparative HILIC yielding fluorophore **44** with a purity of 99.5%. The azido group on the other end of the cleavable anchor was then reduced to an amino group using very mild, slightly basic conditions to produce fluorophore **45**.

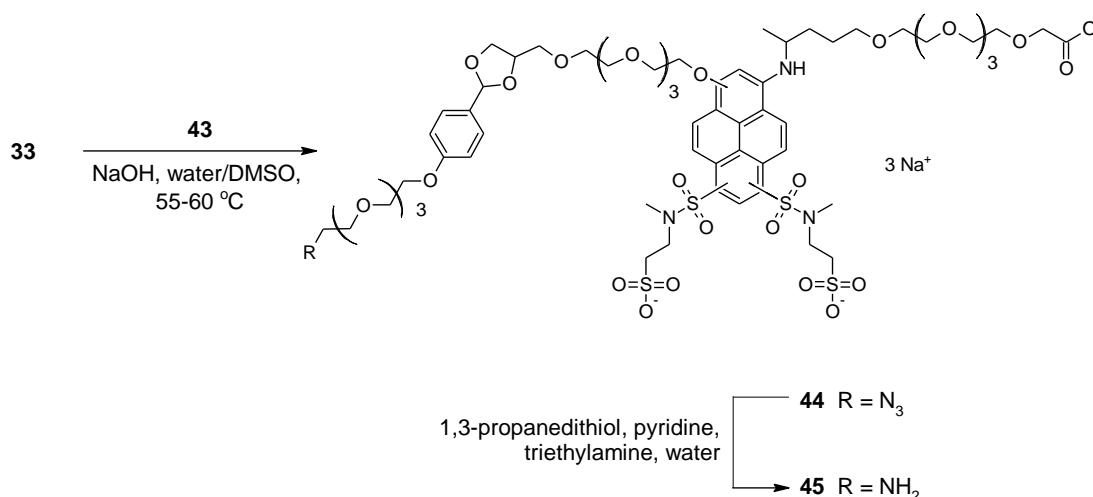


Figure 4.17. Scheme for the attachment of hydroxyl-terminated cleavable anchor intermediate **43** to fluorophore **33** and the subsequent reduction of the azido group to the amino group.

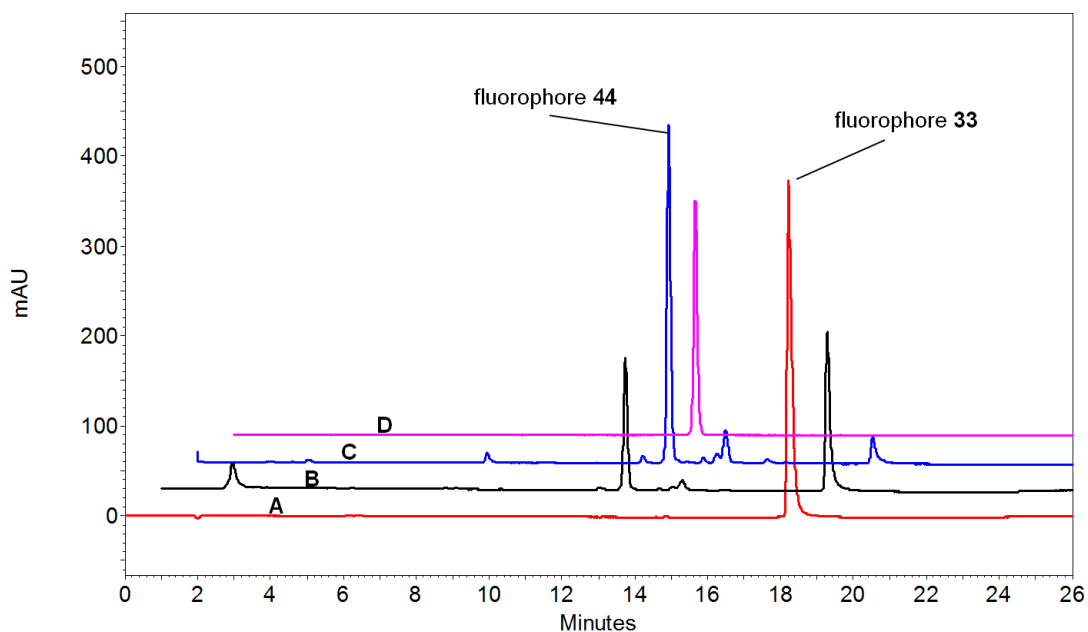


Figure 4.18. HPLC monitoring of the attachment of cleavable anchor intermediate **43** to fluorophore **33** showing the chromatograms for the starting material (A), the reaction mixture after 13 hours (B), the reaction mixture after 30 hours (C) and the target after semi-prep HILIC purification (D).

4.3.3.3 Test Cleavage of Fluorophore **45**

Prior to immobilization onto the solid phase, the fluorophore in its final form was subjected to hydrolysis experiments (Figure 4.16) under acidic conditions in pH 3.1, 3.5 and 4.1 solutions. These pH values were chosen because proteins were expected to tolerate them for short periods of time (thus the need for high cleavage rates). It was important to do the cleavage test at this point and not earlier in order to account for any effects the fluorophore might have on the cleavable anchor. The test solutions were analyzed using CE-LIF with a pH 10 background electrolyte to ensure that there was no further cleavage either in the CE sample or in the separation capillary during

electrophoresis. An internal standard, 8-hydroxypyrene-1,3,6-trisulfonic acid, trisodium salt, was used to compensate for any variation in sample injections.

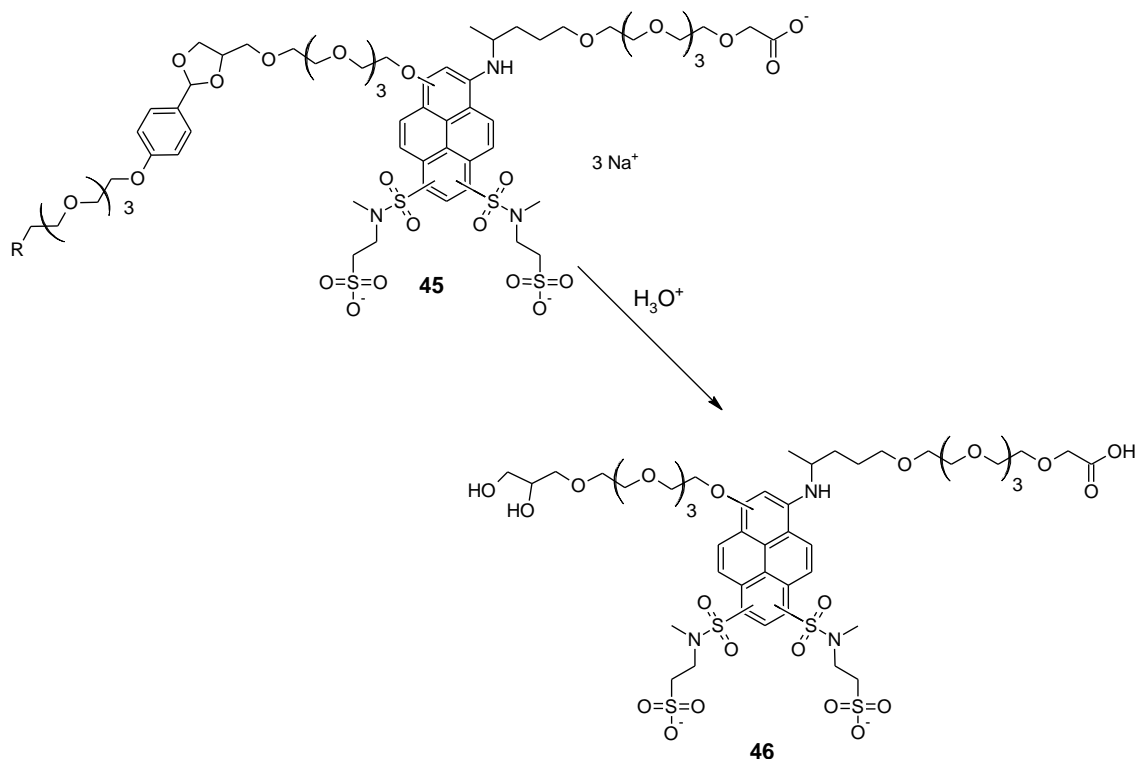


Figure 19. Cleavage of the cleavable group of fluorophore **45** to release diol-terminated fluorophore **46**.

Aliquots were taken from the three hydrolysis mixtures at different times, analyzed by CE and the normalized peak areas corresponding to intact **45** were plotted as a function of hydrolysis time (Figure 4.17) in order to determine the hydrolysis rate constants.

Assuming that cleavage followed a pseudo-first order rate kinetics, the following equation was fitted to the measured data:

$$\frac{A}{A_0} = e^{-k't} \quad (4.1)$$

where A and A_0 are the normalized peak areas at time t and $t = 0$, k' is the pseudo-first order rate constant (s^{-1}) and t is hydrolysis time in seconds. The respective k' values were then used to calculate the $t_{0.5}$ values of the cleavable group for each pH. The time at which only 1% of the cleavable group population was left intact, $t_{0.01}$ was also determined. These values represent the required residence times of the cleaving agent (*i.e.*, acidic buffer) in the SPR to recover 99% of the label and the labeled analytes. A summary of the $t_{0.5}$ and $t_{0.01}$ values is shown in Table 4.2.

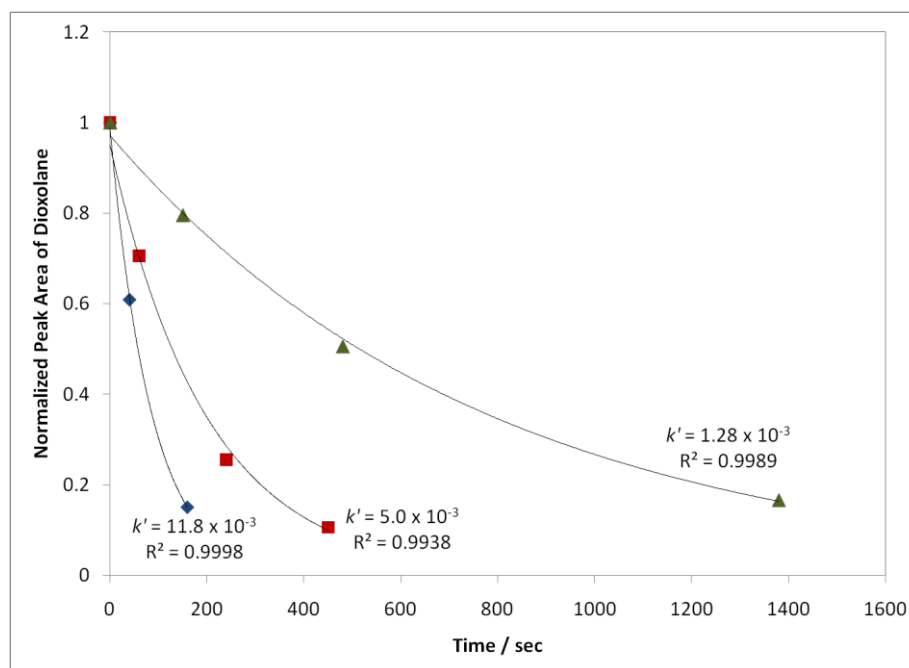


Figure 4.20. Plot of the normalized peak areas versus sampling time for the hydrolysis of the cleavable group at pH 3.1 (◆), pH 3.5 (■) and pH 4.2 (▲). The dark lines are the fitted exponential curves. The respective k' and R^2 values are indicated.

Table 4.2. Summary of the $t_{0.5}$ and $t_{0.01}$ values for the hydrolysis of the cleavable group of fluorophore **45** at different pH.

pH	$t_{0.5}$ / min	$t_{0.01}$ / min
3.1	1.0	6.5
3.5	2.3	15.4
4.1	9.0	59.8

Ideally, the k' values for cleavage of the cleavable group should be proportional to the hydronium ion concentration, $[\text{H}_3\text{O}^+]$. A nonlinear relationship would mean that cleavage depended on other unknown factors as well which would have to be determined. Plotting the k' values against $[\text{H}_3\text{O}^+]$ indicates that the relationship is indeed linear (Figure 4.18). The slope of the fitted line is the second order rate constant of the cleavage, k . Using this equation, one can also predict the $t_{0.5}$ and $t_{0.01}$ values at any pH value.

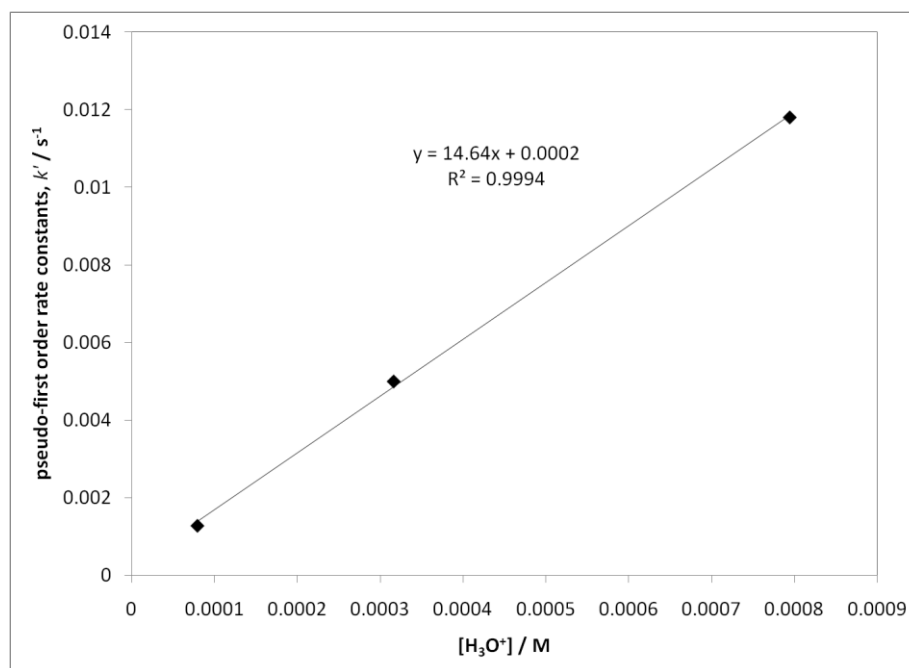


Figure 4.21. Plot of the k' values as a function of $[\text{H}_3\text{O}^+]$ in the hydrolysis buffers.

4.3.3.4 Fluorescence Properties of Fluorophore **46**

The relative fluorescence quantum yield was determined to confirm the initial finding, *i.e.*, that fluorescence improved upon replacement of one of the sulfonamide groups with an alkoxy group in fluorophore **46**. With Rhodamine 6G as standard and using equation 2 in Chapter 2, the relative quantum yield was determined to be 0.86, which is about 15% higher than that of the trisulfonamido APTS, fluorophore **33**.

The fluorescence spectra at different pH values were also recorded to see if the fluorophore, after the derivatization, still had pH-independent fluorescence properties. Figure 4.22 shows that the fluorescence of fluorophore **46** is practically independent of pH in the range of importance for CE. Though there were slight (about 7%) variations in

the intensities, they were not correlated with pH and could have been caused by matrix effects (buffer constituents). The $\lambda_{\text{max}}^{\text{em}}$ was also constant throughout the pH range.

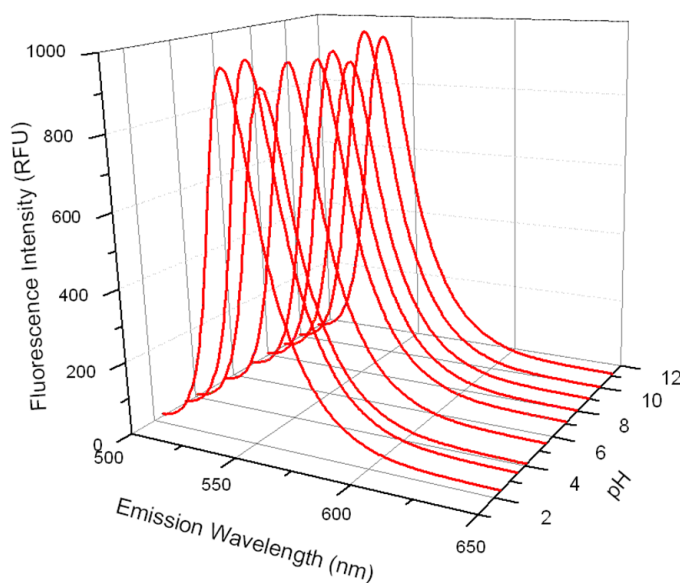


Figure 4.22. Fluorescence spectra of fluorophore **46** recorded at different pH values.

4.4 Synthesis of the Solid Phase and Immobilization of the Fluorophore Through the Cleavable Anchor

4.4.1 Background and Objectives

There are specific requirements for the solid phase of the SCALER SPR to be effective. One, as mentioned in the introduction of this chapter, is good mass transfer properties. This allows the analytes to have speedy access to the reactive sites and ensures efficient recovery of the labeled analytes during cleavage. Another requirement is a high surface area which allows high loading of the fluorescent label, even at large label-to-label

distances. There are different types of solid surfaces that can meet these requirements. Conventional particle-based porous solid supports can have good mass transfer properties and high surface areas, especially when the particle size is very small. However, as the particle size is decreased, the pressure drop across a column packed with the solid phase increases. Monolithic supports form the second group of solid supports. Monoliths are continuous beds of macroporous polymers with through pores that allow mobile phase to flow through the solid support instead of around it [80]. Because of its macroporous nature, a large portion of the surface area of the monolithic solid phase is easily accessible by convection, instead of diffusion alone. They are also easily fabricated into various shapes and sizes, without the need for special column or capillary packing equipment.

Because of the above characteristics, a monolithic support is an attractive choice for the SCALER SPR. There are numerous chemistries in the literature that are used to make functionalized monoliths [62, 81-86]. The ones we preferred are those with functional groups that allow immobilization of the fluorophore. Monoliths with epoxy, carboxylic acid and hydroxyl groups are some of these examples.

As a first generation SCALER SPR support, the monolithic material had to be prepared in a format that would allow easy implementation without the need for special equipment. It should also have a quick turnaround time providing high enough experimental throughput. A strategy for the attachment of fluorophore **45** had to be

developed such that the attachment to the solid surface is stable enough in the subsequent processing steps and under the conditions of the labeling reaction, *i.e.*, the cleavable anchor should not become severed prematurely.

4.4.2 Materials and Methods

2-Hydroxyethylmethacrylate (HEMA), ethylene glycol dimethacrylate (EDMA), 2-methoxyethyl acrylate (MEA), azobisisobutyronitrile (AIBN), 1-octanol, ethanolamine, 2-methoxyethylamine, 3-(trimethoxysilyl)propyl methacrylate (BindSilane), anhydrous dimethylsulfoxide and anhydrous acetonitrile were purchased from Sigma Aldrich.

N,N'-Disuccinimidyl carbonate (DSC) was obtained from Chem-Impex International Inc. HPLC columns were acquired from Phenomenex. Capillary melting point tubes, borosilicate glass (0.8-1.1 mm I.D. x 100 mm) were purchased from VWR.

HPLC analyses were done in a Beckman HPLC system equipped with a 508 autosampler, 126 pump and 168 photodiode detector.

UV photoinitiation of the monolith monomers was done in a closed UV box equipped with four UV strip lights designed to emit at 360nm (Southern New England Ultraviolet Company).

4.4.2.1 Bifunctionalization of the Capillary Melting Point (MP) Tubes

A modification of the bifunctionalization procedure described by Hjerten and coworkers [87] was used. 20 MP tubes were fully immersed in HPLC-grade acetone in a 50 mL centrifuge tube and sonicated for 10 minutes. Acetone was then removed, the tubes were rinsed with water, fully immersed in 0.1M NaOH, sonicated for 30 minutes and allowed to stand for another 2 hours. The NaOH solution was removed, the tubes were rinsed with water, immersed in 0.1M HCl and sonicated for 30 minutes. The HCl solution was removed, the tubes were rinsed with water and acetone, then immersed in acetone and sonicated for 10 minutes. The tubes were stored in acetone.

Between five to ten MP tubes were transferred to a 15-mL centrifuge tube, immersed in a 20% solution of BindSilane in acetone, sonicated for 10 minutes, then allowed to stand overnight. The tubes were washed with HPLC-grade acetone and used in monolith synthesis.

4.4.2.2 HEMA-based Monolith Synthesis in Melting Point Capillaries

Synthesis of the HEMA monolith was based on a procedure by Svec and coworkers [86]. The monomer mixture was prepared by combining 12 mg AIBN, 0.48 g EDMA, 0.195 g HEMA, 0.455 g MEA and 1.8 g 1-octanol. The mixture was sonicated for about a minute to dissolve AIBN and was deaerated by sparging with nitrogen through a needle for about 15 minutes.

While the monomer mixture was deaerated, a bifunctionalized MP tube was flushed with nitrogen to evaporate acetone. Both ends of the melting point tube were then sealed with rubber septa and very carefully flushed with nitrogen using 22-gauge needles as inlet and outlet at the ends of the tube.

Once the monomer solution was ready, a ~0.3 mL aliquot was taken out using a 1-mL syringe. The melting point tube was detached from the nitrogen source and with the needles still pierced through the septa, was very carefully filled with the monomer solution through one of the needles. Care was taken to remove any bubble from the tube. Once filled, the needles were removed and the sealed MP tube was suspended in a UV box for photoinitiation and curing. The monolith mixture became opaque after only about 10 minutes under the UV light. A stream of air was maintained in the box to keep the temperature from increasing due the warmth of the lamps. After overnight curing in the UV box, about 1.5 cm was cut off from each end of the MP tube. The MP tube was connected to an HPLC pump using a union for 1/16 in O.D. tubings. ACN was pumped through the monolithic column at a flow rate of 0.01 mL/min for 5 minutes and then at 0.05 mL/min for about 30 minutes. Pressure was monitored to be sure that the monolith was not plugged. Pressure was initially high when 1-octanol was still present in the column but decreased to a limiting value later on. After the ACN flush, the monolith was stored in a closed tube with several drops of ACN to prevent its drying.

4.4.2.3 Activation of the Monolith Surface

The monolithic column, housed in a MP tube, was connected to a syringe pump using a 1/16 in zero dead volume (ZDV) union. The monolith was rinsed with 0.5 mL of anhydrous ACN at a flow rate of 10 $\mu\text{L}/\text{min}$. A solution of the activating agent was prepared by mixing 25 mg DSC and 1.25 mL anhydrous ACN. This was sonicated and filtered through a 0.45 μm PVDF syringe filter. 13 μL TEA was added to 1.2 mL of the filtrate. 0.8 mL of this solution was pumped through the monolith at 10 $\mu\text{L}/\text{min}$, followed by 0.8 mL of anhydrous ACN at 10 $\mu\text{L}/\text{min}$ to remove unreacted DSC. The hydroxyl groups on the monolith surface now became activated as N-hydroxysuccinimidyl carbonate (NHS-carbonate) groups.

4.4.2.4 Immobilization of Fluorophore **45** on the Activated Monolith Surface

A solution of fluorophore **45** in anhydrous DMSO from Section 4.3.2.2 (90 mg fluorophore **45** in 100 μL DMSO) was mixed with 100 μL anhydrous DMSO, 250 μL anhydrous ACN and 1 μL TEA. This solution was pumped through the activated monolith (length was 75.4 mm) at a flow rate of 2 $\mu\text{L}/\text{min}$. While the fluorophore solution was pumped in, the effluent from the monolith (spent fluorophore solution) was collected into 20- μL fractions which were later analyzed by HPLC to determine the breakthrough volume. As mentioned in Section 4.3.2.1, the DMSO solution of fluorophore **45** contained 10% diol-terminated fluorophore **46** (lacking the primary amino group-terminated cleavable anchor) as contaminant, which was conveniently used as an internal standard for breakthrough analysis. Yellow green unretained **46** visibly

progressed through the monolith while bound fluorophore **45** turned the monolith orange colored. Once the orange colored front reached the end of the monolith, about 80 μL more of the fluorophore mix was pumped through it to ascertain complete loading, after which the monolith was washed with a 200 μL portion of a pH 9, 0.1M sodium bicarbonate solution at 5 $\mu\text{L}/\text{min}$. The alkaline solution was allowed to reside in the monolith for 3 hours to quench any unreacted NHS-carbonate group. The monolith was then rinsed, at a rate of 10 $\mu\text{L}/\text{min}$, with 400 μL of a 1:1 mixture of ACN and water with 0.1% TEA, followed by 600 μL of ACN containing 0.1% TEA. After immobilization, the monoliths were stored in closed vials with a few drops of ACN with 0.1% TEA to prevent their drying.

HPLC of the fractions was carried out using a Luna HILIC column (3 μm , 200 \AA , 150 mm x 4.6 mm) and isocratic elution with 88% B at 1 mL/min (A: 10mM MOPS and 5mM NaOH in water; B: 10mM MOPS and 5mM NaOH in ACN with 5% v/v water).

4.4.2.5 Determination of Cleavage Rate of the Immobilized Fluorophore

A 1.5 to 2.0 mm segment of the melting point tube containing the monolith solid phase reagent was cut using a ceramic cutting tool and a home-made cutting guide/holder (Figure 4.23). The segment was then inserted in a polyethylene tube with a 1/16 in. I.D. and 3/32 in. O.D. A 0.25 mm I.D., 1/16 in. O.D. PEEK tubing that was connected to the outlet of an HPLC pump was inserted to one end of the polyethylene tube. Another PEEK tubing of the same dimension that is connected to the inlet of a PDA detector was

inserted to the other end. The PEEK tubings and the monolith segment were held in place in the polyethylene tube by inserting tightly fitting polyethylene rings around each. A 50 mM formic acid solution titrated to pH 3.1 using LiOH was flushed at a flow rate of either 0.2 or 0.5 mL/min. The signal was recorded at a detection wavelength of 507 nm.

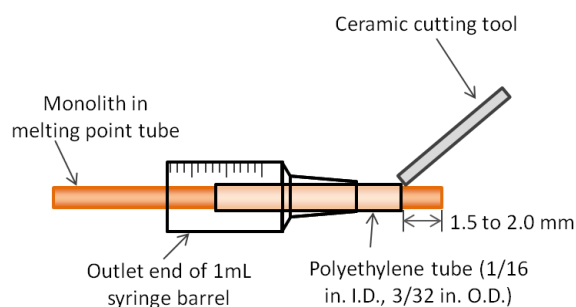


Figure 4.23. Cutting of the melting point tube containing the monolith solid phase reagent using a ceramic cutting tool and a cutting guide/holder consisting of a part of a 1-mL syringe barrel and a polyethylene tube.

4.4.2.6 Preparation of the Monolith Pipette Tip Cartridge

The monolith in the 75 mm long MP tube was cut into short segments (~1.5 mm) using a ceramic cutting tool and cutting guide/holder (Figure 4.23). A short segment was then placed in the tip of the syringe tool shown in Figure 4.24. A polyethylene tubing with a 1/16 in. I.D. was used to keep the monolith segment tightly in place at the syringe tip. The monolith was wetted with a few microliters of water before putting the plunger into the barrel of the syringe. The vent hole in the barrel of the syringe was kept open while pushing the plunger all the way down into the syringe barrel. Then, a finger was placed

over the vent hole and the plunger was pulled out, gently, but fast enough to create a good vacuum, to dislodge the monolith from the melting point tube. The monolith segment was then carefully placed into a 200 μL pipette tip, washed with 500 μL of 0.1% v/v TEA in ACN and stored in the same basic ACN solution.

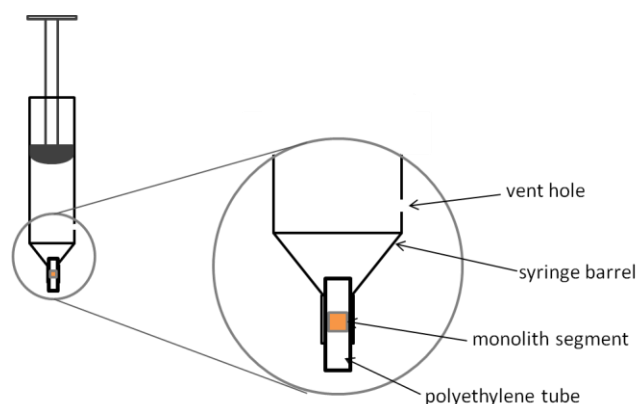


Figure 4.24. Syringe tool for removing the monolith segment from the glass MP tubing mold.

4.4.3 Results and Discussion

4.4.3.1 Preparation of the Monolithic Support for SCALER SPR

The 2-hydroxyethylmethacrylate (HEMA)-based monolith was chosen as a first generation solid support for the SCALER SPR because of the ease of its activation, ease of quenching and the inertness of the hydroxyl groups which do not participate in the derivatization reaction. Monoliths that were functionalized with carboxylic acid and epoxy groups were also considered initially, but were rejected because of various concerns. Free carboxylic acid groups on the monolith surface that were not coupled to

an amine during fluorophore immobilization could become activated during the final activation step of the amine-reactive group of the fluorophore and would permanently bind analytes during labeling. Glycidyl functionalities would require subsequent protection of the secondary amino groups that were formed during immobilization. There is also the possibility of forming tertiary amines which would turn the monolith into a weak anion exchanger, which would bind the multi-anionic fluorophore. The hydroxyl groups of the HEMA-based monolith, on the other hand, are passive during the final activation of the amine-reactive group of the fluorophore and their coupling with the amino group of the cleavable anchor through a carbamate group does not require any protection.

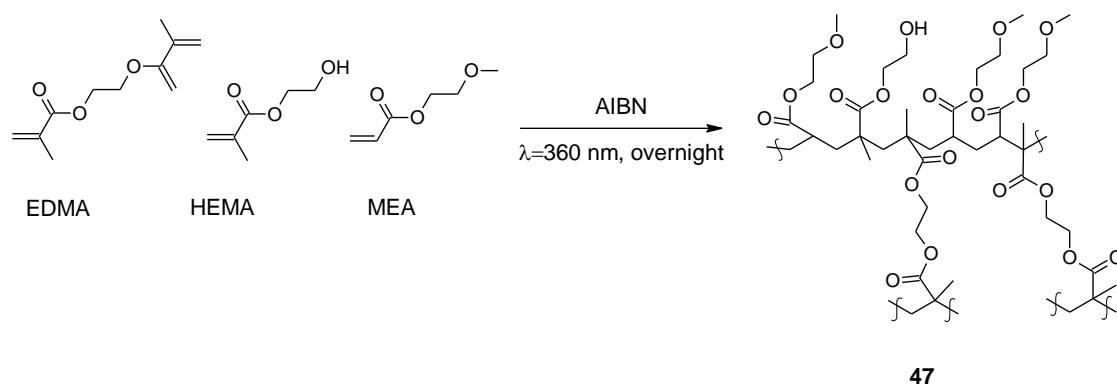


Figure 4.25. Schematic representation of the synthesis of the HEMA-based monolith **47**.

The photoinitiated free-radical polymerization of EDMA, HEMA and MEA to form HEMA-based monolith **47** is depicted in Figure 4.25. MEA, not used as one of the monomers in the original procedure of Svec *et al.* [86] was added as an inert diluent to regulate the number of hydroxyl groups (coupling sites) on the monolith surface

permitting the control, later on, of the surface density of the fluorophore. Different ratios of HEMA and MEA (10/0; 3/7 and 1/9 weight ratio) were tried and all of these monoliths had good permeability and loading of the fluorophore. Other diluents were also tested, such as acrylamide and N,N-dimethylacrylamide, but did not produce satisfactory monoliths.

4.4.3.2 Immobilization of the Fluorophore onto the Monolith Support

Activation of the hydroxyl groups on the monolith surface using N,N'-disuccinimidyl carbonate (DSC) to give activated monolith **48** was facile forming an amine-reactive carbonate ester that could react with the terminal amino group of the cleavable anchor of the fluorophore (Figure 4.26).

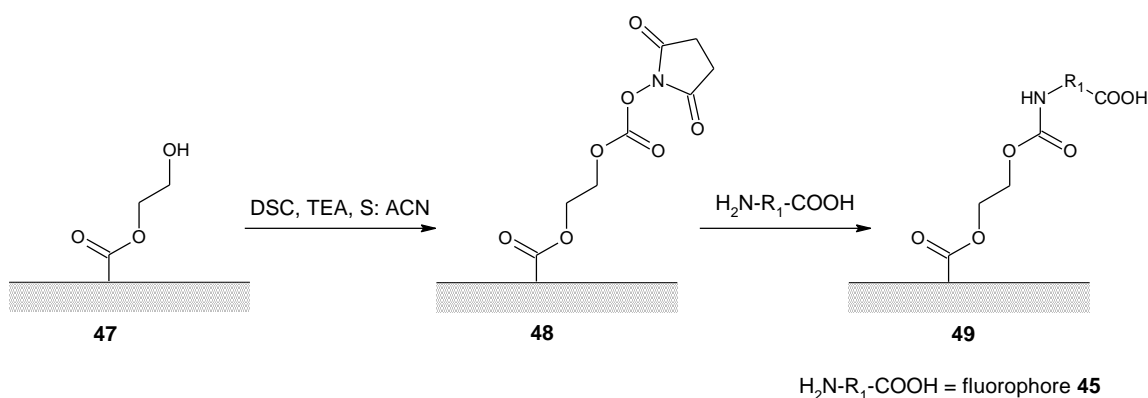


Figure 4.26. Activation of a hydroxyl group on the surface of the HEMA-based monolith using DSC and subsequent immobilization of the fluorophore.

After activation of the monolith, the fluorophore was loaded for immobilization producing monolith **49**. The eluent from the immobilization step was collected in 20- μL

fractions except in the end where 40 μL was collected. These were then analyzed by HILIC. Figure 4.27 shows the plots of the normalized peak areas of diol-terminated fluorophore **46** and amino-terminated fluorophore **45** with respect to fraction volume. Fluorophore **46**, present as a hydrolysis product of fluorophore **45** in the mixture was used as an internal standard and was assumed not to react with the monolith. From the plots, the approximate dead volume of the 75.4mm long monolith column was determined to be about 40 μL , corresponding to about 0.5 $\mu\text{L}/\text{mm}$. The estimated breakthrough point (inflection point) was 220 μL . Using these values, the approximate total amount of fluorophore that was immobilized, X , can be calculated using the following equation:

$$X = C_o \left(1 - \frac{A_{\min}}{A_{\max}} \right) (V_{\text{break}} - V_o) \quad (4.2)$$

where C_o is the concentration of fluorophore **45** in the feed, mM, A_{\min} is the averaged normalized area of fluorophore **45** before the breakthrough, A_{\max} is the maximum normalized peak area of **45**, V_{break} is the volume corresponding to the inflection point of the breakthrough and V_o is the dead volume of the monolith column. Using a feed concentration of 10 mM an approximate total fluorophore load of 1.5 μmol (2.7 mg) or 20 nmol (36 μg) per 1mm section was calculated. It can be seen in Figure 4.27 that a small fraction of fluorophore **45** eluted out before the breakthrough. This may suggest that the rate of carbamate formation was not fast enough for the flow rate used or that there was some sort of channeling in the monolith column.

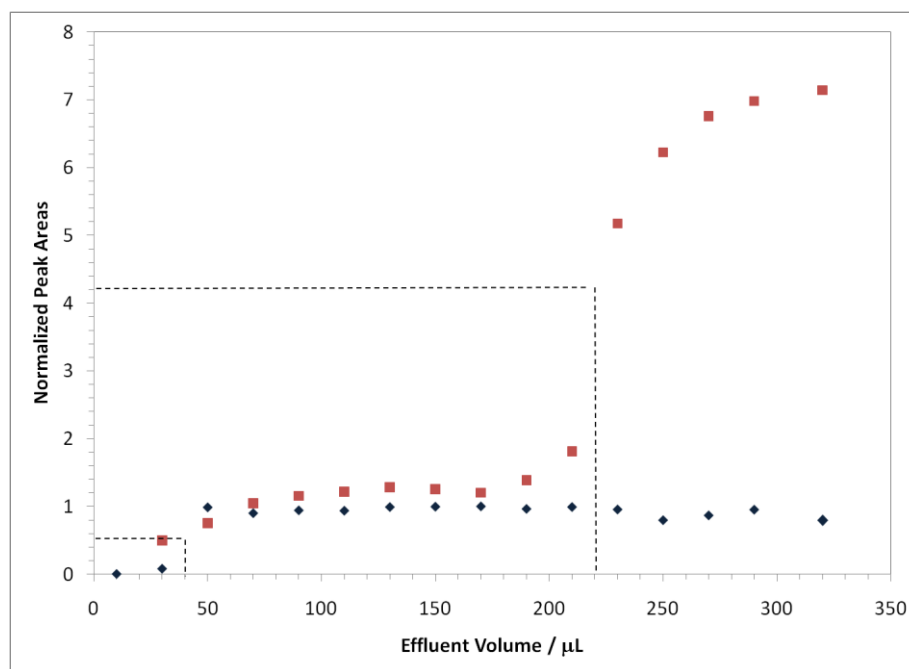


Figure 4.27. Plot of the normalized peak area of the internal standard fluorophore **46** (\blacklozenge) and fluorophore **45** (\blacksquare) versus the effluent volume. Peak areas of **46** were normalized to the largest peak area and their respective volumes. Peak areas of **45** were normalized to the peak areas of the internal standard.

4.4.3.3 Format of the Monolithic SPR

A large diameter (~ 1 mm), shallow bed format was selected for the monolithic SPR over a format that has a small diameter and deep bed (*e.g.*, 100 μm capillaries). The shallow bed format makes elution of reagents, solvents and samples through the SPR easier. For now, SPR activation and derivatization were done manually to allow easy alteration of each step while the methods were under development. The pipette tip SPR format shown in Figure 4.28 allowed easy loading of the reagents and solvents and easy collection of the effluents. It can be seen that the SPR with the immobilized fluorophore

has an orange color and one that has been treated with 3 μL of 1M acetic acid and washed with 7 μL of water had almost no color. The same SPRs were also placed under a UV lamp (Figure 4.29). The monolith with the fluorophore still attached had orange color while the one whose fluorophore had been removed had a faint light yellow green color. The eluted cleaving and wash solution (mixture of 3 μL of 1M acetic acid and 7 μL of water) had an intense yellow green fluorescence. The spent monolith bed had a faint fluorescence because the 7 μL water wash still left some of the fluorophore in the monolith bed.

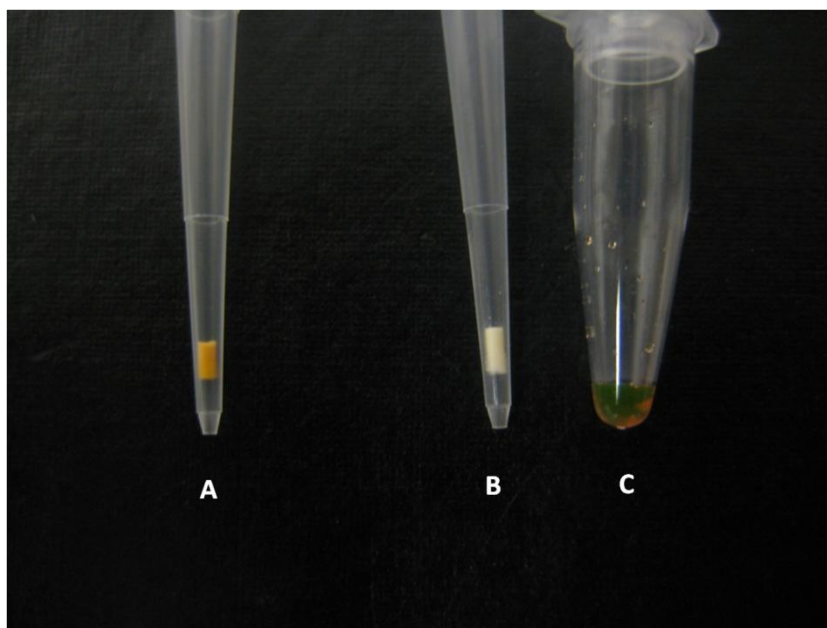


Figure 4.28. Photograph of the pipette tip monolithic SPR with the immobilized fluorophore (A) and after cleaving off the fluorophore (B). The 10- μL volume of the cleaving solution used was collected in a 0.2 mL tube (C).

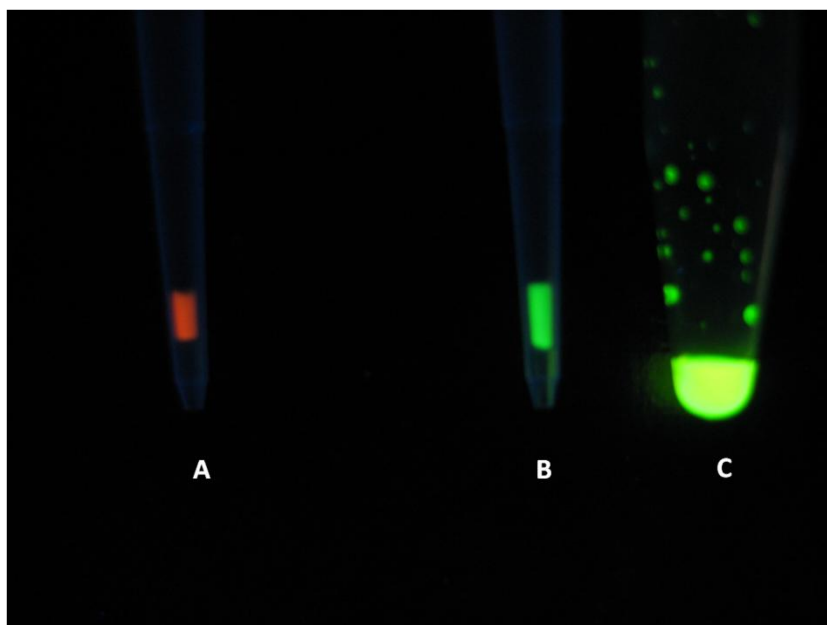


Figure 4.29. Photograph of the pipette tip monolithic SPR shown in Figure 4.28 under a UV lamp. The designations are the same as in Figure 4.28.

4.4.3.4 Rate of Cleavage of the Cleavable Group After Immobilization

Cleavage of the dioxolane group was re-examined to ascertain that formation of the carbamate bond, the close proximity of the solid surface or any other unforeseen or unknown factor associated with the immobilization step did not alter its cleavability at low pH. A short monolith segment (~1.5 mm) was connected in between an HPLC pump and a photodiode detector. A pH 3.1 buffer was flushed through at either 0.2 or 0.5 mL/min flow rate and the detector trace was recorded as displayed in Figure 4.30. The segment of the detector trace where the PDA signal was no longer overloaded yet the fluorophore was still readily detectable (the section between the two vertical dashed lines in Figure 4.30, which is between 7.2 and 15.0 min) was used to determine the

pseudo first order rate constant of the cleavage reaction. The time at the start of the curve is designated as $t = 0$ and the time at the end of the curve as $t = 15.0 - 7.2 \text{ min} = 7.8 \text{ min}$. Because the curve represents the concentration of the cleaved fluorophore (the product) with the passage of time, and not that of the immobilized fluorophore (the starting material or reactant), the latter has yet to be determined to get the rate of cleavage. Therefore, the area under the curve from Figure 4.30 was calculated using Simpson's rule. The curve was divided into short, equal time segments of $\Delta t = 1/240 \text{ min}$. The average absorbance signal in each of these segments, $S(t)$, and Δt were then used to calculate the total area under the curve, A_{total} , using the following equation:

$$A_{total} = \sum_{t=m}^n S(t)\Delta t = \sum_{t=m}^n A(t) \quad (4.2)$$

where m is the time at the beginning of the curve, designated as 0 min., n is the time at the end of the curve, 7.8 min, and $A(t)$ is the area under the curve at a given time. A_{total} is the area that represents the concentration of the immobilized fluorophore at $t = 0 \text{ min}$. To find the corresponding area of the immobilized fluorophore as a function of time, $A_{immob}(t)$, the following equation was used:

$$A_{immob}(t) = A_{total} - \sum_{t=m}^n A(t) \quad (4.3)$$

$A_{immob}(t)$ was then plotted against time in Figure 4.31 and fitted with an exponential decay curve using Equation 4.1. A k' of 0.65 was obtained (for $n=3$, $k' = 0.65$, RSD = 2.3%) leading to a $t_{0.5}$ and $t_{0.01}$ of 1.1 and 7.1 min, respectively. These agree with the

values determined for the cleavable anchor in free solution (1.0 and 6.5 min, Section 4.3.3, Table 4.2). Thus, immobilization did not alter the cleavability of the dioxolane ring and mild conditions can still be used to cleave off the fluorophore.

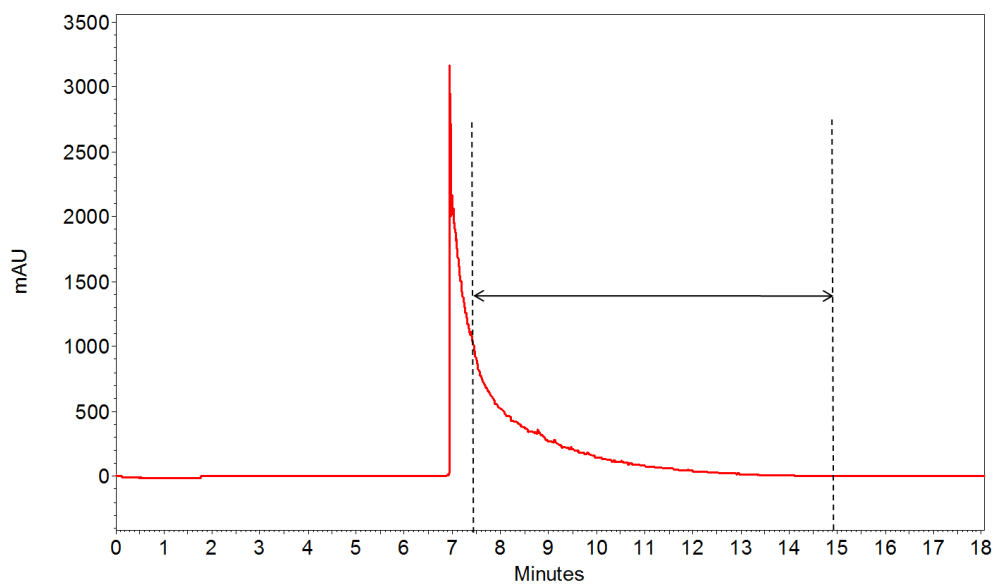


Figure 4.30. PDA signal at 507 nm obtained for the cleaving effluent leaving the 1.5 mm long SPR segment. A pH 3.1 buffer was used as cleaving solution and eluent.

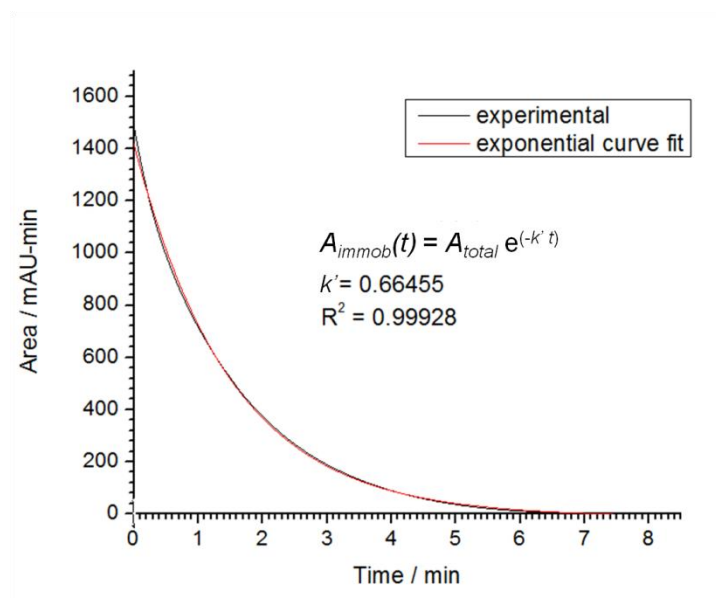


Figure 4.31. Plot of $A_{immob}(t)$ with respect to time. $A_{immob}(t)$ is the area that represents the concentration of the fluorophore as a function of time.

4.5 Labeling Tests using the SCALER SPR

4.5.1 Background and Objectives

Different amines were labeled using the SCALER SPR. Diamines 4-(2-aminoethyl)morpholine (AEM) and 1-methylpiperazine (MP) were used to test the ability of the reagent to effectively label amines at low concentrations. Since the SPR will eventually be used for the ϵ -amino groups of lysine residues in proteins, a lysine derivative, N-acetyl-L-lysine amide was also used as a test compound to mimic their reactivity.

4.5.2 Materials and Methods

4.5.2.1 Activation of the Fluorophore

Using a gel loader pipette tip, 50 μL ACN with 0.1% v/v TEA was added over the monolith segment in the SCALER SPR pipette tip cartridge and eluted through it using a 200 μL autopipette by pushing the plunger of the autopipet down to the first stop. An activating mixture containing 1.7 μL pentafluorophenyl trifluoroacetate, 96 μL anhydrous ACN and 2.8 μL TEA was prepared. A 50 μL aliquot of this solution was loaded into the pipette tip cartridge and slowly eluted through the monolith segment in the span of 1 min. The monolith segment was then washed by eluting, three times, with 50 μL of ACN that contained 0.1% v/v TEA. If the SPR was used for labeling immediately after activation, the cartridge was emptied out. Otherwise, it was kept immersed in the ACN/TEA wash / storage solution.

4.5.2.2 Labeling of Small Amines

A solution of the amine(s) in 0.1M aqueous sodium bicarbonate (pH 9) was loaded into the SPR cartridge using a gel loader pipette tip. The outlet of the SPR cartridge was placed into a collection vial and the sample solution was eluted through it by depressing the plunger of the autopipette to the first stop. The eluted sample was recycled five to twenty times by pipetting it back into the SPR cartridge, depending on the experiment. After labeling, the SPR cartridge was washed with 50 μL of the labeling buffer that was used to prepare the amine sample. The SPR was then quenched by eluting it with 50 μL of 0.1M morpholine in ACN that contained 0.1% v/v TEA. The quenching step was

repeated two more times, then the SPR cartridge was washed with 50 μL 0.1% v/v TEA in ACN, followed by 50 μL of 0.1M aqueous sodium bicarbonate solution and 50 μL of water to remove the salts and buffer. The quenched label and the labeled analytes were then cleaved off by loading 3 μL of a 0.1M solution of acetic acid in water directly on top of the SPR (excluding all air bubbles) and eluting a part of the acidic solution through the monolith segment to soak it. The acidic solution was allowed to stand in the monolith for a few minutes to maximize cleavage. The rest of the acidic solution was eluted out into a collection vial, followed by 7 μL wash water, and the combined collected solution was analyzed by CE.

4.5.2.3 Labeling of Diamines at Low Concentrations

A series of samples having a range of concentrations of 1-methylpiperazine (MP) (from 1mM down to 1nM) were prepared. The concentration of AEM, which was used as an internal standard, was kept constant at 10 μM . For the 1 μM to 1mM MP solutions 20 μL volumes were injected onto the SPR cartridges, for the 1nM and 10 μM MP solutions 200 μL volumes were used following the procedure in Section 4.5.2.2.

4.5.2.4 Labeling of Amino Acids

Amino acids were labeled the same way as in Section 4.5.2.2 except that the labeling buffer used was a mixture of 8 parts (v/v) of 25mM 3-(dimethylamino)-1,2-propanediol titrated to pH 9 with acetic acid and 2 parts (v/v) of water. Also, the quenching solution

contained 2 parts (v/v) of 250mM taurine in water and 8 parts (v/v) of 125mM 3-(dimethylamino)-1,2-propanediol in ACN.

4.5.2.5 Labeling of N-Acetyl-L-Lysine-Amide

The lysine residue mimic, N-acetyl-L-lysine-amide, was labeled as in Section 4.5.2.2, except the labeling buffer contained 3 parts (v/v) of 50mM boric acid titrated to pH 9 with NaOH and 7 parts (v/v) of ACN.

4.5.3 Results and Discussion

4.5.3.1 Activation of the SCALER SPR Amine-reactive Group

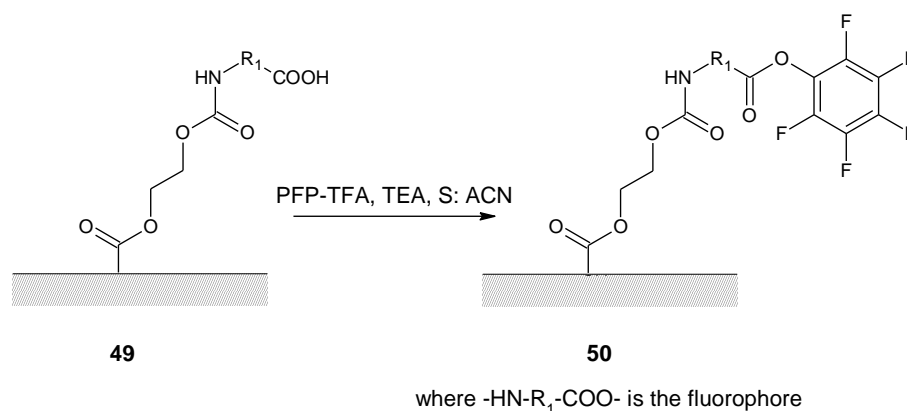


Figure 4.32. Activation of the carboxylic acid of the immobilized fluorophore using PFP-TFA to form the activated SCALER SPR **50**.

The activation of the carboxylic acid group of the fluorophore to form the activated SCALER SPR **50** was accomplished by the use of pentafluorophenyl trifluoroacetate (PFP-TFA) with base as depicted in Figure 4.32. The use of base was necessary to

prevent premature cleavage of the cleavable anchor due to the presence of trifluoroacetic acid and pentafluorophenol from any PFP-TFA hydrolysis. The PFP-TFA activation method gave cleaner activated ester products under basic conditions than those that used carbodiimide. In our previous tests with a similar pyrene derivative, 1-ethyl-3-(3-dimethylaminopropyl)carbodiimide (EDC) under basic conditions resulted in the formation of stable N-acylurea type adducts with the carboxylate of the fluorophore. The resulting fluorophore pentafluorophenyl ester was also found to be significantly more stable under alkaline conditions than the NHS ester.

To determine the degree of activation, SPR **50** was reacted with an excess of morpholine. CE-LIF analysis revealed that relative to the labeled morpholine there was very little of the free carboxylic acid in the cleaving solution when morpholine quenching occurred right after activation (Figure 4.33, A). . This indicates complete activation of the fluorophore in the SPR. We also determined the short-term stability of the PFP-ester in the storage solution, 0.1% v/v TEA in ACN, for 100 min, which was a conservative representation of any lag time between SPR activation and sample loading due to sample preparation. CE-LIF analysis of the cleaving solution obtained when morpholine quenching done 2 hours after the activation is shown in Figure 4.33, electropherogram B. The result showed that the PFP-ester is indeed stable in the storage solution.

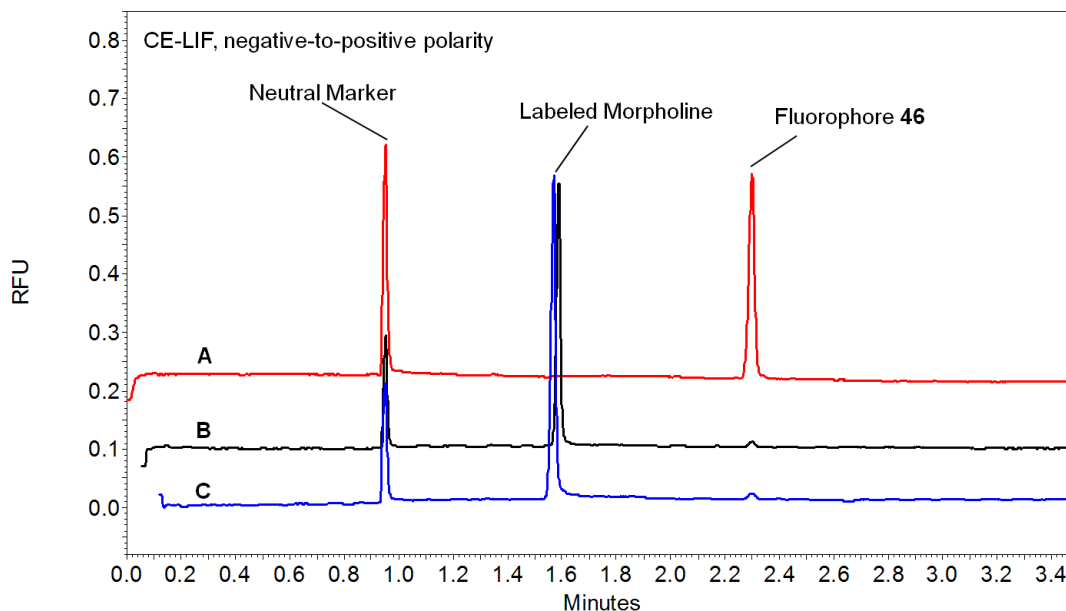


Figure 4.33. CE-LIF analysis of the cleaving solutions of an unactivated SCALER SPR (A), SPR quenched with morpholine immediately after activation (B) and SPR quenched with morpholine 100 minutes after activation (C). The fluorescent neutral marker is a trisulfonamide derivative of APTS obtained with diethanolamine.

4.5.3.2 Labeling of Diamines and Their Analysis by CE-LIF at Different pH Values

A mixture of the diamines, AEM and MP, were labeled using the SCALER SPR and the cleaved solution was analyzed in buffers having different pH values, the same way it was done with fluorophore **33** in Chapter 3. The pH values ranged from 2 to 10 to represent the entire operating pH range for CE. The electropherograms, which are overlaid in Figure 4.34, showed comparable fluorescence intensity between runs signifying that fluorescence is independent of the pH. The peak position of the labeled morpholine, whose charge is solely from the fluorophore, is also the same for all the runs which suggests that the charge state of the fluorophore is also pH-independent. As

with fluorophore **33**, CE separation selectivity for the labeled diamines (marked with *) also changed with pH and had a maximum in the $6.1 < \text{pH} < 8.0$ range.

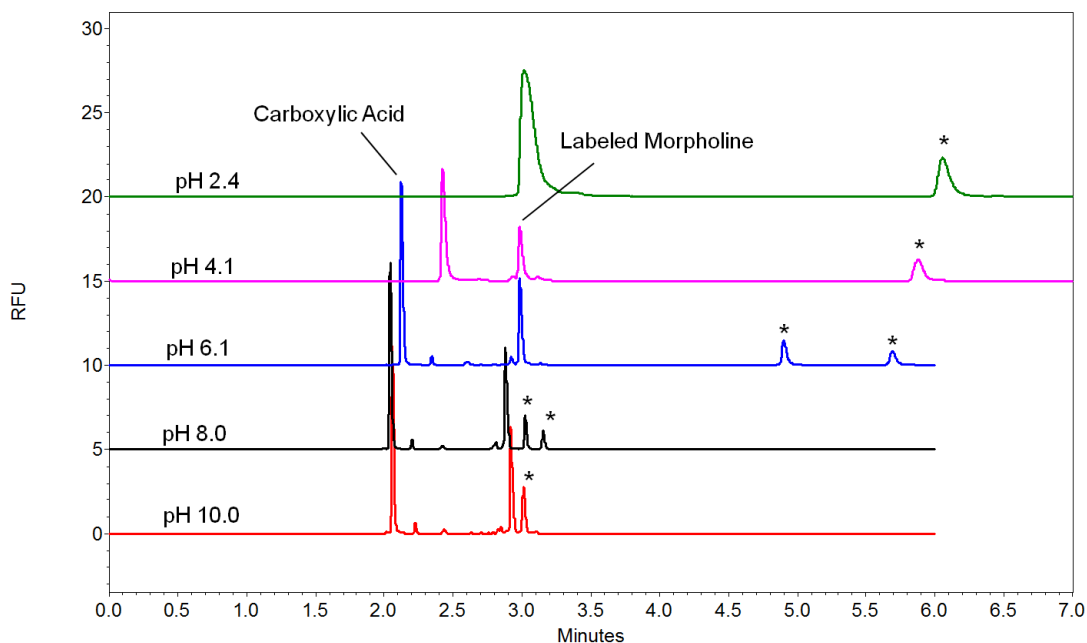


Figure 4.34. CE-LIF analysis, at different pH values, of the cleaving solutions obtained from the diamine labeling experiments.

4.5.3.3 Labeling of Diamines at Low Concentrations

To test the ability of SCALER SPR to label amines at low concentrations, solutions having both diamines AEM and MP were used as samples. The concentration of MP was decreased from 1mM down to 1nM. That of AEM, which was used as internal standard, was kept constant in all of the samples. The sample with the higher

concentrations of MP was labeled using only 20 μL aliquots. To improve detection, samples with the lower concentration of MP were labeled using 200 μL aliquots.

A portion of the electropherograms of the 20- μL set of samples is shown in Figure 4.35. As expected, the size of the peak corresponding to labeled MP went down relative to that of AEM (internal standard) as the concentration of the sample was decreased from 1mM to 1 μM . The samples for the 200- μL set were also analyzed the same way. When the normalized peak areas of MP were plotted against concentration (Figure 4.36), a linear relationship was obtained from 10nM up to 100 μM . Samples with higher concentrations showed a nonlinearity: it could be caused by incomplete labeling due to depletion of the active fluorophore in the SPR. The data for the 1nM sample was not included because it was below the LOQ (S/N=10). Figure 4.36 demonstrates the dynamic range of the labeling of MP and its CE-LIF analysis which is about 4 orders of magnitude. The lower limit of this range could still be improved (lowered) by using a 560 nm emission-side filter, a larger diameter capillary for the CE analysis and employing on-line preconcentration techniques. The reproducibility of the relative peak areas of the CE-LIF analyses were found to be about $\pm 0.2\%$.

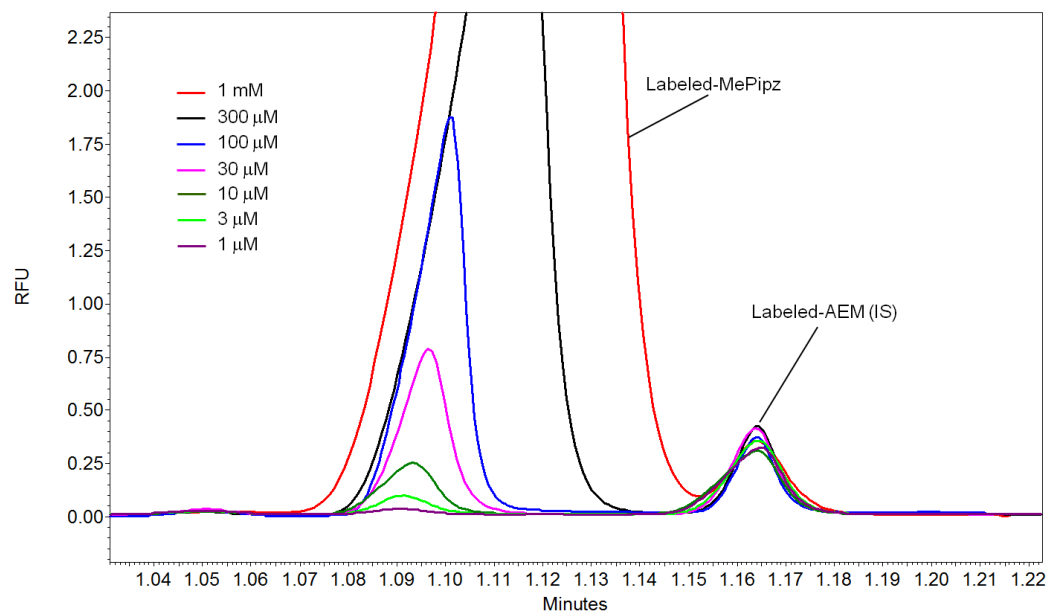


Figure 4.35. CE-LIF analysis of the cleaving solutions from the labeling of the diamine samples having concentrations from 1mM down to 1μM. The electropherograms are normalized to the area of the labeled AEM peak.

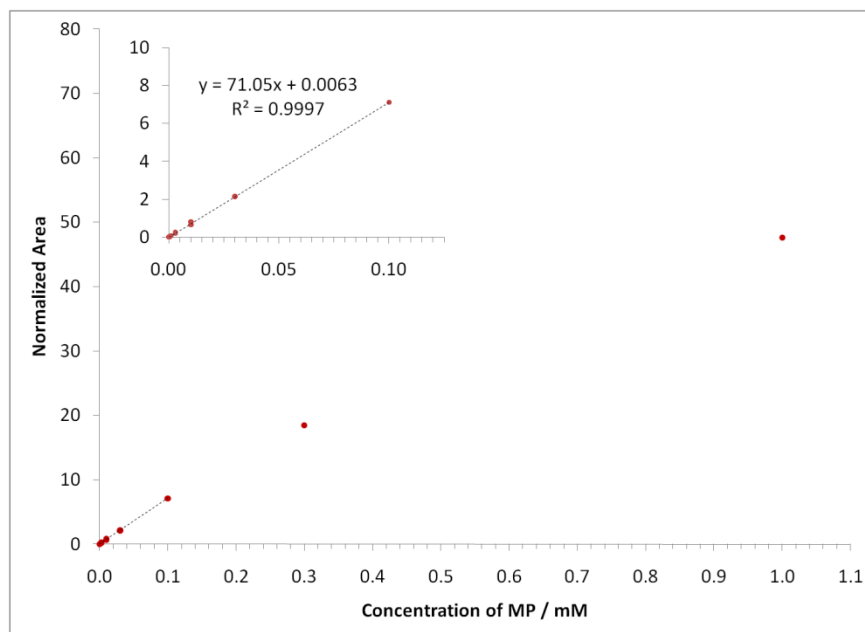


Figure 4.36. Plot of the normalized peak areas of MP against their concentrations. Inset is an expansion for the concentration range of 0 to 0.1 mM. The trend line was fitted from 1×10^{-5} to 0.1 mM (10 nM to 100 μ M). The two highest concentration data points deviate from this linearity and are not included in the fit.

4.5.3.4 Labeling of Amino Acids

Labeling tests using the SPR were done on aspartic and glutamic acid. Since the molecular weights of the labeled analytes are very similar, CE separation selectivity was based on their charge difference. The pH of the background electrolyte that led to maximum separation selectivity was determined by analyzing the samples at different pH values as in Section 4.5.3.2, except a narrower pH range was used. The CE-LIF analysis at pH 4.5 is shown in Figure 4.37 indicating good separation selectivity. The labeling experiments also showed a lower degree of labeling for the acidic amino acids than the diamines at comparable concentrations. This could be caused by steric hindrance on the α -amino group that reacts with the fluorophore or by ionic repulsion

between the anionic fluorophore and analytes. Histidine and arginine were also derivatized and analyzed by CE-LIF (Figure 4.38) at pH 10 where separation selectivity was good. Although the two had the same concentration in the sample, the histidine peak was significantly lower than that of arginine indicating a difference in their reactivities.

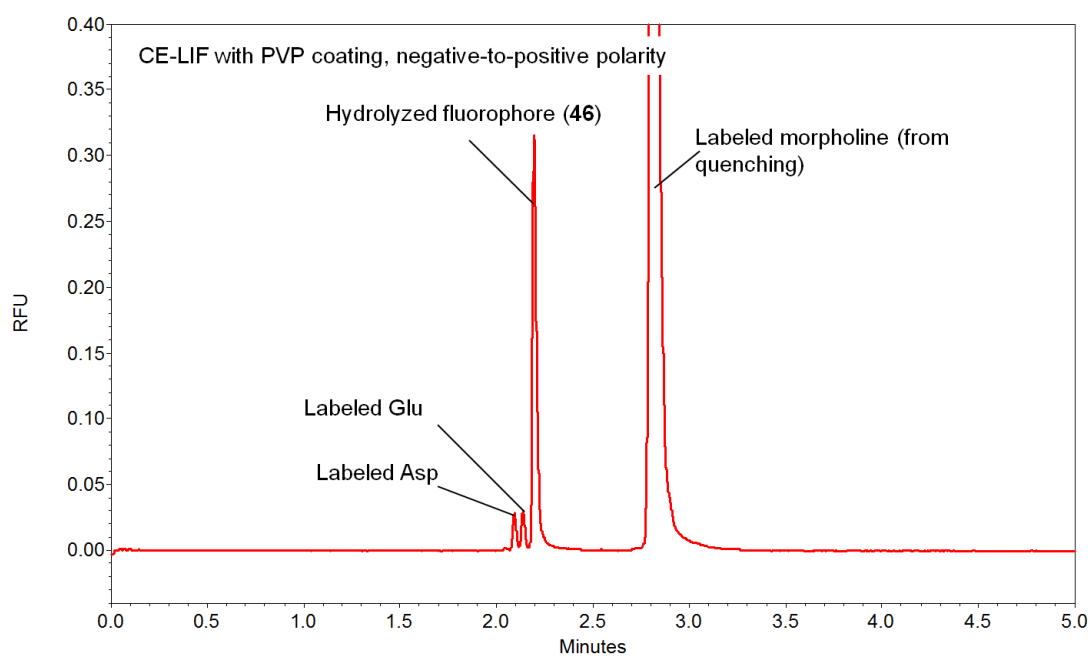


Figure 4.37. CE-LIF of cleaving solution from the labeling of a 20 μ L sample of 0.2mM aspartic and glutamic acid. BGE: 12.5mM acetic acid titrated to pH 4.5 with LiOH.

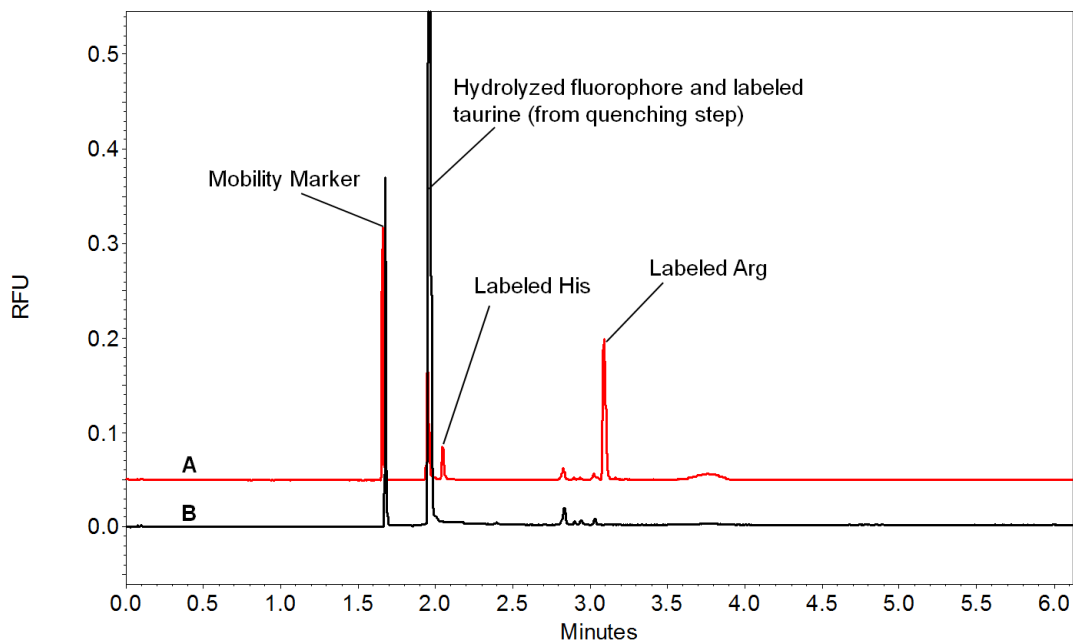


Figure 4.38. CE-LIF of the cleaving solution from the labeling of a 20 μ L sample of 0.2mM histidine and arginine. BGE: 13mM CHES titrated to pH 4.5 with LiOH.

To mimic the reactivity of the ϵ -amino groups of lysine residues in proteins and peptides, N-acetyl-L-lysine amide was labeled. Four labeling experiments were conducted with increasing number of passes of the sample through the SPR. Figure 4.39 shows that there is practically no change in the peak areas between the 2nd and 20th pass. This suggests that labeling was already complete at the 2nd pass and indicates that the fluorophore is very reactive toward the ϵ -amino groups of lysine residues.

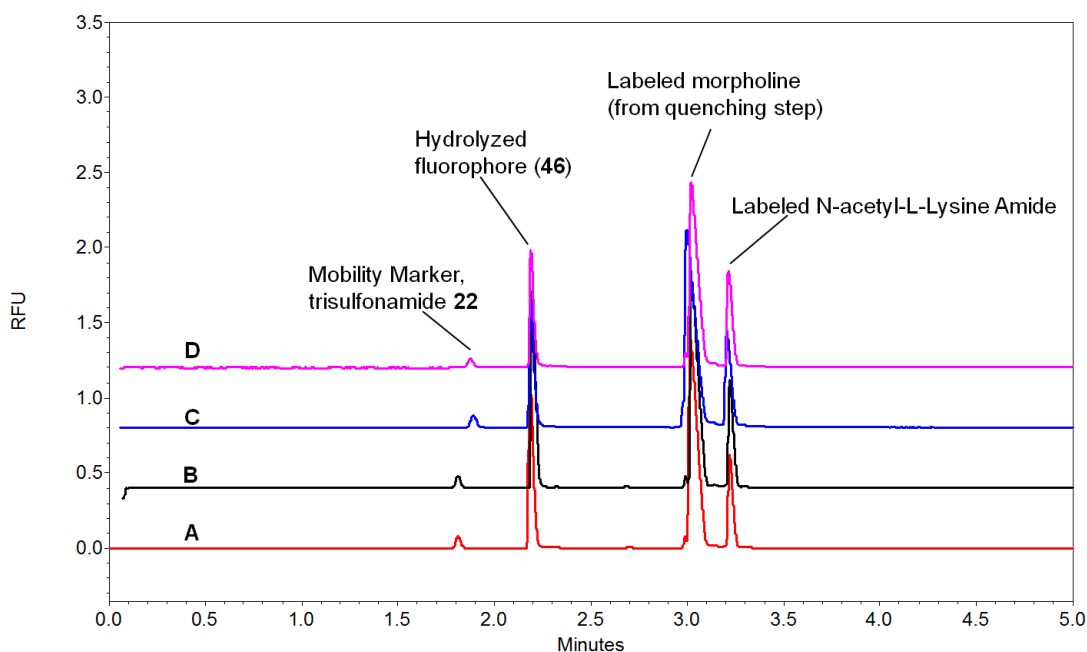


Figure 4.39. CE-LIF of cleaving solution from the labeling of a 20 μ L solution of 0.2mM N-acetyl-L-lysine amide. Different labeling reactions whose samples were passed through the SPR twice (A), 5 times (B), 10 times (C) and 20 times (D) were conducted.

4.6 Concluding Remarks

A solid phase fluorescent labeling reagent (SPR) was designed to simultaneously capture and label analytes, and then efficiently release the labeled-analytes under mild conditions (SCALER). The SCALER SPR design incorporates four separate parts: a fluorophore, an amine-reactive group, a cleavable anchor and a solid phase. A proof-of-principle implementation of the SPR was designed and prepared. The fluorescent label from Chapter 3 (fluorescent label **33**) was used as the starting fluorophore and its amine-reactive group was used as it was. A cleavable group was optimized for stability to sustain the harsh conditions during synthesis and conditions during the labeling reaction,

and cleavability for ease of release of the labeled analytes under mild conditions. A cleavable group based on an alkoxy-benzyl-dioxolane scaffold was shown to be stable under alkaline conditions but was easily cleaved under very mild conditions ($t_{1/2}$ of 1 min at pH 3.1). Tetra(ethylene glycol) spaces were used in between different parts of the SPR to maintain high aqueous solubility and local hydrophilicity.

The attachment of the cleavable anchor to the fluorophore was accomplished through a facile exchange of one of the sulfonamide groups on the pyrene ring with an alkoxy group. The exchange also improved the fluorescence properties of the fluorophore. The new fluorophore was found to have pH-independent fluorescence properties and charge state as well.

An acrylate-based monolithic solid phase was developed as the SPR solid support. The monolith was prepared by photoinitiated free radical polymerization of HEMA, EDMA and MEA monomers with AIBN as catalyst and 1-octanol as porogen. The monomers were chosen to provide hydroxyl groups on the solid surface to which the cleavable anchor of the fluorophore could be attached. The reactivity of the hydroxyl group as a coupling functionality is orthogonal to that of the amine-reactive group of the fluorophore. The immobilization of the completely assembled fluorophore was proven to not affect the cleavability of the cleavable anchor, thus, allowing analyte recovery under mild conditions. Moreover, due to the use of the monolithic solid phase, the elution of the cleaved off sample can be done with a minimal amount of solvent.

Using a pipette tip cartridge format of SCALER SPR, different amines were derivatized and analyzed by CE-LIF. A four orders of magnitude wide linear dynamic range was found for 1-methylpiperazine. Without the use of preconcentration or special techniques to improve detection sensitivity, an LOQ of 10nM was achieved. These experiments proved that SCALER SPR can be used to derivatize and detect analytes at low concentrations even without preconcentration. Amino acids were also derivatized and were found to have differing reactivities. Aspartic acid, glutamic acid and histidine had lower conversions to the labeled species probably due to steric hindrance and, for the first two, ionic repulsion. This is in contrast to the labeling of a lysine derivative, N-acetyl-L-lysine amine, which showed large peak areas at the same concentration and sample volume as the amino acids.

More tests have to be done using SCALER SPR to characterize its labeling behavior at much lower concentrations and look into its ability to proportionally or minimally label analytes having multiple reactive sites. For the latter, the spacing of the fluorophore has to be optimized either by dilution (statistical) or by other more sophisticated means.

5. CONCLUSION

5.1 Fluorescent Labeling Reagents Optimized for Capillary Electrophoretic Separations

Fluorescent labeling of proteins and other analytes have the potential to improve detection sensitivity down to attomolar concentrations. However, the use of fluorophores that are not optimized for CE separations can cause problems in their analysis. An ideal fluorophore for CE is one that has good hydrophilicity to prevent analyte aggregation and adsorption on the wall of the fused silica capillary. It is also advantageous to have pH-independent fluorescence properties and charge states. This permits application of the fluorophore anywhere in the operating pH range of CE.

Having a $\lambda_{\text{max}}^{\text{ex}}$ that is compatible with the emission lines of commonly available lasers is also beneficial because this enables the use of commercially available LIF detectors. For protein derivatization, it is best for the fluorophore to not alter the property of the protein that is being used to effect separation and characterization. The latter can be done by careful design of the property of the fluorophore to complement the separation technique used. Another approach to minimize alteration of the properties of the labeled proteins is minimal labeling, that is, incorporation of only one fluorescent label on one protein molecule. This also results in better quantitation since relative response factors between analytes will be proportional to their molar ratios. A second best approach in place of minimal labeling is proportional multiple labeling where the number of labels incorporated per analyte molecule is proportional to the size of the analyte. Both

minimal and proportional labeling can only be achieved efficiently and reproducibly using a novel approach to solid phase labeling.

5.2 Acridine-based Fluorescent Label

An amine-reactive monocationic fluorescent label had been synthesized. It has pH-independent fluorescent properties and charge states. The fluorophore has a λ_{\max}^{ex} at 493 nm and is compatible with the 488nm emission line of the commonly used Argon ion laser. Small amines have been labeled in solution and were effectively analyzed by CE with LIF detection. Proteins have been derivatized and analyzed using SDS-CGE with an LOD in the low nM range. Chicken ovalbumin was used as a model protein for cIEF analysis. The results show no detectable change of the pI of the protein after labeling. The preservation of the pI value is due to the presence of a monocationic charge on the fluorophore which replaces the cationic charge of the ϵ -amino group that is lost due to labeling. The use of LIF detection permitted lower loading of sample in cIEF which, in turn, resulted in better resolution: peaks with a Δ pI of about 0.05 could be resolved using a wide range, pH 3 to 10 carrier ampholyte mixture.

5.3 Pyrene-based Fluorescent Label

An amine-reactive, highly water soluble, tri-anionic pyrene-based fluorescent label was synthesized from the APTS core structure. Two strategies were used together to improve the λ_{\max}^{ex} of the core fluorophore, which is 425 nm, without changing its desirable properties. One of these strategies is the complete sulfonamidation of APTS

by a protected N-methyltaurine which, after deprotection in a later step of the synthesis scheme restores the tri-anionic charge of APTS. This brought about a bathochromic shift of ~45 nm. The other strategy involved the alkylation of the anilinic amine which was also served as a means to attach a tether that connects the analyte-reactive group to the core fluorophore. Alkylation brought about another ~25 nm shift bringing λ_{\max}^{ex} to 502 nm thus making it compatible with the 488 nm Argon ion laser. The fluorescent label has very good fluorescence quantum yield ($\Phi_{fluro33} = 0.76$) and has pH-independent fluorescence properties. The fluorescent label was designed to have a minimal hydrophobic alkyl and aromatic footprint, to have good water solubility and to avoid non-specific hydrophobic interactions with proteins and hydrophobic surfaces in aqueous solutions.

Efficient methods were developed for the synthesis and preparation of the fluorescent label. A method for the efficient reductive alkylation of very weak amines under dehydrating conditions using phosphorus pentoxide was optimized. Cleavage of the very stable neopentyl ester was improved to give fewer byproducts than those reported in literature. A method for high throughput purification of highly anionic compounds by semi-preparative HILIC was also established.

The newly synthesized fluorescent label was used to derivatize small diamines which were then analyzed by CE-LIF. Analysis at different pH values demonstrated its pH-independent fluorescence properties in actual CE separations. Proteins were labeled by

the tri-anionic fluorophore and were separated by SDS-CGE. Plots of the logarithm of the protein molecular weight versus migration time were linear indicating that labeling did not interfere with the size-based separation of proteins that occurs in a sieving matrix. Calculated LODs for these proteins were in the low nM range.

5.4 SCALER Solid Phase Fluorescent Labeling Reagent

A novel way of implementing a solid phase supported fluorescent labeling reaction has been developed. The distinguishing feature of SCALER is that as the analyte is labeled, it is removed from the solution and becomes immobilized on the solid matrix, preventing uncontrolled, multiple labeling of analytes with multiple reactive groups. The new solid phase reagent uses a cleavable anchor to connect a fluorophore to a solid phase. The fluorophore has a separate functional group for coupling with the analyte. The cleavable anchor was designed to be stable under the conditions used in the fluorophore synthesis yet efficiently cleavable under very mild conditions insuring efficient recovery and minimum dilution of the labeled analytes. The above scheme can achieve simultaneous capture and labeling, and efficient release (SCALER) of analytes. SCALER can lead to the *in situ* concentration of analytes which improves detection sensitivity on top of that from the fluorescence labeling. It also brings the promise of multiple proportional labeling and upon further development, mono-labeling of analytes that have multiple possible labeling sites.

A prototype of the SCALER SPR was built from the ground up. The fluorophore used was the tri-anionic pyrene-based fluorophore **33** because of its good fluorescence properties and high water solubility. An alkoxy-benzyl-1,3-dioxolane cleavable group was used as part of the anchor optimized to have high rate of cleavage under mild acidic conditions ($t_{1/2}$ of 1 min at pH 3.1) but remain stable under alkaline conditions. Again, to maintain good water solubility and hydrophilicity of the entire fluorophore, tetra(ethylene glycol) spacers flanked both sides of the cleavable dioxolane group. The cleavable anchor was connected to fluorophore **33** using a serendipitously observed displacement of one of its sulfonamide groups by an alkoxy group. This strategy connected the cleavable anchor and the fluorophore in a single step and at the same time improved the fluorescence quantum yield of the latter ($\Phi_{fluor46} = 0.86$). The solid phase used was a HEMA-based monolith with an EDMA crosslinker and a MEA diluent providing a means to control the density of hydroxyl groups on the monolith surface which serve as the attachment points of the cleavable anchor of the fluorophore. Cleavability of the dioxolane group was not affected by its attachment to the fluorophore and its immobilization on the solid surface ($k' = 0.7 \text{ min}^{-1}$, $t_{1/2} = 1 \text{ min}$, $t_{0.01} = 7 \text{ min}$ at pH 3.1).

SCALER SPR was used to label diamines and amino acids. The labeling experiments demonstrated its utility in the labeling of low concentration analytes without sample preconcentration. A lower limit of quantitation of 10nM was achieved for the CE-LIF analysis in a 25 μm capillary without the use of any online enrichment scheme. The

lower limit of efficient reaction for the SPR is expected to be lower than 10nM due to the linearity of the response factors even at this low concentration. The amino acids proved to have structure-dependent reactivities with the SPR. Samples of the same concentration and volumes gave different peak sizes: aspartic acid and glutamic acid were found to be least reactive, histidine was slightly better and arginine was significantly more reactive than the others. N-acetyl-L-lysine amide was also labeled which proved that the SPR is very reactive toward the ϵ -amino group of lysine residues. Several experiments and characterizations still need to be done for the SCALER SPR. The solid phase has yet to be well characterized to determine its actual morphology in order to optimize its surface area and mass transfer properties. Proteins will have to be labeled and their products characterized to determine the degree of labeling and distribution of the labels. Based on these results, the surface density of the hydroxyl groups on the monolith surface will have to be optimized to achieve multiple proportional labeling and, ideally, mono-labeling of proteins.

REFERENCES

- [1] Rabilloud, T., *Proteomics* 2002, 2, 3-10.
- [2] Michels, D. A., Brady, L. J., Guo, A., Balland, A., *Analytical Chemistry* 2007, 79, 5963-5971.
- [3] Huang, T. M., Pawliszyn, J., *Analyst* 2000, 125, 1231-1233.
- [4] Craig, D. B., Wong, J. C. Y., Dovichi, N. J., *Analytical Chemistry* 1996, 68, 697-700.
- [5] Lee, T. T., Yeung, E. S., *Journal of Chromatography* 1992, 595, 319-325.
- [6] Lee, T. T., Yeung, E. S., *Analytical Chemistry* 1992, 64, 3045-3051.
- [7] Paquette, D. M., Sing, R., Banks, P. R., Waldron, K. C., *Journal of Chromatography B-Analytical Technologies in the Biomedical and Life Sciences* 1998, 714, 47-57.
- [8] Banks, P. R., *Trac-Trends in Analytical Chemistry* 1998, 17, 612-622.
- [9] Uchiyama, S., Santa, T., Fukushima, T., Homma, H., Imai, K., *Journal of the Chemical Society-Perkin Transactions 2* 1998, 2165-2173.
- [10] Santa, T., Okamoto, T., Uchiyama, S., Mitsuhashi, K., Imai, K., *Analyst* 1999, 124, 1689-1693.
- [11] Sjoback, R., Nygren, J., Kubista, M., *Spectrochimica Acta Part a-Molecular and Biomolecular Spectroscopy* 1995, 51, L7-L21.
- [12] Richards, D. P., Stathakis, C., Polakowski, R., Ahmadzadeh, H., Dovichi, N. J., *Journal of Chromatography A* 1999, 853, 21-25.
- [13] Wu, X. Z., Wu, J. Q., Pawliszyn, J., *Electrophoresis* 1995, 16, 1474-1478.
- [14] Strong, R. A., Liu, H. J., Krull, I. S., Cho, B. Y., Cohen, S. A., *Journal of Liquid Chromatography & Related Technologies* 2000, 23, 1775-1807.
- [15] Stoyanov, A. V., Ahmadzadeh, H., Krylov, S. N., *Journal of Chromatography B-Analytical Technologies in the Biomedical and Life Sciences* 2002, 780, 283-287.
- [16] Sze, N. S. K., Huang, T. M., Pawliszyn, J., *Journal of Separation Science* 2002, 25, 1119-1122.
- [17] Stoyanov, A. V., Fan, Z. H., Das, C., Ahmadzadeh, H., *et al.*, *Anal Biochem* 2006, 350, 263-267.

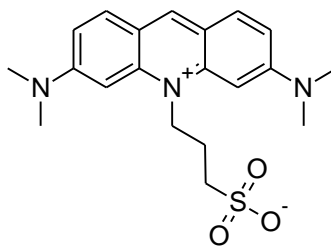
- [18] Henriksson, G., Englund, A. K., Johansson, G., Lundahl, P., *Electrophoresis* 1995, *16*, 1377-1380.
- [19] Unlu, M., Morgan, M. E., Minden, J. S., *Electrophoresis* 1997, *18*, 2071-2077.
- [20] Mckay, I. C., Forman, D., White, R. G., *Immunology* 1981, *43*, 591-602.
- [21] Brandtzaeg, P., *Annals of the New York Academy of Sciences* 1975, *254*, 35-54.
- [22] Valdesaguilera, O., Neckers, D. C., *Accounts of Chemical Research* 1989, *22*, 171-177.
- [23] Panchuk-Voloshina, N., Haugland, R. P., Bishop-Stewart, J., Bhalgat, M. K., *et al.*, *Journal of Histochemistry & Cytochemistry* 1999, *47*, 1179-1188.
- [24] Haugland, R. P., Kang, H. C., *US Patent 4,774,339*, 1988.
- [25] Hilal, S. H., Karickhoff, S. W., Carreira, L. A., *Quantitative Structure-Activity Relationships* 1995, *14*, 348-355.
- [26] Wolfbeis, O. S., Urbano, E., *Journal of Heterocyclic Chemistry* 1982, *19*, 841-843.
- [27] Kaewsuya, R., Miller, J. D., Danielson, N. D., Sanjeevi, J., James, P. F., *Analytica Chimica Acta* 2008, *626*, 111-118.
- [28] Yang, Y. K., Tae, J., *Organic Letters* 2006, *8*, 5721-5723.
- [29] Adamczyk, M., Chen, Y. Y., Mattingly, P. G., Pan, Y., Rege, S., *Journal of Organic Chemistry* 1998, *63*, 5636-5639.
- [30] Adamczyk, M., Rege, S., *Tetrahedron Letters* 1998, *39*, 9587-9588.
- [31] Williams, B. A., Vigh, C., *Analytical Chemistry* 1996, *68*, 1174-1180.
- [32] Williams, A. T. R., Winfield, S. A., Miller, J. N., *Analyst* 1983, *108*, 1067-1071.
- [33] Fukushima, T., Usui, N., Santa, T., Imai, K., *Journal of Pharmaceutical and Biomedical Analysis* 2003, *30*, 1655-1687.
- [34] Kiyohito Shimura, K.-I. K., *Electrophoresis* 1995, *16*, 1479-1484.
- [35] Shimura, K., Kamiya, K.-i., Matsumoto, H., Kasai, K.-i., *Analytical Chemistry* 2002, *74*, 1046-1053.
- [36] Bohne, C., Abuin, E. B., Scaiano, J. C., *Journal of the American Chemical Society* 1990, *112*, 4226-4231.

- [37] de Borba, E. B., Amaral, C. L. C., Politi, M. J., Villalobos, R., Baptista, M. S., *Langmuir* 2000, 16, 5900-5907.
- [38] Sasaki, R., Murata, S., *Langmuir* 2008, 24, 2387-2394.
- [39] Evangelista, R. A., Liu, M. S., Chen, F. T. A., *Analytical Chemistry* 1995, 67, 2239-2245.
- [40] Guttman, A., Pritchett, T., *Electrophoresis* 1995, 16, 1906-1911.
- [41] Guttman, A., *Nature* 1996, 380, 461-462.
- [42] Mohr, G. J., Wolfbeis, O. S., *Analytica Chimica Acta* 1995, 316, 239-246.
- [43] Jaros, M., Hruska, V., Stedry, M., Zuskova, I., Gas, B., *Electrophoresis* 2004, 25, 3080-3085.
- [44] Firouzabadi, H., Iranpoor, N., Jafarpour, M., Ghaderi, A., *Journal of Molecular Catalysis A: Chemical* 2006, 252, 150-155.
- [45] Amore, K. M., Leadbeater, N. E., Miller, T. A., Schmink, J. R., *Tetrahedron Letters* 2006, 47, 8583-8586.
- [46] Hussenether, T., Hubner, H., Gmeiner, P., Troschutz, R., *Bioorganic & Medicinal Chemistry* 2004, 12, 2625-2637.
- [47] Surendra, K., Krishnaveni, N. S., Sridhar, R., Rao, K. R., *Tetrahedron Letters* 2006, 47, 2125-2127.
- [48] Huang, D. W., Jiang, H., Nakanishi, K., Usherwood, P. N. R., *Tetrahedron* 1997, 53, 12391-12404.
- [49] Verardo, G., Giumanini, A. G., Strazzolini, P., Poiana, M., *Synthesis-Stuttgart* 1993, 121-125.
- [50] Amokhtari, M., Andersen, K., Ibazizene, M., Dhilly, M., *et al.*, *Nuclear Medicine and Biology* 1998, 25, 517-522.
- [51] Obrien, P. M., Sliskovic, D. R., Blankley, C. J., Roth, B. D., *et al.*, *Journal of Medicinal Chemistry* 1994, 37, 1810-1822.
- [52] McLaughlin, M., Palucki, M., Davies, I. W., *Organic Letters* 2006, 8, 3307-3310.
- [53] Baxter, E. W., Reitz, A. B., *Organic Reactions* 2002, 59, 1-714.

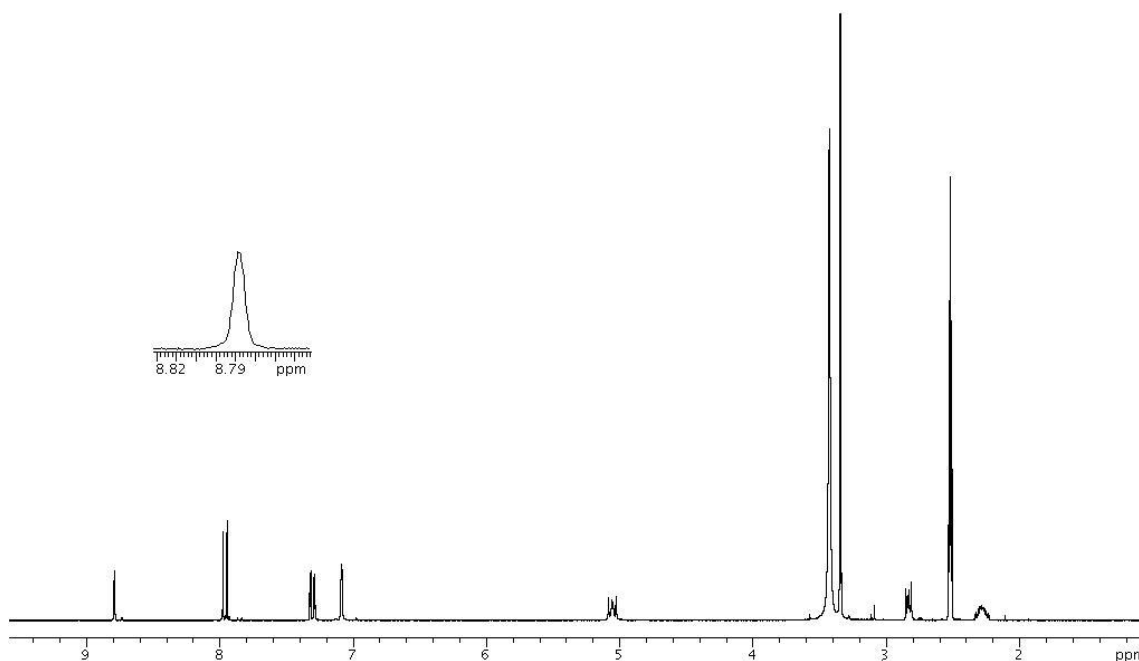
- [54] Roberts, J. C., Gao, H., Gopalsamy, A., Kongsjahju, A., Patch, R. J., *Tetrahedron Letters* 1997, 38, 355-358.
- [55] Lindner, H., Sarg, B., Helliger, W., *Journal of Chromatography A* 1997, 782, 55-62.
- [56] Lindner, H., Sarg, B., Meraner, C., Helliger, W., *Journal of Chromatography A* 1996, 743, 137-144.
- [57] Zhang, H., Guo, Z. M., Li, W., Feng, J. T., *et al.*, *Journal of Separation Science* 2009, 32, 526-535.
- [58] Neue, U. D., Mazza, C. B., Cavanaugh, J. Y., Lu, Z., Wheat, T. E., *Chromatographia* 2003, 57, S121-S127.
- [59] Krenkova, J., Lacher, N. A., Svec, F., *Analytical Chemistry* 2009, 81, 2004-2012.
- [60] Krenkova, J., Lacher, N. A., Svec, F., *Journal of Chromatography A* 2009, 1216, 3252-3259.
- [61] Svec, F., *Electrophoresis* 2006, 27, 947-961.
- [62] Dulay, M. T., Baca, Q. J., Zare, R. N., *Analytical Chemistry* 2005, 77, 4604-4610.
- [63] Krenkova, J., Bilkova, Z., Foret, F., *Journal of Separation Science* 2005, 28, 1675-1684.
- [64] Gao, C. X., Chou, T. Y., Krull, I. S., *Analytical Chemistry* 1989, 61, 1538-1548.
- [65] Zhou, F. X., Thorne, J. M., Krull, I. S., *Trac-Trends in Analytical Chemistry* 1992, 11, 80-85.
- [66] Li, G., Yu, J., Krull, I. S., Cohen, S., *Journal of Liquid Chromatography* 1995, 18, 3889-3918.
- [67] Szulc, M., Swett, P., Krull, I. S., *Biomedical Chromatography* 1997, 11, 207-223.
- [68] Holmes, C. P., Jones, D. G., *Journal of Organic Chemistry* 1995, 60, 2318-2319.
- [69] Holmes, C. P., *Journal of Organic Chemistry* 1997, 62, 2370-2380.
- [70] Kumar, P., Mahajan, S., Gupta, K. C., *Journal of Organic Chemistry* 2004, 69, 6482-6485.
- [71] Kumar, P., Bose, N. K., Gupta, K. C., *Tetrahedron Letters* 1991, 32, 967-970.

- [72] Jaeger, D. A., Chou, P. K., Bolikal, D., Ok, D., *et al.*, *Journal of the American Chemical Society* 1988, *110*, 5123-5129.
- [73] Jaeger, D. A., Jamrozik, J., Golich, T. G., Clennan, M. W., Mohebalian, J., *Journal of the American Chemical Society* 1989, *111*, 3001-3006.
- [74] Ross, A. R. S., Lee, P. J., Smith, D. L., Langridge, J. I., *et al.*, *Proteomics* 2002, *2*, 928-936.
- [75] Zeller, M., Brown, E., Bouvier, E., Konig, S., *J Biomol Tech* 2002, *13*, 1-4.
- [76] Konig, S., Schmidt, O., Rose, K., Thanos, S., *et al.*, *Electrophoresis* 2003, *24*, 751-756.
- [77] Yu, Y. Q., Gilar, M., Lee, P. J., Bouvier, E. S. P., Gebler, J. C., *Analytical Chemistry* 2003, *75*, 6023-6028.
- [78] Ashton, P. R., Huff, J., Menzer, S., Parsons, I. W., *et al.*, *Chemistry-a European Journal* 1996, *2*, 31-44.
- [79] Bouzide, A., Sauve, G., *Organic Letters* 2002, *4*, 2329-2332.
- [80] Svec, F., Frechet, J. M. J., *Analytical Chemistry* 1992, *64*, 820-822.
- [81] Viklund, C., Svec, F., Frechet, J. M. J., Irgum, K., *Chemistry of Materials* 1996, *8*, 744-750.
- [82] Palm, A., Novotny, M. V., *Anal. Chem.* 1997, *69*, 4499-4507.
- [83] Xie, S. F., Svec, F., Frechet, J. M. J., *Journal of Polymer Science Part a-Polymer Chemistry* 1997, *35*, 1013-1021.
- [84] Peters, E. C., Petro, M., Svec, F., Frechet, J. M. J., *Analytical Chemistry* 1998, *70*, 2288-2295.
- [85] Dulay, M. T., Quirino, J. P., Bennett, B. D., Kato, M., Zare, R. N., *Analytical Chemistry* 2001, *73*, 3921-3926.
- [86] Yu, C., Xu, M. C., Svec, F., Frechet, J. M. J., *Journal of Polymer Science Part a-Polymer Chemistry* 2002, *40*, 755-769.
- [87] Li, Y. M., Liao, J. L., Nakazato, K., Mohammad, J., *et al.*, *Analytical Biochemistry* 1994, *223*, 153-158.

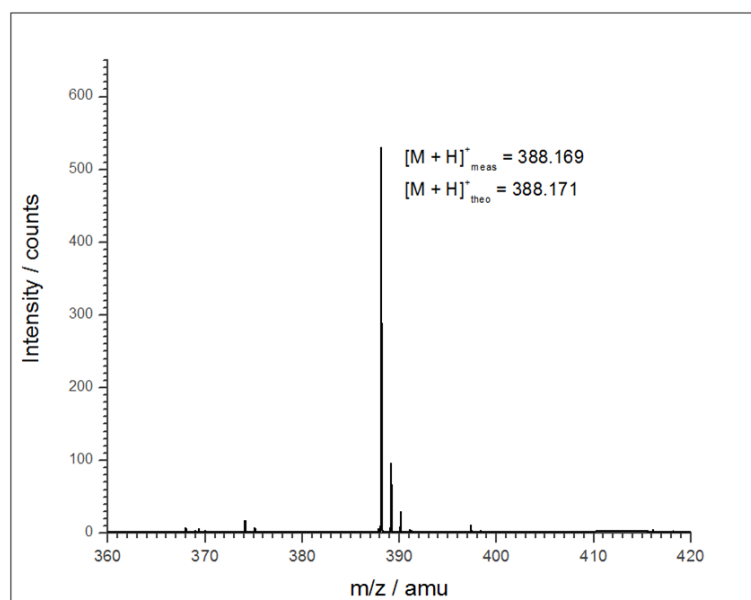
APPENDIX A**EXPERIMENTAL DATA FOR SECTION 2**

Sulfopropylated Acridine Orange (6)

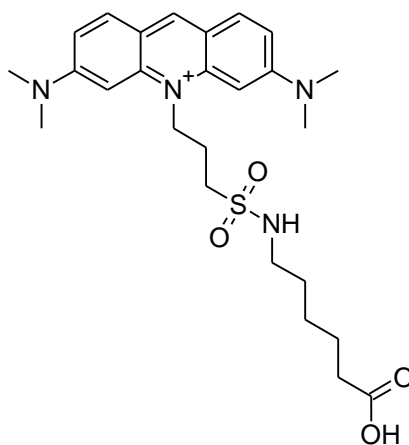
$^1\text{H-NMR}$ (300 MHz, d_6 -DMSO-triflic acid) δ 8.79 (s, 1H), 7.96 (d, 2H), 7.30 (d, 2H), 7.08 (s, 2H), 5.05 (t, 2H), 3.34 (s, 12H), 2.83 (t, 2H), 2.28 (m, 2H); ESI-TOF-MS $[\text{M}+\text{H}]^+$ meas. 388.170, $[\text{M}+\text{H}]^+$ calc. 388.171.



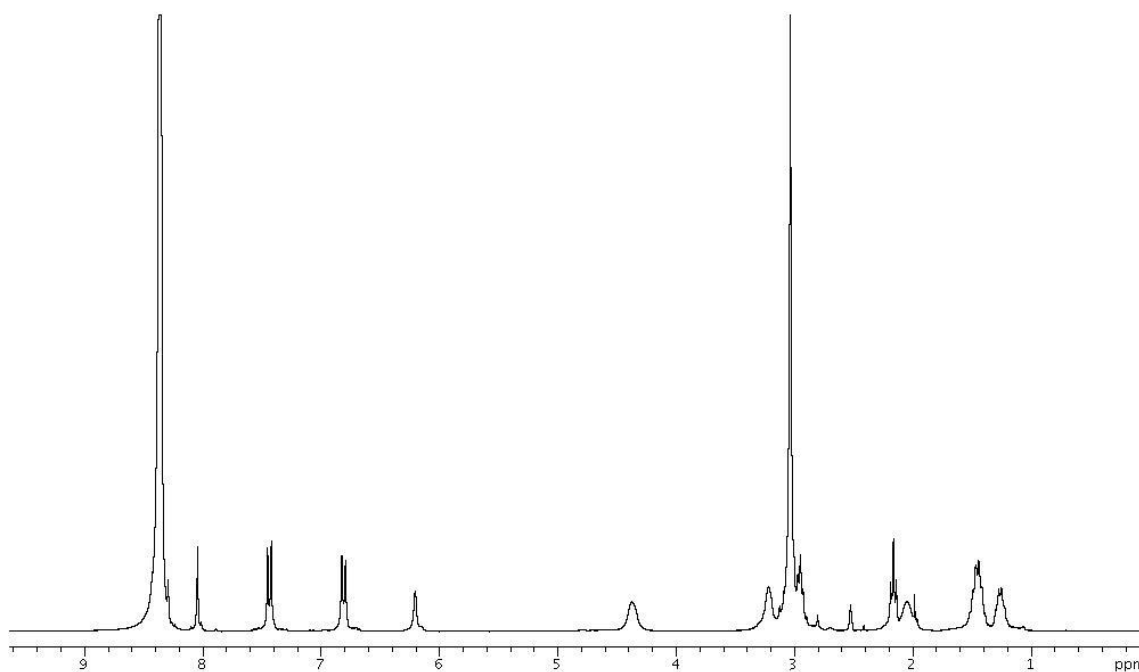
$^1\text{H NMR}$ (d_6 -DMSO with triflic acid)



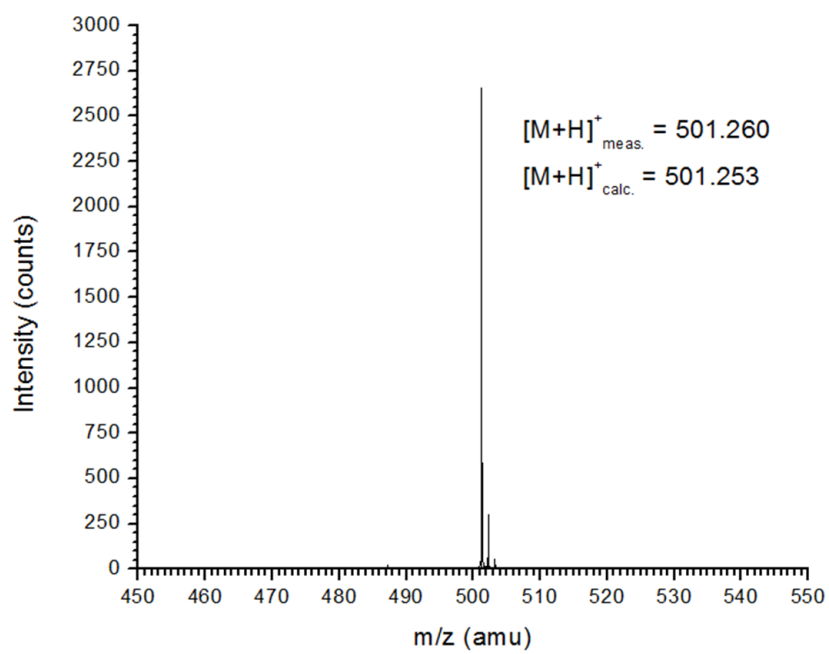
ESI-TOF-MS

Carboxylic Acid-Terminated Acridine Orange (9)

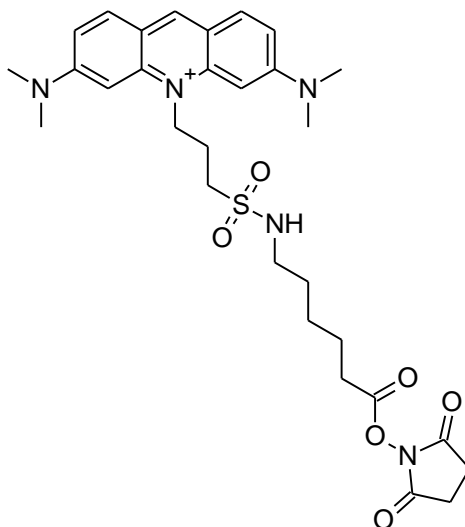
$^1\text{H-NMR}$ (300 MHz, d_6 -DMSO with trifluoroacetic acid) δ 8.04 (s, 1H), 7.43 (d, 2H), 6.81 (d, 2H), 6.2 (s, 2H), 4.37 (broad t, 2H), 3.22 (broad t, 2H), 3.03 (s, 12H), 2.92 (t, 2H), 2.16 (t, 2H), 2.04 (broad t, 2H), 1.52-1.39 (m, 4H), 1.30-1.25 (m, 2H); ESI-TOF-MS $[\text{M}+\text{H}]^+_{\text{meas.}}$ 501.288, $[\text{M}+\text{H}]^+_{\text{calc.}}$ 501.253.



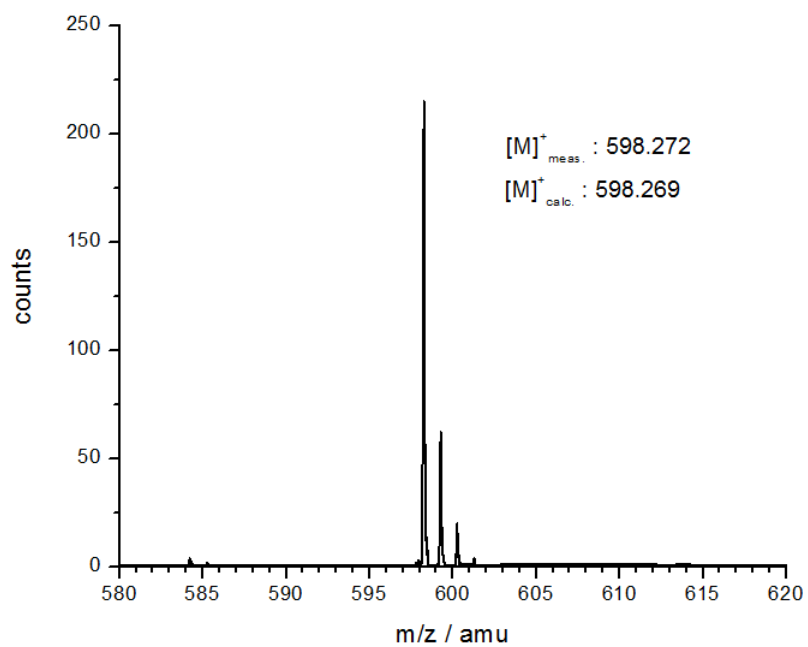
^1H NMR (d_6 -DMSO with TFA)



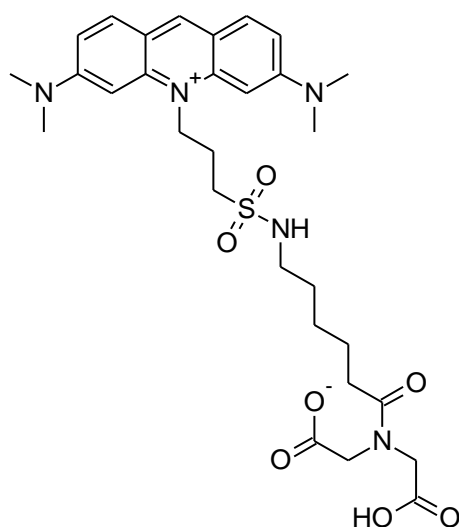
ESI-TOF-MS

Synthesis of Acridine Orange N-Hydroxysuccinimidyl Ester (10)

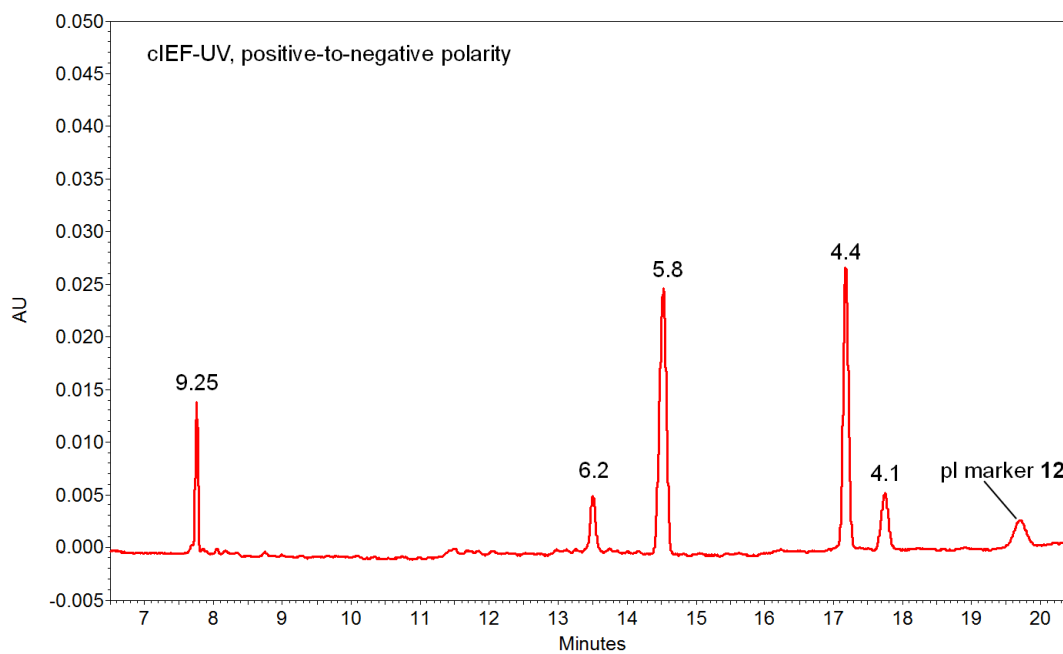
ESI-TOF-MS $[M+H]^+$ _{meas.} 501.288, $[M+H]^+$ _{calc.} 501.253.



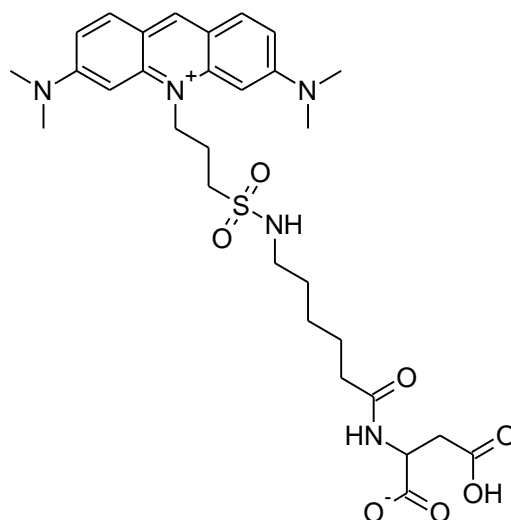
ESI-TOF-MS

pI Marker 12

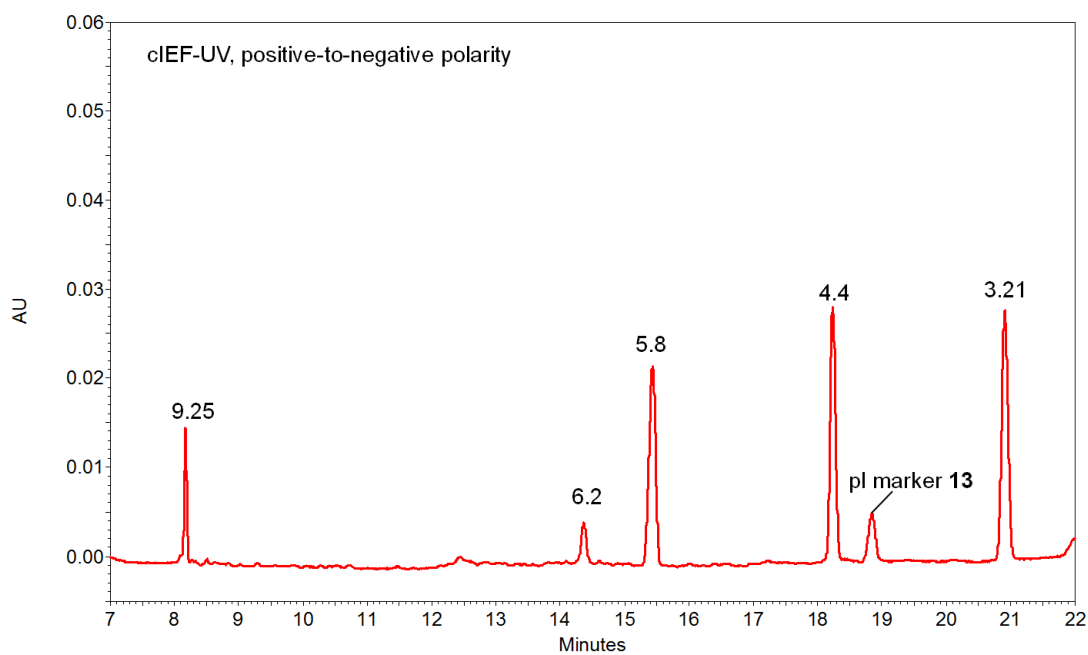
pI marker **12**: ESI-TOF-MS $[M+H]^+$ _{meas.} 616.282 , $[M+H]^+$ _{calc.} 616.280.



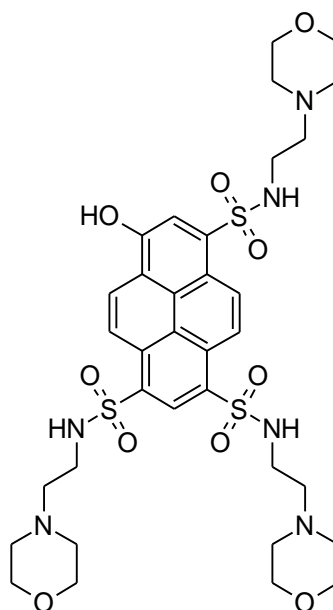
Mobilization trace of the cIEF-UV analysis of pI marker 12. Other peaks are UV-absorbing pI markers with known pI values

pI Marker 13

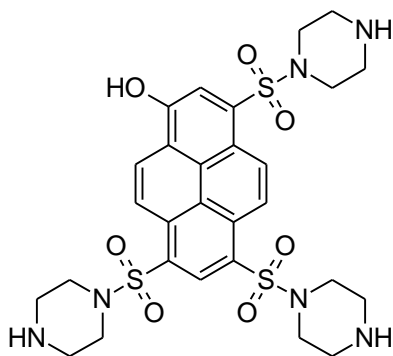
pI marker **13**: ESI-TOF-MS $[M+H]^+$ _{meas.} 616.281 , $[M+H]^+$ _{calc.} 616.280.



Mobilization trace of the cIEF-UV analysis of pI Marker 13. Other peaks are UV-absorbing pI markers with known pI values

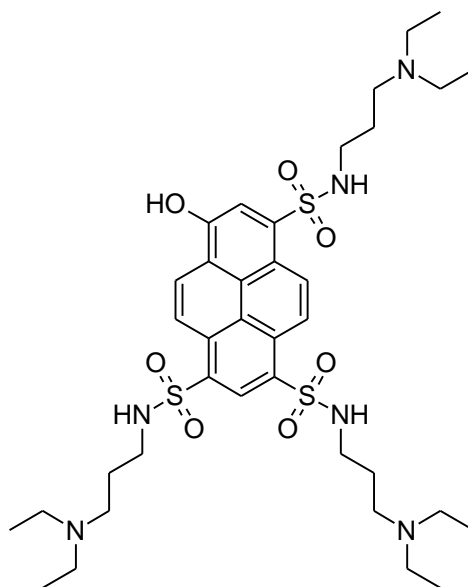
pI Marker 14

pI marker **14**: ESI-TOF-MS $[M+2H]^{2+}_{\text{meas.}}$ 398.1295, $[M+2H]^{2+}_{\text{calc.}}$ 398.1292.

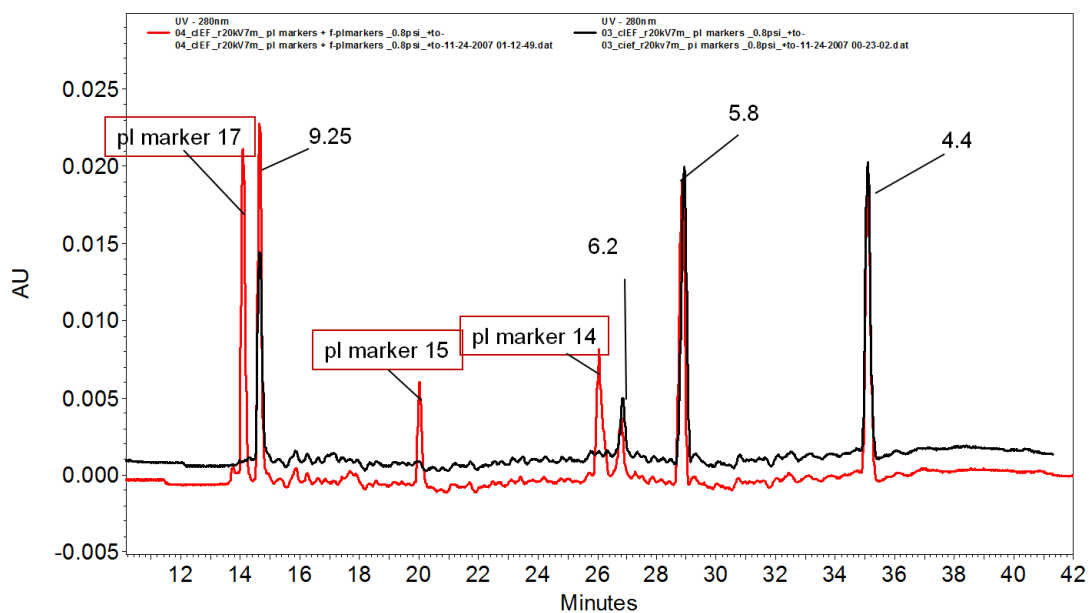
pI Marker 15

pI marker **15**: ESI-TOF-MS $[M+2H]^{2+}_{\text{meas.}}$ 332.0898, $[M+2H]^{2+}_{\text{calc.}}$ 332.0898.

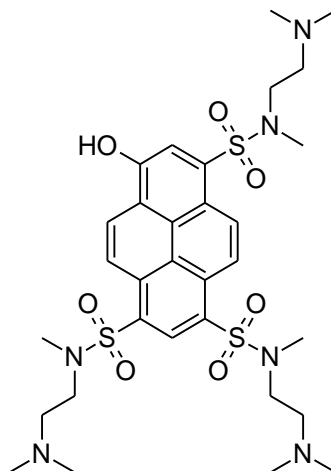
pI Marker 17



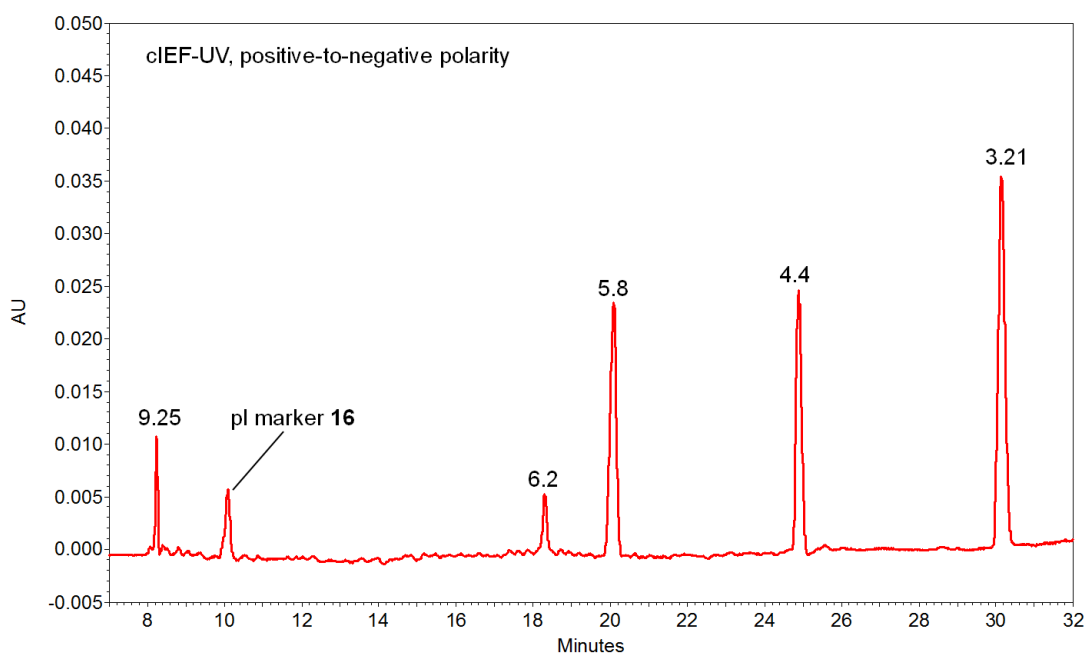
pI marker 17: ESI-TOF-MS $[M+2H]^{2+}$ meas. 398.1861 , $[M+2H]^{2+}$ calc. 398.1837.



Mobilization trace of the cIEF-UV analysis of pI Marke 13. Other peaks are UV-absorbing pI markers with known pI values (black trace is UV pI markers only, red trace is UV and fluorescent pI markers)

pI Marker 16

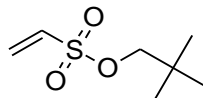
pI marker **16**: ESI-TOF-MS $[M+H]^+$ _{meas.} 711.2658 , $[M+H]^+$ _{calc.} 711.2663.



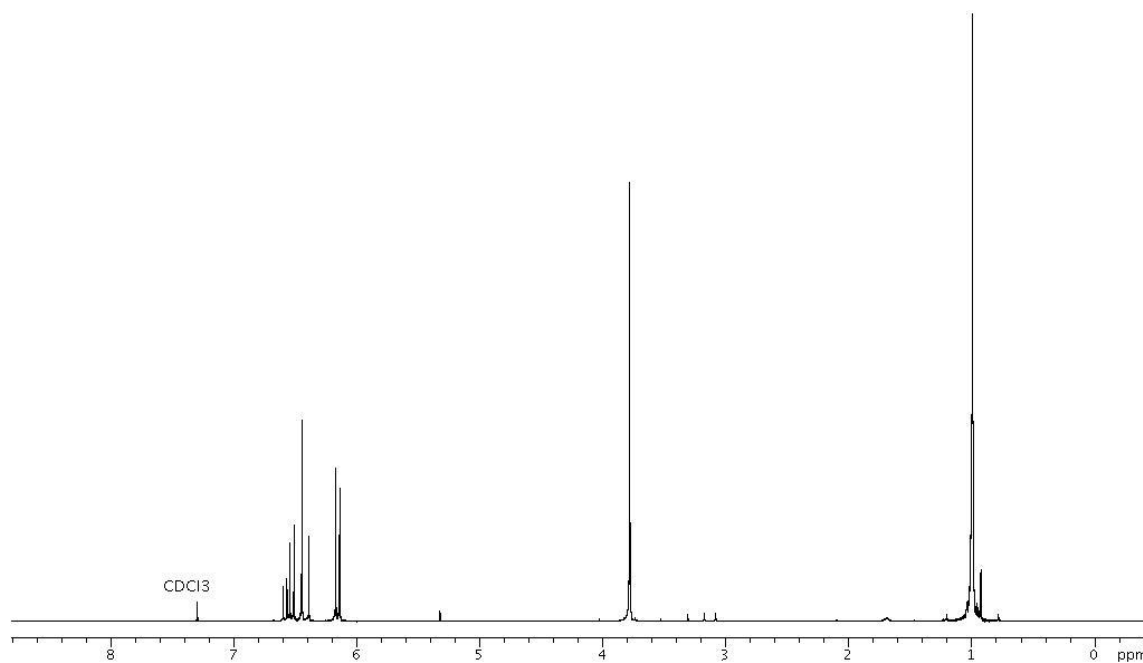
Mobilization trace of the cIEF-UV analysis of pI Marker 16. Other peaks are UV-absorbing pI markers with known pI values

APPENDIX B

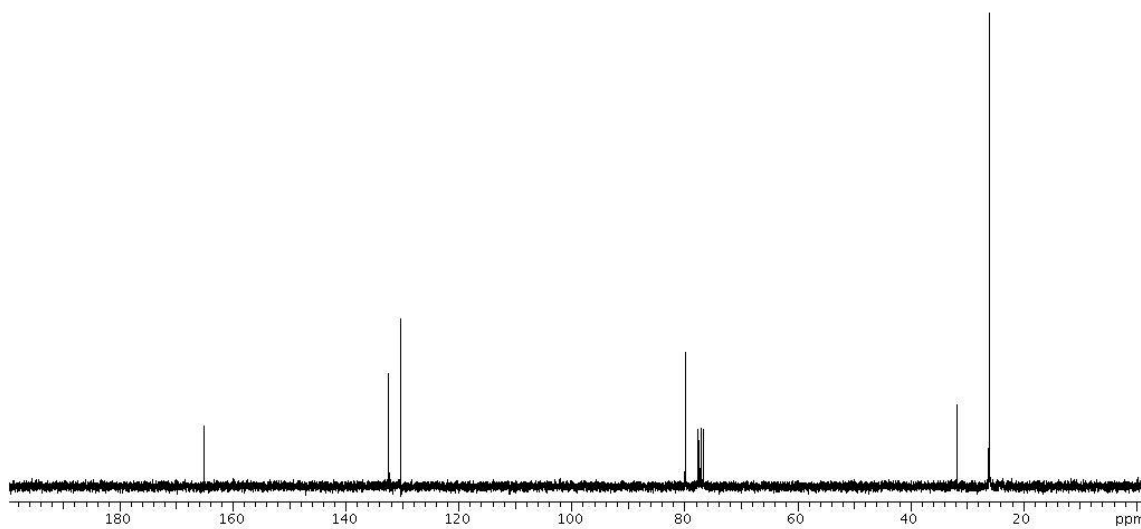
EXPERIMENTAL DATA FOR SECTION 3

2,2-Dimethylpropyl Ethenesulfonate (18)

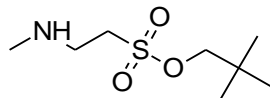
$^1\text{H-NMR}$ (300 MHz, CDCl_3) δ 6.60-6.14 (m, 3H), 3.78 (s, 2H), 0.98 (s, 9H); $^{13}\text{C-NMR}$ (300 MHz, CDCl_3) δ 132.3, 130.2, 79.6, 31.7, 26.1.



$^1\text{H NMR}$ (CDCl_3)

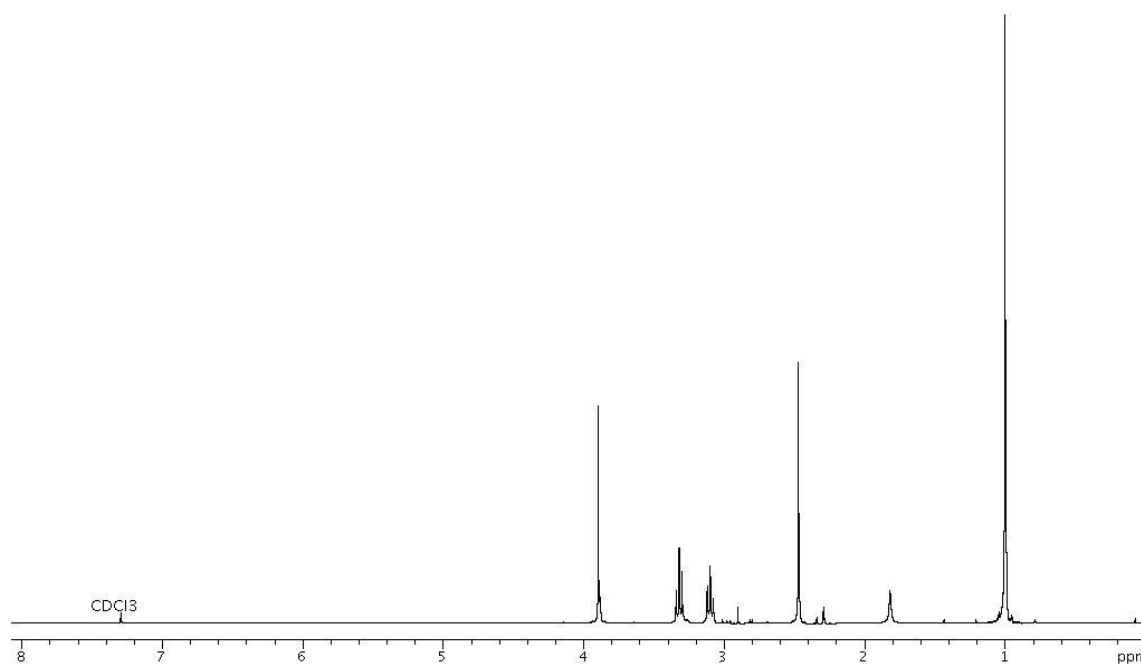


^{13}C NMR (CDCl_3)

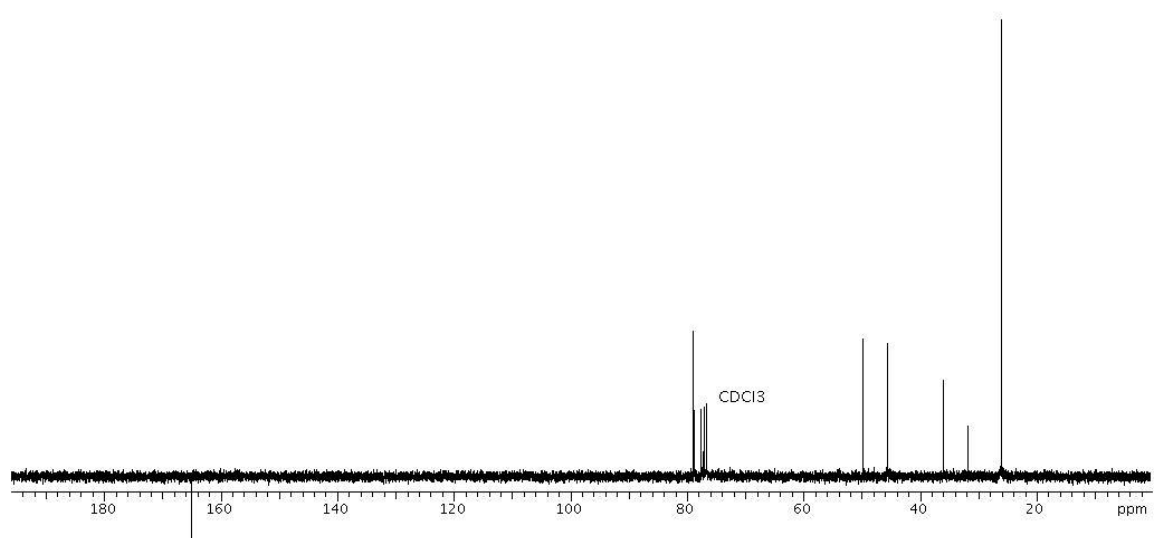
2,2-Dimethylpropyl 2-(methylamino)ethanesulfonate (19)

$^1\text{H-NMR}$ (300 MHz, CDCl_3) δ 3.89 (s, 2H), 3.34 (t, 2H), 3.310 (t, 2H), 2.47 (s, 3H),
1.82 (broad s, 1H), 1.01 (s, 9H); $^{13}\text{C-NMR}$ (300 MHz, CDCl_3) δ 78.8, 49.7, 45.6, 36.0,
31.8, 26.1.

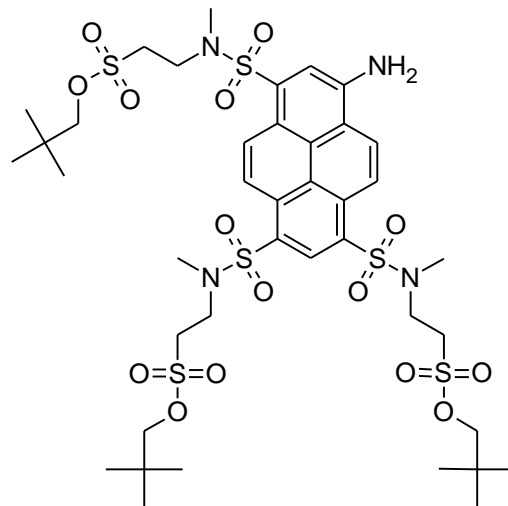
$[\text{M}+\text{H}]^+_{\text{meas.}} = 210.1161$, $[\text{M}+\text{H}]^+_{\text{calc.}} = 210.1158$



$^1\text{H NMR}$ (CDCl_3)

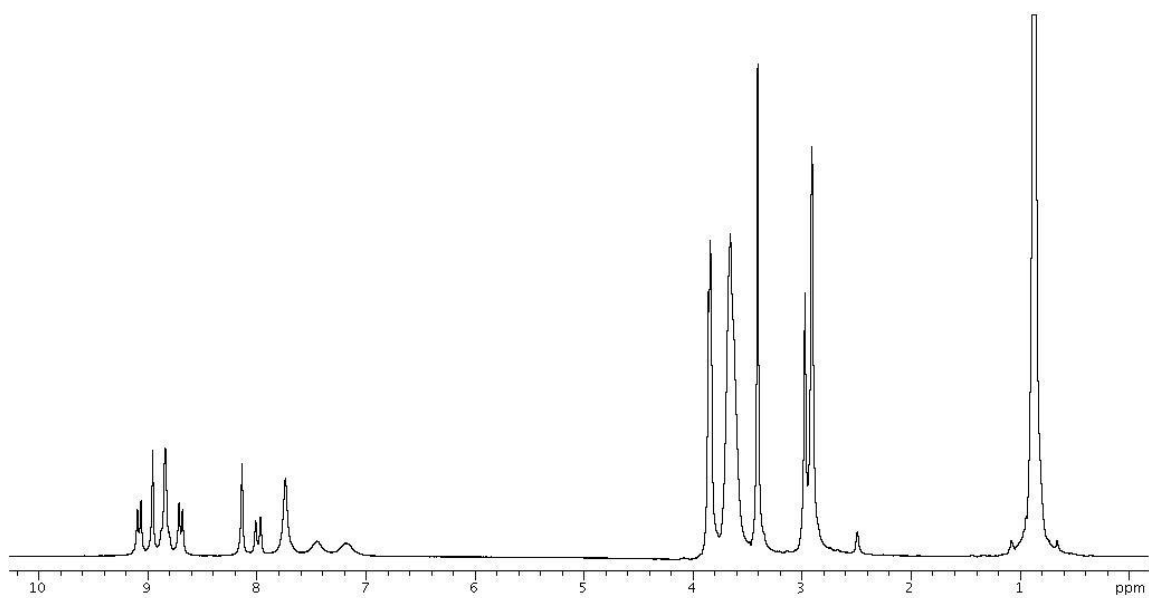
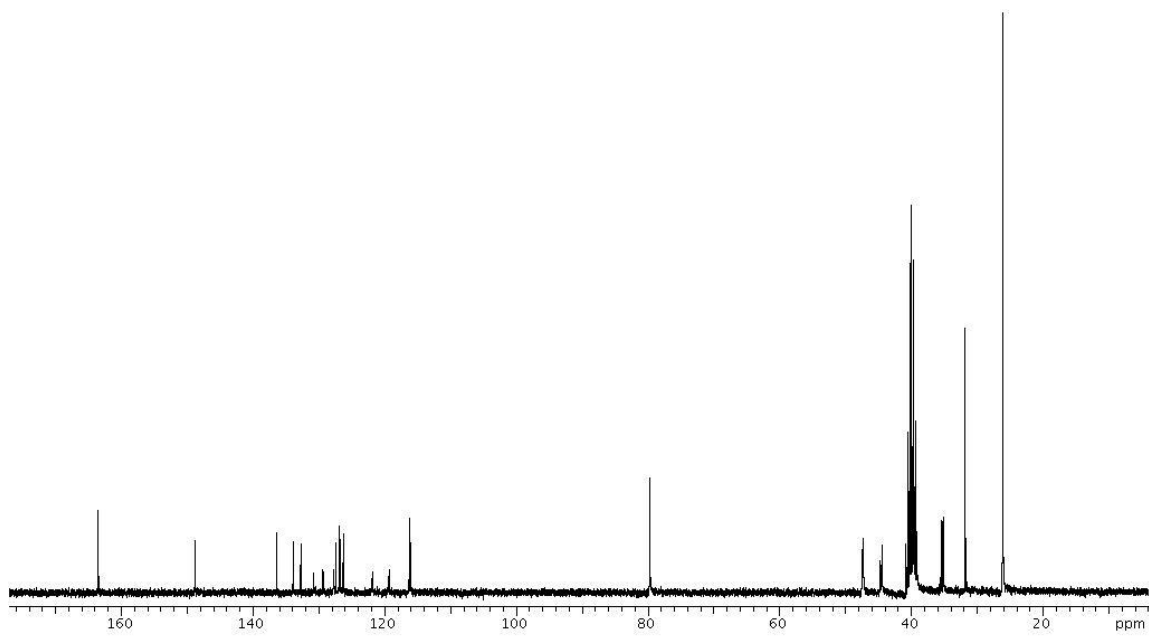
 ^{13}C NMR (CDCl_3)

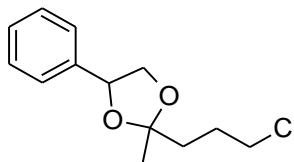
8-Aminopyrene-1,3,6-trisulfonamide (21)



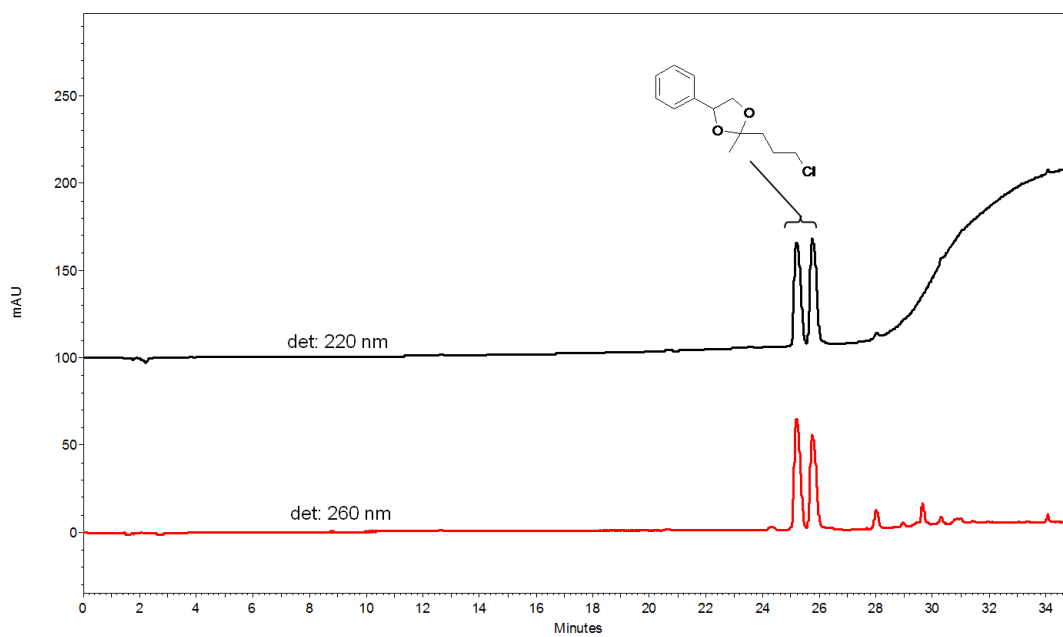
$^1\text{H-NMR}$ (300 MHz, d_6 -DMSO) δ 9.08 (d, 1H), 8.95 (s, 1H), 8.84 (broad s, 2H), 8.70 (d, 1H), 8.13 (s, 1H), 7.74 (broad s, 2H), 3.87-3.82 (m, 6H), 3.71-3.58 (m, 12H), 2.97 (s, 3H), 2.92-2.89 (m, 6H), 0.87 (broad s, 27H); $^{13}\text{C-NMR}$ (300 MHz, d_6 -DMSO) δ 163.4, 148.8, 136.4, 133.9, 132.7, 130.7, 129.3, 127.7, 127.4, 126.9, 126.7, 126.2, 121.8, 119.3, 116.2, 116.0, 79.71, 79.69, 79.64, 47.44, 47.30, 47.23, 44.70, 44.43 (broad), 35.44, 35.12, 35.04, 31.8, 26.0.

$[\text{M-H}]^-_{\text{meas.}} = 1029.2463$, $[\text{M-H}]^-_{\text{calc.}} = 1029.2463$

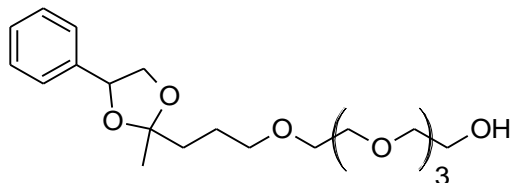
 ^1H NMR (CDCl₃) ^{13}C NMR (CDCl₃)

Dioxolane 24

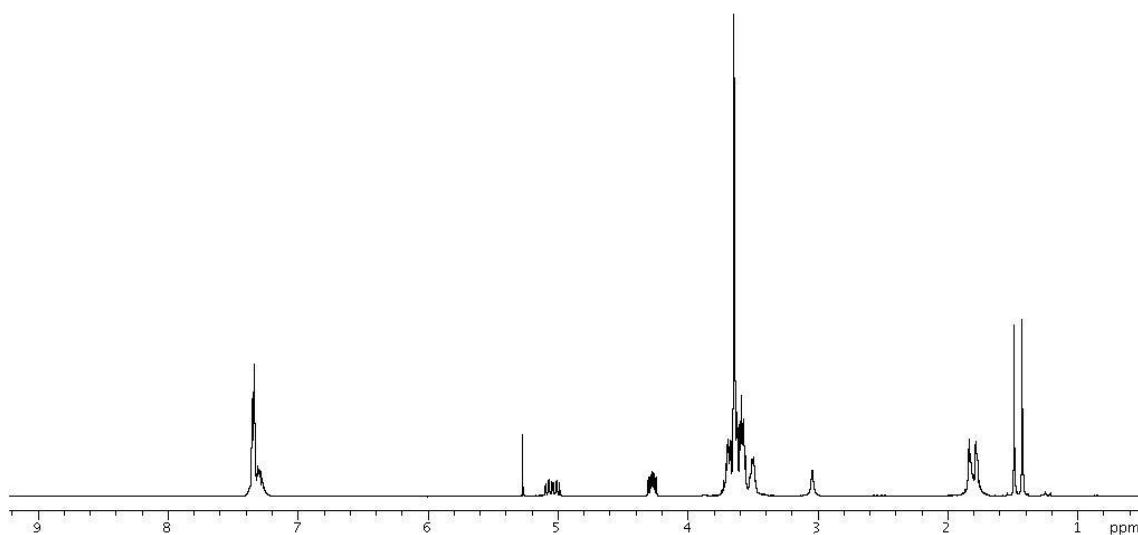
ESI-TOF-MS $[M+Li]^+$ _{meas.} 247.13, $[M+Li]^+$ _{calc.} 247.11.

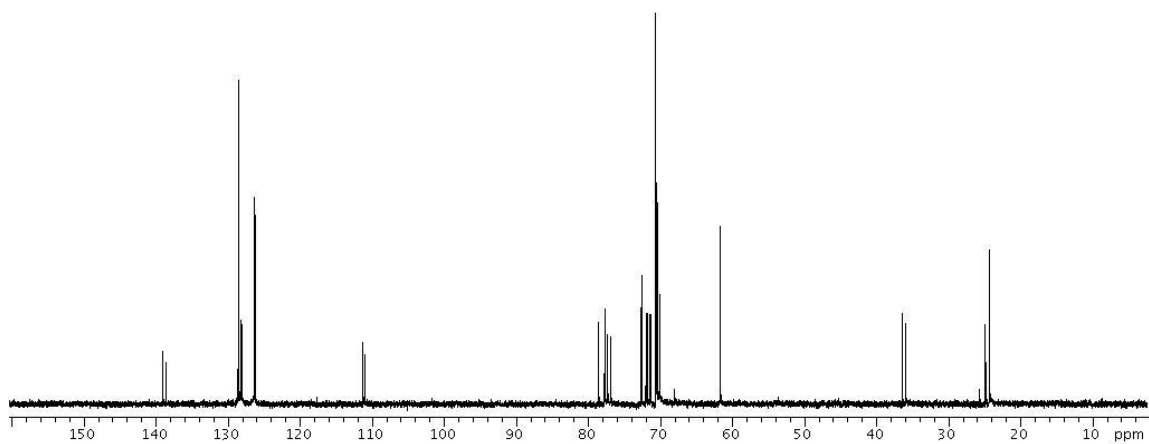
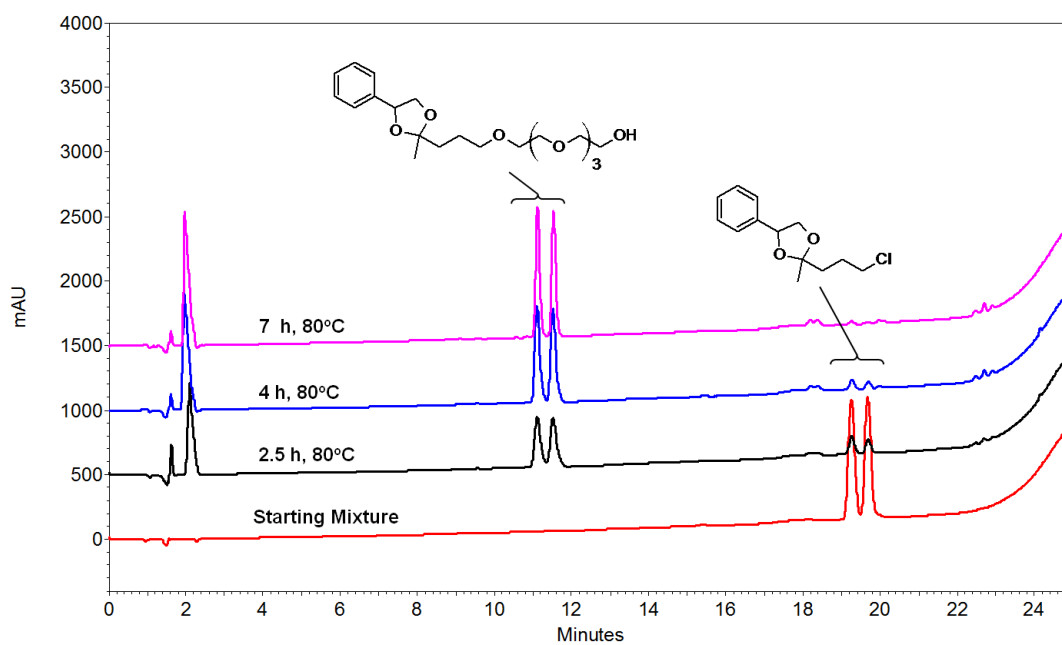


HPLC of dioxolane **24**. HPLC details in materials and methods section.

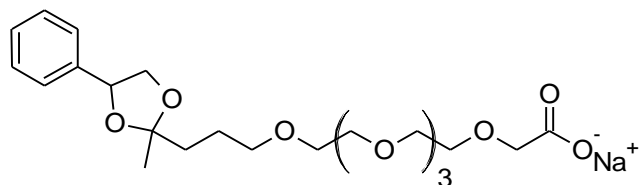
Tetraethyleneglycol-decorated Dioxolane 25

$^1\text{H-NMR}$ (300 MHz, CDCl_3) δ 7.37-7.26 (m, 5H), 5.09-4.98 (m, 1H), 4.30-4.24 (m, 1H), 3.73-3.47 (m, 19H), 3.04 (s, 1H), 1.87-1.74 (m, 4H), 1.46 (d, 3H); $^{13}\text{C-NMR}$ (300 MHz, CDCl_3) δ 139.0, 138.5, 128.5, 128.1, 128.0, 126.3, 126.2, 111.2, 111.0, 78.5, 77.7, 72.6, 71.9, 71.7, 71.4, 71.3, 70.60, 70.55, 70.3, 70.05, 70.03, 67.9, 61.6, 36.4, 35.9, 25.6, 24.8, 24.32, 24.29.

 $^1\text{H NMR}$ (CDCl_3)

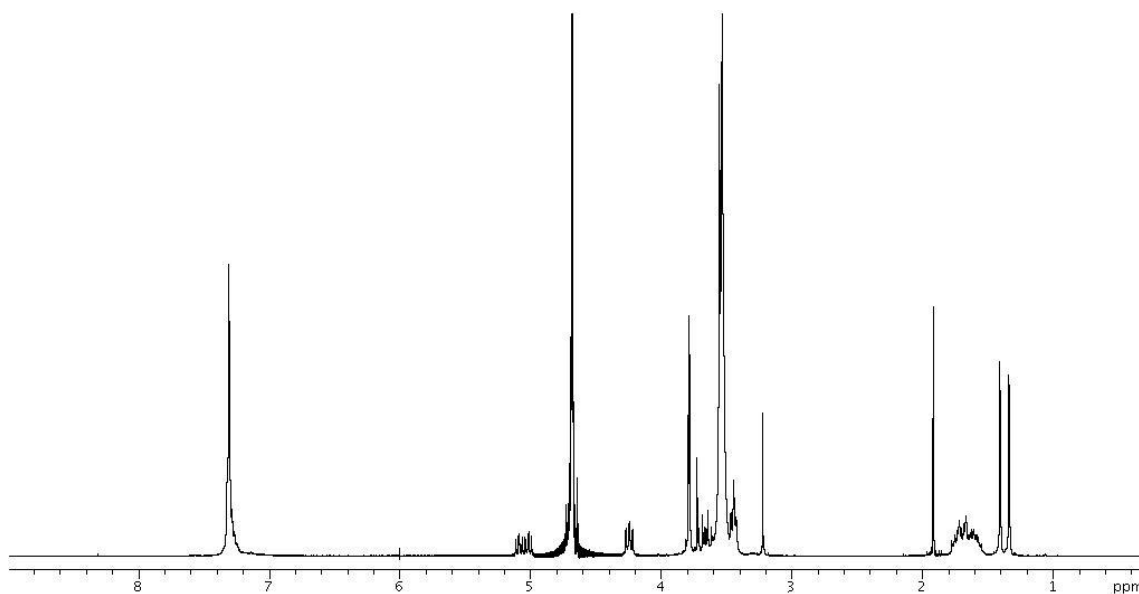
 ^{13}C NMR (CDCl_3)

RP-HPLC monitoring of the reaction

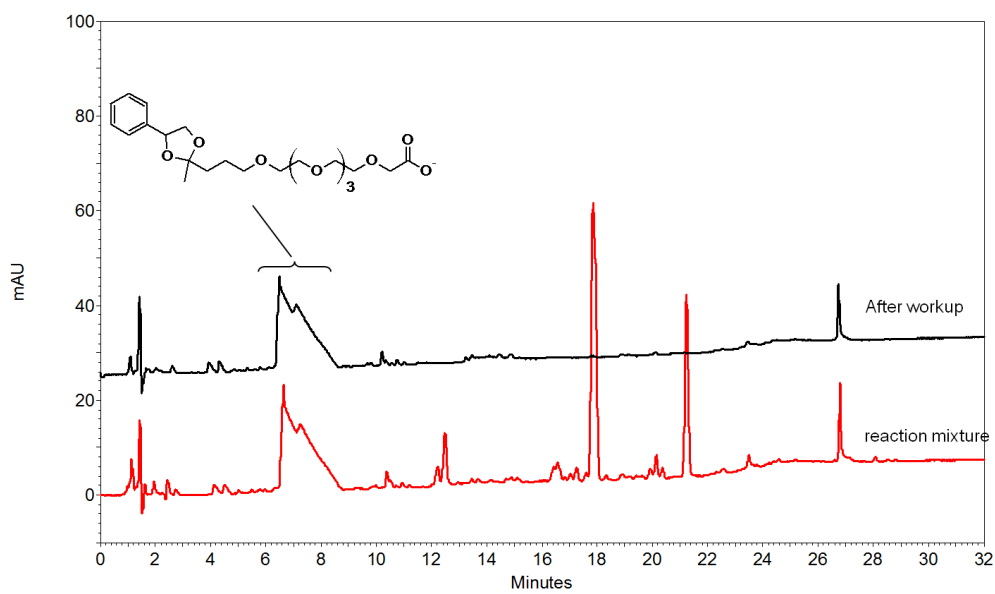
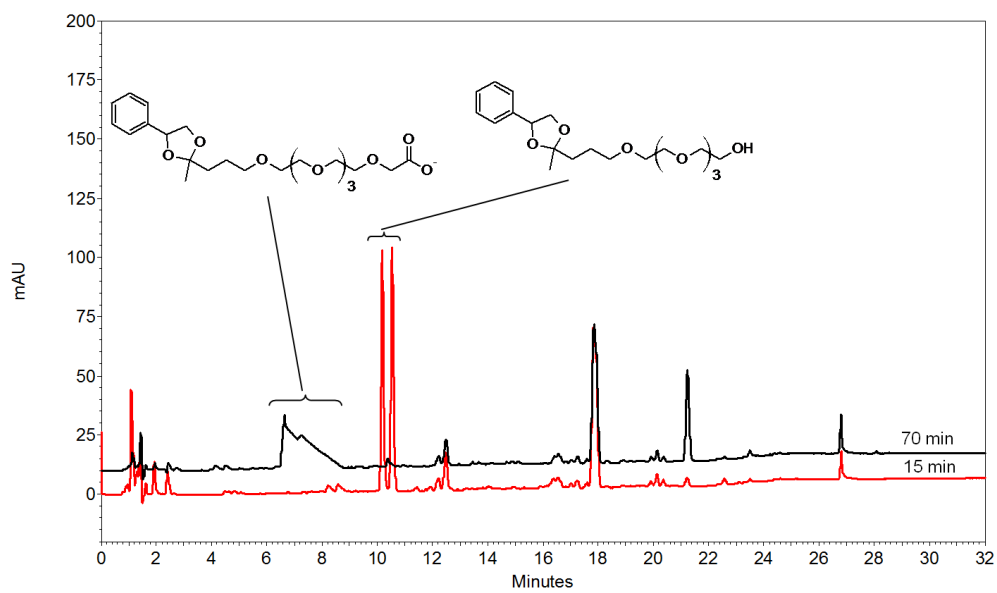
Dioxolane/Carboxylic Acid-Terminated Tetraethyleneglycol 26

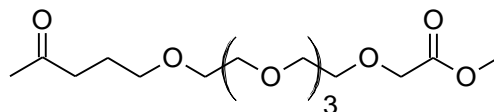
$^1\text{H-NMR}$ (300 MHz, D_2O) δ 7.33-7.28 (m, 5H), 5.11-4.99 (m, 1H), 4.27-4.22 (m, 1H), 3.79-3.42 (m, 21H), 1.79-1.54 (m, 4H), 1.37 (d, 3H).

$[\text{M-H}]^-_{\text{meas.}} = 455.228$, $[\text{M-H}]^-_{\text{calc.}} = 455.229$



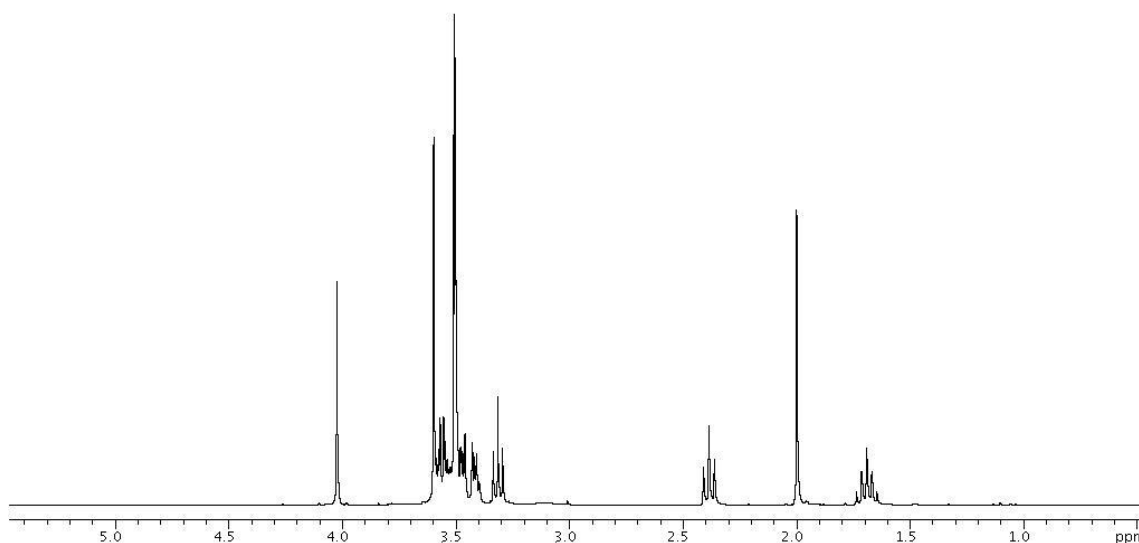
$^1\text{H NMR}$ (D_2O)



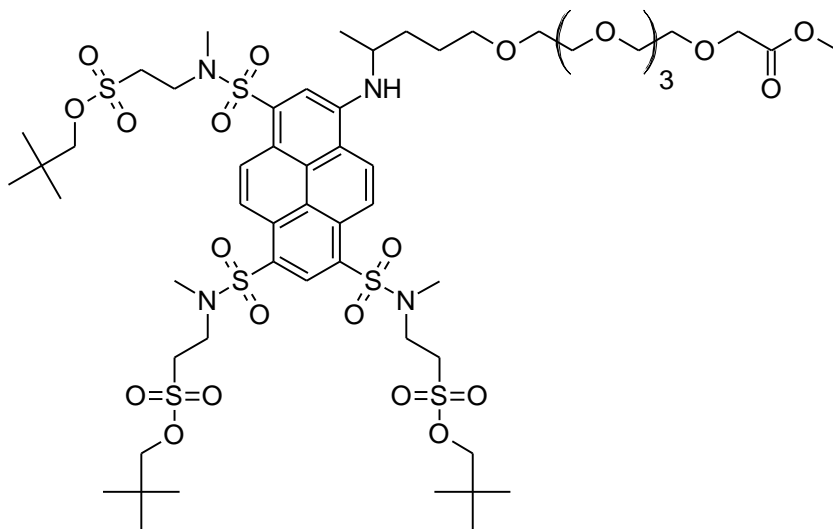
PEG-based Fluorophore Tether Intermediate 28

$^1\text{H-NMR}$ (300 MHz, CDCl_3) δ 4.02 (s, 2H), 3.61-3.39 (m, 19H), 3.32 (t, 2H), 2.38 (t, 2H), 2.00 (s, 3H), 1.73-1.64 (m, 2H); $^{13}\text{C-NMR}$ (300 MHz, CDCl_3) δ 208.5, 170.8, 165.0, 70.7, 70.45, 70.39 (broad), 70.37, 70.0, 69.9, 68.4, 51.6, 40.1, 29.8, 23.6.

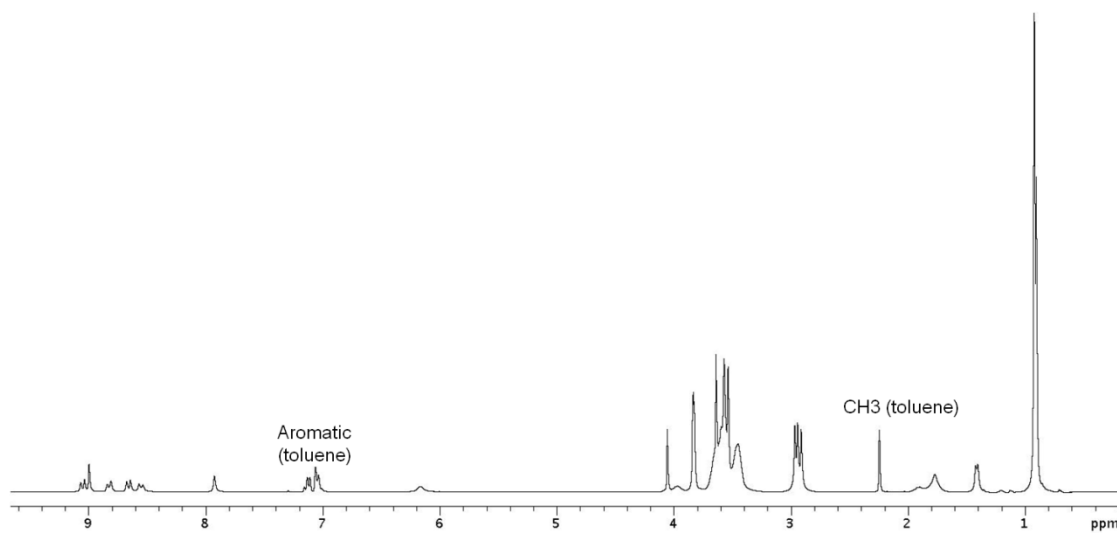
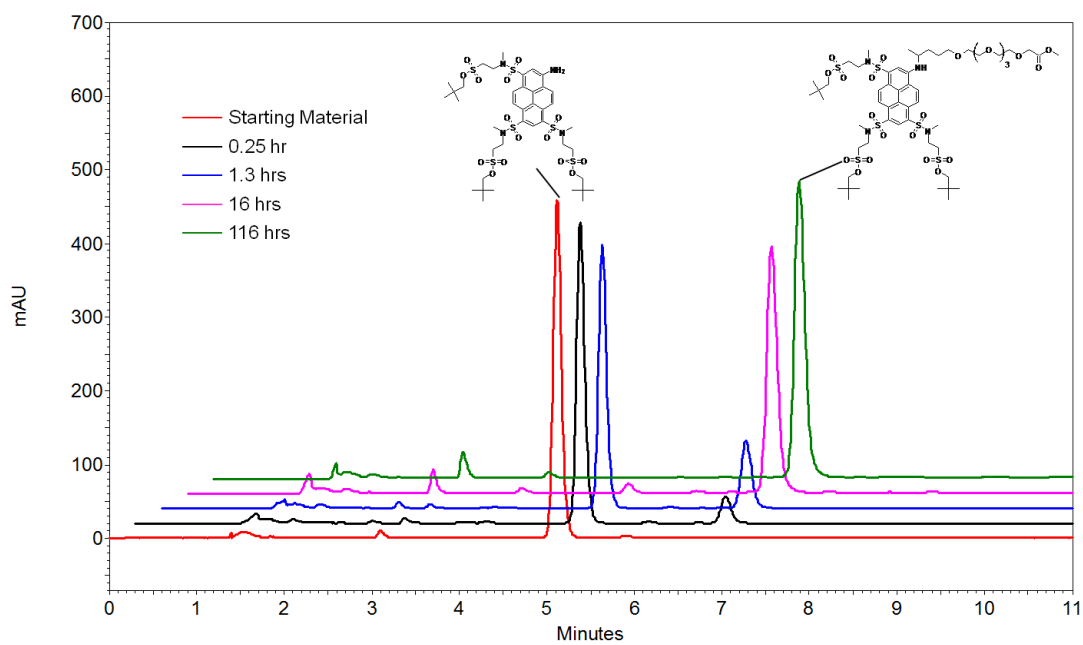
$[\text{M}+\text{Na}]^+_{\text{meas.}} = 373.1834$, $[\text{M}+\text{Na}]^+_{\text{calc.}} = 373.1833$



$^1\text{H NMR}$ (CDCl_3)

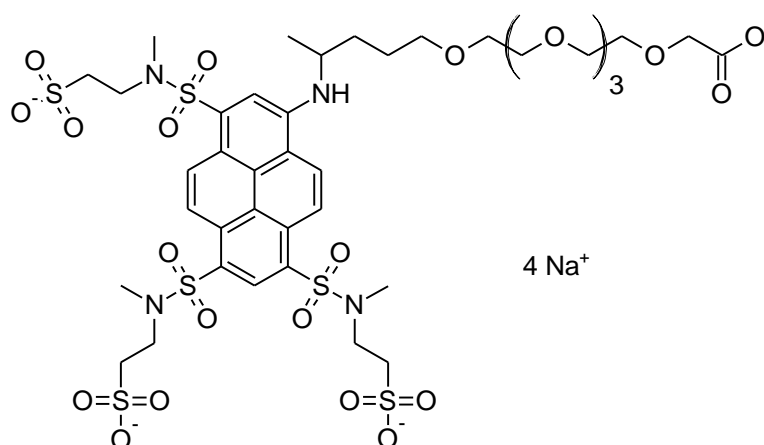
Alkylated APTS tris Sulfonamide 29

$^1\text{H-NMR}$ (300 MHz, CDCl_3) δ 9.05 (d, 1H), 9.00 (s, 1H), 8.82 (d, 1H), 8.66 (d, 1H), 8.55 (d, 1H), 7.93 (s, 1H), 6.19 (broad s, 1H), 4.056 (s, 2H), 4.0-3.4 (m, 42H), 2.97-2.91 (m, 9H), 2.0,-1.68 (m, 3H), 1.41 (d, 2H), 0.91 (s, 27H).

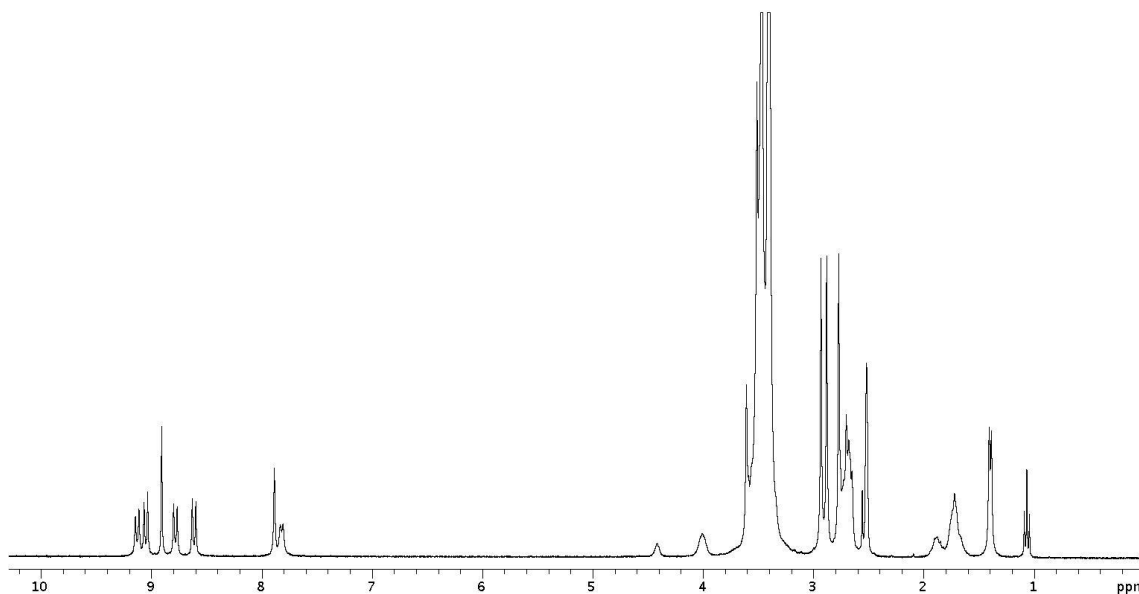
 $^1\text{H NMR (CDCl}_3)$ 

RP-HPLC monitoring of reductive amination reaction.

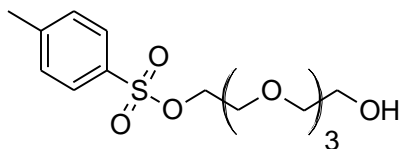
Tetra-anionic Trisulfonamide APTS 33



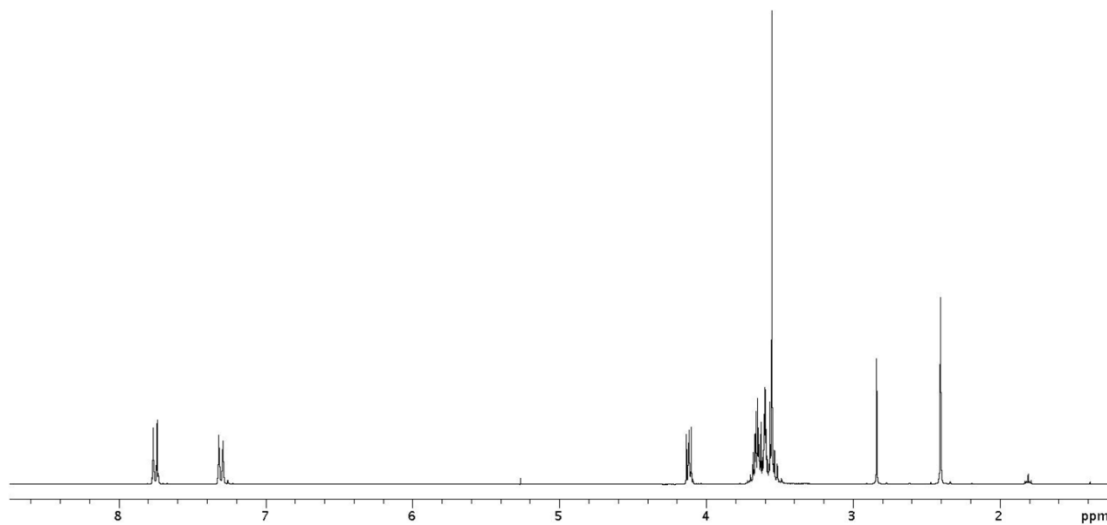
¹H-NMR (300 MHz, *d*₆-DMSO) δ 9.11 (d, 1H), 9.05 (d, 1H), 8.91 (s, 1H), 8.78 (d, 1H), 8.61 (d, 1H), 7.89 (s, 1H), 7.82 (broad d, 1H), 3.61-3.40 (m, more than theoretical), 2.90 (d, 6H), 2.70,-2.65 (m, 9H), 1.88-1.72 (broad m, 3H), 1.39 (d, 2H); [M+Na-3H]²⁻_{meas.} = 580.180, [M+Na-3H]²⁻_{calc.} = 580.085



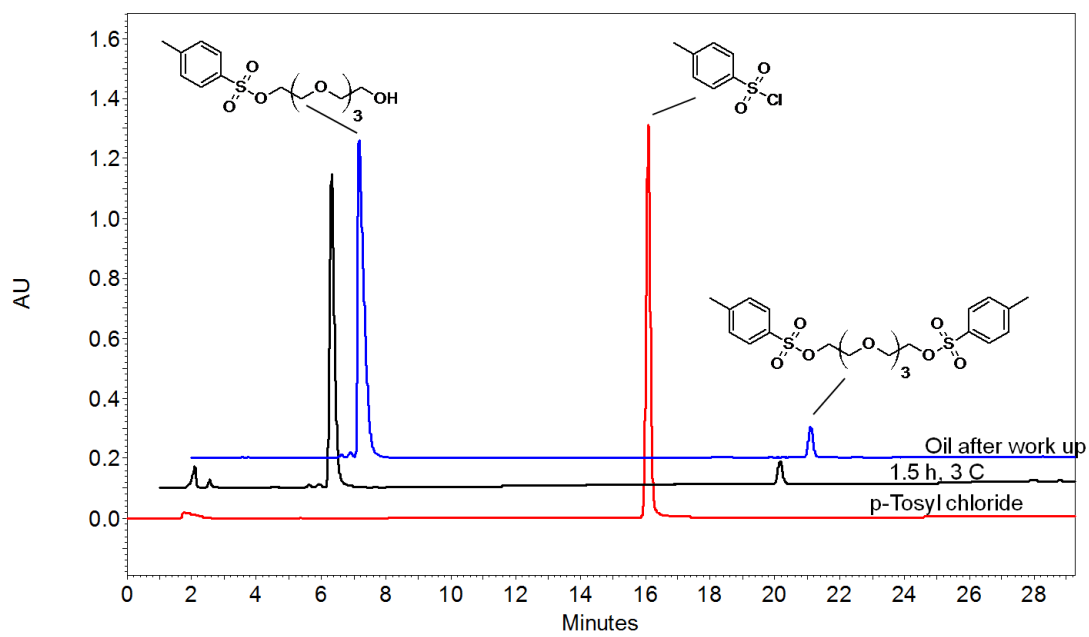
APPENDIX C**EXPERIMENTAL DATA FOR SECTION 4**

Monotosylated Tetra(ethylene glycol) 35

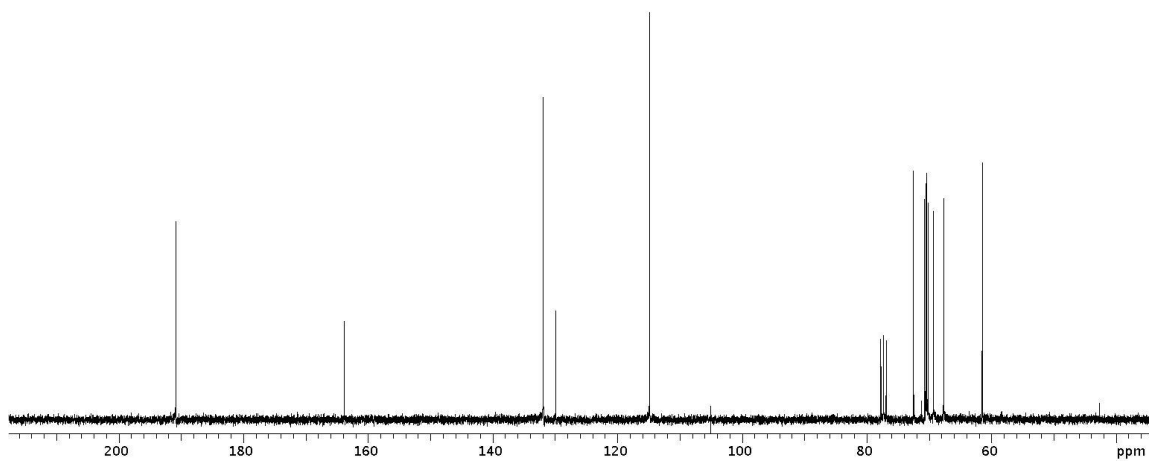
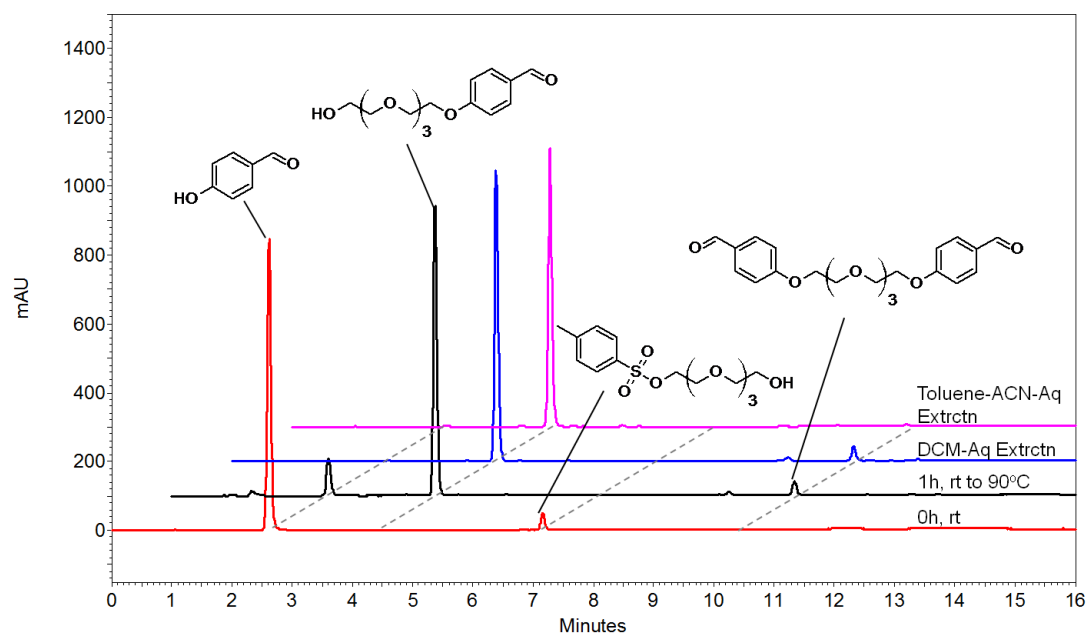
¹H-NMR (300 MHz, CDCl₃) δ 7.76 (d, 2H), 7.30 (d, 2H), 4.12 (t, 2H), 3.70-3.49 (m, 14H), 2.84 (s, 1H), 2.40 (s, 3H);



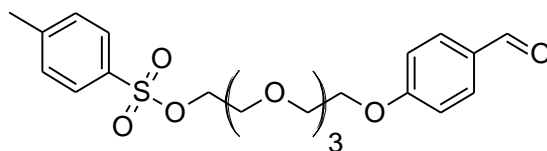
¹H-NMR (CDCl₃)



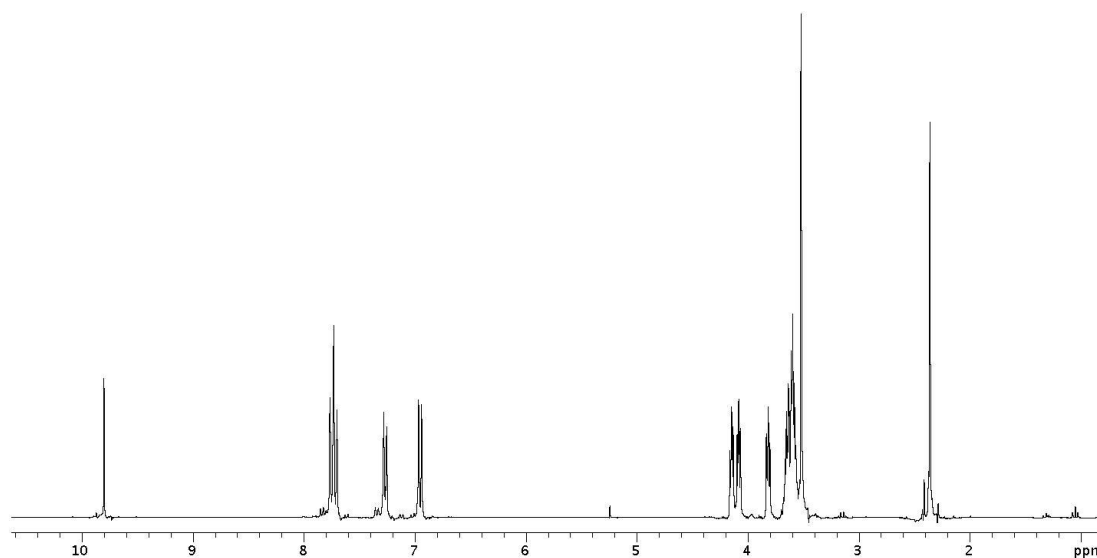
RP-HPLC monitoring of the tosylation reaction and workup

 $^{13}\text{C-NMR (CDCl}_3)$ 

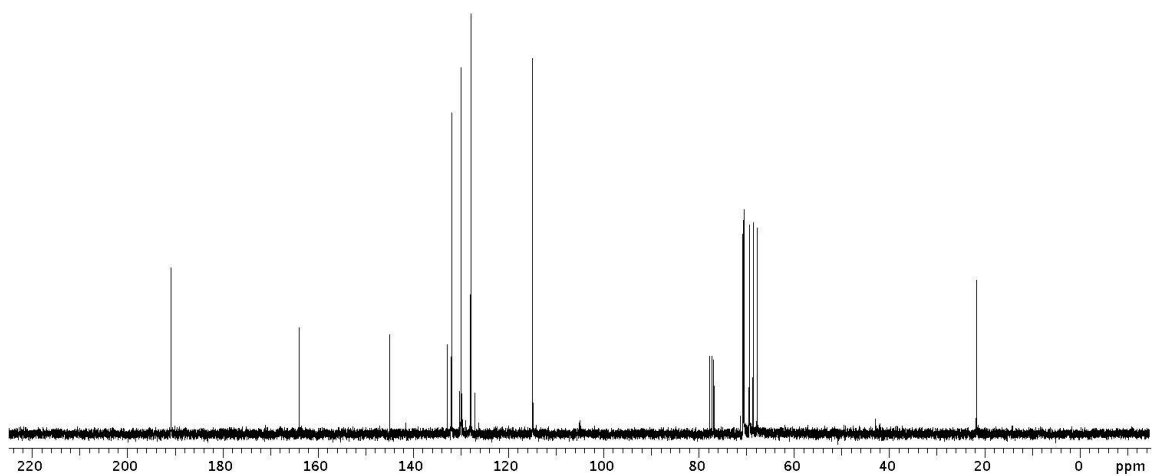
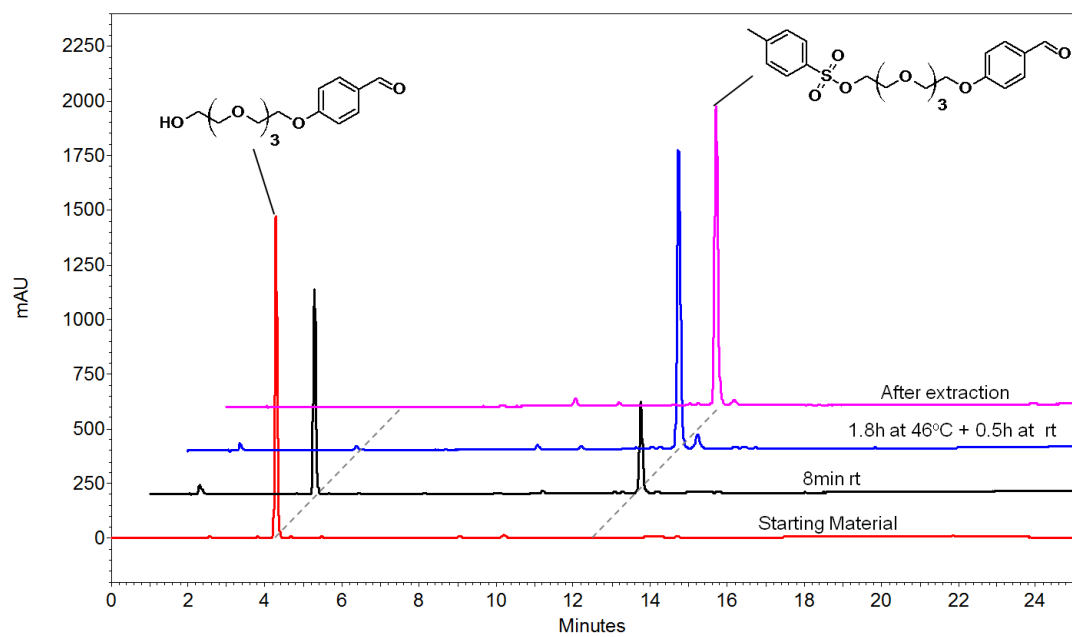
RP-HPLC monitoring of ether formation

Tosylated-TEG-Benzaldehyde 37

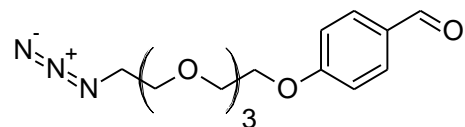
$^1\text{H-NMR}$ (300 MHz, CDCl_3) δ 9.80 (s, 1H), 7.74 (t, 4H), 7.27 (d, 2H), 6.95 (d, 2H), 4.15 (t, 2H), 4.08 (t, 2H), 3.82 (t, 2H), 3.68-3.49 (m, 10H), 2.36 (s, 3H); $^{13}\text{C-NMR}$ (300 MHz, CDCl_3) δ 190.8, 163.8, 144.8, 132.8, 131.9, 129.9, 129.8, 127.9, 114.9, 70.6, 70.56, 70.51, 70.45, 69.4, 69.3, 68.6, 67.7, 21.6.



$^1\text{H-NMR}$ (CDCl_3)

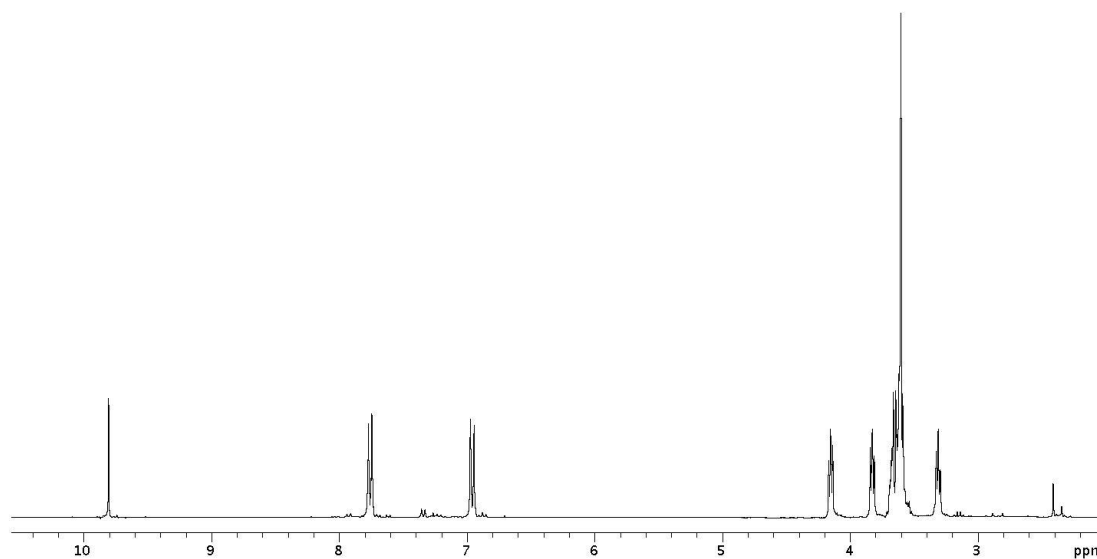
 $^{13}\text{C-NMR}$ (CDCl_3)

RP-HPLC monitoring of tosylation reaction

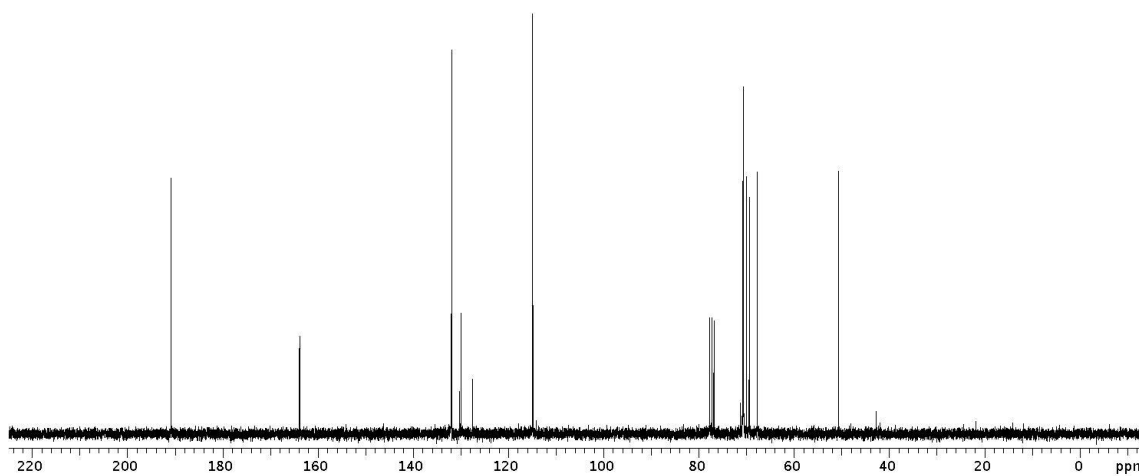
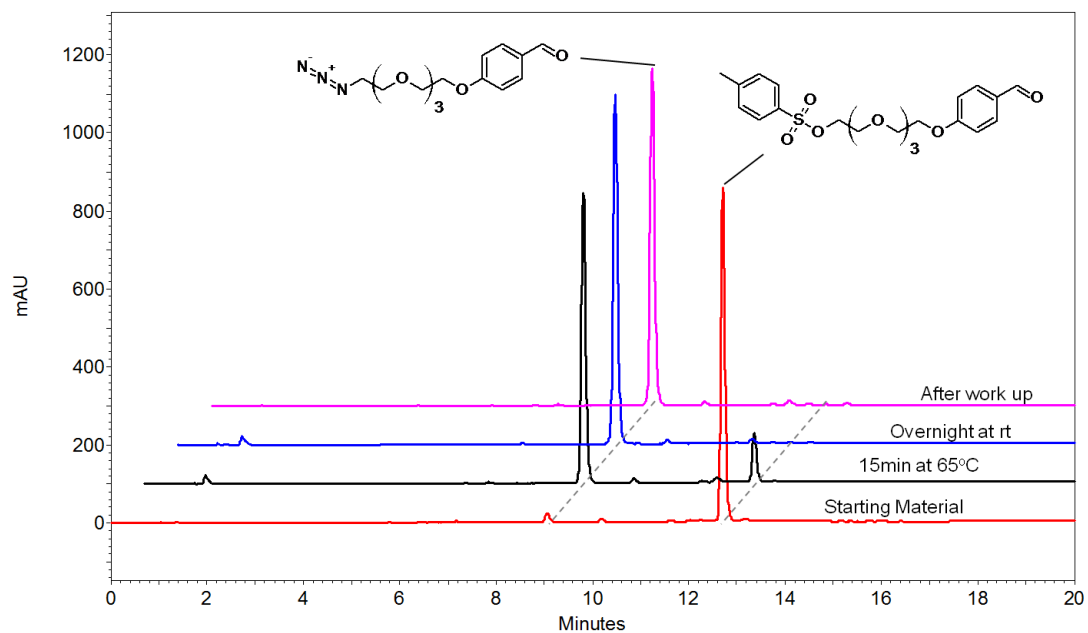
Azido-TEG-Benzaldehyde 38

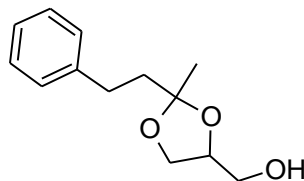
¹H-NMR (300 MHz, CDCl₃) δ 9.81 (s, 1H), 7.76 (d, 2H), 6.96 (d, 2H), 4.15 (t, 2H), 3.82 (t, 2H), 3.69-3.57 (m, 10H), 3.31 (t, 2H); ¹³C-NMR (300 MHz, CDCl₃) δ 190.8, 163.8, 131.9, 129.9, 114.8, 72.3, 70.8, 70.59, 70.57, 70.0, 69.4, 67.7, 50.6.

[M+Na]⁺_{meas.} = 346.1373, [M+Na]⁺_{calc.} = 346.1373

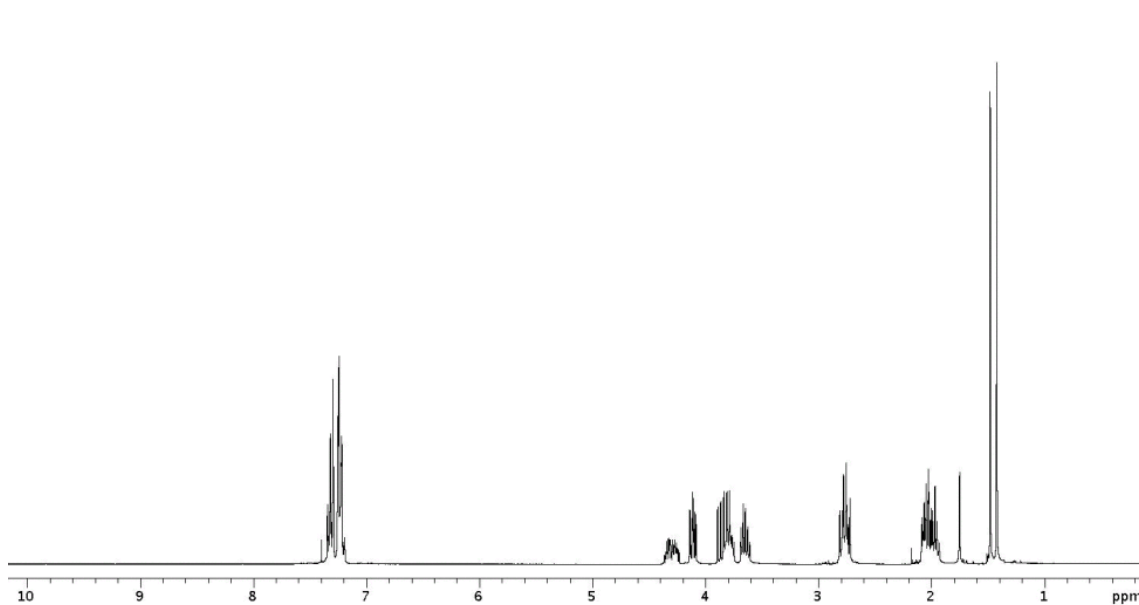


¹H-NMR (CDCl₃)

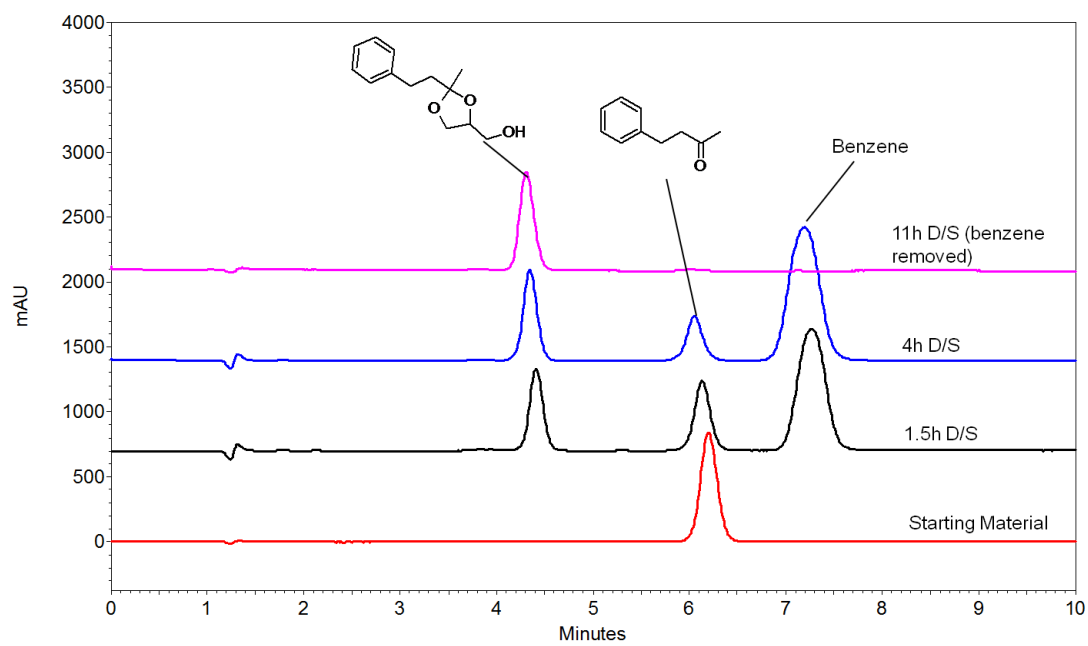
 $^{13}\text{C-NMR}$ (CDCl_3)

Dioxolane 39

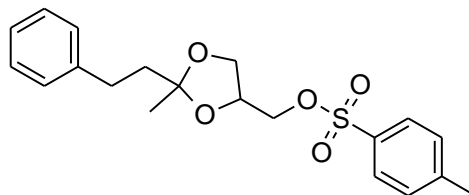
¹H-NMR (300 MHz, CDCl₃) δ 7.34-7.19 (m, 5H), 4.34-4.26 (m, 1H), 4.14-4.08 (m, 1H), 3.89-3.76 (m, 2H), 3.7-3.6 (m, 1H), 2.81-2.72 (m, 2H), 2.08-1.95 (m, 3H), 1.45 (d, 3H).



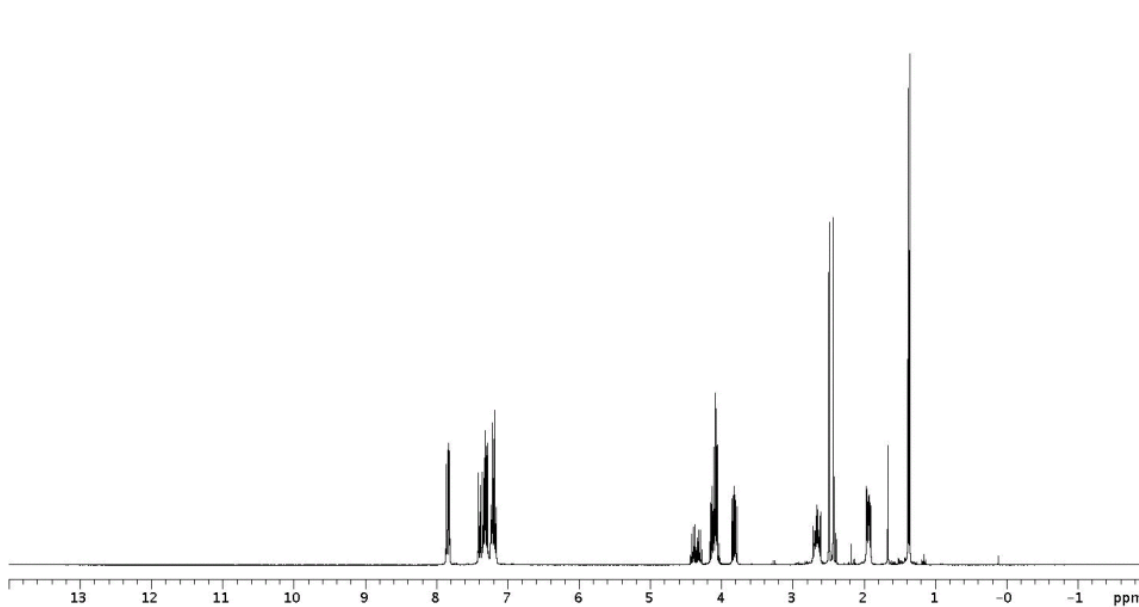
¹H-NMR (CDCl₃)



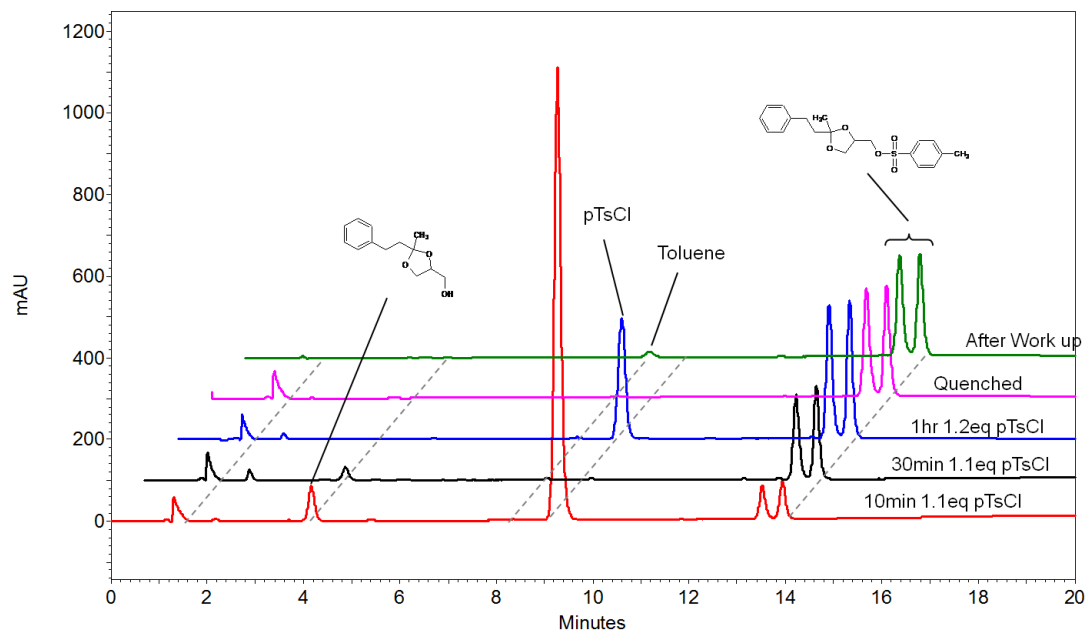
RP-HPLC monitoring of dioxolane formation

Tosylated Dioxolane 40

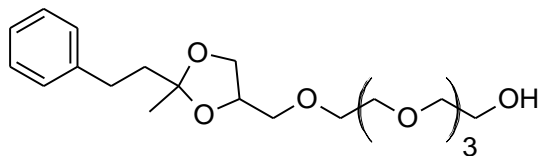
$^1\text{H-NMR}$ (300 MHz, CDCl_3) δ 7.86-7.81 (m, 2H), 7.41-7.16 (m, 7H), 4.40-4.34 (m, 1H), 4.16-4.06 (m, 3H), 3.85-3.78 (m, 1H), 2.7-2.6 (m, 2H), 2.46 (d, 3H), 1.97-1.9 (m, 2H), 1.37 (d, 3H).



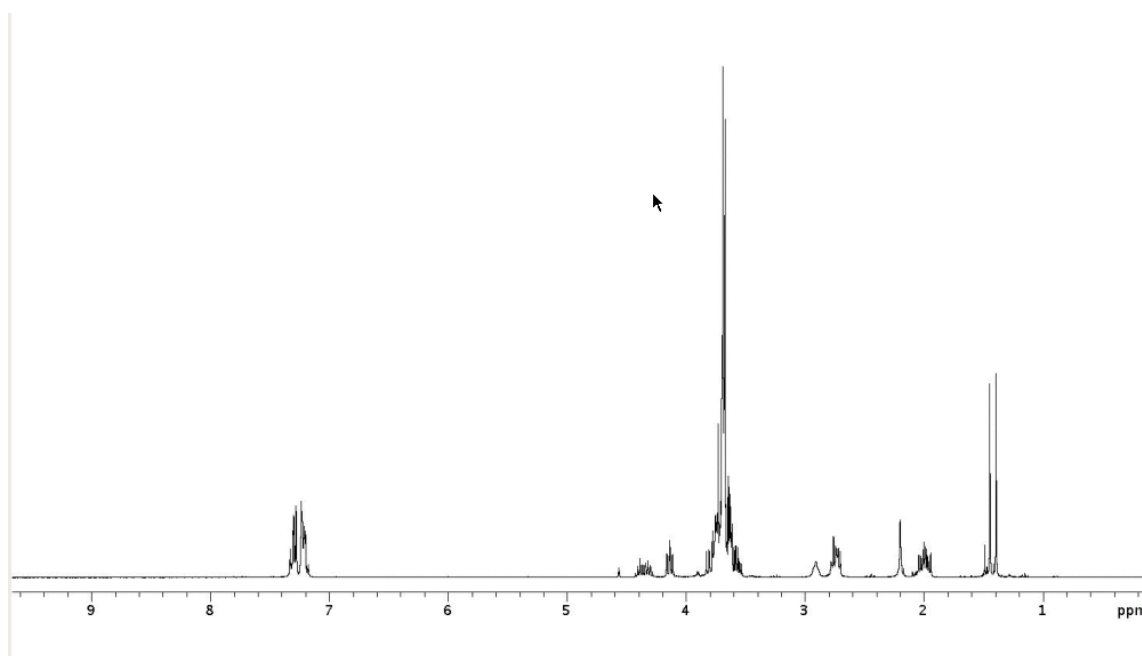
$^1\text{H-NMR}$ (CDCl_3)



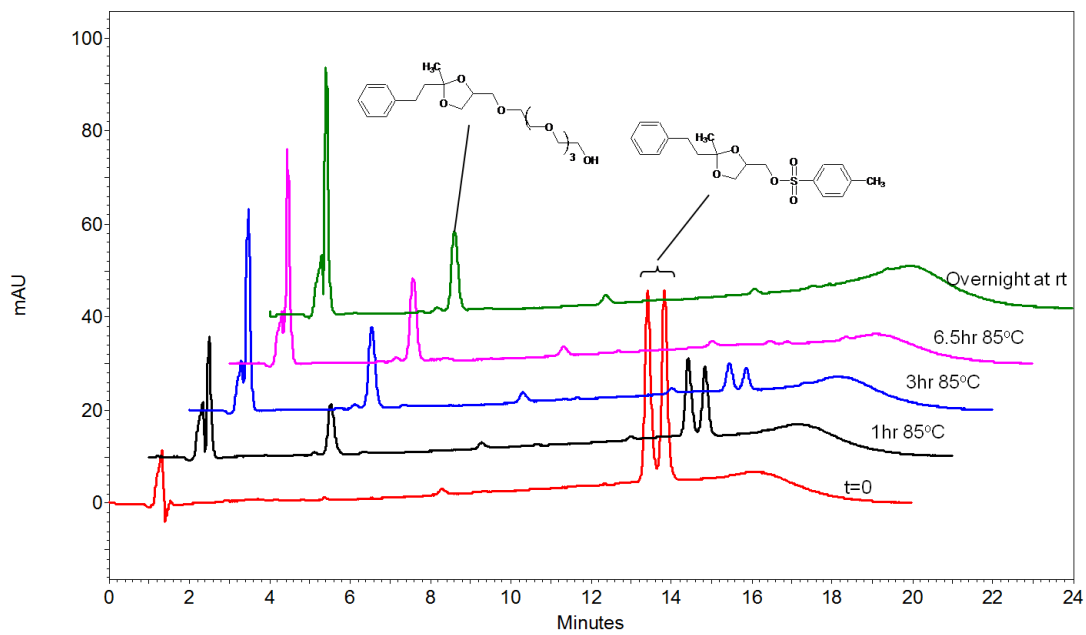
RP-HPLC monitoring of tosylation reaction

Tetra(ethylene glycol)-decorated Dioxolane 41

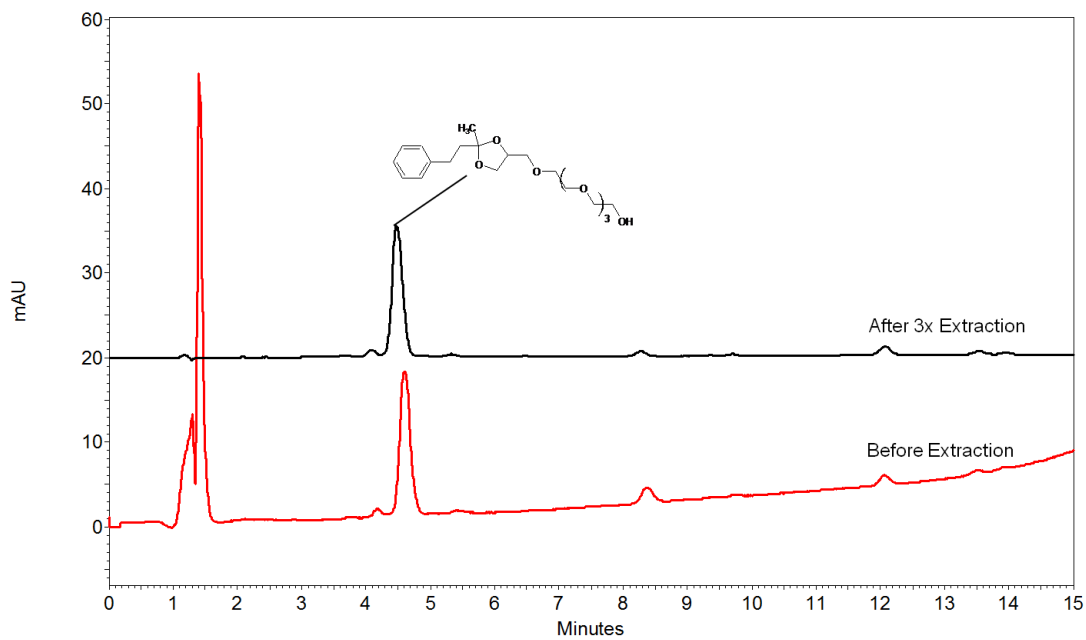
$^1\text{H-NMR}$ (300 MHz, CDCl_3) δ 7.33-7.20 (m, 5H), 4.42-4.30 (m, 1H), 4.14-4.11 (m, 1H), 3.83-3.57 (m, 18H), 2.92 (broad peak, 1H), 2.76-2.70 (m, 2H), 2.20 (s, 1H), 2.04-2.96 (m, 2H), 1.42 (d, 3H).



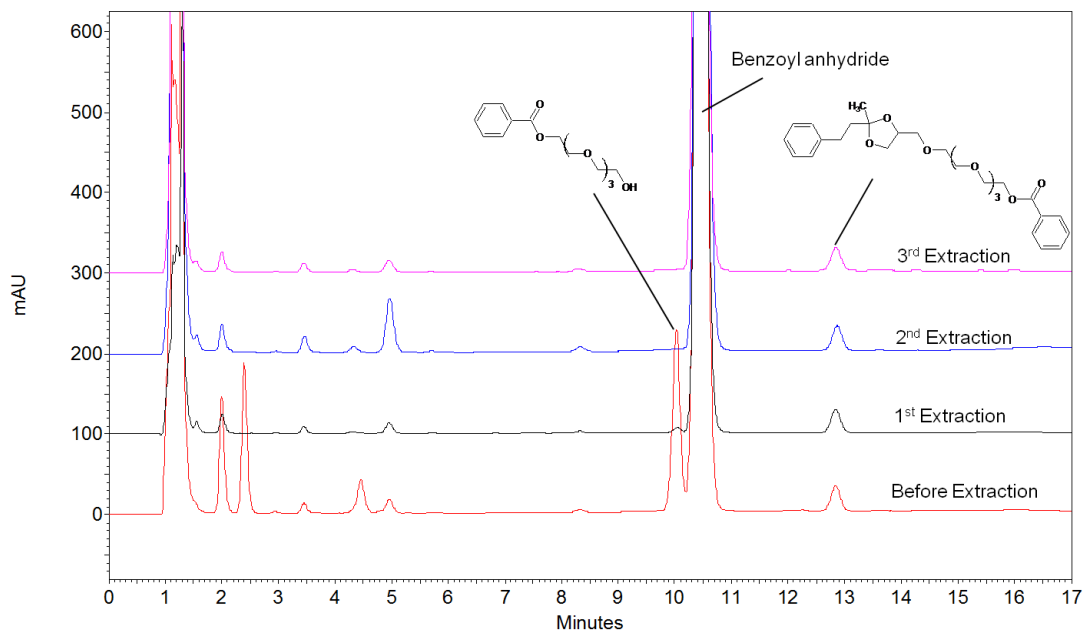
$^1\text{H-NMR}$ (CDCl_3)



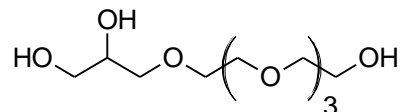
RP-HPLC monitoring of reaction with tetraethylene glycol



RP-HPLC monitoring of workup

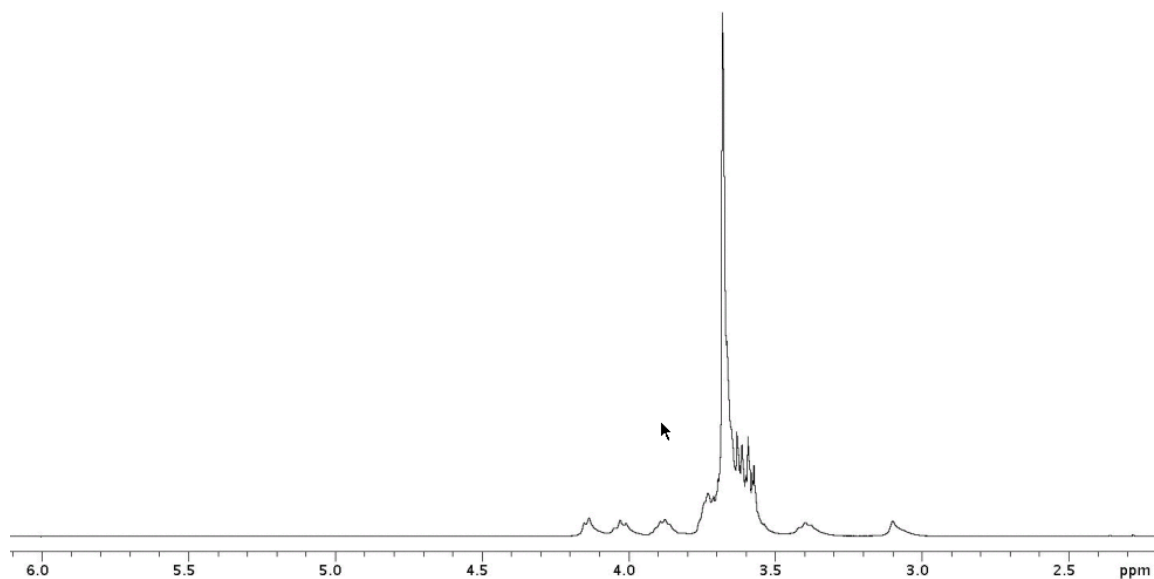


RP-HPLC monitoring of removal of tetraethylene glycol (with benzoyl chloride labeling)

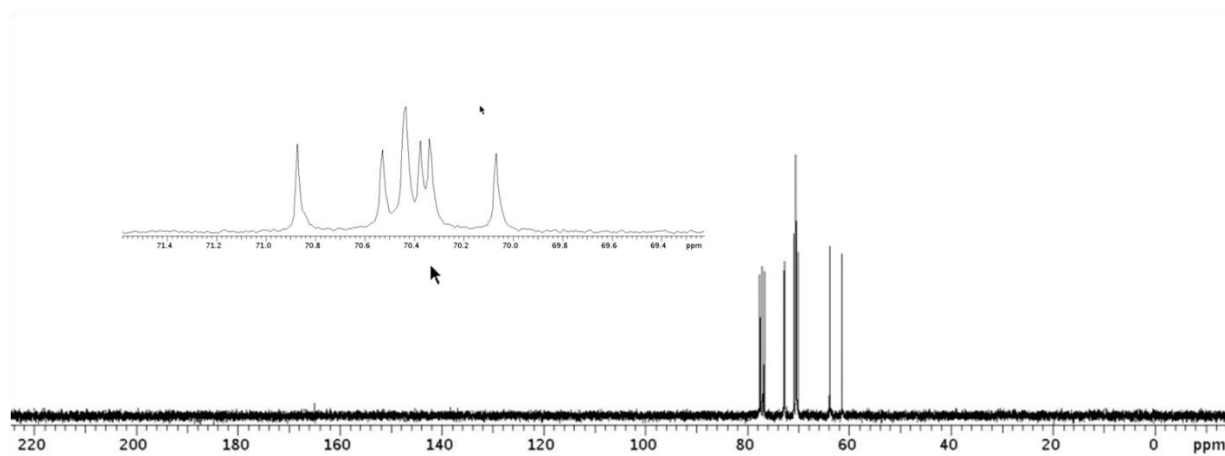
Diol-terminated Tetra(ethylene glycol) 42

$^1\text{H-NMR}$ (300 MHz, CDCl_3) δ 4.14 (broad m, 1H), 4.03 (broad m, 1H), 3.88 (broad m, 1H), 3.7-3.5 (m, 19H, actual ~23H), 3.40 (broad m, 1H), 3.1 (m, 1H); $^{13}\text{C-NMR}$ (300 MHz, CDCl_3) δ 72.9, 72.7, 70.9, 70.5, 70.43, 70.38, 70.34, 70.1, 63.8, 61.4 (two peaks are not resolved).

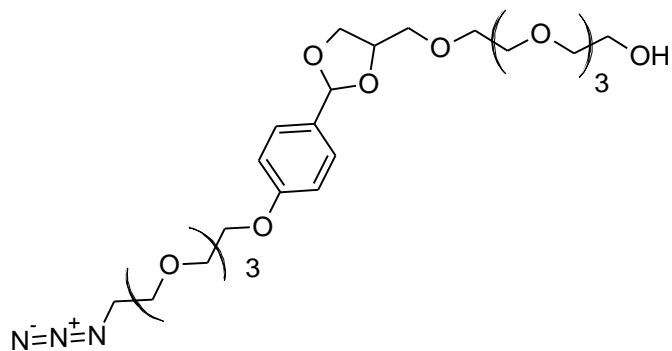
$[\text{M}+\text{H}]^+_{\text{meas.}} = 269.1607$, $[\text{M}+\text{H}]^+_{\text{calc.}} = 269.1595$



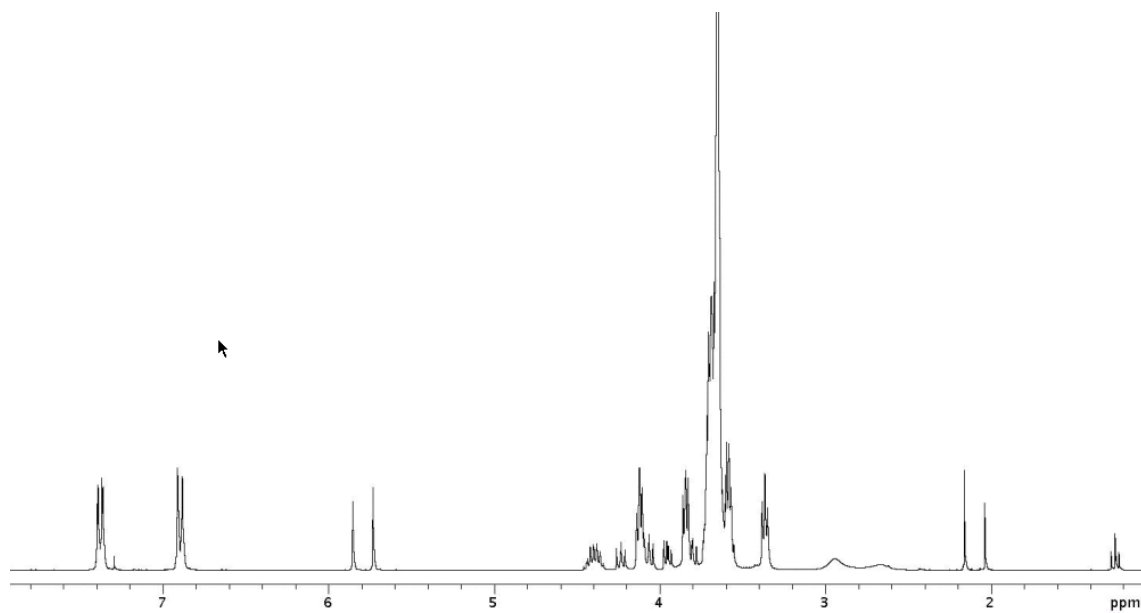
$^1\text{H-NMR}$ (CDCl_3)

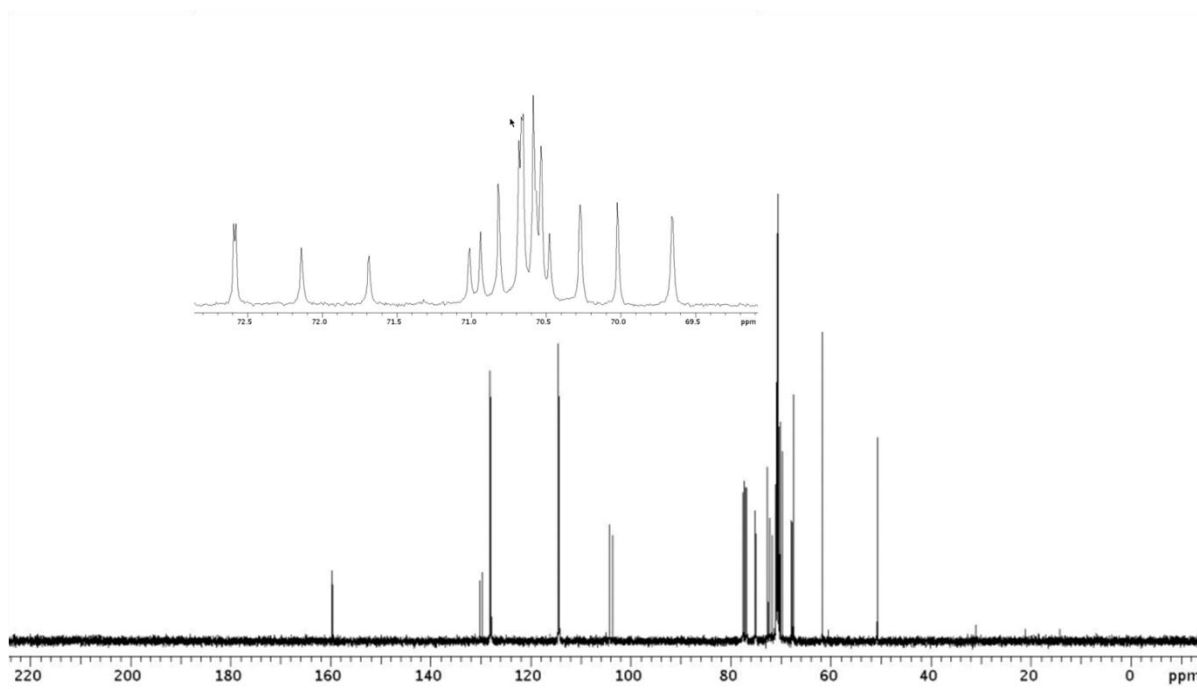


^{13}C -NMR (CDCl_3)

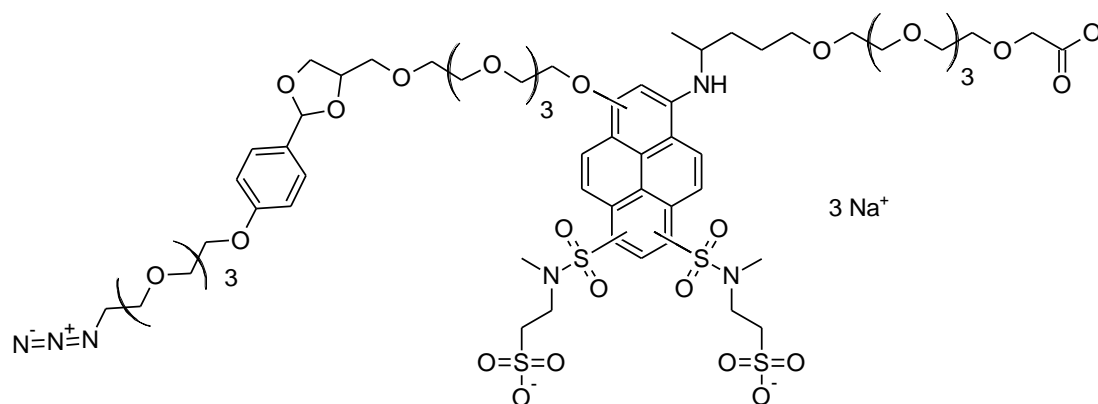
Cleavable Anchor Intermediate 43

$$[M+H]^+_{\text{meas.}} = 574.2971, \quad [M+H]^+_{\text{calc.}} = 574.2970$$

 $^1\text{H-NMR}$ (CDCl_3)

 ^{13}C -NMR (CDCl_3)

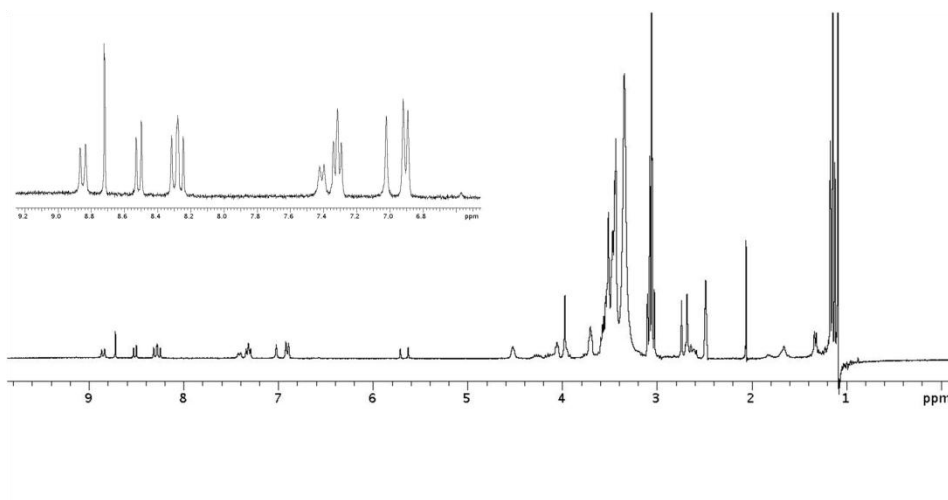
Azide-Terminated Fluorophore 44

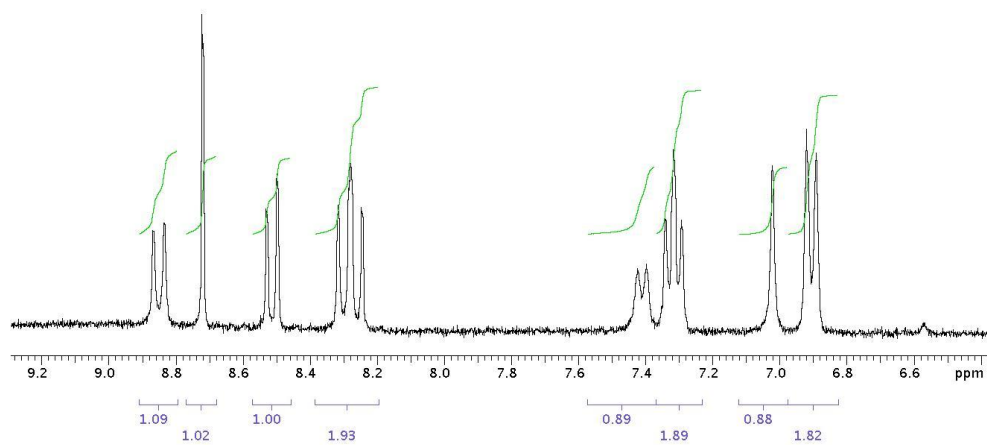


$$[\text{M-H}]^-_{\text{meas.}} = 1509.446, [\text{M-H}]^-_{\text{calc.}} = 1509.493$$

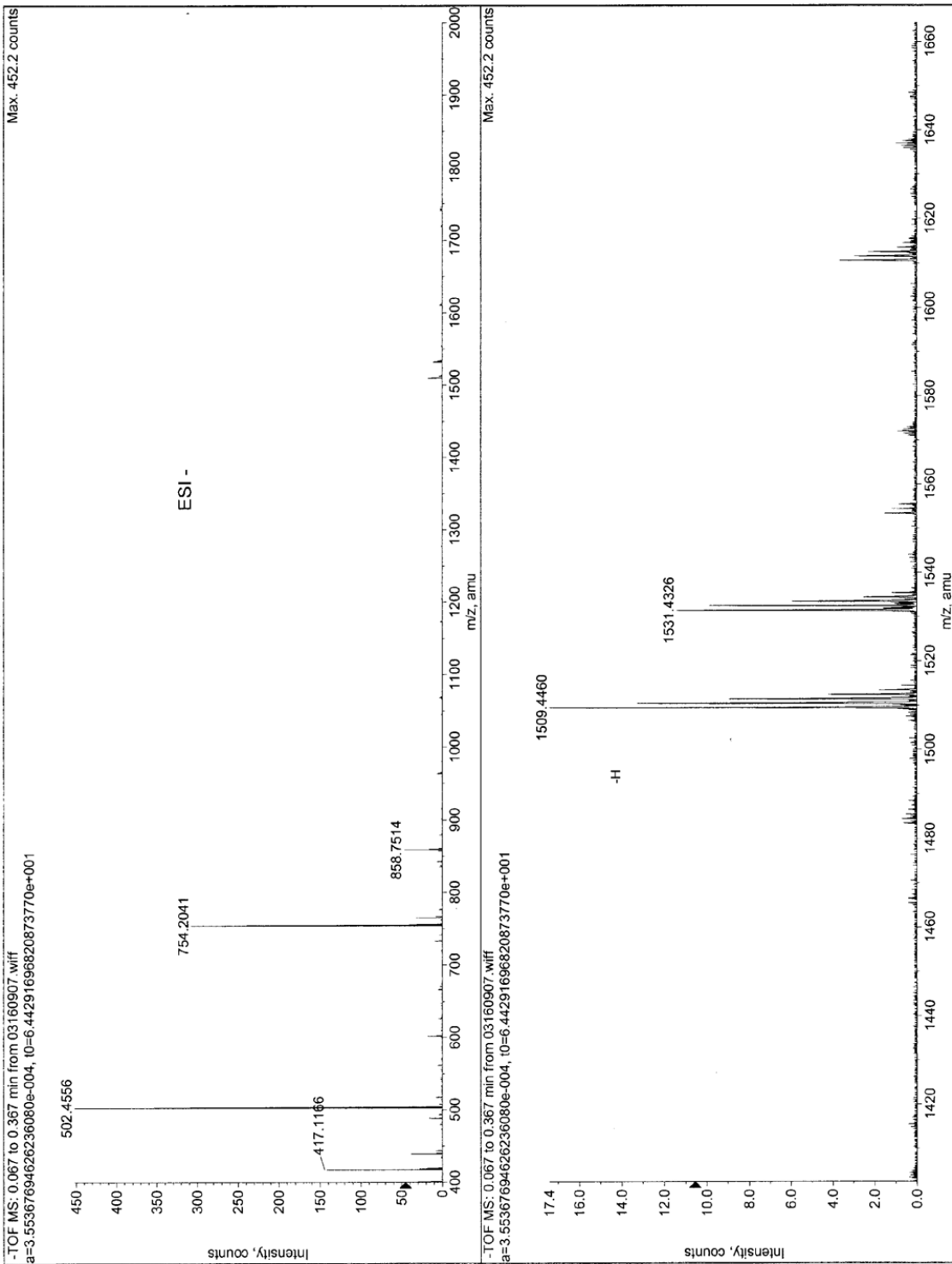
$$[\text{M-2H}]^{2-}_{\text{meas.}} = 754.204, [\text{M-2H}]^{2-}_{\text{calc.}} = 754.243$$

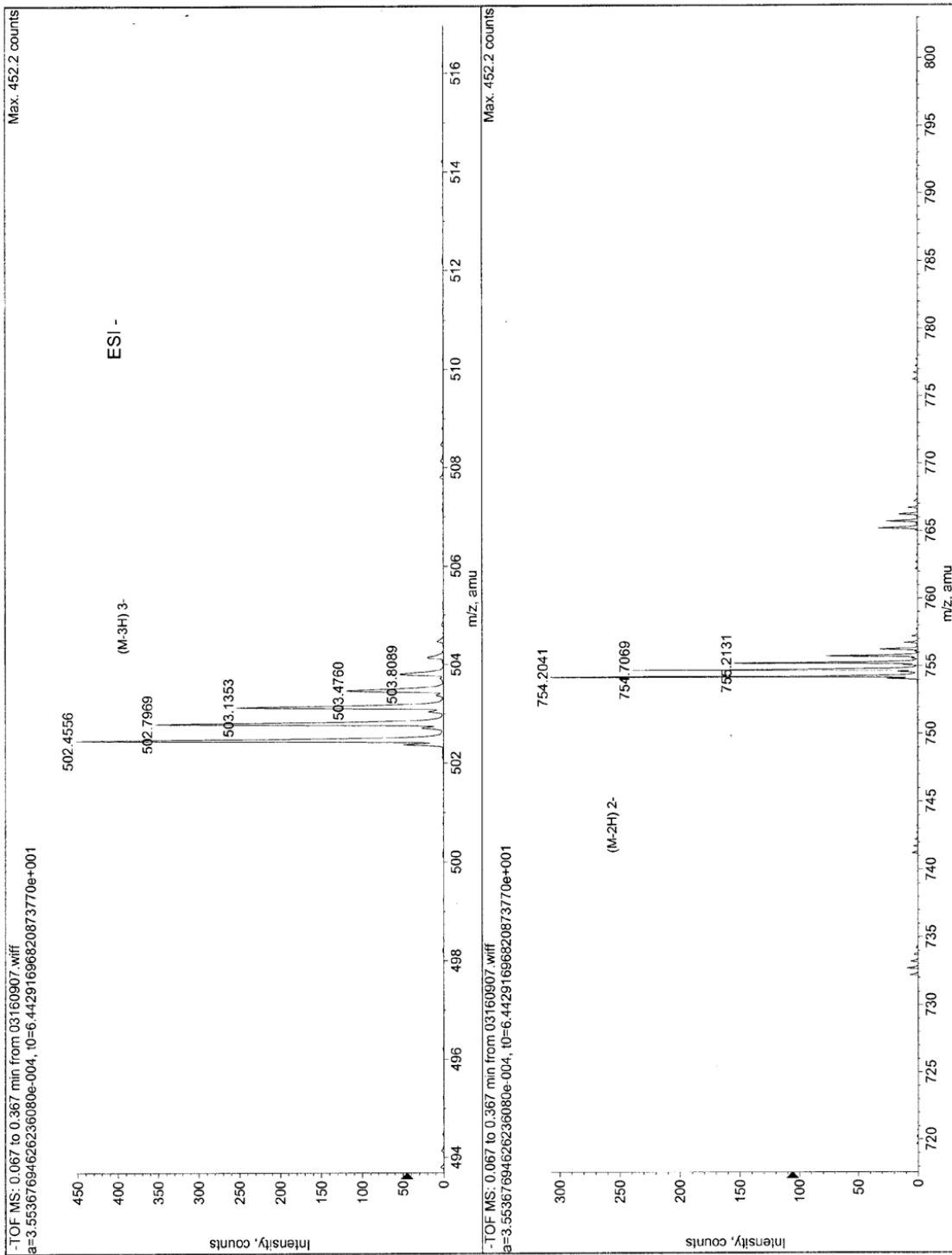
$$[\text{M-3H}]^{3-}_{\text{meas.}} = 502.456, [\text{M-3H}]^{3-}_{\text{calc.}} = 502.493$$


 $^1\text{H-NMR}$ ($d_6\text{-DMSO}$)

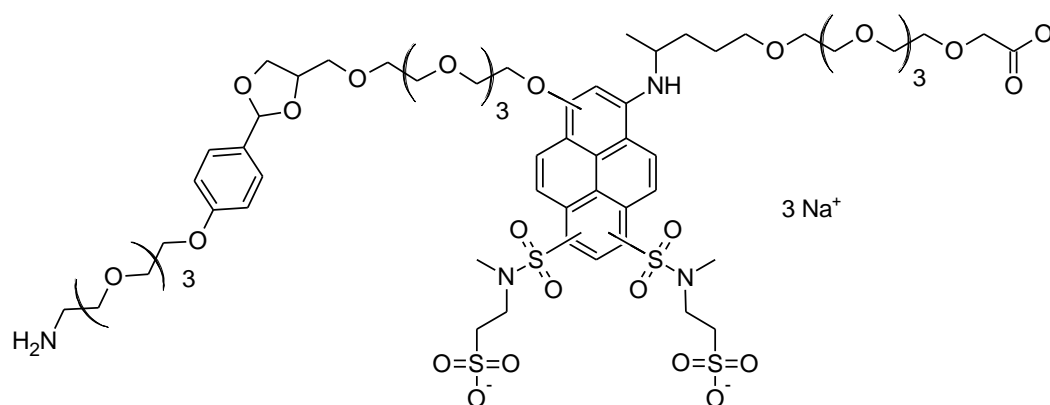


$^1\text{H-NMR}$ ($d_6\text{-DMSO}$), aromatic region.





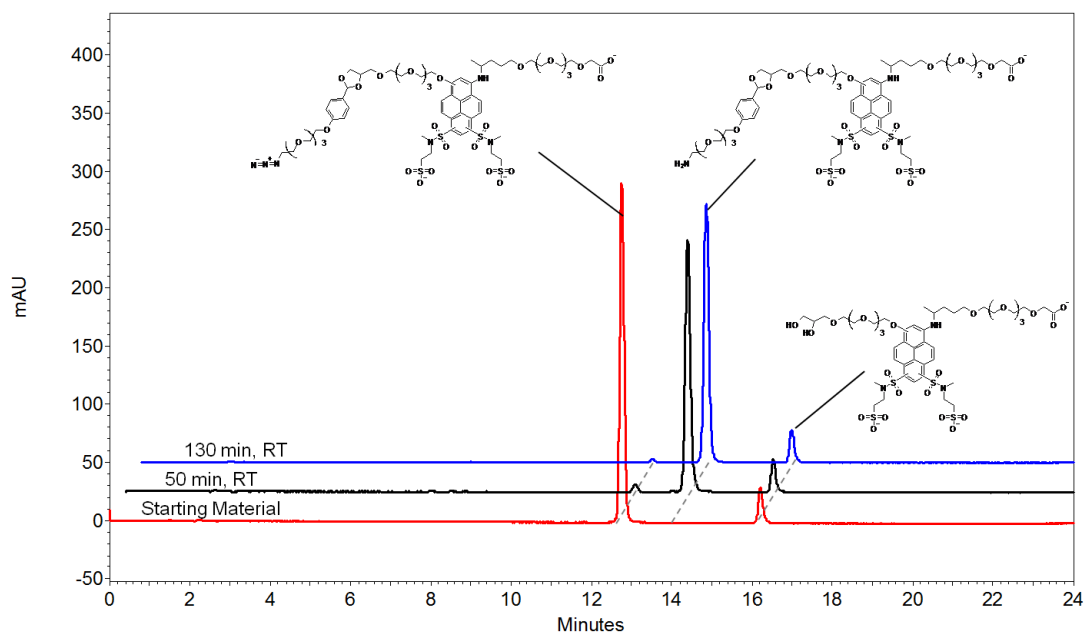
Amine-Terminated Fluorophore 45



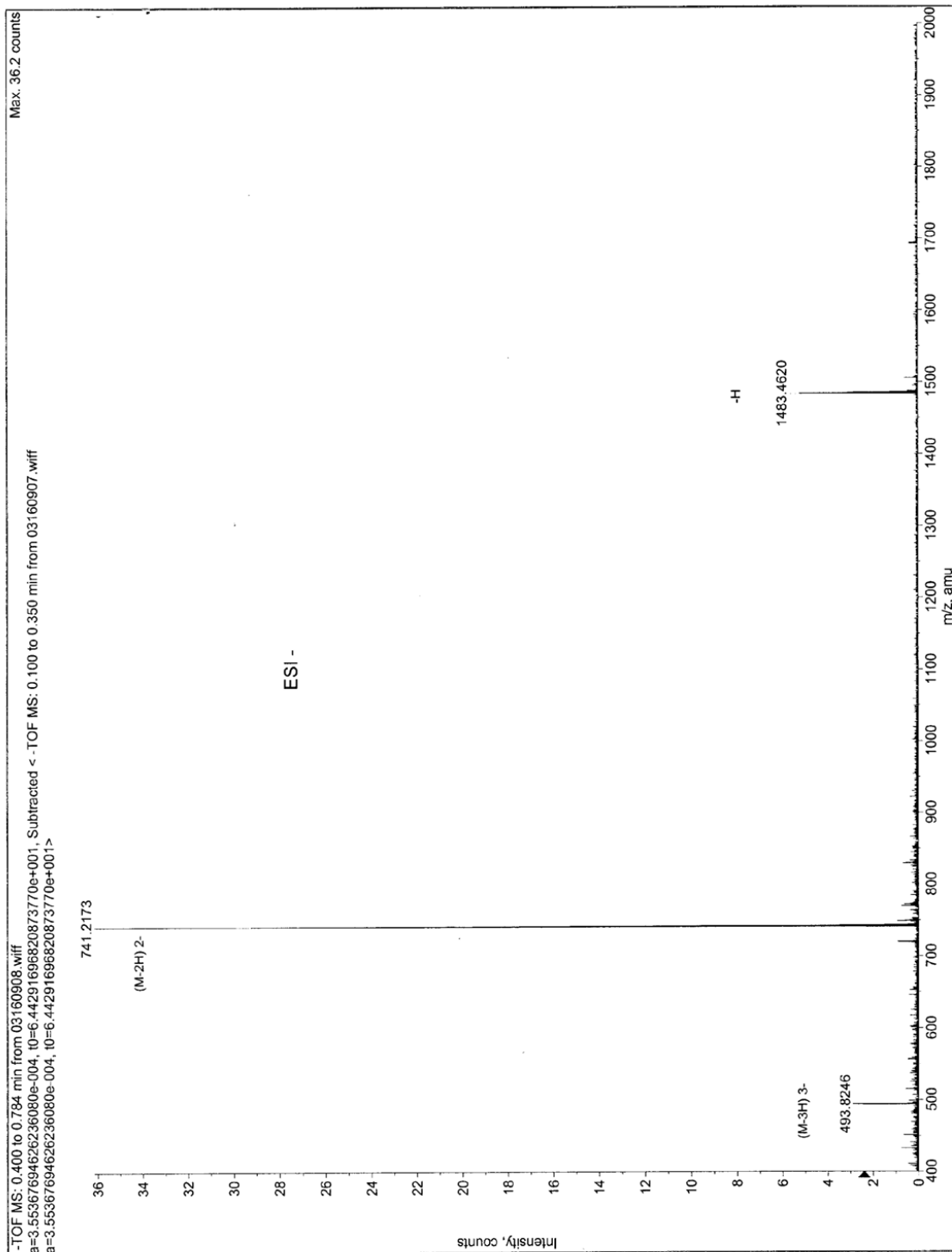
$$[\text{M-H}]^-_{\text{meas.}} = 1483.462, [\text{M-H}]^-_{\text{calc.}} = 1483.502$$

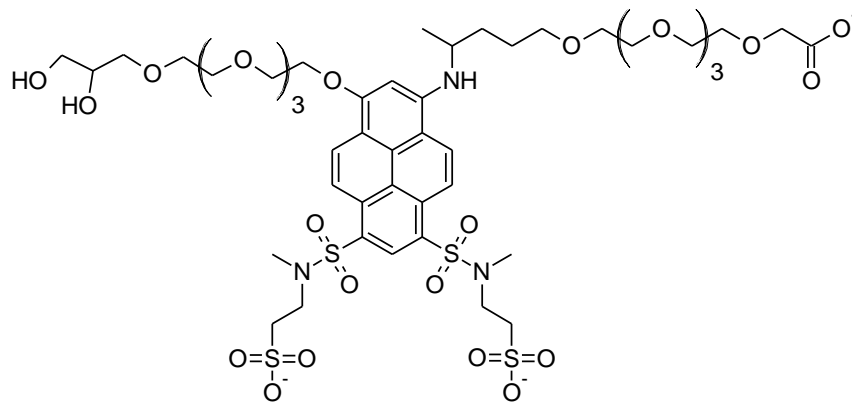
$$[\text{M-2H}]^{2-}_{\text{meas.}} = 741.217, [\text{M-2H}]^{2-}_{\text{calc.}} = 741.247$$

$$[\text{M-3H}]^{3-}_{\text{meas.}} = 493.825, [\text{M-3H}]^{3-}_{\text{calc.}} = 493.829$$



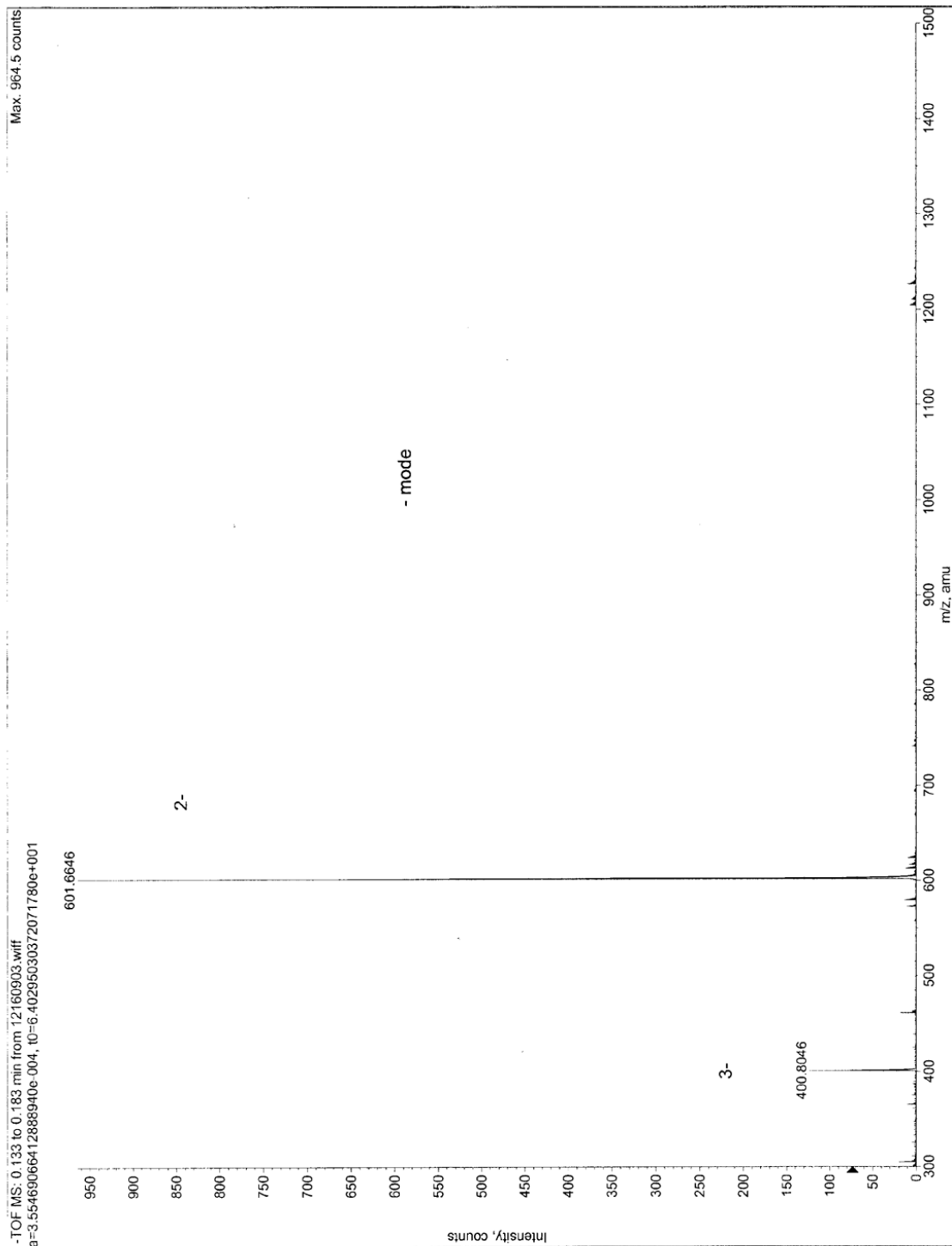
HILIC monitoring of reduction of azide to amine



Diol-Terminated Fluorophore 46

$$[M-2H]^{2-}_{\text{meas.}} = 601.665, [M-2H]^{2-}_{\text{calc.}} = 601.674$$

$$[M-3H]^{3-}_{\text{meas.}} = 400.805, [M-3H]^{3-}_{\text{calc.}} = 400.780$$



VITA

Name: Roy Tonacao Estrada, III

Address: TM Chemicals Limited Partnership
2525 Battleground Road
La Porte, TX 77571

Email Address: roy3rd@gmail.com

Education: B.S. Chemical Engineering, University of San Carlos, Cebu City,
Cebu, Philippines, 1999

Ph.D. Chemistry, Texas A&M University, College Station, Texas
USA, 2010